A dual isotope approach to the study of nitrogen cycling in shelf seas

Thesis submitted in accordance with the requirements of the University of Liverpool for the degree of Doctor in Philosophy by Calum George Preece.

May 2018

I certify that the work described in this thesis is my own except where otherwise stated and has not previously been submitted for any degree at this or any other university

Calum George Preece

……

Acknowledgements

First and foremost, I would like to thank my supervisor Claire Mahaffey for giving me the opportunity to be part of such an interesting project; whose guidance has been invaluable and continued support has provided me with a drive to continue in the field. I would also like to thank my other supervisors Jonathan Sharples and Keith Weston for their help over the years.

I would also like to thank my colleagues at Liverpool, in particular Clare Davis and Nealy Carr who spent many long days on research cruises filtering seawater for my isotope samples. I would also like to thank the fellow PhD students of office 206 for keeping me sane and helping me enjoy the past four years.

I would like to thank my family for their unwavering support both before and throughout my PhD. Finally, thank you to Sabria for putting up with me for the past few years, and in particular the stress of the past couple of months before submission.

Abstract

A dual isotope approach to the study of nitrogen cycling in shelf seas

Calum George Preece

Shelf seas are highly productive and economically important regions of our ocean, and therefore play a significant role in the global ocean carbon cycle. While accounting for only 8% of the ocean surface area they support between 15 and 30% of global ocean primary productivity (Wollast 1998) and are responsible for up to 40% of global ocean carbon sequestration (Muller-Karger et al. 2005). Their productivity is thought to be sustained through dynamic physical mixing processes combined with the supply of both terrestrial and oceanic nutrients and internal regeneration of nutrients. However, the relative importance of these different nutrient pools is currently not clear. Nitrogen is often a key limiting nutrient for biological production within the open ocean and shelf seas and therefore has an important role in ocean biogeochemistry influencing the marine carbon and phosphorus cycles. The processes within the nitrogen cycle are complex. This study aims to identify the sources of nitrogen to the NW European shelf and to understand how nitrogen is cycled on the shelf.

In this thesis, the nitrogen stable isotope composition the $\delta^{15}N$ and stable oxygen isotope ($\delta^{18}O$) composition of dissolved nitrate has been used to quantitatively assess the relative magnitude and importance of the oceanic source of nitrate versus on shelf regeneration of nitrate in sustaining the on shelf nitrate pool that supports the high primary productivity in temperate shelf seas.

In the Celtic Sea there was greater *in-situ* remineralisation of nitrate across the inner shelf during the summer ($\leq$ 30 %) and autumn ($\leq$ 60 %) in 2015 indicated by the decoupling of the $\delta^{15}N_{NO3}$ and $\delta^{18}O_{NO3}$ in bottom water with the introduction of isotopically light $\delta^{18}O_{NO3}$. The influence of riverine water was also greater at the inner shelf stations as evidenced by a mixing of riverine and oceanic isotope end-members. In contrast, the proportion of nitrate remineralised *in-situ* across the outer shelf region of the Celtic Sea during the summer and autumn period was lower (0 to 10 %), with an off shelf supply of nitrate being more important than previously thought. Across the Hebrides shelf a significant proportion (up to 94 %) of the nitrate was remineralised *in-situ* at the inner and middle shelf stations during autumn 2014. The shelf edge was influenced by the off shelf supply of nitrate and the inner shelf regions were influenced by the Scottish Coastal Current and greater *in-situ* remineralisation.

The results of this study have provided the first assessment of the regeneration of nitrogen in the North West European shelf seas using the stable isotopes of nitrate. This has improved the knowledge of nitrogen cycling on the shelf and identified the

magnitude of the sources of nitrogen to the shelf over an annual cycle. These results have significant implications for the efficiency of shelf sea carbon pump and the method of subsequent carbon export from shelf seas.

References

Muller-Karger, Frank E, Ramon Varela, Robert Thunell, Remy Luerssen, Chuanmin Hu, and John J Walsh. 2005. 'The importance of continental margins in the global carbon cycle', *Geophysical research letters*, 32.

Wollast, Roland. 1998. 'Evaluation and comparison of the global carbon cycle in the coastal zone and in the open ocean', *The sea*, 10: 213-52.

Contents

List of Figures

List of Tables

Chapter 1. Introduction

1.1 The Celtic Sea and North West European Shelf Seas

Shelf seas have been identified as one of the most important biomes on earth (Wollast 1998). Shelf seas cover just 8 % of the ocean surface area yet are highly productive, supporting between 15 and 30 % of global ocean primary productivity. They also support up to 90 % of global fisheries (Pauly et al. 2002). The global ocean is estimated to absorb one third of the anthropogenic carbon that is emitted into the atmosphere every year through the burning of fossil fuels (Bates et al. 2014). Shelf seas are thought to play a disproportionate role in carbon sequestration; up to 0.68 Pg C y^{-1} sinks below the thermocline on continental margins, and over 0.62 Pg C y^{-1} settles on the seafloor. For comparison 1.01 Pg C y^{-1} sinks below the thermocline in the deep ocean, and 0.31 Pg C y^{-1} reaches the deep ocean sediments. Therefore, the continental margins are responsible for >40 % of the global carbon sequestration in the ocean (Muller-Karger et al. 2005). Shelf seas must receive nutrients to sustain this enhanced productivity, but it is still unclear how these nutrients are supplied to, cycled within and exported from the shelf regions. The North West European shelf seas are an important study region due to their environmental and economic importance; support large fisheries, oil and gas industry and tourism. This PhD formed part of the NERC Shelf Sea Biogeochemistry Programme that was developed in order to improve our understanding of the fundamental biogeochemical processes that underpin primary and secondary production. This knowledge will be used to improve and implement marine policy to maintain the ecosystem services of the region for the future.

The focus area of this PhD was the North West European shelf in particular the Celtic Sea. The Celtic Sea is part of the North West European Shelf Seas and the North Atlantic Ocean, extending across the continental shelf south of Ireland and west of France, with the Bristol and English Channel as its eastern limits (Figure 1.1). It is a highly productive shelf sea ecosystem, which displays seasonal cycles in productivity with a large spring phytoplankton bloom event followed by a smaller autumn bloom. The Celtic Sea supports major fisheries, with total annual catches of 1.8 million tonnes in 2007 (Sparholt et al. 2007). The major commercial species

caught in the Celtic Sea include the Norway lobster (*Nephrops norvegicus*), sardine (*Sardina pilchardus*) and sprat (*Sprattus sprattus*). Numerous other fisheries across other areas of the shelf include: hake (*Merluccius merluccius*), cod (*Gadus morhua*) and herring (*Clupea harengus*). The productivity of the Celtic Sea shelf region supports a large and complex trophic web with basking sharks (*Cetorhinus maximus*), blue sharks (*Prionace glauca*), and large cetaceans such as minke whale (*Balaenoptera acutorostrata*), common dolphins (*Delphinus delphis*) and grey seals (*Halichoerus grypus*) all regularly observed (Sparholt et al. 2007).

The Celtic Sea and surrounding shelf regions are also subject to numerous anthropogenic influences for example enhanced nutrient loading, overfishing, habitat disturbance from fishing, and climate change. The coastal and shelf seas around the United Kingdom are predicted to experience increases in sea surface temperature of up to 3 °C by 2100 and increases in sea level of up to 0.6 m by 2100 (Solomon 2007). These physical changes could drastically alter their productivity, and potential for carbon export (Forster et al. 2007).

The Celtic Sea is a useful region to investigate nitrogen and carbon sources and cycling due to its important economic location and highly productive ecosystem linked to the strong frontal system that exists all year round. The region is also being put under stress by humans but without a complete understanding what drives the productivity of this region. The new data collected for this thesis is complimented by an abundance of long term measurements made not only in the Celtic Sea but across the whole NW European Shelf, including the long-term time-series at stations E1 and L4 making up the Western Channel Observatory.

The overall focus of this thesis is to investigate the sources, sinks and cycling of nitrate within the North-West European shelf seas.

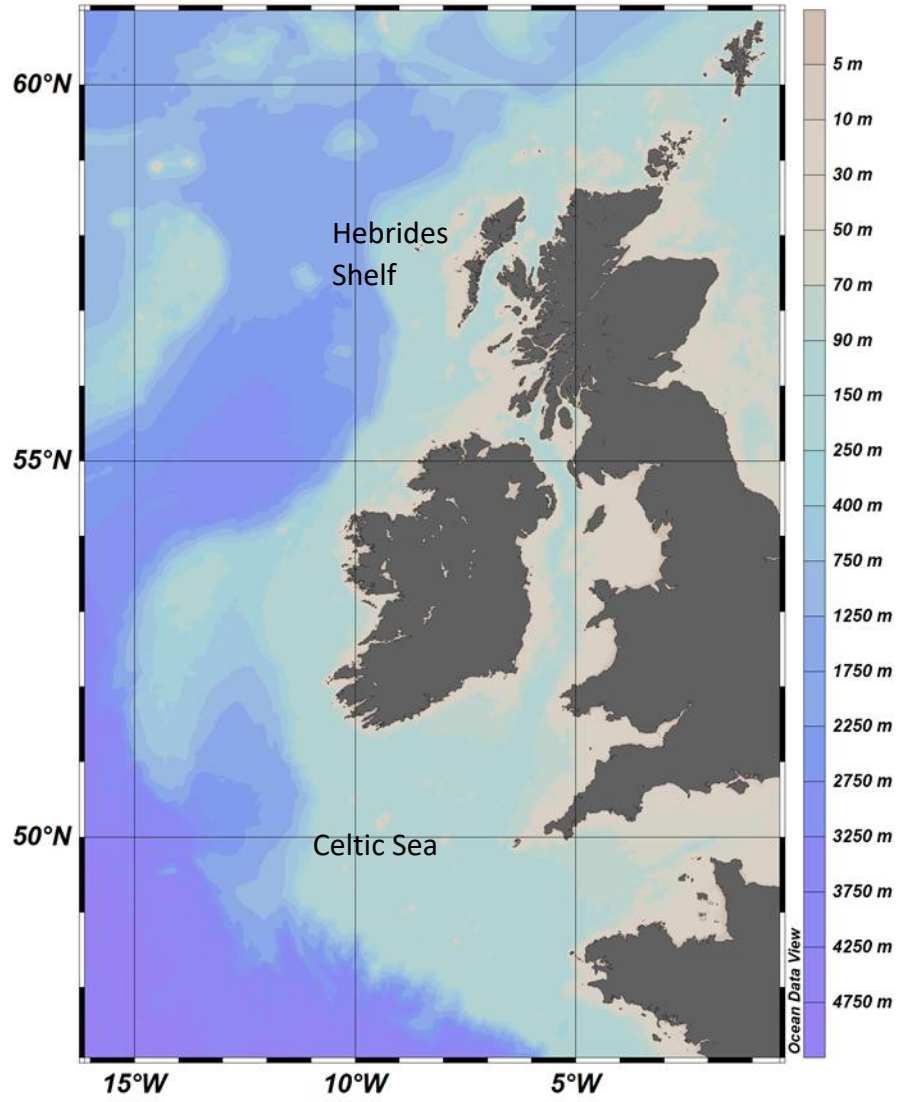

Figure 1.1. Map of the western edge of the North West European Shelf Sea system, showing the Celtic Sea and Hebrides shelf where the majority of samples for this thesis were collected

1.2 The marine nitrogen cycle

Carbon (C) and nitrogen (N) are two of the most crucial elements for life. The supply and cycling of these elements within the marine environment has important consequences for marine productivity and global climate. This study will focus on the cycling of nitrogen in a shelf sea environment. N is often a limiting nutrient for biological production and has an important role in ocean biogeochemistry, having direct impacts on other nutrient cycles including the marine C and phosphorus (P) cycles. The N cycle within the ocean is complex, driven by numerous biological

transformations of N that include nitrogen fixation, denitrification, nitrification, and anammox (Figure 1.2).

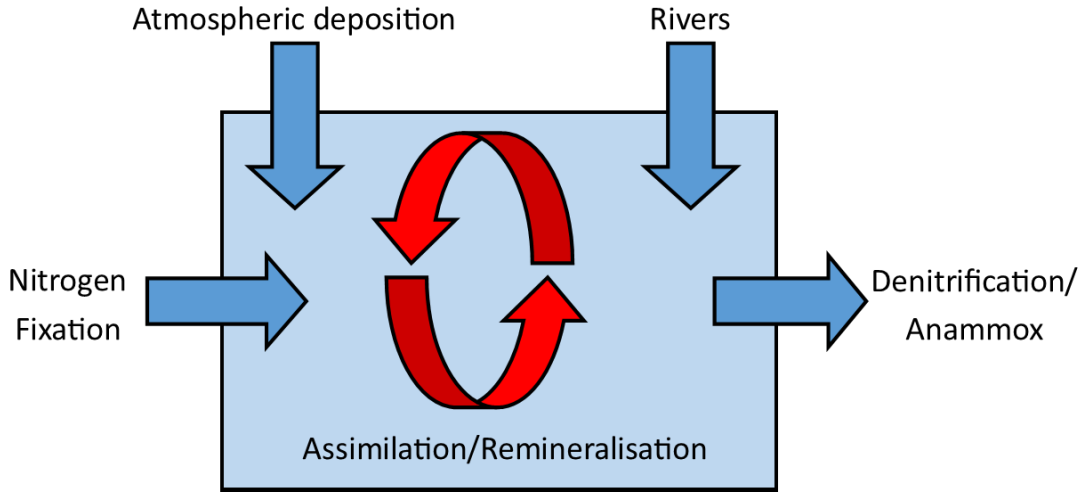

Figure 1.2. A schematic of the marine nitrogen cycle, highlighting the sources, sinks and cycling of nitrogen within the global ocean.

1.2.1 Inputs and Outputs (nitrogen fixation, atmospheric deposition, rivers and denitrification)

Nitrogen fixation and denitrification are the main source and sink pathways of nitrogen in the global ocean. If the losses of nitrogen were not balanced by inputs then the ocean would quickly lose nitrogen, which has consequences for productivity as nitrogen is the most important nutrient controlling phytoplankton growth in the surface ocean (Antia et al. 1991). Estimates of water column and benthic denitrification fall into a range of 190 – 550 Tg a^{-1}, with a total 550 $x10^3$ Tg which puts the residence time of fixed nitrogen somewhere between 1000 and 3000 years. This implies that there is a similar rate of nitrogen fixation occurring to balance the ocean nitrogen budget. Current estimates of nitrogen fixation are between 51 and 110 Tg a^{-1}, meaning that either denitrification has been overestimated or nitrogen fixation has been underestimated (Luo et al. 2014). Evidence that the nitrogen budget is close to being in balance is that the ratio of N:P is relatively constant at 16:1, and given that the residence time of P is an order of magnitude greater than N there must be a tight coupling of N addition and loss to maintain this ratio (Gruber and Sarmiento 1997).

Nitrogen fixation, the conversion of nitrogen gas into ammonium is the primary input of fixed nitrogen into the global ocean. Dissolved nitrogen gas as N_2 is the most abundant form of nitrogen within the oceans, but nitrogen is generally unavailable for marine organisms meaning nitrogen fixation is a particularly important process. Diazatrophs are bacteria (or archaea) that fix atmospheric nitrogen into ammonium. One of the most ubiquitous diazotrophs is the marine cyanobacterium *Trichodesmeum* which was first identified as a diazotroph in 1961 (Capone et al. 1997). Since then *Trichodesmeum* is known to be cosmopolitan across the tropical oligotrophic oceans and until recently was thought to account for the bulk of nitrogen fixation in the ocean. Only in recent years have other groups of diazotrophs such as *Crocosphaera watsonnii, Nodularia* spp., *Anabaena* spp., and *Richelia intracellularis* been recognized as important (Sohm et al. 2011).

Numerous factors limit nitrogen fixation within the ocean including light, temperature, nutrients and trace metals (Carpenter et al. 1997; Karl et al. 2002). *Trichodesmium* spp. and other planktonic cyanobacteria were thought to be limited to the 20°C isotherm, meaning that they are limited to the tropical and subtropical regions. The Baltic Sea also experiences summer time diazotroph blooms when the surface waters are particularly warm and there is strong water column stability (Wasmund et al. 1998; Finni et al. 2001). Recently there has been increasing evidence of water column marine diazotrophy in high latitude regions where temperatures are much lower, including Arctic nitrogen fixation on the ice free Alaskan coast of up to 3.5–17.2 nmol N L^{-1} d^{-1} (Sipler et al. 2017). Nitrogenase activity within autotrophic diazotrophs is also correlated with light, as it is a photosynthetic process (Gallon 2001). *Trichodesmium* fixes nitrogen in the upper layer of euphotic waters and exclusively during the daytime periods, with maximum rates of N_2 fixation around midday when light is the strongest (Capone et al. 1990). Two of the most common controls on nitrogen fixers are iron and phosphorus. Areas of excess nitrate relative to phosphate using Redfield ratios (expressed as a positive N* value, calculated as nitrate – 16 x phosphate; (Gruber and Sarmiento 1997)) have been found in regions of high aeolian dust deposits from the deserts of the world (Jickells et al. 2005). Nitrogen fixers require up to 10 times more iron than non-nitrogen fixing phytoplankton (Kustka et al. 2003).

Phosphorus has also been highlighted as a potential limiting nutrient for nitrogen fixers. (Wu et al. 2000) reported that the sub-tropical North Atlantic was more phosphorus depleted than the sub-tropical North Pacific, this suggests more iron reaches the North Atlantic from the Sahara, which increases nitrogen fixation and leads to the draw-down of all available phosphorus. *Trichodesmium* also has the ability to produce the enzyme alkaline phosphatase (AP), which enables them to remove phosphate from dissolved organic phosphorus compounds. Much higher rates of AP activity have been found in the Atlantic, where P concentrations are extremely low compared to the Pacific, supporting the hypothesis that P is a limiting nutrient for nitrogen fixers in high iron regions (Mulholland et al. 2002; Mahaffey et al. 2014).

Atmospheric deposition is another source of fixed nitrogen to the ocean, which deposits dissolved and particulate nitrogen. Rainwater may include dissolved inorganic nitrogen such as nitrate, nitrite and ammonium, along with dissolved organic nitrogen (DON). Gaseous nitrogen inputs to the ocean include ammonia, nitric acid and other nitrogen compounds. Particulate nitrogen is added through dust or organic debris, which can be included in rainfall. Atmospheric deposition is particularly important within coastal regions, and can make up a significant proportion of the nitrogen input (Jickells et al. 2017). Anthropogenic sources of fixed nitrogen can also be important to take into account and globally account for 70% of the nitrous oxide and 65% of ammonium deposition (Galloway et al. 2004). Anthropogenic inputs from atmospheric deposition are estimated to have increased overall ocean carbon sequestration by approximately 0.4%, equivalent to 0.15 Pg C Y^{-1} (Jickells et al. 2017).

Rivers provide an important pathway for nitrogen into the coastal shelf seas, supplying between 36 and 66 Tg total nitrogen per year to the coastal zone (Beusen et al. 2016). Human activities associated with food production have drastically altered the riverine inputs from the continents into the coastal ocean zones (Boyer et al. 2006). More than half of the current input of nitrogen to the ocean is associated with anthropogenic activity (Yan et al. 2010) and this means that in the last 50 years the inputs from rivers and coastal atmospheric deposition have doubled. Previous estimates of the nitrogen from rivers reaching the open ocean was low, however

recent estimates predict that a total of 17 Tg of DIN reaches the open ocean (Sharples et al. 2017).

Denitrification is the primary loss process for fixed N in the ocean, with denitrifying bacteria converting nitrate into nitrogen gas using nitrogen as a terminal electron acceptor in respiration. In the oceans denitrification occurs when dissolved oxygen concentrations are lower than 5 µM (low oxygen regions (Cohen and Gordon 1978). There are three main regions of the global ocean where water column denitrification occurs, the eastern tropical North Pacific, the eastern tropical South Pacific and the northern Arabian Sea (Codispoti et al. 2001). Sub-oxic regions are also found in marine sediments across the world. However, the majority of benthic denitrification occurs across the continental shelves and shelf slopes where there is a much greater input of organic material to the sediments. Up to 44 % of the total N-removed globally is in shelf sea sediments (Seitzinger et al. 2006). Sub-oxic and anoxic regions have also been artificially created in shelf regions as a result of anthropogenic nutrient loading, which stimulates primary production. This is a problem in many coastal regions including the shelf seas surrounding the Mississippi delta (Rabalais and Turner 2006; Rabalais et al. 2010), Chesapeake Bay (Li et al. 2016), the Danish coastal ecosystems (Riemann et al. 2016), and the Baltic Sea (Huttunen et al. 2015).

Anammox is an abbreviation of **an**aerobic **amm**onioum **ox**idation and is an important process converting ammonium and nitrite into nitrogen gas. Anammox bacteria are chemoautotrophs and have only recently been discovered 25 years ago, although the reaction was postulated before their discovery (Kuenen 2008). They are a major sink for fixed nitrogen within the oceans and have been estimated to produce between 30-50% of the nitrogen gas within the oceans (Dalsgaard et al. 2005).

1.2.2 Internal cycling (assimilation and remineralisation)

Biological production converts inorganic nutrients and carbon into organic matter. Photosynthetic phytoplankton take up fixed nitrogen, predominantly as nitrate (but can include other forms e.g. ammonium and urea), in the surface ocean converting it into organic nitrogen, which depletes fixed nitrogen in the surface ocean. Sources of organic nitrogen include direct release from phytoplankton, bacteria, macroalgae, zooplankton, fecal pellets, ‘sloppy feeding’ by zooplankton and

larger organisms (Sterner 1990; Tupas and Koike 1990; Saba et al. 2011). Some of this particulate organic matter is broken down into dissolved organic nitrogen (DON), whilst some sinks as particulate organic nitrogen (PON). A proportion of this particulate organic nitrogen can be remineralised back into inorganic fixed N, either in the surface waters or at depth. The process of remineralisation (conversion of organic N back into its inorganic forms) occurs in three steps:

1. The breakdown of organic nitrogen into ammonium (degradation or ammonification)
2. The bacterial conversion process of ammonium into nitrite (ammonium oxidation)
3. The bacterial conversion of nitrite into nitrate (nitrite oxidation)

The DON pool has become increasingly recognized as an important component of the ocean nitrogen cycle, having a role in primary production. The DON pool is the largest pool of nitrogen within the global ocean, with the exception of dissolved nitrogen gas. Historically, the majority of the DON pool was thought to be composed of refractory compounds, unavailable as sources of nitrogen for phytoplankton and bacteria. However, since the 1980s studies have found that there are high turnover and flux rates for pools of more labile DON. In coastal waters DON turnover rates are rapid; the turnover rate in the coastal waters of Southern California for total DON and labile DON were 21 and 17 days, respectively. This was up to 14 times more rapid than the Central North Pacific Gyre (Jackson and Williams 1985). The DON flux into and out of DON pools is better understood, with phytoplankton now known to release DON (Diaz and Raimbault 2000), and elevated DON concentrations also being associated with *Trichodesmium* blooms (Capone et al. 1994). Sinks for DON include algae, cyanobacteria, bacteria, and archaebacterial that can either exploit the DON pool directly or after degradation (Antia et al. 1991; Berman 2001; Bronk 2002; Bronk et al. 2007).

1.3 The shelf sea nitrogen cycle

The nitrogen cycle within shelf sea environments is the same as the overall ocean nitrogen cycle, however the balance of certain components such as river input, local regeneration and sedimentary denitrification may be more important. The relative magnitude of these inputs and outputs for shelf seas are outlined in Figure 1.3.

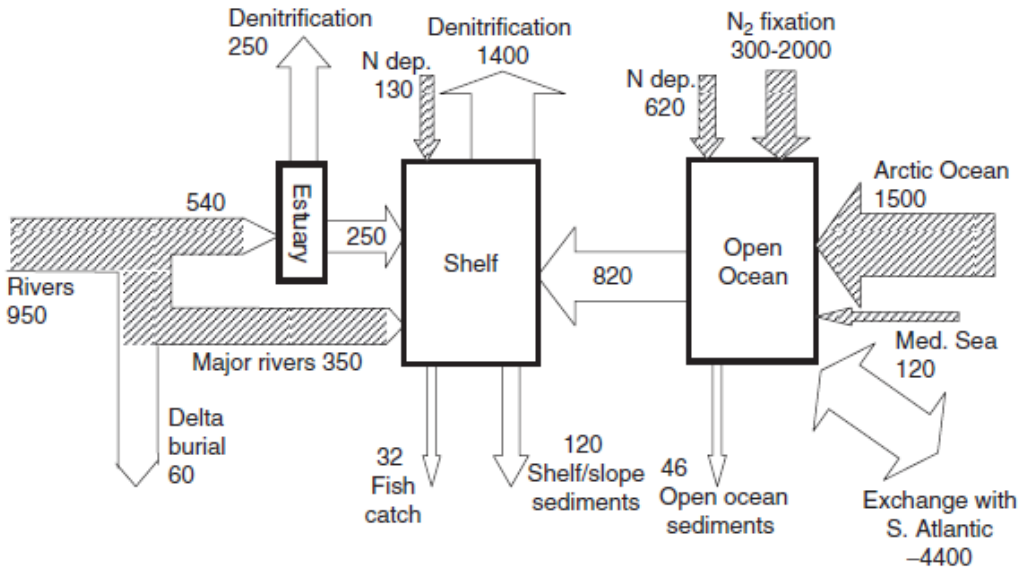

Figure 1.3. The nitrogen budget for the North Atlantic, showing the major N fluxes ($x10^9$ mol year $^{-1}$) taken from (Gruber 2004).

Nitrogen supply to shelf seas comes from three major sources, the open ocean riverine and atmospheric input (Figure 1.3). In the North Atlantic over 50 % of the nitrogen supply to the shelf is from the open ocean with the remainder from rivers and atmospheric deposition. There is potential for inner shelf regions to be isolated from the deep ocean, and so these regions may rely on increased *in situ* regenerated nutrients. Coastal regions are highly influenced by river run off, including agricultural run-off. Although previously thought to be limited to the tropics evidence of nitrogen fixation as a source of nitrogen has been observed in the North Atlantic, with nitrogen fixation measured in the English Channel (Rees et al. 2009a).

Local remineralisation of organic matter to nitrate is important for sustaining primary productivity in some shelf regions during periods of the year. This occurs as a result of constrained exchange of water with the shelf edge and the possibility of shelf areas being isolated from the deep ocean supply of nitrogen. This directly influences not only on the nitrogen cycle, but also the ability of shelf seas to act as a sink for carbon depending on where the recycling takes place either in the surface waters, deep waters or sediments (Simpson and Sharples 2012). If organic matter is exported off shelf and reaches waters below the winter thermocline in the open ocean, then it has effectively been removed from atmospheric contact over a multi-decadal timescale.

Denitrification in the sediments can also be important in shelf seas due to the larger amount of organic matter reaching the seabed compared to the open ocean. Over half of the total sedimentary denitrification takes place on continental shelves although rates are highly variable (Seitzinger and Giblin 1996). The turbulent environment within shelf seas can cause resuspension and oxygenation of the sediments potentially reducing denitrification (Seitzinger et al. 2006)

1.4 The shelf sea carbon cycle

The ocean sequesters fifty times more carbon than the atmosphere and plays a large role in the control of the planet's climate. The marine carbon cycle is intricately linked to the marine nitrogen cycle. Shelf seas are thought to be extremely important in the global carbon cycle acting as a global carbon sink due to their high productivity and potential for carbon export, being responsible for the uptake of approximately 20 % of the total uptake of anthropogenic carbon dioxide by the oceans (Thomas et al. 2004). The role of shelf seas has been described as a continental shelf pump (Tsunogai et al. 1999), where carbon is exported from the shelf sea surface waters to the deep ocean in either particulate or dissolved forms.

Bacterial remineralisation of organic matter releases both inorganic nitrogen and dissolved inorganic carbon (DIC). The export of carbon will depend on where remineralisation takes place. If remineralisation takes place in the euphotic zone, then the recycled carbon can be utilised by phytoplankton or transferred back to the atmosphere and there will be no net flux of carbon into the ocean from the atmosphere. However, if organic matter sinks below the seasonal thermocline before it remineralised then DIC can be exported off shelf. Additional carbon can then equilibrate from the atmosphere and be fixed by phytoplankton providing there is a source of N, meaning there is a net flux of atmospheric carbon dioxide into the surface waters (and potentially export off shelf).

Phytoplankton production sustained by nitrate along with nitrogen fixation is termed new production (Dugdale and Goering 1967). However, on a global scale nitrification in surface waters can account for half of the nitrate consumed in surface waters making it difficult to quantify 'new' production and carbon export (Yool et al. 2007). Due to the dynamic and seasonal nature of shelf sea physics it is difficult to quantify the amount of carbon exported. This is because carbon that is sinking below

the surface mixed layer, may be exported for a short time period (months) until it is resupplied to the surface waters and utilised by phytoplankton. Export by definition requires particulate organic matter to be transported off shelf.

1.5 Physical processes

The processes transporting nutrients from the open ocean onto the shelf are important for cycling of carbon and nutrient in shelf seas (Wollast 1993; Liu et al. 2000). Numerous observational studies have highlighted the importance of ocean-shelf exchange in regard to carbon export, these include: the Middle Atlantic Bight, the US Western Shelf and the European Shelves including the NERC funded FASTNEt programme focussed on the Celtic Sea, Malin shelf, and North Scotland Shelf (Biscaye et al. 1994; Jahnke et al. 2008; Huthnance et al. 2009; Porter et al. 2016).

The topography of the shelf edge prevents large scale geostrophic flow from crossing the shelf slope. Typical depths along the North West European range from 100 to 150 m on shelf. The continental shelf slope is steep from Portugal to north-west Scotland. This shelf region is subject to forcing by numerous processes including the slope current (the adjacent ocean density layer), winds and tides. The off shelf North Atlantic warm water (NAW) flows northwards past Ireland towards Norway sitting at around 500 m on the slope (Huthnance 1986). Mediterranean waters flow northwards at depths between 500-1500 m in a layer of higher salinity. A bottom Ekman layer lies beneath the slope current where friction reduces the slope current to zero. In this Ekman layer off shelf transport in the order of 1 Sv/(1000 km) has been observed (Huthnance 1995) (Figure 1.4). This forms the hypothesis for the ‘Ekman drain’ for the off shelf flux of waters, where downslope Ekman transport at the base of the slope current allows export of water and suspended material from the shelf. In combination with this Ekman drain, the uneven shape and depth of the shelf edge, cross-shelf flow, meanders and eddies can all transport nutrients across the shelf edge (Trowbridge and Lentz 1998).

Wind forcing moves water across the shelf edge, with strong winds associated with depressions driving storm surges and waves causing up- and downwelling events. Summer upwelling is caused by northerly trade winds and can cause

upwelling with on and off shelf fluxes, although this is constrained to southern areas such as Iberia. Internal tides are also generated across the shelf edge in many regions by tidal flow across the steep slopes. Cold, dense water formed in the winter due to the cooling of the relatively shallow shelf can also cascade down the slope due to gravity. Cascading fluxes have been estimated to be between 0.5 m^2 s^{-1} and are significant where they occur intermittently (Shapiro et al. 2003).

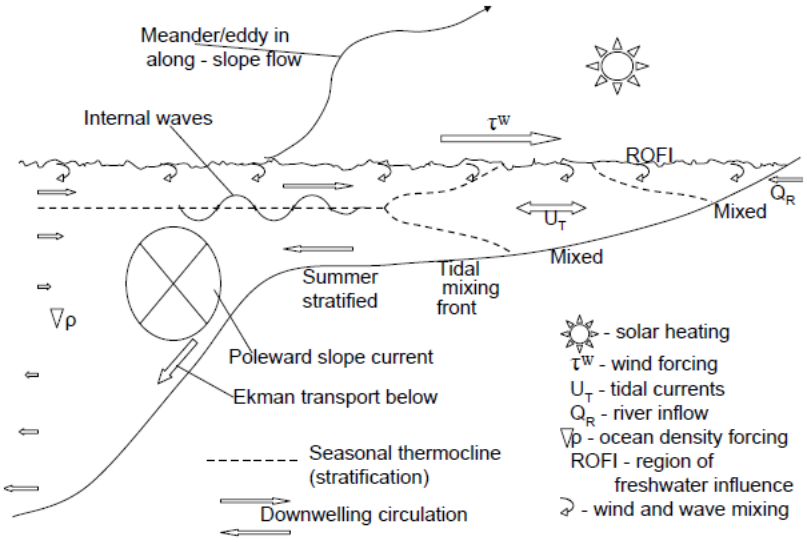

Figure 1.4. A schematic of shelf edge exchange processes and stratification. Taken from Huthnance et al., (2009)

Seasonal stratification caused by summer heating and winter cooling of the water column occurs in most areas across the shelf, with the exception of those closest to the coast, which are influenced by freshwater and increased mixing events due to the shallow water column. In these stratified areas, organic matter has the potential to sink below the seasonal thermocline and be exported off shelf below the permanent thermocline. In the Celtic Sea, enhanced mixing caused by internal tides results in a nitrate flux that drives a subsurface chlorophyll maximum supporting production that is independent of the spring bloom and cooler water brought to the surface are exposed to wind mixing (Sharples et al. 2009). The on shelf wind forced flow in the Celtic Sea flows eastwards through the English Channel and northwards through the Irish Sea. Overall, the processes in the Celtic Sea suggest large ocean-

shelf exchanges (3 m^2 s^{-1}), exceeding the exchange estimates in other parts of the NW European shelf (Huthnance et al. 2009).

1.6 Nitrogen and oxygen stable isotopes in marine biogeochemistry

Nitrogen has two stable isotopes ^{14}N and ^{15}N with atomic masses of 14 and 15, respectively. ^{14}N is the more abundant of the two comprising of 99.67 % of the nitrogen found in nature. Nitrogen gas is the nitrogen isotope reference with mass of 28, 29 or 30 for nitrogen. Oxygen has 3 stable isotopes ^{16}O, ^{17}O, and ^{18}O with atomic masses of 16, 17, and 18 respectively. ^{16}O is the most abundant comprising of 99.8 % of the oxygen found in nature. O in the VSMOW (Vienna Standard Mean Ocean Water) is the O isotopic reference. Physical, chemical, and biological processes discriminate between isotopes of particular elements and this is referred to as isotopic fractionation. This leads to measurable differences in the ratio of heavy and light isotopes of elements such as ^{15}N to ^{14}N among the different forms of nitrogen, and differences in the ^{16}O and ^{18}O in oxygen. The small deviations between the heavy and light isotopes are reported using delta notation:

$$\delta^{15}N\ (‰) = \left(\frac{\left(^{15}N/^{14}N\right)_{sample}}{\left(^{15}N/^{14}N\right)_{standard}} - 1\right) \text{ x } 1000 \qquad \text{Eqn 1.1}$$

Enzymatic (kinetic) isotope fractionation arises from small differences in the rates of reactions containing heavy and light isotopes. If a reaction rate can be characterized by a first order dependence on substrate concentration then the fractionation factor, α, can be defined as $^{1}k/^{h}k$, where ^{1}k is the first order rate constant for the reaction of the light isotope containing molecule and ^{h}k is the first order rate constant for the reaction of the heavy isotope containing molecule. The fractionation factor can be expressed in a per mil notation as an isotope effect, ε, defined as (α-1) x1000. For example, using nitrogen:

$$\varepsilon\ (‰) = (^{14}k/^{15}k\text{-}1) \text{ x } 1000 \qquad \text{Eqn. 1.2}$$

where ^{14}k and ^{15}K are the rate constants for light ^{14}N and heavy ^{15}N isotopes, respectively

This isotopic fractionation results in predictable differences between the isotope ratio of the substrate and the product of a reaction. Usually the products of an enzymatic reaction are depleted in heavy isotopes due to preferential reaction of the light isotope containing molecules.

For example, the preferential reaction of ^{14}N and ^{16}O during assimilation of nitrate by phytoplankton leads to progressive enrichment in euphotic zone nitrate as it is consumed (Casciotti et al. 2002). However, this can be reversed for example, such as when ^{15}N and ^{18}O containing NO_2^- is preferentially oxidised to NO_3^-, leaving residual NO_2^- progressively depleted in ^{15}N and ^{18}O (Granger et al. 2004).

When studying stable isotopes, two different idealised models are used to interpret stable isotope data; the Rayleigh Model and the Steady State Model. Here, the models are described using nitrogen isotopes. These models describe the isotopic composition of a reactant pool, using the degree of consumption of the reactant N pool, the $\delta^{15}N$ of the initial reactant N pool, and the kinetic isotope effect (ε). If the transformation proceeds at a constant rate and there is no resupply to the N pool then it can be described using Rayleigh fractionation kinetics (or a 'closed system'):

$$\delta^{15}N_{reactant} = \delta^{15}N_{initial} - \varepsilon \, (\ln (f)) \qquad \text{Eqn. 1.3}$$

$$\delta^{15}N_{instantaneous} = \delta^{15}N_{reactant} - \varepsilon \qquad \text{Eqn. 1.4}$$

$$\delta^{15}N_{integrated} = \delta^{15}N_{initial} + \varepsilon \, (f / (1 - f)) \ln (f) \qquad \text{Eqn. 1.5}$$

Where (f) is the fraction of the reactant N pool remaining, $\delta^{15}N_{initial}$ is the $\delta^{15}N$ of the initial N pool, and ε is the kinetic isotope effect. The alternative to the Rayleigh Model is the Steady State Model. In this model reactant N is continually supplied and partially consumed, with residual N being exported at a steady rate so that the gross supply of reactant N equals the sum of the product N and the residual reactant N exported:

$$\delta^{15}N_{reactant} = \delta^{15}N_{initial} + \varepsilon \, (1 - f) \qquad \text{Eqn. 1.6}$$

$$\delta^{15}N_{product} = \delta^{15}N_{initial} - \varepsilon \, (f) \qquad \text{Eqn 1.7}$$

The steady state model is used to quantify uptake processes where supply and uptake are occurring simultaneously, such as consumption of nitrate by denitrification. Both the Rayleigh and Steady State models are demonstrated in Figure 1.5.

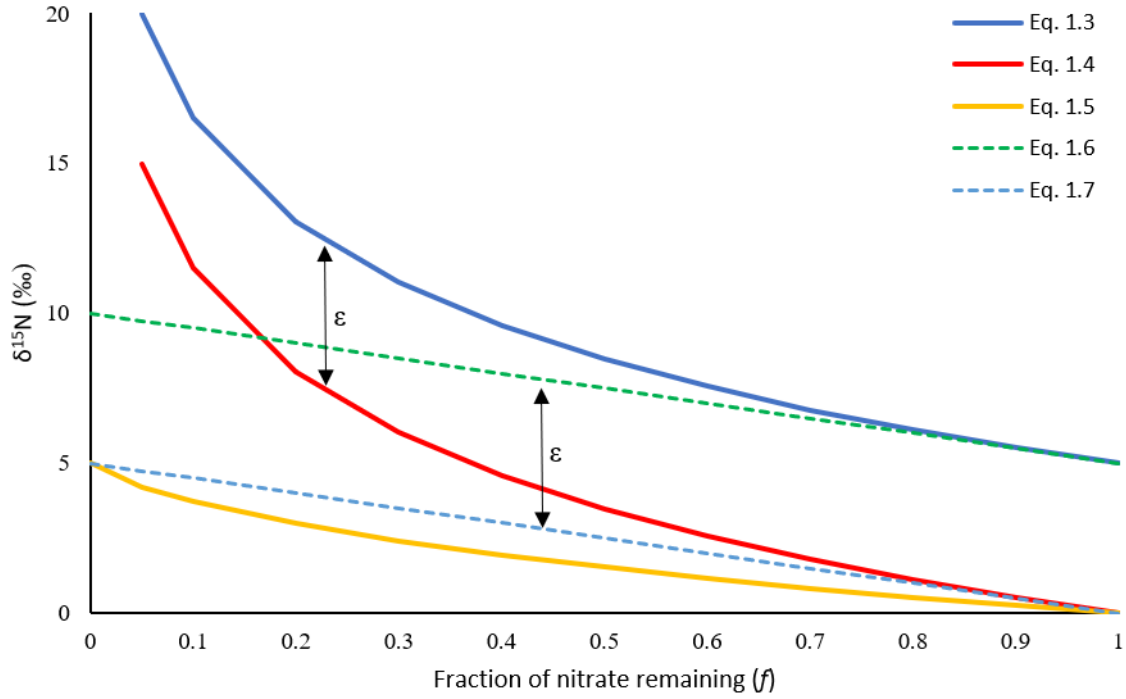

Figure 1.5. The isotopic fractionation of reactant and product N following both the Rayleigh (solid lines) and steady state (dashed lines) systems. The fractionation factor (ε) is 5‰ and the $\delta^{15}N$ of the initial reactant supply is also 5‰ for both Rayleigh and Steady State models. ε is equal to the difference between the reactant N and its product.

The isotopic fractionation models as described can be used as biogeochemical tracers to investigtate spatially and temporally complex biogeochemical processes in the ocean.

1.7 $\delta^{15}N_{NO3}$, $\delta^{18}O_{NO3}$ and $\delta^{15}N_{PON}$ in ocean and shelf sea biogeochemistry

As previously discussed, nitrogen is a key component of marine ecosystems and one of the key elements required by marine phytoplankton. The primary source of fixed nitrogen to the ocean is by marine nitrogen fixation and the primary loss of fixed nitrogen is through marine denitrification either in the water column or in sediments. The stable nitrogen and oxygen isotopes of nitrate, and the stable nitrogen

isotopes of particulate matter are useful in studying both the input, output and internal cycling of nitrogen within the marine realm and understanding the overlapping processes (Figure 1.6). Each pool has a different $\delta^{15}N$ value and each process has a different fractionation factor (ε), with different processes affecting the nitrogen and oxygen isotopes differently.

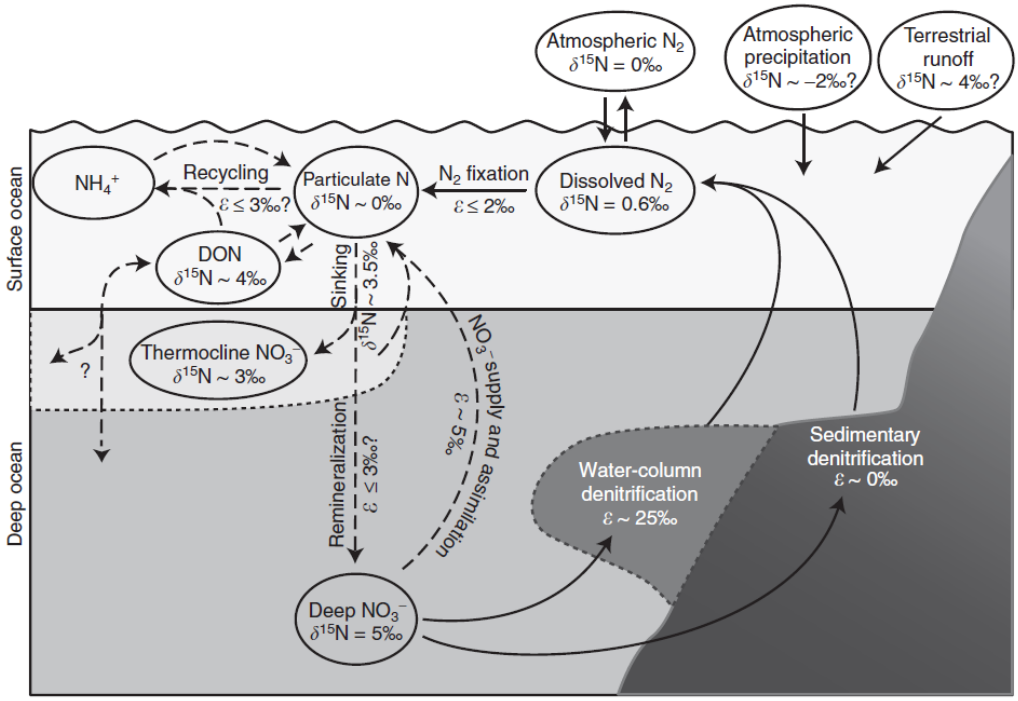

Figure 1.6. Processes that affect nitrogen isotopes in the ocean. Solid arrows indicate inputs and outputs while dashed arrows indicate internal cycling. Adapted from Sigman *et al*., (2009).

1.7.1 Inputs and Outputs

The mean deep ocean $\delta^{15}N_{NO3}$ and $\delta^{18}O_{NO3}$ are 5 ‰ and 2 ‰ respectively. Deep ocean nitrate $\delta^{15}N_{NO3}$ and $\delta^{18}O_{NO3}$ can be thought of as a balance between the inputs and outputs of N to the ocean, balancing nitrogen fixation and denitrification (Sigman et al. 2009a). In shelf seas the supply of nutrients is constrained by the topography at the shelf edge so this deep ocean supply of nitrate can be thought of as an input to shelf seas (Simpson and Sharples 2012), supplying new nitrogen with a $\delta^{15}N_{NO3}$ and $\delta^{18}O_{NO3}$ of 5 ‰ and 2 ‰ respectively (Sigman et al. 2000).

The primary input of fixed nitrogen into the global ocean is by nitrogen fixation. Field studies that collected *Trichodesmium* have yielded $\delta^{15}N$ values between -2 ‰ and +0.5 ‰ (Sigman et al. 2009a). Nitrate and particulate nitrogen (PN) derived from nitrogen fixation have values close to 0 ‰ as there is no fractionation during nitrogen uptake (Carpenter et al. 1997)(Figure 1.7). These surface water inputs add newly nitrified nitrate that is relatively depeleted in ^{15}N when compared to the average subsurface nitrate, which is influenced by denitrification that consumes nitrate within the water column with an isotopic effect of approximately 25 ‰. Therefore in regions of strong nitrogen fixation the $\delta^{15}N_{NO3}$ will decrease with increased nitrogen fixation (Carpenter et al. 1997; Mahaffey et al. 2003). Although nitrogen fixers were thought to be generally limited to within 30° to 40° of the equator and unlikely to influence the surface nitrogen isotopes in the North West European shelf seas, more recent work has identified nitrogen fixation in more northerly latitudes including the English Channel (Rees et al. 2009a), so it has the potential to introduce light $^{15}N_{NO3}$.

Terrestial run off can be particularly important in coastal and shelf regions (Figure 1.6). The isotopic composition of nitrate from rivers are poorly constrained. However, pure river run off from pristine systems ranges between 0 ‰ and 5 ‰ (Xue et al. 2009). However anthropgenic loading of nutrients in estuaries can cause low oxygen concentrations leading to denitrification, which can drastically alter the isotopic compostion.

Denitrification is the main N loss process from the the global ocean. Water column denitrification has an isotope effect between 20 ‰ and 30 ‰ (Altabet et al. 1999; Sigman et al. 2003; Sigman et al. 2005) leaving the $\delta^{15}N_{NO3}$ increasingly enriched as denitrification proceeds. The enrichment seen in waters associated with denitrifcation can be identified in water masses far from the site where it initially occured. Depth profiles along the North Pacific margin displayed enriched values associated with the denitrification signal from the oxygen deficient waters of the eastern tropical North Pacific (Sigman et al. 2005). Nitrate reduction is the main cause of fractionation during denitrification and the isotope effect of water column denitrification is the same for both $\delta^{15}N_{NO3}$ and $\delta^{18}O_{NO3}$ ($^{15}\varepsilon=^{18}\varepsilon$) (Karsh et al. 2012). Benthic denitrification in sediments leads to little increase in the $\delta^{15}N$ and $\delta^{18}O$ of water column nitrate as the high $\delta^{15}N_{NO3}$ within pore waters shows isotopic

discrimination at the level of the organism but any sediment/water exchange is minimised owing to complete consumption of nitrate within the pore waters (Sigman et al. 2009a).

1.7.2 Internal cycling

Nitrate consumption by phytoplankton also enriches the residual pool of nitrate by discriminating between the light and heavy isotopes (Figure 1.7). The N isotope effect associated with uptake by phytoplankton is appoximately 5 ‰ (Altabet et al. 1999). The O isotope effect associated with phytoplankton uptake is the same as N ($^{15}\varepsilon=^{18}\varepsilon$) (Casciotti et al. 2002). Again, nitrate reduction is the the cause for fractionation. As nitrate is depleted by phytoplankton the N and O isotopes become increasingly enriched at a ratio of 1:1 (Sigman et al. 2009a). Other forms of nitrogen such as ammonium, nitrite and urea are produced and usually completely consumed within the surface mixed layer and have a minmal effect on the overall oceanic N isotopes. In some areas e.g. estuaries, ammonium can accumulate and display strong increases in the $\delta^{15}N$ of the remaining ammonium pool with estimates of an isotope effect being between 6.5 ‰ and 18.5 ‰ (Casciotti 2016).

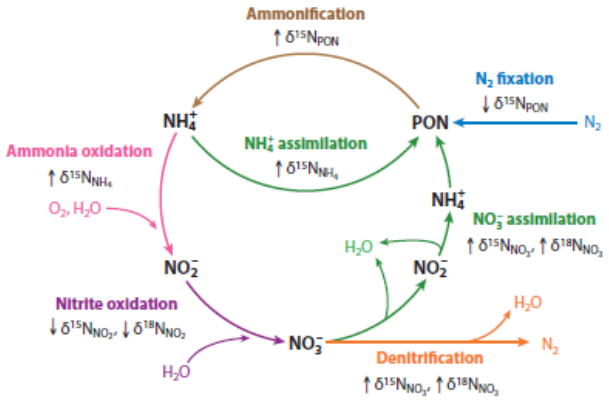

Figure 1.7. The processes and pools associated with the nitrogen and oxygen sources, sinks and cycling in the ocean. Taken from Casciotti, 2016.

Remineralisation is the cycling of organic N back into nitrate and occurs in three steps. The breakdown of organic N into ammonium and the bacterial mediated oxidation of ammonium to nitrite (ammonia oxidation) and bacterial mediated oxidation of nitrite to nitrate (nitrite oxidation; Figure 1.7). During the production of nitrate from organic matter there are different effects on the $\delta^{15}N_{NO3}$ and $\delta^{18}O_{NO3}$.

The nitrate added to the ocean via remineralisation of organic matter is sourced from the phytoplankton that have assimilated the *in situ* nutrients from the water column (or nitrogen fixers which have a $\delta^{15}N$ of approximately 1 ‰). Therefore, the remineralised nitrate will reflect these processes in the $\delta^{15}N$. In high nitrate environments this would lead to a low $\delta^{15}N$ as the lighter isotope would be preferentially used by bacteria, but in low nitrate environments the value would be higher (approximately 5 ‰) representing the integrated product.

Unlike the $\delta^{15}N$ of remineralised nitrate, the $\delta^{18}O$ is disconnected from the internal cycle and is directly obtained from the ambient seawater dissolved O_2. This effectively 'resets' the $\delta^{18}O_{NO3}$ with the signature of new nitrate, at approximately 1.1 ‰ above the *in situ* $\delta^{18}O$ of ambient seawater (Sigman et al. 2009a). The specific $\delta^{18}O$ value of 1.1 % above ambient seawater was estimated from $\delta^{18}O_{NO3}$ in the eastern Mediterranean where subsurface nitrate originates exclusively from in-situ remineralisation (Sigman et al. 2009a). Apart from areas of extremely high evaporation such as the Red Sea where the $\delta^{18}O$ of ambient seawater ($\delta^{18}O_{H2O}$) can be as high as 2 ‰ (Bigg and Rohling 2000) and glacial run off where $\delta^{18}O_{H2O}$ can be as low as -20 ‰, the $\delta^{18}O_{H2O}$ in the ocean is fairly homogenous, with values between -0.4 ‰ to +0.5 ‰ (Bigg and Rohling 2000). This decoupling in isotopic signature between the $\delta^{15}N_{NO3}$ and $\delta^{18}O_{NO3}$, when analysed together, can be a powerful tool for assessing multiple N cycle processes. Coupling between $\delta^{15}N_{NO3}$ and $\delta^{18}O_{NO3}$ allows the relative magnitude of processes such as nitrate uptake by phytoplankton, which fractionates both $\delta^{15}N_{NO3}$ and $\delta^{18}O_{NO3}$ at a 1:1 ratio to be distinguished from the addition of newly fixed N (via nitrification or nitrogen fixation), which affects $\delta^{15}N_{NO3}$ and $\delta^{18}O_{NO3}$ differently.

The application of dual isotopes of $\delta^{15}N_{NO3}$ and $\delta^{18}O_{NO3}$ has been particularly useful in shelf seas as they are highly dynamic systems, where multiple N processes may be occuring simultaneously. The sensitivity of $\delta^{18}O_{NO3}$ to nitrification allows an estimate of the contribution of nitrate that has been newly nitrified on shelf to the overall shelf nitrate pool, as this new nitrate will have a lower $\delta^{18}O$ value than nitrate originating from off shelf (Granger et al. 2013). Estimates from the Bering Shelf Sea indicate that large parts of the inner shelf are fueled by nitrate remineralised in-situ, with estimates indicating that between 20-100 % of nitrate in winter water is derived

from regeneration rather than seasonal entrainment of slope waters (Granger et al. 2011; Granger et al. 2013).

The application of $\delta^{15}N_{NO3}$ and $\delta^{18}O_{NO3}$ led to the development of Δ(15-18) parameter, defined as $\delta^{15}N_{NO3}$ - $\delta^{18}O_{NO3}$; (Rafter et al. 2013). This derived parameter has been used in dual isotope studies to investigate the sources of remineralised nitrate. Deviations away from a 1:1 relationship cause a shift in the Δ(15-18) and give information on how the nitrate was formed. Low Δ(15-18) values indicate the addition of low ^{15}N, which would occur in places where there was remineralisation of newly fixed organic matter, while high values would indicate regeneration in regions of deplete nitrate (Figure 1.8).

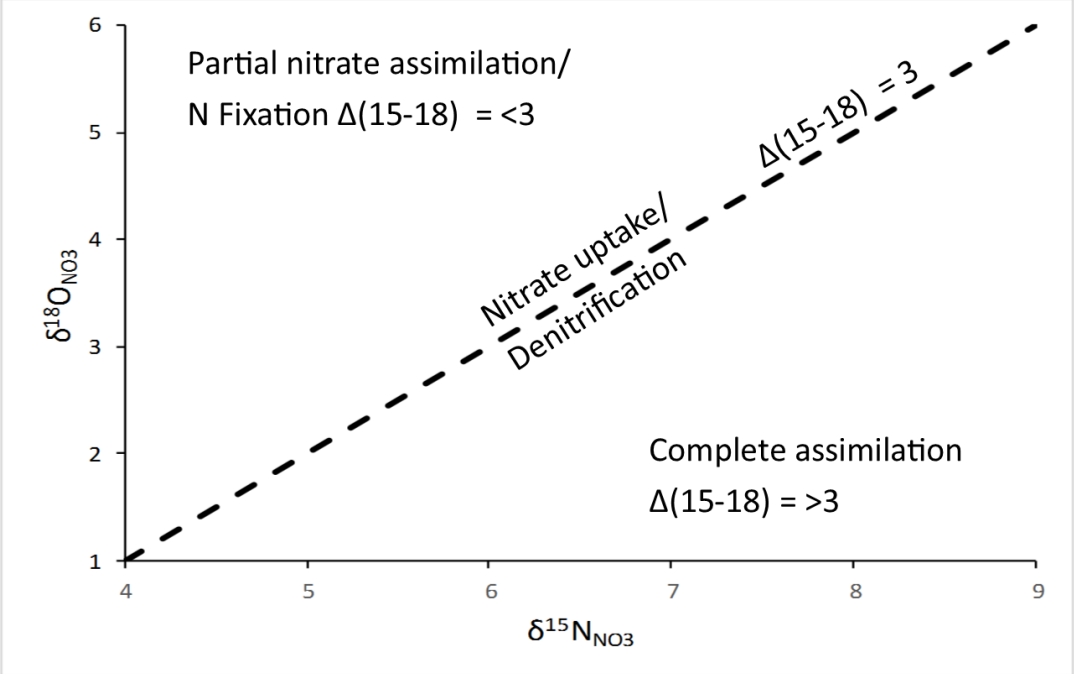

Figure 1.8. Nitrate regeneration systematics showing regeneration above and below the 1:1 ratio

1.7.3 The $\delta^{15}N$ of particulate organic matter

The $\delta^{15}N$ of particulate organic matter can also provide useful insights into the links between fixed N and organic matter, and the links between the surface, deep

ocean and sediments. The $\delta^{15}N$ of suspended particles are generally lightest at the surface and increase with depth. This low surface value is typically lower than what would be expected if assimilation was the only process occuring. The low surface $\delta^{15}N$ has two explanations: nitrogen fixation adding low $\delta^{15}N$ to the surface waters, and N recyling from heterotrophic processes. Zooplankton release ammonium which has a lower $\delta^{15}N$ than their food source, making their solid waste and tissues higher in $\delta^{15}N$. The low $\delta^{15}N$ ammonium is consumed in the surface while the heavier partiulate matter is exported to depth. This leads to low $\delta^{15}N$ of surface particulates in regions where recycled nitrogen is important (Sigman et al. 2009a). The $\delta^{15}N$ of deep suspended particles is consistent with the hypothesis that bacteria preferentially remineralise low $\delta^{15}N_{PN}$, leaving the remaining particulates enriched. Sinking particulate matter collected in sediment traps tends to show a small decrease in $\delta^{15}N$, which is contrary to the expected pattern and currently lacks an explanation. There is however, a good correlation between sinking particulates and the $\delta^{15}N$ of surface sediments below, particularly on continental shelves where increased sinking matter is preserved in the sediments. This can provide a useful insight into historical surface isotopes. End member mixing models can also be used to estimate the contribution of nitrogen fixation and nitrate fuelling surface ocean productivity using $\delta^{15}N_{PN}$ from sediment traps (Kao et al. 2012; Böttjer et al. 2017),

1.8 Research aims

This project was conducted as part of the NERC/DEFRA Shelf Sea Biogeochemistry Programme. The overall aims of which were to:

(a) take a holistic approach to the cycling of nutrients (nitrogen, phosphorus, silicon and iron) and carbon and the controls on primary and secondary production in UK and European shelf Sea and

(b) to increase understanding of these processes and their role in wider biogeochemical cycles.

Outcomes from (a) and (b) would therefore significantly improve predictive marine biogeochemical and ecosystem models over a range of scales (see SSB Website https://www.uk-ssb.org/). Work package one, *Controls and nutrient dynamics over shelf systems (CANDYFLOSS)* aims to establish the role of the shelf sea in global

carbon and nutrient cycles. My contribution to CANDYFLOSS was to collect, analyse and interpret the $\delta^{15}N_{NO3}$, $\delta^{18}O_{NO3,}$ and $\delta^{15}N_{PN}$ from the Celtic Sea, Site L4 and the Hebrides Shelf.

Research aims for my project were:

To increase our understanding of the sources of nutrients to the NW European shelf seas and to understand how these nutrients are cycled through the use of $\delta^{15}N_{NO3}$, $\delta^{18}O_{NO3,}$ and $\delta^{15}N_{PN}$ along with supplementary data collected on the same research cruises. My overarching hypothesis was that a large proportion of the nitrate pool in shelf seas is from local regeneration with limited supply from the open ocean.

1.9 Thesis Outline

Chapter 2: Chapter 2 outlines the sample collection, field work and analytical methodology used throughout this thesis. Quality control measures and results are also included.

Chapter 3: In Chapter 3, I present $\delta^{15}N_{NO3}$ and $\delta^{18}O_{NO3}$ measurements (2014 to 2016) from the L4 station at the Western Channel Observatory. These measurements were used to investigate the onset of the spring bloom and the sources of nitrate which drive it. I investigated the hypothesis that a large proportion of the nitrate at the L4 site consumed during the spring bloom period is supplied from run-off from the River Tamar and this source can be differentiated from oceanic nitrate using $\delta^{15}N_{NO3}$ and $\delta^{18}O_{NO3}$.

Chapter 4: In Chapter 4, the nitrate supply, cycling and remineralisation across the Celtic Sea over a seasonal cycle were investigated using $\delta^{15}N_{NO3}$ and $\delta^{18}O_{NO3}$ as part of the NERC funded Shelf Sea Biogeochemistry programme. I investigated the hypothesis that a large proportion of the nitrate was regenerated *in situ* on shelf with limited exchange with the open ocean.

Chapter 5: In Chapter 5, the post autumn bloom nutrient cycling and remineralisation signal was investigated across the Hebrides shelf using $\delta^{15}N_{NO3}$ and $\delta^{18}O_{NO3}$ as part of the NERC funded Shelf Sea Biogeochemistry programme. I investigated the hypothesis that the inner shelf stations were more isolated from the

oceanic supply of nitrate with the post autumn bloom production relying on nitrate regenerated *in situ*.

Chapter 6: In Chapter 6, the $\delta^{15}N_{NO3}$ and $\delta^{18}O_{NO3}$ data presented in Chapters 3, 4 and 5 is compared to published $\delta^{15}N_{NO3}$ and $\delta^{18}O_{NO3}$ data from Shelf Sea and estuarine regions. Finally, the conclusions for each chapter are synthesised and the overarching implications of the work are discussed.

Chapter 2. Methods, Sample Collection & Fieldwork

Sample collection and fieldwork was conducted as part of the co-funded (NERC and Defra) Shelf Sea Biogeochemistry (SSB) research programme. The programme aims to increase understanding of nutrient and carbon cycling and the controls on primary and secondary production in the European and UK shelf seas. It will thereby significantly improve predictive marine biogeochemical and ecosystem models.

Even in the relatively well-studied European shelf seas, fundamental biogeochemical processes are still poorly understood. The SSB programme consisted of five work packages, with work package 1 (WP1) focusing on the Carbon and Nutrient Dynamics and Fluxes over Shelf Systems (CANDYFLOSS).

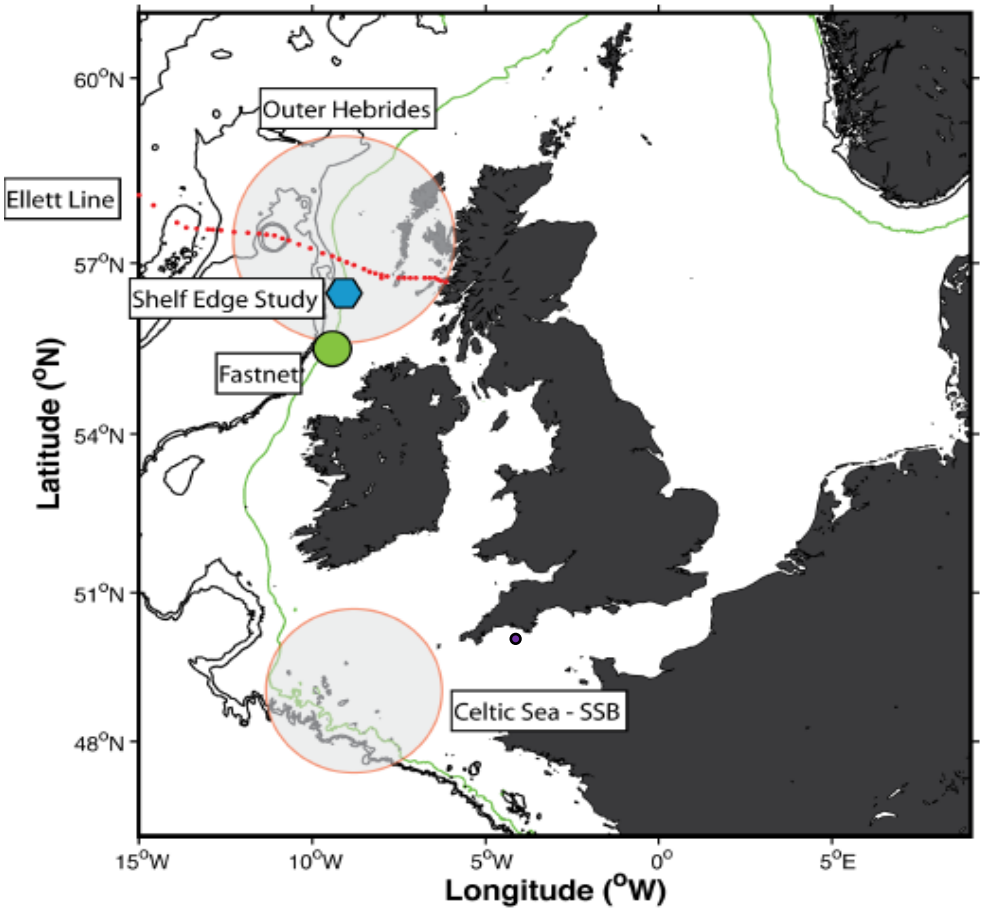

Figure 2.1. Chart showing the main working areas of the Shelf Sea Biogeochemistry programme research cruises in the Celtic Sea, previous NERC funded research activities on the western shelf, including the Extended Ellett Line (red diamonds), the Shelf Edge Study (blue hexagon), FastNet (green circle), the L4 site in purple, and the approximate working area of the Outer Hebrides process cruise. The green line represents the 200m bathymetric contour.

Stable isotopes are an important tool in unravelling the uncertainty regarding the source of nutrients, specifically nitrate to shelf seas. Using the distribution of inorganic nutrients and oxygen, the stable nitrogen isotope ($\delta^{15}N$) composition of particles and the $\delta^{15}N$ and stable oxygen ($\delta^{18}O$) isotope composition of nitrate, along with other physical, chemical and biological measurements. My goal was to quantify the relative magnitude and importance of local regeneration in sustaining an on shelf nitrate pool and use these data to infer physical transport processes. Collection and measurement of the stable isotopes of nitrate has not been conducted on this scale before across the North West European Shelf Seas and adds to our understanding of the processes which control the nitrate inventory within a temperate shelf sea.

2.1 Sample Collection

2.1.1 Process Cruises

Samples for $\delta^{15}N_{NO3}$ and $\delta^{18}O_{NO3}$, $\delta^{15}N$ of particulate matter and $\delta^{18}O$ of water were collected during process cruises to the Celtic Sea in 2014 and 2015 (Table 2.1, Figure 2.2).

Table 2.1. Process cruises undertaken during the SSB sampling campaign, detailing number of isotope samples collected, their inclusion in this thesis and who they were collected by.

Cruise	**Dates**	**$\delta^{15}N/\delta^{18}O$-Nitrate**	**$\delta^{15}N$-POM**	**$\delta^{18}O$ of H_2O**	**Data included in Thesis**	**Collected by:**
DY026	03/08/14 to 24/08/14	20	×	×	× (Method Testing)	Calum Preece
DY018	09/11/14 to 02/12/14	215	19	×	✓	Clare Davis (UoL)
DY021	01/03/15 to 26/03/15	30	18	×	✓	Nealy Carr (UoL)
DY029	01/04/15 to 30/04/15	310	63	30	✓	Calum Preece/Clare Davis (UoL)
DY033	11/07/15 to 03/08/15	94	46	×	✓	Clare Davis (UoL)

The sampling strategy included: (a) repeat visits to 3 main stations, Site A, CCS and CS2, (b) on shelf transects, O and J and (c) cross shelf edge transects as part of the SSB iron sampling programme (Figure 2.2).

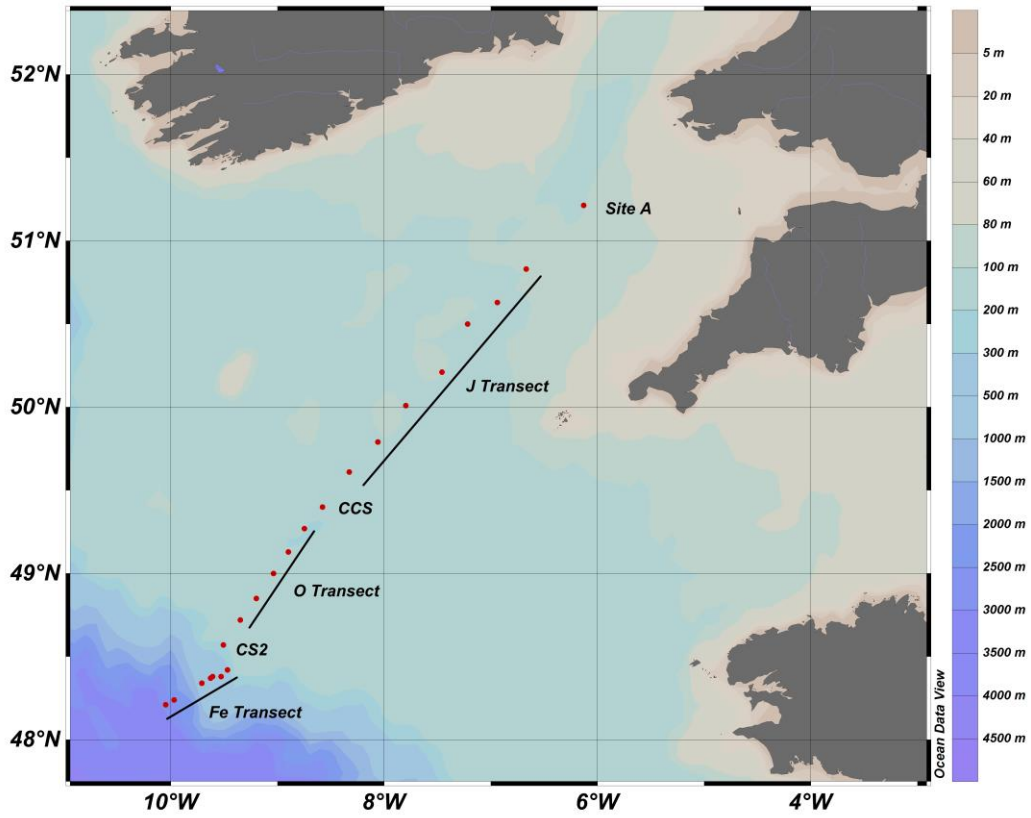

Figure 2.2. Celtic Sea process stations (CS2, CCS, and Benthic A), and transects (O, J and Fe) visited during each of the SSB process cruises during 2014 and 2015. Map generated with Ocean Data View (Schlitzer, 2002).

2.1.2 Additional Cruises

DY017 (October 20th 2014 – November 11th 2014) was an additional SSB process cruise to the Outer Hebrides. This region immediately to the west of the UK and North of Ireland is thought to be a key region for the exchange of nutrients, carbon and water between the continental shelf and North Atlantic Ocean (Painter et al. 2016). Six of the seven planned transects were completed with the seventh transect (B) abandoned due to poor weather (Figure 2.3).

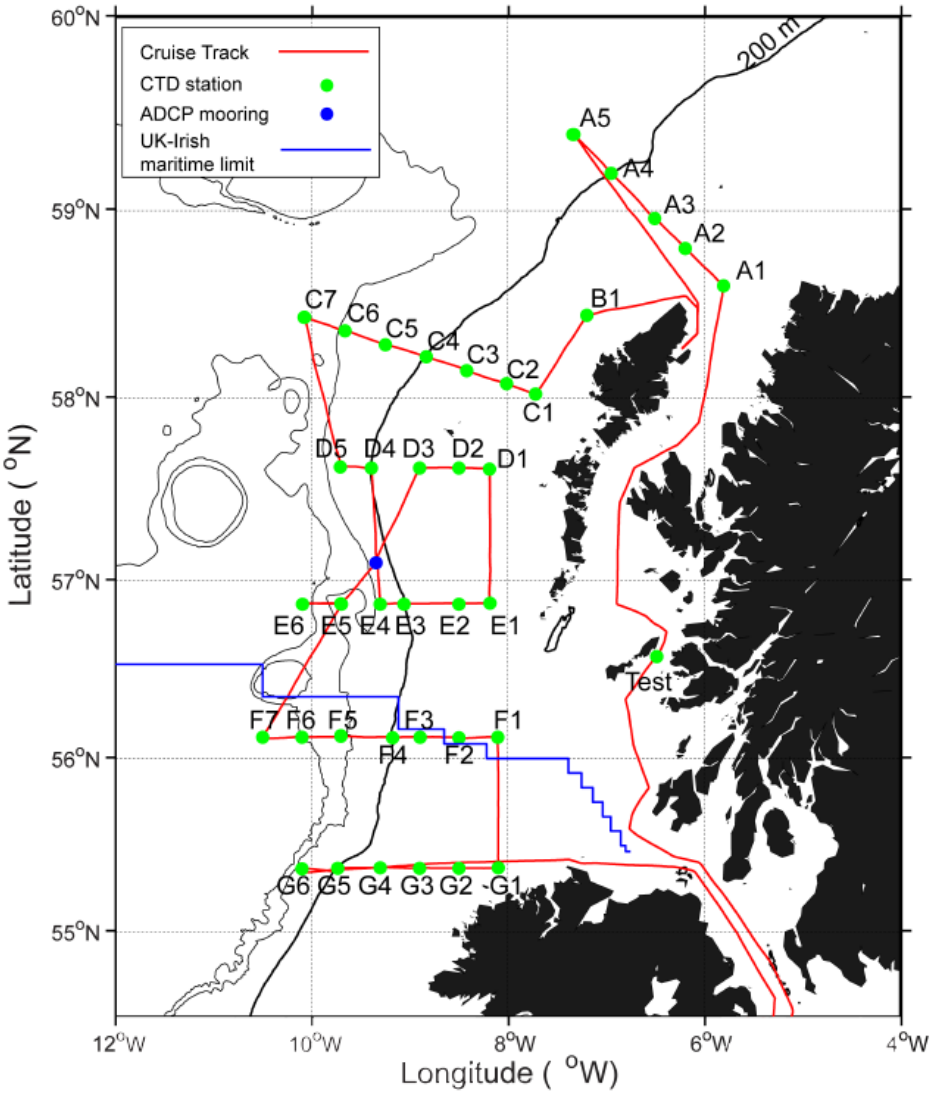

Figure 2.3. Chart showing Outer Hebrides work area with DY017 cruise track (red line), position of completed CTD stations (green dots), benthic ADCP lander location (blue dot), and the UK/Irish maritime limits (blue line). The thick black line represents the 200m bathymetric contour.

2.1.3 Western Channel Observatory Time series

Water samples for $\delta^{15}N_{NO3}$ and $\delta^{18}O_{NO3}$ analysis were also collected on a bimonthly basis from the Western Channel Observatory Long Term Buoys L4 and E1 in the English Channel spanning late 2014 - late 2016 (Figure 2.4). The Western Channel Observatory (WCO) is an oceanographic time-series and marine biodiversity reference site in the Western English Channel. *In situ* measurements were undertaken using the research vessels of the Plymouth Marine Laboratory (PML) and Marine Biological Association (MBA) by Malcolm Woodward.

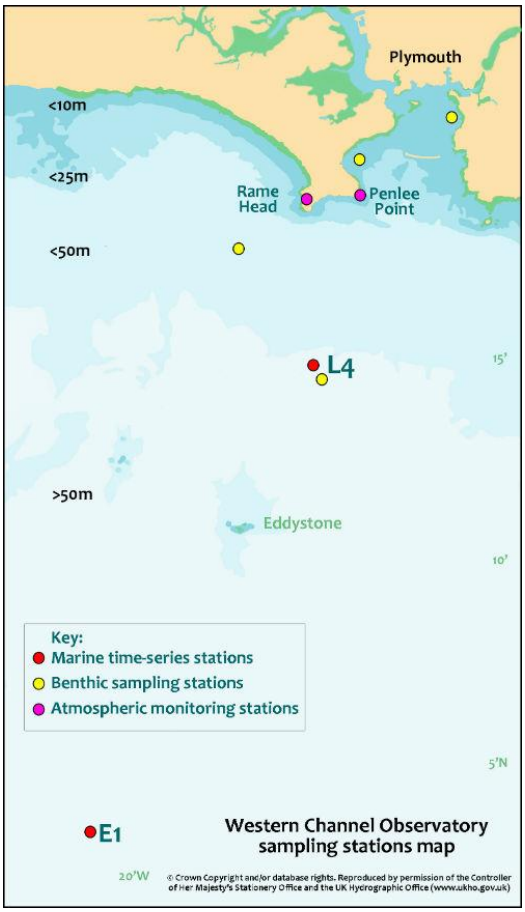

Figure 2.4. Map of the Western Channel Observatory sampling stations with water depth, including the L4 sampling site where water samples were collected for isotope analysis.

Additional information on sampling strategy and samples collected is provided in each of the relevant chapters of this thesis.

2.2 Hydrography, Oxygen, and Inorganic Nutrients

During all process cruises, hydrographical measurements were made using a Seabird 911 conductivity – temperature – depth profiler (CTD) equipped with a 24-bottle rosette of 20L Niskin bottles to collect vertical profiles of salinity, temperature, oxygen concentration and seawater samples. Dissolved oxygen concentration was from *in situ* CTD oxygen probe calibrated using Winkler titrations (Williams and Jenkinson, 1982).

Inorganic nutrients (NO_3^-, NO_2^-, PO_4^{3-}, $Si(OH)_4$, NH_4^+) were analysed onboard using standard colormetric autoanalyser techniques by Malcolm Woodward (Brewer and Riley 1965; Mantoura and Woodward 1983; Kirkwood 1989; Zhang and Chi 2002).

2.3 Stable isotope analysis

The $\delta^{15}N$ of POM and $\delta^{15}N_{NO3}$ and $\delta^{18}O_{NO3}$ were analysed at the LIFER laboratory at the University of Liverpool. Isotope ratios are reported as parts per thousand deviations from a known international standard. The isotope ratios are reported using delta notation (δ) with units per mil (‰):

$$\delta(X) = \left[\frac{R_{sample} - R_{standard}}{R_{standard}}\right].10^3[‰]$$

Where $R=^{15}N/^{14}N$, the ratio of the atom occurrence of the rare to common isotope. The reference values for $^{15}N/^{14}N$ and $^{18}O/^{16}O$ are N_2 in air and Vienna Standard Mean Ocean Water (VSMOW), respectively.

Samples were analysed using a continuous flow mass spectrometer (IRMS); atoms (or molecules) are ionised to give a charge and accelerated. The ions are then deflected by a magnetic field according to their mass to charge ratio (m/z). Lighter ions have a greater deflection, as do ions that have a higher charge. The beam of ions is then detected electrically (Figure 2.5). The continuous flow system uses helium as a carrier gas to carry the sample gas into the ion source chamber. An 'open-split' device ensures equivalent inlet conditions for both standard and sample gases.

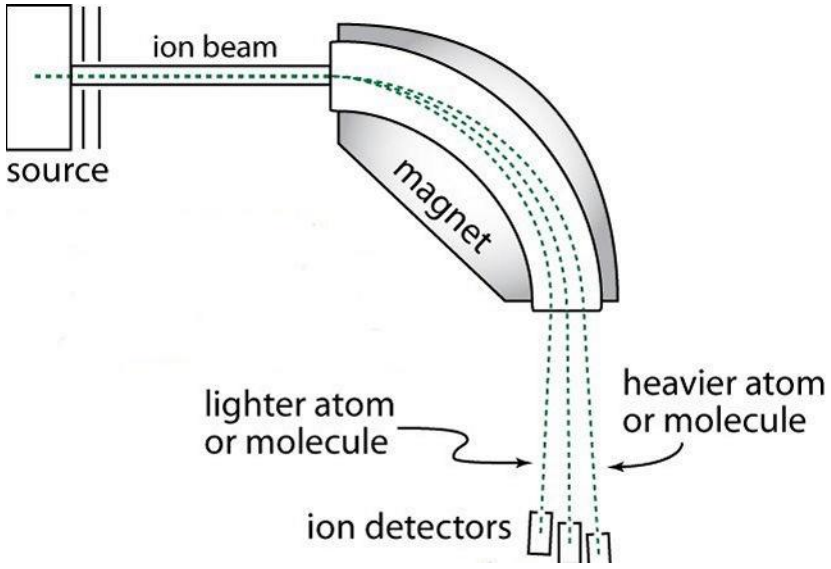

Figure 2.5. Mass spec ion beam, showing molecular masses being deflected after ionisation.

2.3.1 $\delta^{15}N$ analysis of particulate material

Analysis of particulate material was carried out at the University of Liverpool. Particulate samples were freeze dried overnight to remove moisture from the 24mm diameter filter and then half the filter was pelletized using pre-combusted tin capsules into two pellets of equal size. Samples were not decarbonated. Stable N isotope analysis was carried out using a Costech Elemental Analyser coupled with a Conflo IV interfaced with a Thermo Fisher Delta V Advantage IRMS. Tin capsules are first dropped into the combustion column containing Copper (II) oxide where both carbon and nitrogen are combusted to CO_2 and N_2. The gases then pass through a GC column and over copper oxide wires and silver wool to remove sulphur and halides. Finally, gases are passed through to the IRMS and then output is presented for carbon and nitrogen as raw ratios. Isotope ratios are reported using delta notation (δ) with units per mil (‰) as in section 2.3. Samples were calibrated using internationally recognized L-glutamic acid standards, USGS40 ($\delta^{15}N$ = -4.5 ‰), USGS41 ($\delta^{15}N$ = +47.6 ‰ (Qi et al. 2003)), IAEA-N-1 (δ15N = +0.4 ‰ (Gonfiantini 1978)), and IAEA-N-2 ($\delta^{15}N$ = +20.3 ‰ (Gonfiantini 1978)). Standard concentrations were matched to approximately the same nitrogen mass as samples being analysed to avoid the need for size effect corrections. Standards were analysed in duplicate at the start, middle and end of each run of 49 samples to identify potential drift during a run. An independent organic standard of glycine was also used to check for any drift between runs. The instrument precision for nitrogen was 0.2 ‰ and the limits of detection were 10 µg.

2.3.2 Denitrifier Method

$\delta^{15}N_{NO3}$ and $\delta^{18}O_{NO3}$ in water samples was analysed using the 'Denitrifier Method' (Sigman et al. 2001; Casciotti et al. 2002; McIlvin and Casciotti 2011). The samples were analysed using a customised Thermo – Finnigan Gas Bench II (with backflush) interfaced with a Thermo Fisher Delta V Advantage IRMS. The same IRMS was used for both the particulate analysis (with the Elemental Analyser) and nitrate analysis (using the Gas Bench II).

Figure 2.6 Gas Bench II setup at the Liverpool Lifer laboratory

The denitrifier method uses denitrifying bacteria to convert the sample nitrate into nitrous oxide gas, which is then analysed using head space analysis on the Gas Bench-IRMS. Before the denitrifier method was developed, nitrogen isotopic composition of nitrate from seawater involved reduction of nitrate to ammonia followed by distillation or diffusion of the ammonia and reaction to N_2 gas (Sigman et al. 1997). There was no published method for oxygen isotopic analysis previously. These analyses required micromoles of nitrate-N and were both time and labour intensive. Using the bacterial method, both nitrogen and oxygen isotopes in nitrate can be analysed in fluids and the throughput is improved compared to previous methods (Sigman et al. 1997).

Dentitrifiying bacteria convert nitrate to nitrite to nitric oxide to nitrous oxide. *Pseudomonas chlororaphis* was originally used to determine the $\delta^{15}N$ of nitrate (Sigman et al. 2001) but was replaced by *Pseudomonas aureofaciens* which allows measurement of both the $\delta^{15}N$ and $\delta^{18}O$ of nitrate to a much higher degree of precision. Both *Pseudomonas chlororaphis* and *Pseudomonas aureofaciens* lack the final N_2O reductase gene to convert nitrous oxide to N_2 gas. Bacterial strains of *P. aureofaciens* were supplied by Karen Casciotti, (Univeristy of Stanford) in 2013, and then from Sian Henley, (University of Edinburgh) in 2016 after the integrity of the original strain was questioned. Strains were supplied on streaked agar and then cultured and stored as -80 °C frozen stock.

Pseudomonas aureofaciens was cultured under clean laboratory conditions in the School of Biological Sciences, Univeristy of Liverpool. Bacteria were cultured from the frozen stock on tryptic soy agar (Table 2.4) plates overnight in the dark at 30 °C. Bacteria were streaked to provide individual colonies for starter tubes (Figure 2.7).

Figure. 2.7 *Pseudomonas aureofaciens* cultured under clean laboratory conditions in the School of Biological Sciences, University of Liverpool

Table 2.2. Tryptic soy broth recipe (400 ml) autoclaved @121 °C 50 mins and left to cool overnight

Ingredient	Amount (g)	Concentration	Supplier (part number)
Tryptic Soy Broth	12	30 g/L	Sigma Aldrich (T8907-1kg)
Potassium Nitrate	0.4	10 mM	Sigma Aldrich (221295)
Ammonium Chloride	0.16	7.5 mM	Sigma Aldrich (A9434)
Potassium Phosphate	1.952	36 mM	Sigma Aldrich (60218)

Table 2.3. NO_3^- Free tryptic soy broth recipe (500 ml) autoclaved @121 °C 30 mins and left to cool overnight

Ingredient	Amount (g)	Concentration	Supplier (part number)
Tryptic Soy Broth	15	30 g/L	Sigma Aldrich (T8907-1kg)
Ammonium Chloride	0.2	7.5 mM	Sigma Aldrich (A9434)
Potassium Phosphate	2.44	36 mM	Sigma Aldrich (60218)

Table 2.4. Tryptic soy agar recipe (500 ml) autoclaved @121 °C 30 mins

Ingredient	Amount (g)	Concentration	Supplier (part number)
Tryptic Soy Agar	20	40 g/L	Sigma Aldrich (22091)
Potassium Nitrate	0.5	10 mM	Sigma Aldrich (221295)

Bacteria were monitored so that any contaminated plates were discarded. Plates were stored in a fridge at less than 3 °C with plates wrapped in parafilm and discarded after a week. All work was done using aseptic technique and gloves were

worn at all times. Starter tubes containing approximately 10 mls of Tryptic Soy Broth (Table 2.2) media were inoculated with an individual colony of bacteria using a sterilised inoculating loop. The loop was sterilised between each starter culture using a Bunsen burner flame, or a new sterile disposable loop was used. The starter tubes were then grown on a shaker table at 60 rpm overnight in the dark. 500 ml media bottles containing 400 ml of the same Tryptic Soy Broth were inoculated with 1 ml of bacterial sample from the starter tubes. These larger bottles were then incubated on a to shaker table for between 6 and 8 days to ensure there was sufficient biomass of bacteria and to ensure that all nitrate in the media was consumed during the growth phase.

After the incubation period the media was divided into 50 ml disposable plastic centrifuge tubes (approximately 7 tubes per 400 ml of media). These tubes were centrifuged at 9600 *g* (7500 rpm) for 12 minutes at room temperature. The supernatant media was then discarded and 14 mls of nitrate free media (Table 2.3) (with antifoaming agent, 3 mls per 500 ml of nitrate free media) were added to each tube and cells were re-suspended. This step concentrated cells by 3.7 fold. The media was then homogenised in one 500 ml bottle and pipetted in 3 ml aliquots into 20 ml headspace glass vials (Sigma Aldrich SU860030) and crimp sealed using butyl septa (Cole Parmer W224200-405) (McIlvin and Casciotti 2011). Vials were purged with high purity N_2 gas for 3 hours on a custom built degassing line to ensure that any N_2O and O_2 was removed, creating an anaerobic environment for the bacteria to begin denitrifying before the addition of the seawater sample (Figure 2.8).

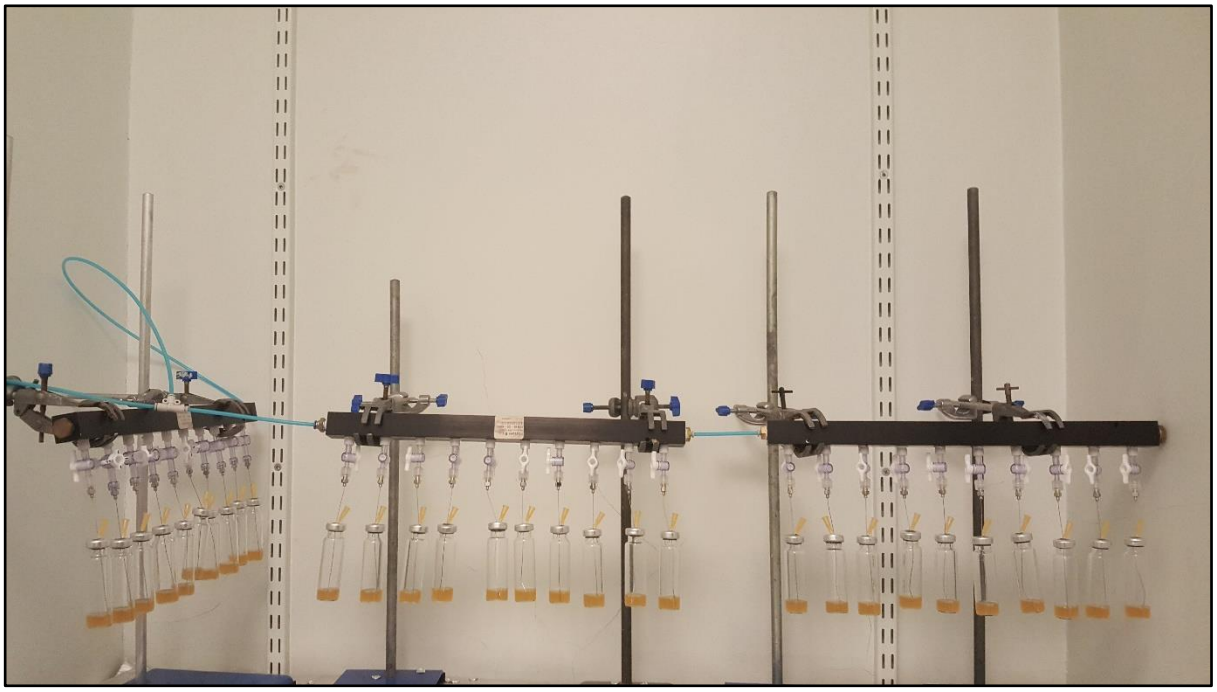

Figure 2.8 High purity N_2 Purging line set-up for 30 vials at University of Liverpool

After purging, a known volume of seawater sample or standard (USGS-34, USGS35, and IAEA-NO-3) was added to achieve an amount of nitrate between 10 and 40 nmol, giving a peak height of 1000 mV and 4000 mV on the IRMS, respectively. The amount of nitrate in samples were matched to standards to avoid the need to correct for linearity problems on the Gas Bench-IRMS. Below a peak height of 1000 mV sample reproducibility was compromised. The limits of detection of the method were 1 µM nitrate as only 10 mls can be added to headspace vials (while maintaining the bacteria to sample ratio). This limit is due to the injection procedure on the Gas Bench system, as any more than 10 mls of sample causes liquid to be drawn into the system. Limits of detection could be improved by increasing the volume of the culture and using manual injections, however due to time constraints this was unfeasible. The isotope standards used were USGS-34, USGS35, and IAEA-NO-3. Originally USGS32 was also used although the $\delta^{18}O$ and $\delta^{15}N$ values differed from the samples and the high $\delta^{15}N$ of +180 led to problems with carry over. Standards were made up daily to a working concentration of 40 µM from a 10 mM stock solution, which was prepared monthly.

After sample or standard addition samples were left in the dark at room temperature overnight to allow the bacterial conversion of NO_3^- to N_2O. The following day the bacteria were lysed by adding 0.1 ml of 10 N NaOH to each

headspace vial. Along with lysing the bacterial cells, the addition of NaOH scavenges and immobilises any CO_2 within the vial, which has the same molecular mass as N_2O. Samples were then ready for analysis. Samples using the butyl septa can be stored for over 165 days, this meant that samples were be made up in large batches as complete preparation time is between 8 and 10 days (McIlvin and Casciotti 2011).

As the denitrifier method does not distinguish between nitrate and nitrite in samples, it was necessary to remove nitrite from samples before spiking the broth so that the isotope ratio of both $\delta^{15}N$ and $\delta^{18}O$ reflects only the nitrate within the sample. Sulfamic acid addition and neutralisation was used to remove any excess nitrite from a sample before adding the sample to the bacterial broth in the headspace vials (Granger and Sigman 2009). The method used follows the protocol described for field campaigns (Granger and Sigman 2009).

The nitrite removal process was conducted when nitrite represented more than 5 % of the total nitrite plus nitrate in the sample. Briefly, samples were spiked with 10 µl per ml of 4 % w/v sulfamic acid solution (Table 2.5) and left for approximately 20 minutes for all nitrite within the sample to react. Samples were then neutralised with 5.5 µl ml^{-1} of 2N NaOH. Neutralisation was required to avoid bacterial cell lysis in the vials. Sulfamic acid and NaOH were added to standards to detect and therefore correct for potential contamination of reagents.

Table 2.5. Sulfamic Acid recipe (1000 ml) made up in deionised water.

Ingredient	**Amount**	**Concentration**	**Supplier (part number)**
Sulfamic Acid	38.8 g	0.4 M	Sigma Aldrich (383120-500g)
Hydrochloric Acid	1.2 N	100 ml	Sigma Aldrich (258148-M)

2.3.3 Analysis of nitrous oxide

The setup used to analyse samples was a customised Thermo – Finnigan Gas Bench II (with backflush) interfaced with a continuous flow IRMS. Figure 2.9 shows

the configuration of the Gas Bench-IRMS in two modes, load and inject. These modes will be discussed further below.

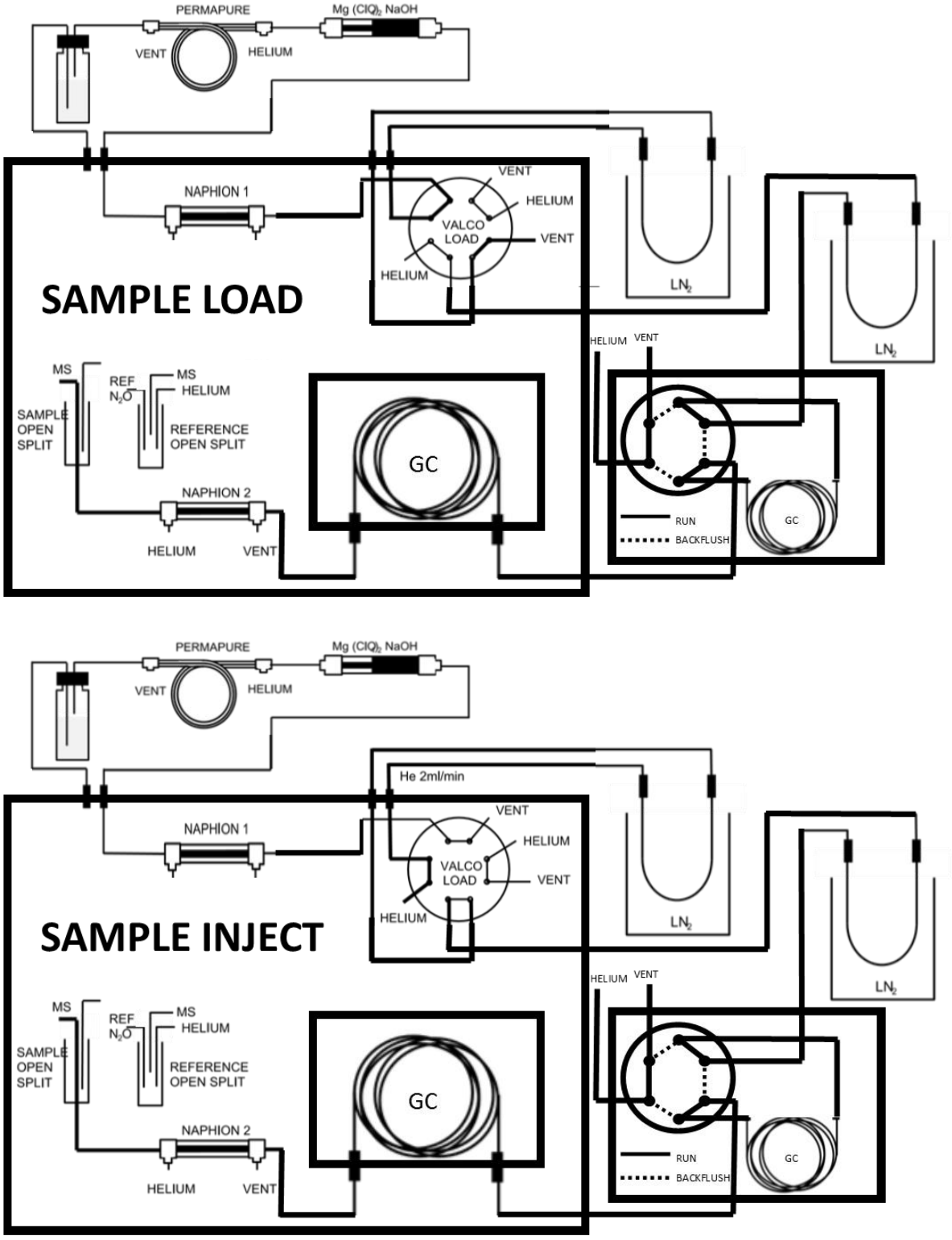

Figure 2.9. Gas Bench set up at the University of Liverpool. Sample load shows the flow of helium and sample while it is added to the first liquid nitrogen trap, during this time the backflush is active (dotted line). Inject mode shows the flow of helium and sample through the GC columns to the IRMS. Details are described in the text.

Gas-Bench preparation: Before samples were analysed, the main gas chromatography (GC) column (HP-Plot-Q 30 m x 0.53 mm x 40 µm) was baked at 140 °C for approximately 1 hour each day. Once the column had cooled to room temperature N_2O zero enrichments were run (short bursts of N_2O from a tank) until the background for masses 18, 32 and 40 have reached acceptable levels (≤5000 mV, ≤3000 mV and ≤180 mV, respectively), and the standard deviation between peaks is acceptable, ≤0.02 for $\delta^{15}N$ and ≤0.1 for $\delta^{18}O$.

Transfer of sample from vials to Gas-Bench: 20 ml glass headspace vials containing samples of N_2O were flushed using Helium carrier gas and single needle setup as described by McIlvin and Casciotti, (2011). Helium gas was flushed through the needle at a flow rate of 30 ml $min^{-1}$from the bottom of the needle, creating positive pressure and forcing the sample into the second hole near the top of the needle, where a counter-flow He gas stream carried the nitrous oxide into the Gas Bench. Samples first passed through a chemical trap containing Ascarite II, a sodium hydroxide coated silica and magnesium perchlorate and then through a Nafion drier to remove water. Ascarite II rapidly and quantitatively adsorbs CO_2 and acid gases. The sample passed into the first liquid nitrogen trap, where the sample was cryo-focussed. During this procedure, the valco valve (Figure 2.9) is in load position. After 860 seconds of cryo-focusing, the Gas Bench switches to inject mode and the sample gas is transferred to a second liquid nitrogen trap for further focusing. This step also reduces the CO_2 and H_2O content of the sample gas. After 800 seconds in the second trap, the trap is released, warms to room temperature and the gas is transferred to the pre-column (Poraplot-Q column 10 m x 0.32 mm x 10 µm) and main GC column (HP-Plot-Q 30 m x 0.53 mm x 40 µm), which separates the gases by mass before they are introduced into the IRMS via an open split (Table 2.7).

Backflush: After the sample passes from the second liquid nitrogen trap into the IRMS the system is switched to backflush mode, which allows carrier gas (and any remaining residual sample) through the pre- column which lies between the second liquid nitrogen trap and the main column. The backflush helps prevent any residual carry over from one sample to the next. The procedure is then repeated for each sample. The backflush remains on as the next sample was focussed in the first liquid nitrogen trap (Figure 2.9).

IRMS analysis: In the ion source of the IRMS the gas molecules ionised and are accelerated though high voltage. The ions then pass through a magnetic field before reaching faraday cup detectors. The strength of the magnetic field and the voltage of acceleration determine the trajectory of the ions and therefore which ions will enter the faraday cups. The use of multiple collectors allows simultaneous analysis of ions. The stable isotope analysis of N_2O requires three collectors. The MS measures the m/z ratio of the samples and standards versus reference N_2O gas. Ion measurements for N_2O at masses 44, 45 and 46 are referenced to N_2 and VSMOW using the N_2O reference peak. The absolute value of the $\delta^{15}N$ and $\delta^{18}O$ value is calculated by analysing USGS-34, USGS35, and IAEA-NO-3 standards prepared from the same batch of bacterial media and associated procedures as the samples (Table 2.6). As sample and standard nitrate concentration were matched, any non-linearity from the mass spectrometer was corrected for. The slope and intercept of the linear regression between USGS-34 and IAEA-NO-3 values for measured standards and absolute values were used to correct samples to their absolute values (Table 2.6). USGS-35 was also used as an extra standard. An independent standard of deep-sea water (1000 m, collected during D361, 2011) was also analysed alongside each sample set. Pure N_2O gas standards were prepared from 20 ppm high purity N_2O gas cylinder (BOC, 160528-AK-C) and analysed in duplicate at the end of each run to check for any variation or drift in the IRMS. This standard was useful as it is separate from the samples/standards made up using the denitrifier method. This allowed easy differentiation between issues with the denitrifier method and problems with the Gas Bench-IRMS. During each run, a set of broth blanks are analysed to detect and quantify residual nitrate in the broth or contamination. Throughout this study these peak areas for the blanks were consistently below the limit of detection of the IRMS, and thus a blank was not quantified.

Table 2.6. Reference standards used for nitrate isotopic analysis. Isotopic values are stated relative to Air and VSMOW, respectively.

	$\delta^{15}N_{NO3}$ (‰ vs. AIR)	$\delta^{18}O_{NO3}$ (‰ vs. VSMOW)
IAEA-NO-3	+4.7	+25.6
USGS-34	-1.8	-27.9
USGS-35	+2.7	+57.5

Samples were initially run in triplicate. Samples were then run in duplicate when the method was running optimally to allow greater throughput of samples. In one daily run, 40 vials could be analysed, consisting of 8 samples in duplicate, plus standards, deep sea water and blanks. The reproducibility for $\delta^{15}N$ was typically 0.2 ‰, while the $\delta^{18}O$ was typically 0.5 ‰. Reproducibility using this method was comparable to other studies (Sigman et al. 2001; Granger et al. 2004; Granger et al. 2011; Granger et al. 2013).

During the time frame of my PhD (2014-2018), I further developed and optimized the method to increase sample throughout and reduce instrument downtime. These changes included:

(a) The main GC column was changed from a 25 m x 0.32 mm x10 µm column to a HP-Plot-Q 30 m x 0.53 mm x 40 µm column.
(b) The nafion tubing and Ascarite II traps were also changed, and a schedule for regular replacement was implemented.
(c) The major change to the configuration was the addition of a backflush system to help reduce residual carryover between samples. It is not feasible to backflush the main column within the time-frame of a sample run and therefore the backflush containing a pre-column was inserted between the second liquid nitrogen trap and the main GC column (Figure 2.9). The backflush pre-column was a shorter Poraplot-Q column 10 m x 0.32 mm x 10 µm. The pre-column backflush was active from the start of the run until the first liquid nitrogen trap was removed (0-800 seconds), and then was reactivated when the sample peak is measured from 1600 seconds to the end of the run at 1900 seconds (Table 2.7).

Table 2.7. Isodat timing for gas bench denitrifier method analysis (total run time = 1900 s), with ticks indicating on, and crosses indicating off.

Time (s)	Ref 1 (Backflush)	Ref 3 (N_2O Ref)	Split	Valco Inject	Trap 1	Trap 2
0	✓		×	×	✓	×
630		✓				
650		×				
680		✓				
700		×				
730		✓				
750		×				
800	×			✓		✓
860					×	
1200			✓			
1600	✓					×

2.3.4 Denitrifier method quality control

The accuracy and precision associated with the denitrifier method improved with the alterations made (described above). The values of standards and independent check standards run were analysed over the time period of most intensive analysis to check for any drift in absolute values (values once corrected with USGS34 and IAEA-NO-3). The $\delta^{15}N$ values of USGS34 and IAEA-NO-3 were stable over the intensive run period (September 2017 – December 2017) (Figure 2.10). The mean value of USGS34 was -1 ‰, with a standard deviation of 0.09 ‰. The mean value of IAEA-NO-3 was +5.4 ‰ with a standard deviation of 0.1 ‰. Despite some variation in measured values between runs, the corrected values of $\delta^{15}N$-nitrate in deep sea water and USGS35 remained stable throughout the period (Figure 2.12).

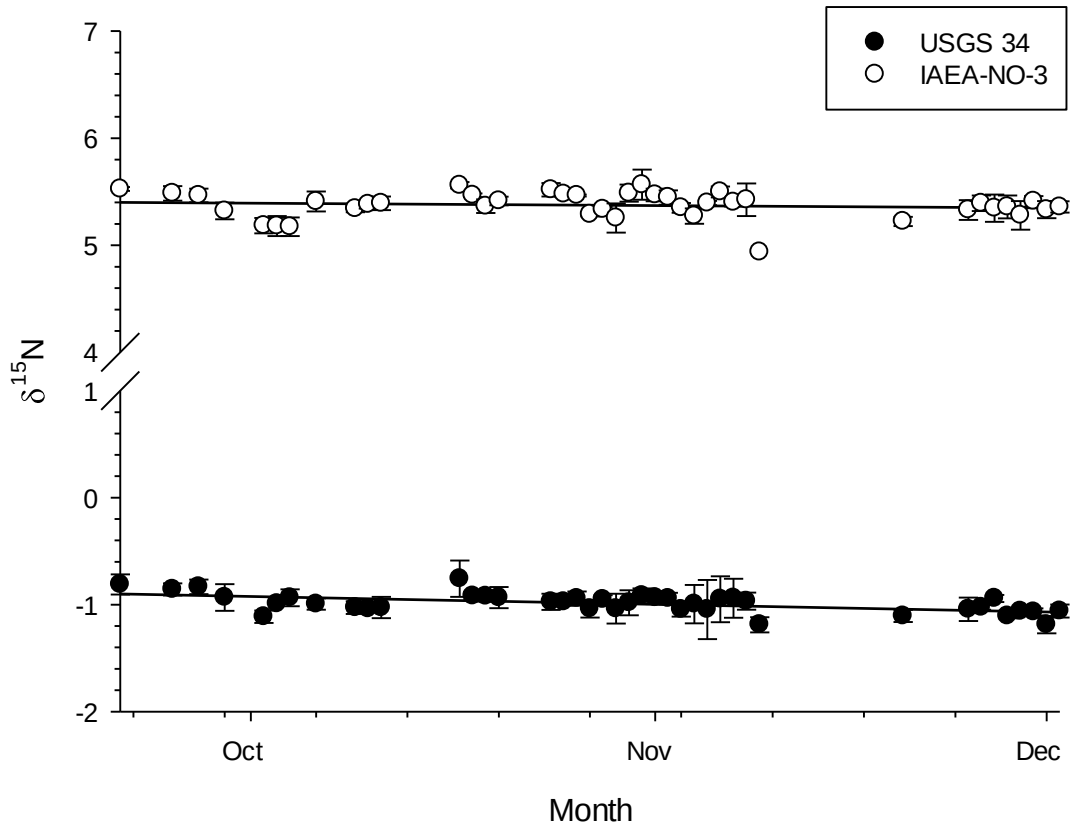

Figure 2.10. The mean $\delta^{15}N$ value of standards USGS 34 (filled circles) and IAEA-NO-3 (unfilled circles) during the most intensive period of analysis (September 2017 to December 2017)

The $\delta^{18}O$ values of USGS34 and IAEA-NO-3 showed more variation than the $\delta^{15}N$ over the intensive run period (September 2017 – December 2017) (Figure 2.11). The mean value of USGS34 was -29.7 ‰, with a standard deviation of 0.75 ‰. The mean value of IAEA-NO-3 was +20 ‰ with a standard deviation of 0.49 ‰. Despite the variation in measured values between runs, the corrected values of $\delta^{18}O$-nitrate in deep sea water and USGS35 also remained stable throughout the period (Figure 2.12).

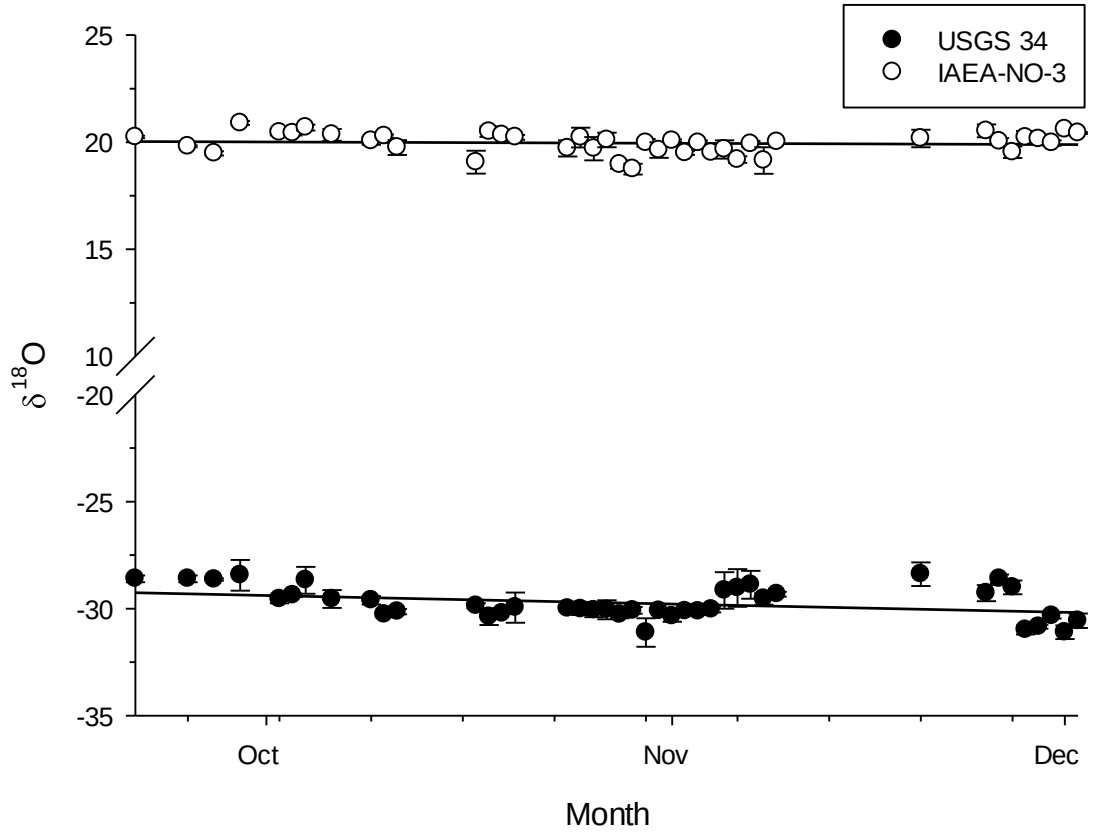

Figure 2.11. The mean $\delta^{18}O$ value of standards USGS 34 (filled circles) and IAEA-NO-3 (unfilled circles) during the most intensive period of analysis (September 2017 to December 2017)

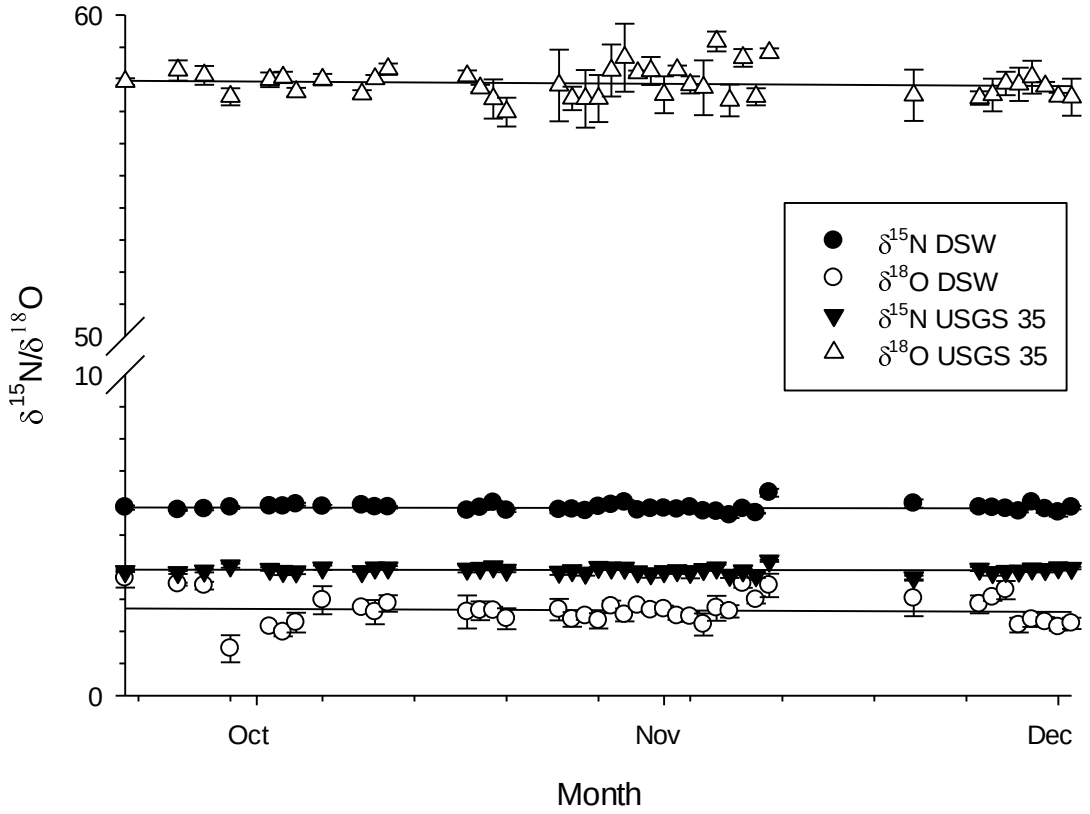

Figure 2.12. The mean $\delta^{15}N$ (filled circles) and $\delta^{18}O$ (filled triangles) values of deep sea water (1000m) (DSW) independent check standard during the most intensive period of analysis (September 2017 to December 2017). The mean $\delta^{15}N$ (unfilled circles) and $\delta^{18}O$ (unfilled triangles) of independent check standard USGS 35 during the most intensive period of analysis (September 2017 to December 2017). These check standards were corrected using the corresponding USGS 34 and IAEA-NO-3 values.

2.3.5 Analysis of $\delta^{18}O$ of H_2O samples

Analysis of $\delta^{18}O$ of H_2O samples collected during DY029 was carried out at the NERC isotope facility which is part of the British Geological Survey.

2.4 Supplementary Data

Additional data was used in complement with the stable isotope datasets. This data was collected and analysed by numerous scientists from other scientific institutions as part of the SSB project and other projects.

Inorganic nutrient data (nitrate, nitrite, phosphate, silicate and ammonium) for the SSB process cruises **DY026** (August 3rd 2014 –August 24th 2014), **DY018** (November 09th 2014 – December 02nd 2014), **DY021** (March 01st 2015 – March 26th 2015), **DY029** (April 01st 2015 – April 30th 2015), and **DY033** (July 11th 2015 to August 03rd 2015) was primarily analysed by Malcolm Woodward (Plymouth Marine

Laboratory). Western Channel observatory samples were also analysed by Malcolm Woodward. Inorganic nutrient data (nitrate + nitrite, phosphate and silicate) for **DY017** (October 20th 2014 – November 11th 2014) was analysed by Chris Daniels, NOC Southampton. Inorganic nutrient samples spiked with $HgCl_2$ from the CEFAS Smartbuoy (Central Celtic Sea site) were analysed by Calum Preece, University of Liverpool and by CEFAS staff, Lowestoft.

Dissolved oxygen samples were analysed by Claire Mahaffey & Calum Preece, University of Liverpool, Vassilis Kitidis, Plymouth Marine Laboratory and Chata Seguero, University of East Anglia.

All supplementary data was collated, and quality control checked by the British Oceanographic Data Centre and made available online.

Chapter 3. Nitrate cycling and supply at L4

3.1 Introduction

The Western Channel Observatory: The Western Channel Observatory (WCO) is in the western English Channel (Figure 3.1). The WCO consists of two sites, station L4 (50° 15′N, 4° 13′W) and station E1 (50° 02′N, 4° 22′W). Investigation into the western English Channel has been carried out since the Marine Biological Association was opened in 1888 (Southward et al. 2005). *In situ* measurements are undertaken using the research vessels of the Plymouth Marine Laboratory (PML) and Marine Biological Association (MBA). The WCO is an important oceanographic region, with stations influenced by Atlantic influx into the shelf seas, the neritic zone, and coastal outflows (Southward et al. 2005). This chapter will focus on station L4.

The L4 time-series: The L4 station is situated approximately 19 km from Plymouth lying just over the 50 m depth isobar, at approximately 55 m deep, where the open ocean water and the coastal zone meet. The site is weakly, seasonally stratified during the summer, but experiences periodically mixed waters and estuarine outflow from Plymouth Sound (Southward et al. 2005). The site is strongly tidally influenced with a maximum surface stream of 0.6 ms^{-1} during the mean spring tide. L4, along with the other coastal sampling stations is heavily influenced by the ambient weather conditions. The L4 site is primarily sandy (Smyth et al. 2009).

A host of physical, biological and chemical measurements are carried out at L4, with the site sampled on a weekly basis since 1988, apart from periods of bad weather. The initial emphasis of the time series was focused on phytoplankton and zooplankton species composition. The collection of data for more than 20 years now allows the impact of climate variation and climate change to be assessed. Analysis of surface inorganic nutrients has been performed on samples collected from L4 since 2000, with full depth vertical resolution of inorganic nutrients being resolved since 2002. PML has operated two autonomous surface moorings since 2009. The autonomous buoys for L4 were funded by the NERC Oceans 2025 project. The buoys are equipped with *in situ* sensors to collect data on sea surface temperature, salinity, oxygen, turbidity, fluorescence, air temperature, humidity, wind speed and direction and atmospheric pressure, CDOM fluorescence and nitrate.

In this study, I investigate nitrogen cycling at station L4 and the sources of inorganic nutrients, which drive primary production. I use $\delta^{15}N_{NO3}$ and $\delta^{18}O_{NO3}$ measurements from 2014-2016 along with temperature, salinity, oxygen and inorganic nutrients to demonstrate how stable isotopes can be used to capture not only the biological uptake signature during the spring bloom period but also give evidence of the sources of nitrate to the L4 site and how it is cycled.

3.2 Methods

Water samples for the analysis of $\delta^{15}N_{NO3}$ and $\delta^{18}O_{NO3}$ were collected on a bimonthly basis from the Western Channel Observatory Long Term Buoy L4 (Figure 3.1) in the English Channel from late 2014 to late 2016. Samples for analysis of inorganic nutrient (NO_3^-, NO_2^-, PO_4^{3-}, $Si(OH)_4$, NH_4^+) and $\delta^{15}N_{NO3}$ and $\delta^{18}O_{NO3}$ were collected using a CTD equipped with a 24 bottle rosette. Samples were filtered and stored frozen at -20˚C until analysis. Inorganic nutrients (NO_3^-, NO_2^-, PO_4^{3-}, $Si(OH)_4$, NH_4^+) were analysed at PML using standard colormetric autoanalyser techniques (Brewer and Riley 1965; Mantoura and Woodward 1983; Kirkwood 1989; Zhang and Chi 2002). Fluorometric analysis of chl *a* was conducted by filtering 100 ml of seawater through 25 mm glass fibre filters and extracted in 90 % acetone at 4 °C. Chl a concentration was then measured using a Turner fluorometer using the Welschmeyer method (Welschmeyer 1994). Water column temperature, oxygen and salinity were recorded using a Seabird SBE 19+ CTD.

The water samples for $\delta^{15}N_{NO3}$ and $\delta^{18}O_{NO3}$ analysis were collected in 60 ml HDPE bottles and filtered through a 0.7 micron glass fibre filter before being frozen at -20 °C and sent for analysis in Liverpool. The Denitrifier Method (McIlvin and Casciotti 2011) was used to prepare samples for analysis. Samples were analysed on a Gas bench II interfaced with a GC IRMS. The method used is described in detail in Chapter 2.

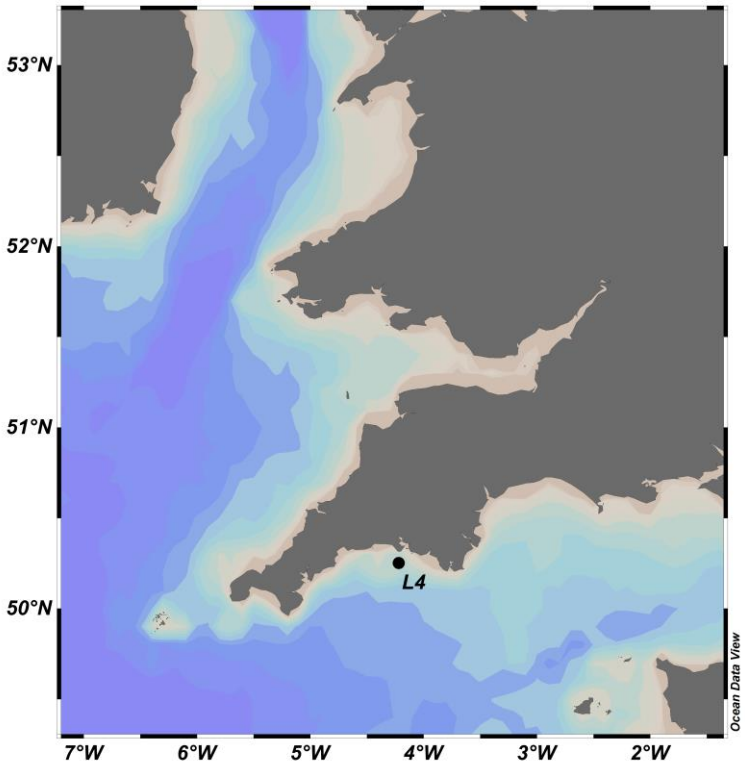

Figure 3.1. Map of the Western Channel Observatory L4 station where water samples were collected for nitrate isotope analysis.

3.3 Results

3.3.1 Water column conditions 2014-2016

Samples for stable isotope analysis of $\delta^{15}N_{NO3}$ and $\delta^{18}O_{NO3}$ were collected over a 16-month period from December 2014 to May 2016. Over this timescale, temperature was similar between surface and bottom between September and June, but between June and September, surface waters were 1.6 °C warmer in surface waters (14.9 ± 1.5 °C) relative to 50 m waters (13.3 ± 1.1 °C); (Figures 3.2a, 3.3a and 3.4a). Temperature was lowest during February and March of each year with the mean water column being at 9.4 °C (±0.2) for the 2014-2016 period. Temperature increased from March to August or September in each year. Maximum surface temperature occurred in September in 2014 (16.6 ± 0.5 °C) and 2016 (16.6 ± 0.4 °C) but August in 2015 (16.2 ± 0.7 °C). Over the sampling period (2014-2016), the mean salinity was 35.18 ± 0.16). Salinity decreased in surface waters in January 2015 (34.83) and January 2016 (34.41) Salinity was lower in winter 2016 (35.10 ± 0.19) compared to winter 2015 (35.21 ± 0.12; Figures 3.2b, 3.3b and 3.4b).

Oxygen saturation in surface waters was highest (> 100 %) in September 2014 August 2015 and May 2016. Oxygen concentrations were below saturation but above 90 % saturation in October 2014, September 2015 and September 2016. At 50 m there was more variation in the oxygen saturation, being highest (> 100 %) during April and May each year and lowest during August and September. Oxygen saturation was below 85 % at 50 m in September 2016 (Figures 3.2c and 3.4c).

Chlorophyll-a concentrations increased rapidly from 0.2 mg m^{-3} in February 2015 to over 3 mg m^{-3} in April 2015. Concentrations were above 0.4 mg m^{-3} until December 2015 and frequently increased to over 2 mg m^{-3} during the summer months. Chlorophyll dynamics in 2015 were markedly different to 2014 and 2016, with concentrations increasing to over 2 mg m^{-3} between April and December instead of increasing during the spring bloom period alone (Figures 3.2d and 3.3d). Mean chlorophyll concentrations between April and October were higher in 2015 (1.6 ± 0.6 mg m^{-3}) compared to 2014 (0.9 ±0.6 mg m^{-3}) and 2016 (1.2 ± 0.8 mg m^{-3}).

Total rainfall varied between each of the years 2014, 2015 and 2016. The highest rainfall was during 2014 (929 mm), followed by 2016 (753 mm) and 2015 (677 mm) (Figure 3.5). Rainfall during the winter period (December, January and February) was much higher during the 2015 to 2016 period (325 mm) compared to the 2014 to 2015 period (187 mm) (Figure 3.5). Rainfall in the spring period during 2015 (84 mm) was lower than both 2014 (196 mm) and 2016 (147 mm). Summer rainfall was lowest in 2016 (117 mm) compared to 2014 (209 mm) and 2015 (220 mm) (Figure 3.5).

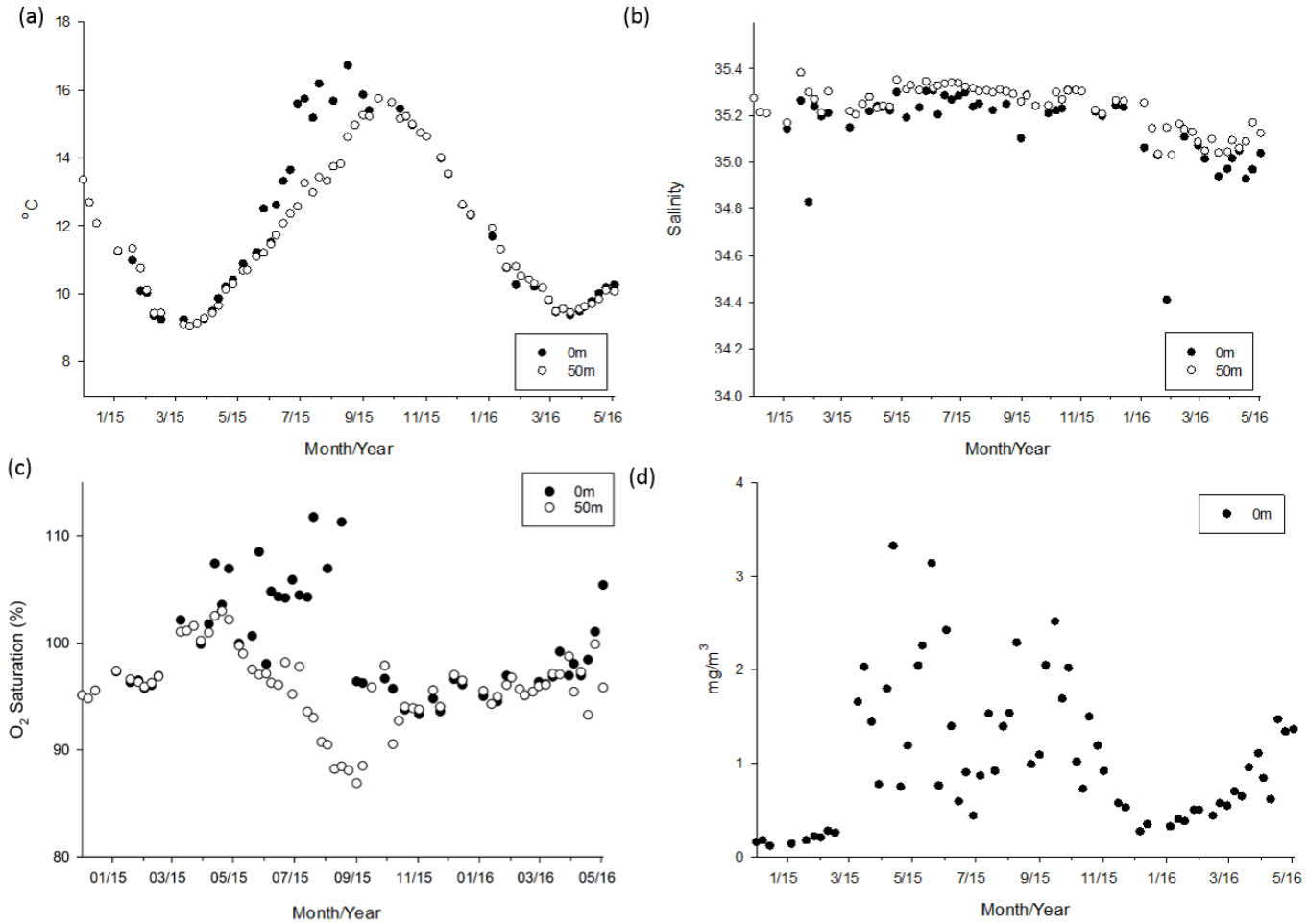

Figure 3.2. L4 time series data between December 2014 and May 2015 (when water samples were collected for stable isotope analysis) at surface (0 m) and 50 m depth including a) Temperature (°C), b) Salinity, c) Oxygen saturation (%), d) Chlorophyll-a (mg m^{-3})

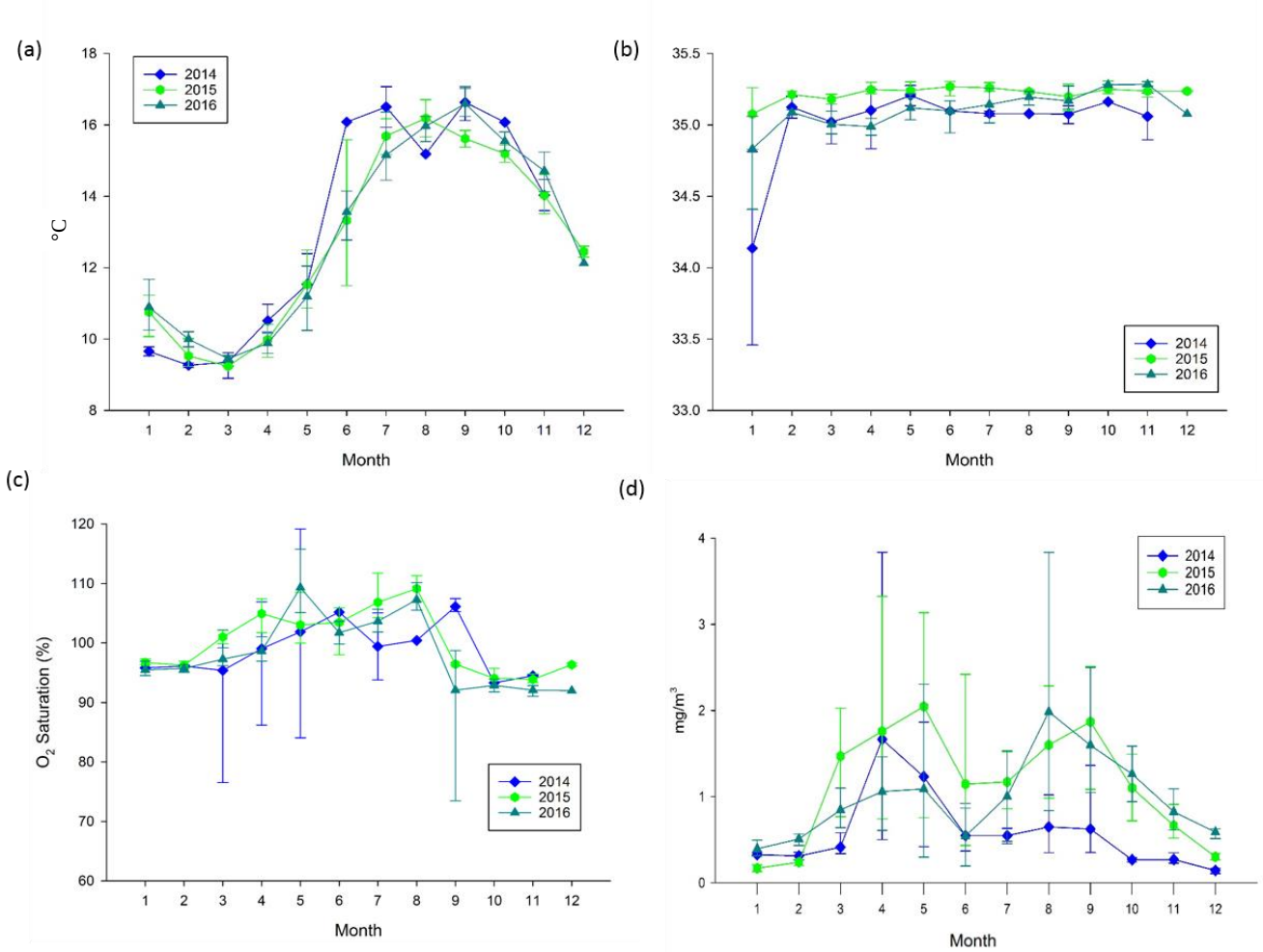

Figure 3.3. Long term L4 time series data at surface (0 m), months 1-12 (Jan-Dec) for 2014-2016 including a) Temperature (°C), b) Salinity, c) Oxygen saturation (%), d) Chlorophyll-a (mg m^{-3})

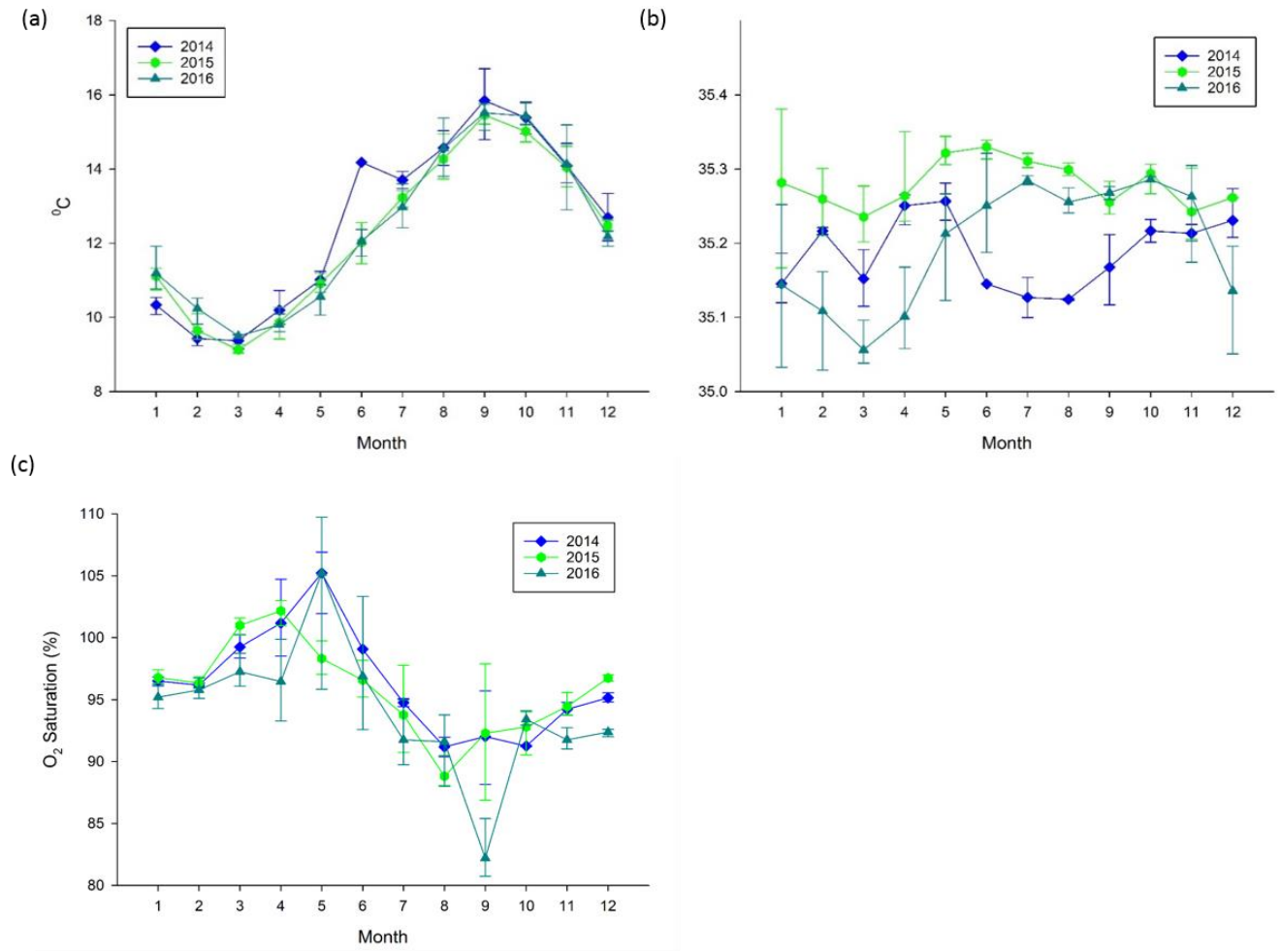

Figure 3.4 Long term L4 time series data at surface (50 m), months 1-12 (Jan-Dec) for 2014-2016 including a) Temperature (°C), b) Salinity, c) Oxygen saturation (%)

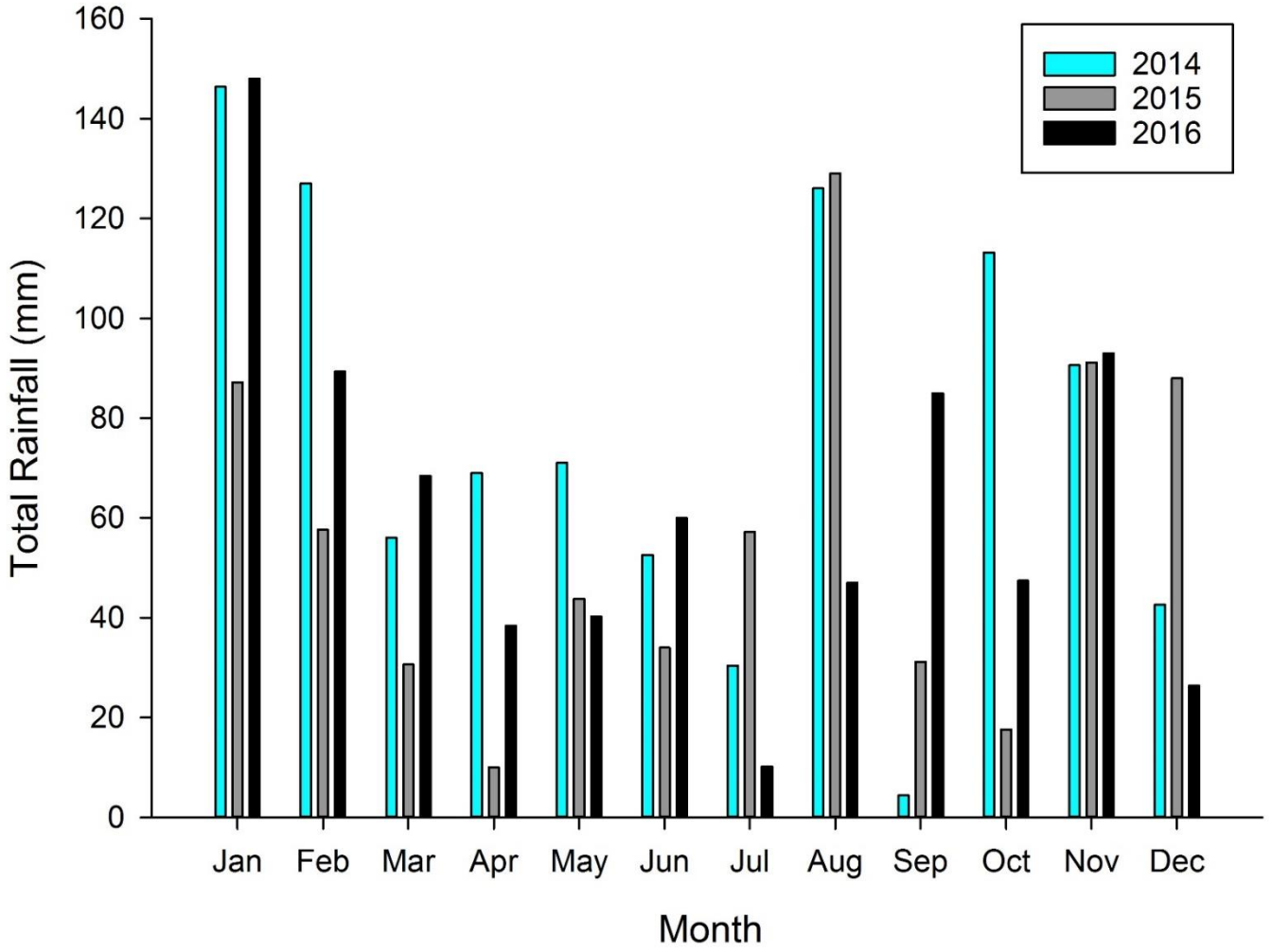

Figure 3.5 Total monthly rainfall (mm) for the years 2014 to 2016 at Crownhill, Plymouth weather station

3.3.2 Nutrient distributions 2014-2016

Nitrate concentrations in surface waters in winter 2014/2015 (6.9 ± 1.1 µM) and winter 2015/2016 (7.3 ±1.6 µM), were higher than at 50 m in winter 2014/2015 (6.3 ± 0.7 µM) and winter 2015/2016 (6.5 ±0.9 µM), possibly reflecting the external input of nitrate to surface waters (Figure 3.6a, Table 3.1). Concentrations in the surface and at 50 m decreased rapidly to near zero in April and May as the onset of stratification and initiation of the spring bloom consumed nutrients. The decline in nitrate to near zero concentrations occurred over a shorter time period in 2015 (48 days) compared to 2016 (70 days; Figure 3.7a), decreasing to the limits of detect on earlier in 2015 (27th April) compared to 2016 (16th May). Surface concentrations remained low (below 1 µM in the surface, and below 2 µM at 50 m) during the summer until increasing through autumn back to winter maximum concentrations (Figures 3.7a and 3.8a). The rate of increase from September until the end of December (15th December 2015, and 19th December 2016) was 0.05 µM d^{-1} in 2015, and 0.04 µM d^{-1} in 2016. In July and August, there were small sporadic increases in nitrate concentrations at 50 m depth to over 1 µM (Figures 3.6a and 3.8a).

In 2015, nitrite concentrations increased in February (0.2 ± 0.04 µM) and October (0.7 ± 0.3 µM) in surface waters, and February (0.2 ± 0.04 µM) and October (0.8 ± 0.2 µM) at 50 m (Figures 3.6b, 3.7b, and 3.8c). The second larger peak was in October in both the surface and at 50 m (mean concentrations of 0.7 ± 0.3 µM and 0.8 ± 0.2 µM, respectively; Figures 3.7b and 3.8b). During 2016, the spring time increase in nitrite occurred later in March in surface waters (0.2 ± 0.01 µM) and April at 50 m (0.3 ± 0.1 µM) and in November in both surface waters (0.9 ± 0.3 µM) and at 50 m (1.0 ± 0.3 µM). During both years, nitrite concentrations were < 0.1 µM between May and August in both the surface and bottom water before increasing throughout the autumn months (Figures 3.6b, 3.7b and 3.8b).

In surface waters, ammonium concentrations increased from a minimum in January (< 0.2 µM) to maximum concentration in May 2015 (0.5 µM) and April 2016 (0.4 ± 0.2 µM; Figures 3.6c and 3.7c). Ammonium concentrations then decreased throughout the summer months in surface waters, with intermittent increases in ammonium up to 0.6 µM (Figures 3.6c and3.7c). At 50 m depth,

ammonium concentrations peaked in July in 2015 (1.6 µM ±0.5) and 2016 (1.9 µM ±0.4; Figure 3.8c) and declined to 0.5 µM in November.

During the summer months ammonium was the dominant form of total dissolved inorganic nitrogen pool, making up approximately 75 % during June, July and August. During the rest of the year nitrate is the dominant form of DIN (Figure 3.8d).

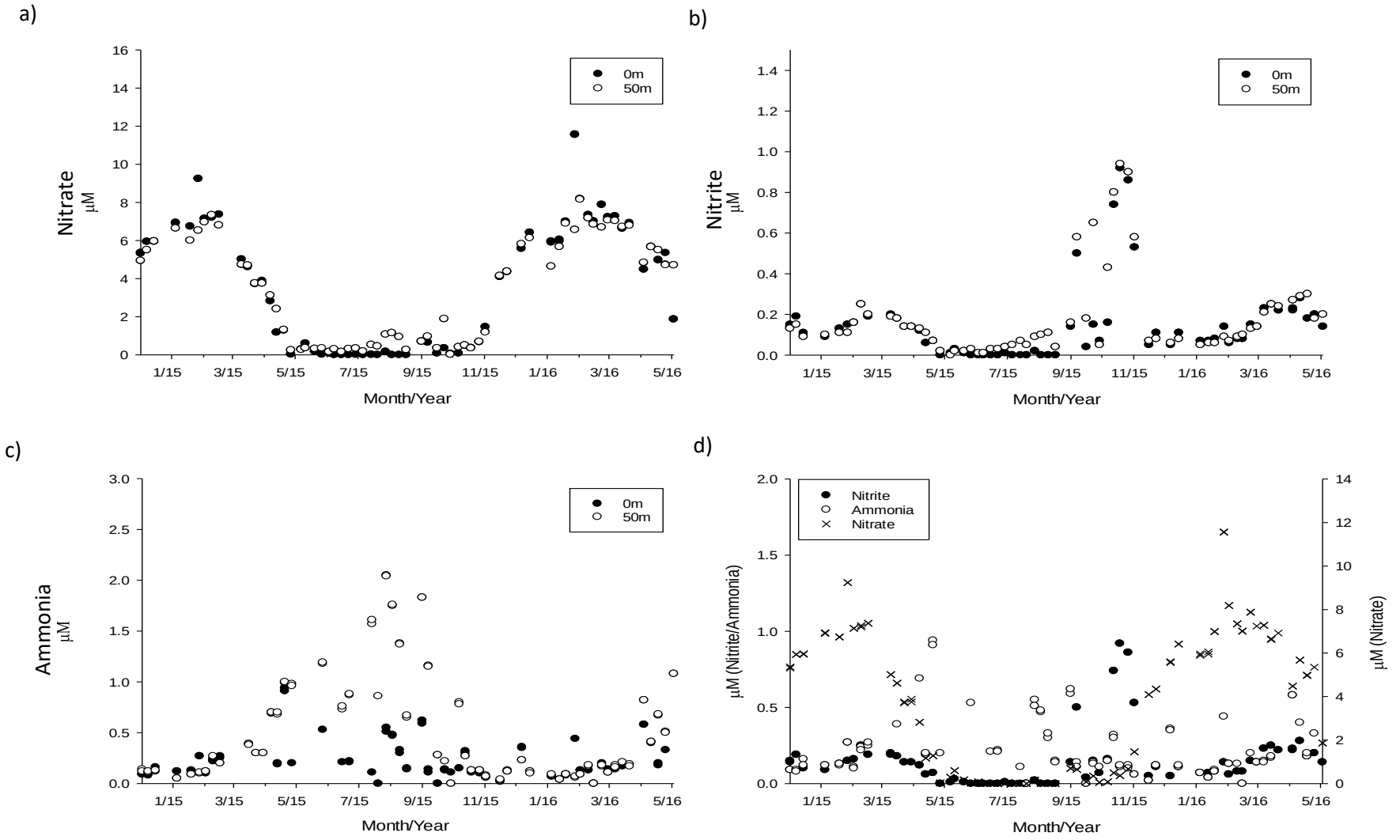

Figure 3.6. L4 time series data between December 2014 and May 2015 (when water samples were collected for stable isotope analysis) at surface (0 m) and 50 m depth including (a) Nitrate concentration (µM), (b) Nitrite concentration (µM), (c) Ammonia concentration (µM), (d) Composite of surface (0 m) nitrate, nitrite and ammonia (µM)

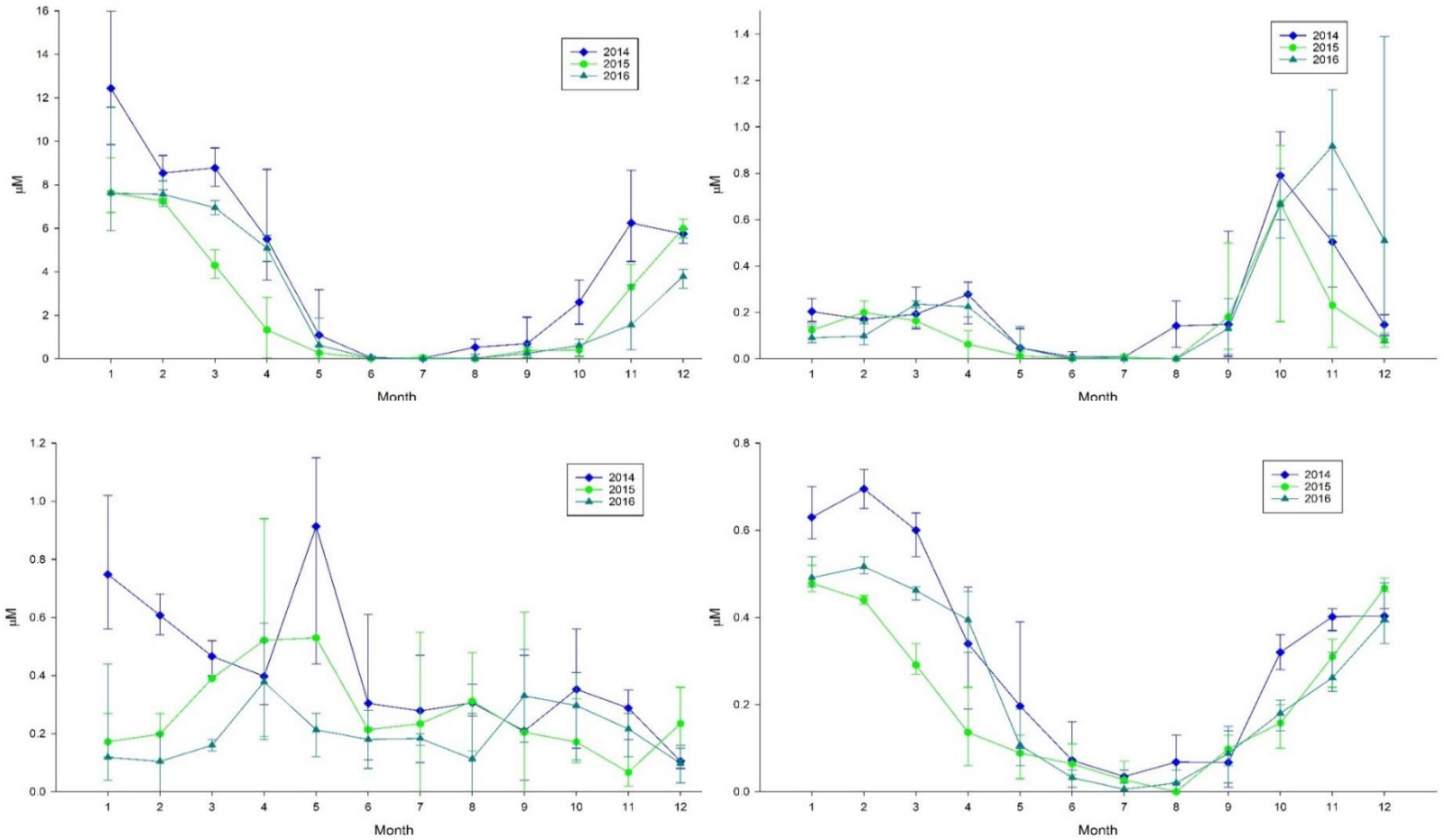

Figure 3.7. Long term L4 time series data at surface (0 m), months 1-12 (Jan-Dec) for 2014-2016 including a) Nitrate concentration (µM), b) Nitrite concentration (µM), c) Ammonia concentration (µM), d) Phosphate concentration (µM)

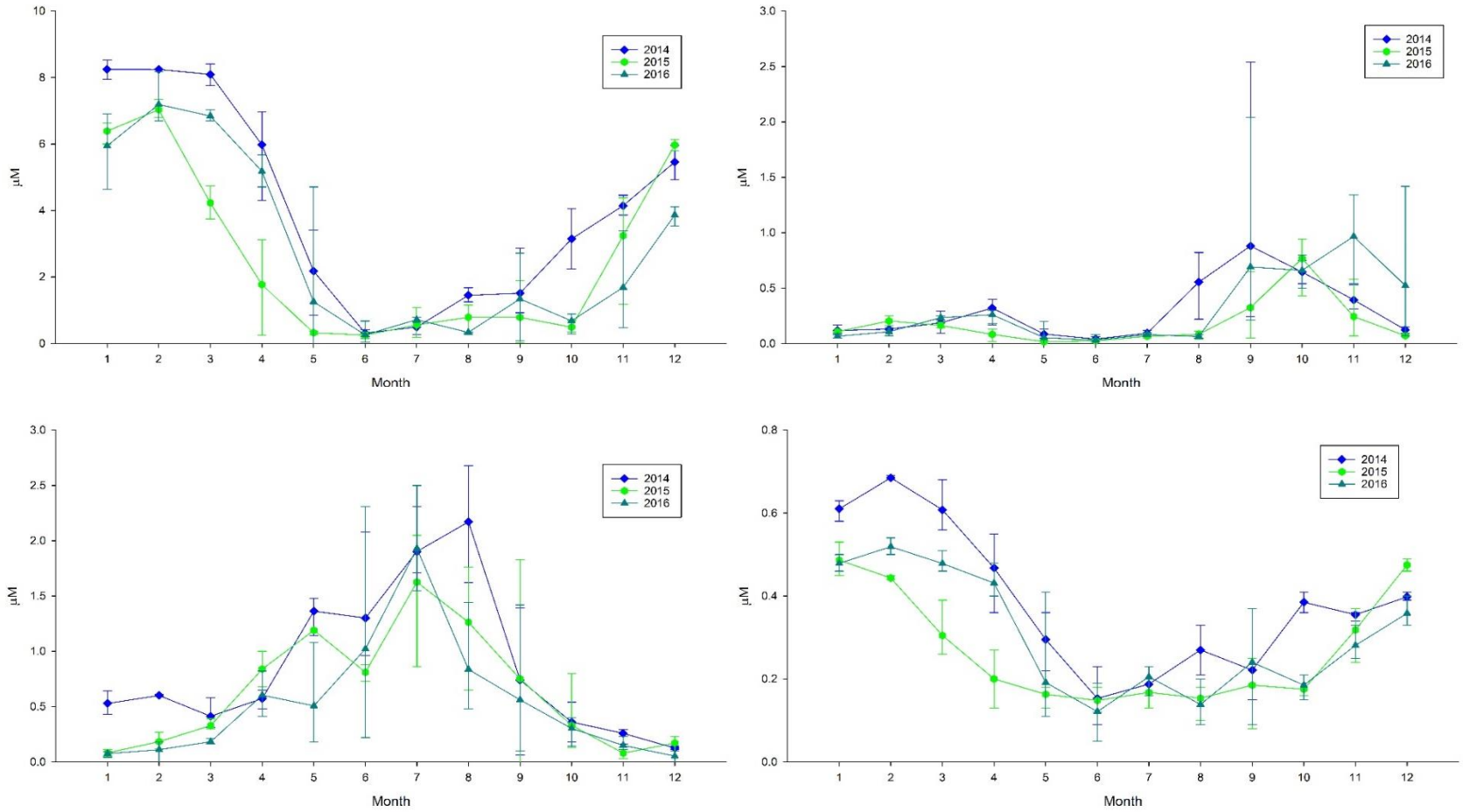

Figure 3.8. Long term L4 time series data at 50 m, months 1-12 (Jan-Dec) for 2014-2016 including a) Nitrate concentration (µM), b) Nitrite concentration (µM), c) Ammonia concentration (µM), d) Phosphate concentration (µM)

The relationship between nitrate and salinity at L4 was variable between each of the two winter periods sampled (Figure 3.9). During winter 2014 to 2015, there was no relationship between nitrate and salinity in surface and bottom waters at L4. Salinity was particularly low in surface waters on 27th January 2015, at 34.83 PSU (Figure 3.9a). During the winter of 2015 to 2016 linear regression highlighted that there was a relationship between nitrate and salinity in the surface ($y= -9.5237x + 338.56$, $r^2 = 0.34$, $p = \leq 0.05$) and bottom waters ($y = -22.412x + 793.33$, $r^2 = 0.69$, $p = \leq 0.05$) (Figure 3.9b). The increase in nitrate from close to zero to over 8 µM at 50 m was associated with a decrease in salinity of almost 0.3, while the increase in nitrate at the surface from close to zero to 7.3 µM was associated with a decrease in salinity of over 0.2 (Figure 3.9b).

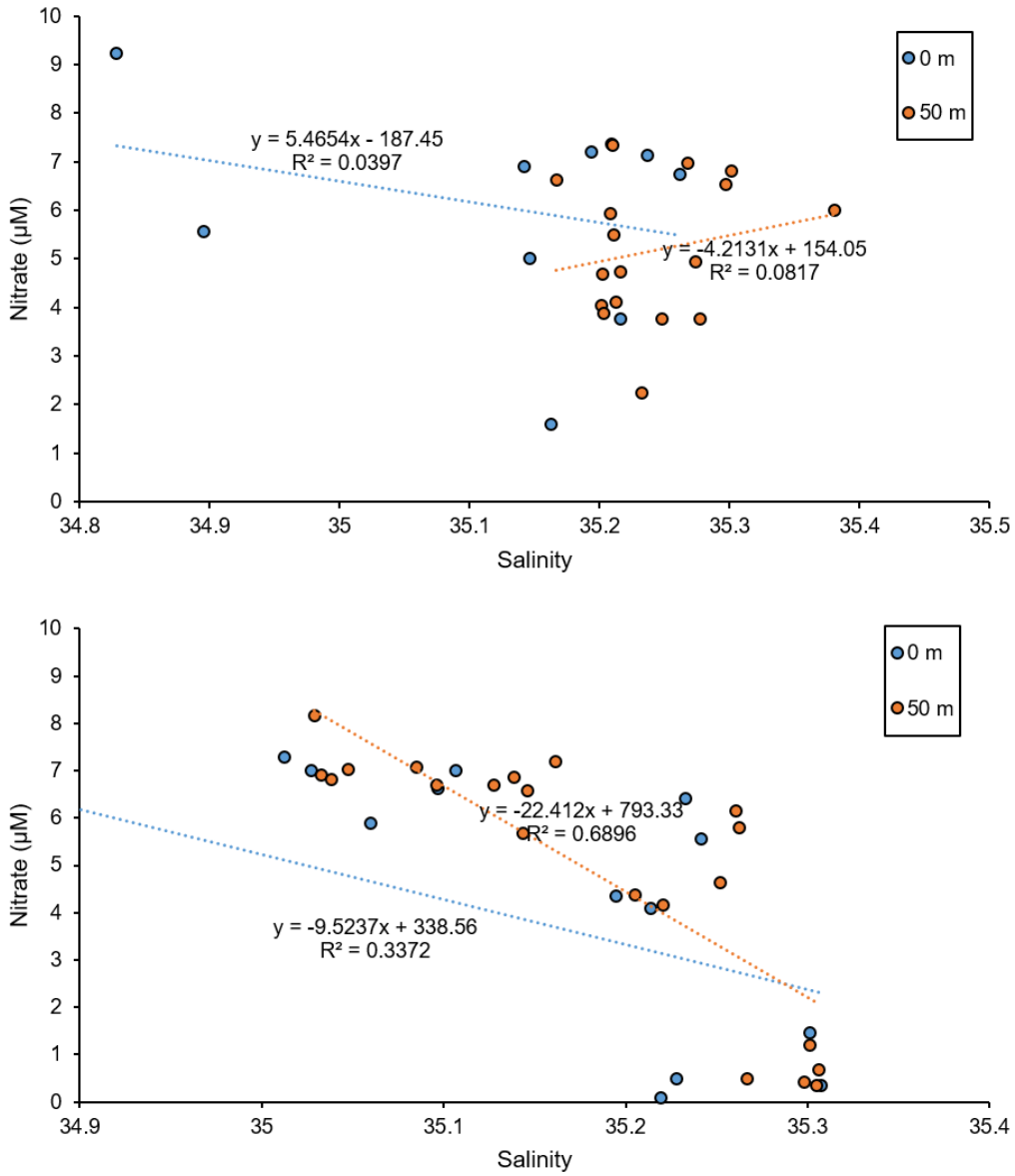

Figure 3.9. The salinity nitrate relationship in wintertime transition periods (a) October 2014 to March 2015, (b) October 2015 to March 2016

3.3.3 Stable isotopes of nitrate

Over the time period sampled, the $\delta^{15}N$ and $\delta^{18}O$ of nitrate ranged from 5.8 ‰ to 10.2 ‰ and 4.3‰ to 17.8 ‰, respectively (Figures 3.10a, 3.10b). From December 2014 to February 2015, winter time values of $\delta^{15}N$ in surface waters were constant at 6.7 ± 0.2 ‰. The $\delta^{15}N_{NO3}$ then increased to 8.7 ‰ and 8.6 ‰ during March and April 2015, respectively. The following winter, the $\delta^{15}N_{NO3}$ increased more gradually from 6 ‰ in November 2015 to 6.9 ‰ in March, and then increased

rapidly to a maximum of 9.9 ‰ in April. The $\delta^{15}N$ at 50 m showed a similar pattern to the surface during the winter 2014 to spring 2015 transition, rapidly increasing from 6.5 ± 0.2 ‰ December 2014 and February 2015 to a maximum of 10.2 ‰ during April. Between 2015 and 2016, the $\delta^{15}N_{NO3}$ at 50 m also increased from a mean of 6.3 ± 0.2 ‰ between November 2015 and February 2016 to mean of 8.3 ± 0.2 ‰ in April/May 2016, reaching a maximum of 8.5 ‰ in May 2016 (Figure 3.10a).

During the winter 2014 to spring 2015 period, the surface $\delta^{18}O_{NO3}$ ranged from a minimum of 7.4 ‰ in February 2015 to 17.8 ‰ in April 2015 (Figure 3.10b). Between December 2014 and March 2015 $\delta^{18}O$ fluctuated between 12.7 ‰ and 7.4 ‰. The winter 2015 to spring 2016 period was less variable than the previous year. Surface $\delta^{18}O$ was below 6 ‰ in November 2015 and March 2016, with a minimum $\delta^{18}O$ value of 4.3 ‰ in January, and a rapid increase during March and April to a maximum value of 11‰ in May (Figure 3.10b).

$\delta^{18}O$ at 50 m increased from 8.3 ‰ at the start of December 2014 to an average of 10.9 ± 0.3 ‰ during December and January. ^{18}O values then decreased during February to 7.4 ‰ before increasing to 13.4 ‰ in April 2015. During the winter 2015 to spring 2016 period $\delta^{18}O$ was low in November and December with a mean value of 4.5 ± 0.1 ‰. Throughout February, March and April there was an increase in $\delta^{18}O$ to a maximum of 10.1 ‰ in May 2016 (Figure 3.10b).

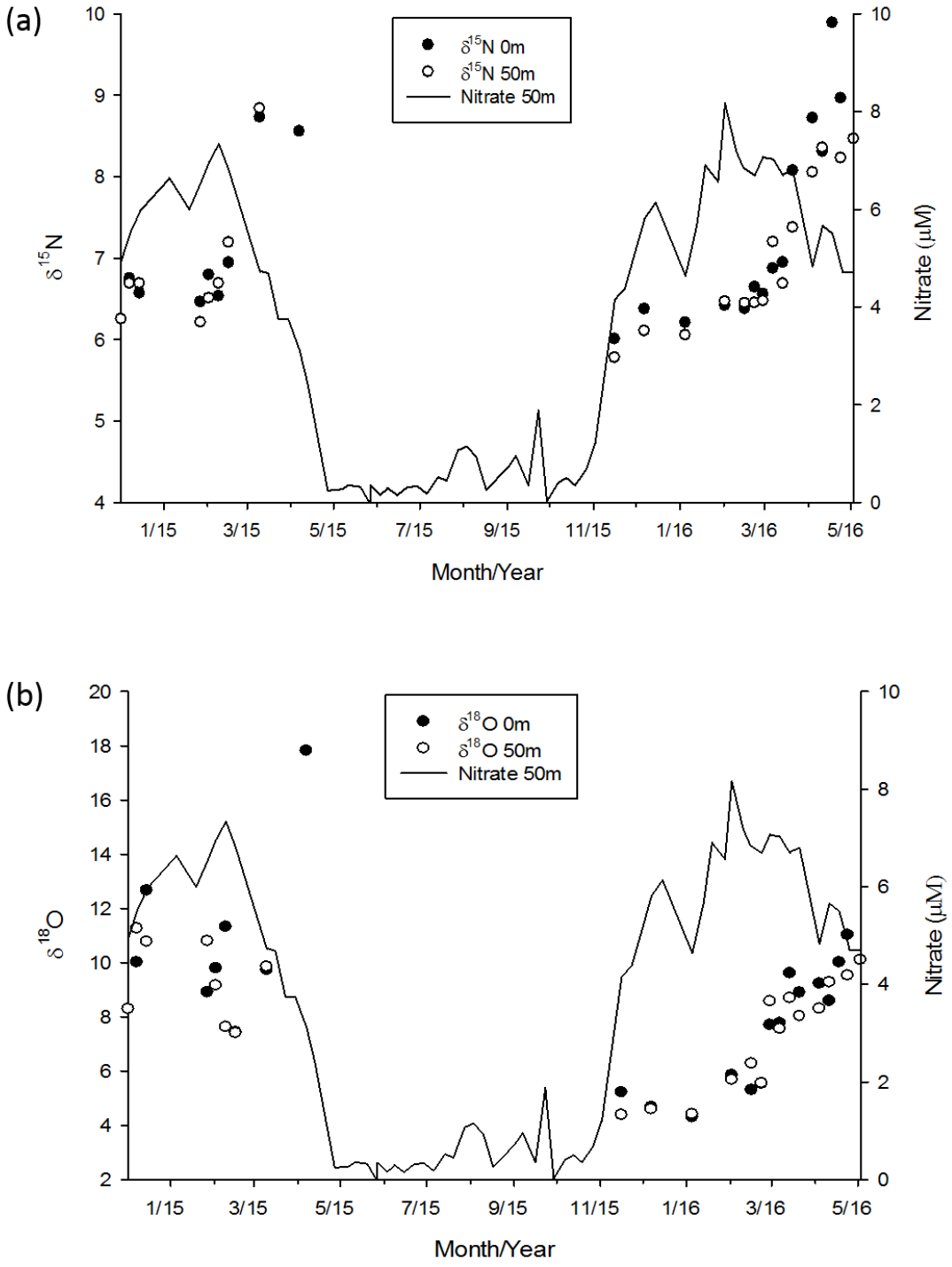

Figure 3.10. $\delta^{15}N$ (a) and $\delta^{18}O$ (b) of nitrate between December 2014 and May 2016 at L4. Solid Line denotes nitrate at 50 m depth between December 2014 and May 2016.

Linear regression highlights the relationship of $\delta^{15}N_{NO3}$ with both nitrate and dissolved oxygen concentrations (Figure 3.11a, 3.12a, 3.12c). Generally, as nitrate concentration decreased $\delta^{15}N_{NO3}$ increased as expected during Rayleigh fractionation

dynamics, although the increase in $\delta^{15}N_{NO3}$ was slightly below the expected curve (Figure 3.11a). Over the winter period in 2014 to 2015 and 2015 to 2016, there was a small increase in $\delta^{15}N_{NO3}$ of 0.9 ‰ and 0.3 ‰ as winter nitrate concentrations increased (Figure 3.10a, 3.11a), with these changes being greater than the precision of analysis (0.1 ‰). Multiple linear regression analyses showed that 69 % of the variation in surface $\delta^{15}N_{NO3}$ could be explained by the change in the natural log of nitrate concentration and dissolved oxygen concentration (R^2 = 69 %, p = 0.001). At 50 m multiple linear regression analyses showed that 85 % of the variation in $\delta^{15}N_{NO3}$ could be explained by the change in the natural log of nitrate concentration and dissolved oxygen concentration (R^2 = 85 %, p = <0.001).This is indicative of a nutrient uptake signal according to Rayleigh fractionation kinetics.

The relationships between $\delta^{18}O_{NO3}$ and nitrate, and dissolved oxygen concentrations were weaker than observed for $\delta^{15}N_{NO3}$ (Figure 3.11b, 3.12b, 3.12d). This relationship was similar to $\delta^{15}N_{NO3,}$ as nitrate concentration decreased $\delta^{18}O_{NO3}$ increased as expected during Rayleigh fractionation dynamics (Figure 3.11b). $\delta^{18}O_{NO3}$ increased during winter from 4.5 ‰ (at 50 m) in January 2016 to 6 ‰ in March 2016 as nitrate concentrations increased (Figure 3.10b, 3.11b). In contrast, $\delta^{18}O_{NO3}$ decreased during the previous winter as nitrate increased (Figure 3.10b, 3.11b). Only 39 % of the variation in surface $\delta^{18}O_{NO3}$ could be explained by the natural log of nitrate concentration and dissolved oxygen concentration (R^2 = 38 % p (O_2) = 0.016, p (NO_3 conc.) = 0.061) with only oxygen concentration being statistically significant. $\delta^{18}O_{NO3}$ showed no significant correlation with either nitrate concentration or dissolved oxygen concentration at 50 m depth (Figure 3.11d).

There were two main patterns observed in $\delta^{15}N_{NO3}$ to $\delta^{18}O_{NO3}$ relationship. Firstly, there was a 1:1 relationship between $\delta^{15}N_{NO3}$ to $\delta^{18}O_{NO3}$ associated with Rayleigh fractionation during uptake of nitrate (Figure 3.11c). Secondly, there was a larger increase in $\delta^{18}O_{NO3}$ relative to $\delta^{15}N_{NO3}$, lying close to a 3:1 ratio (Figure 3.11c), likely indicating both uptake of nitrate and nitrification occurring at L4 together.

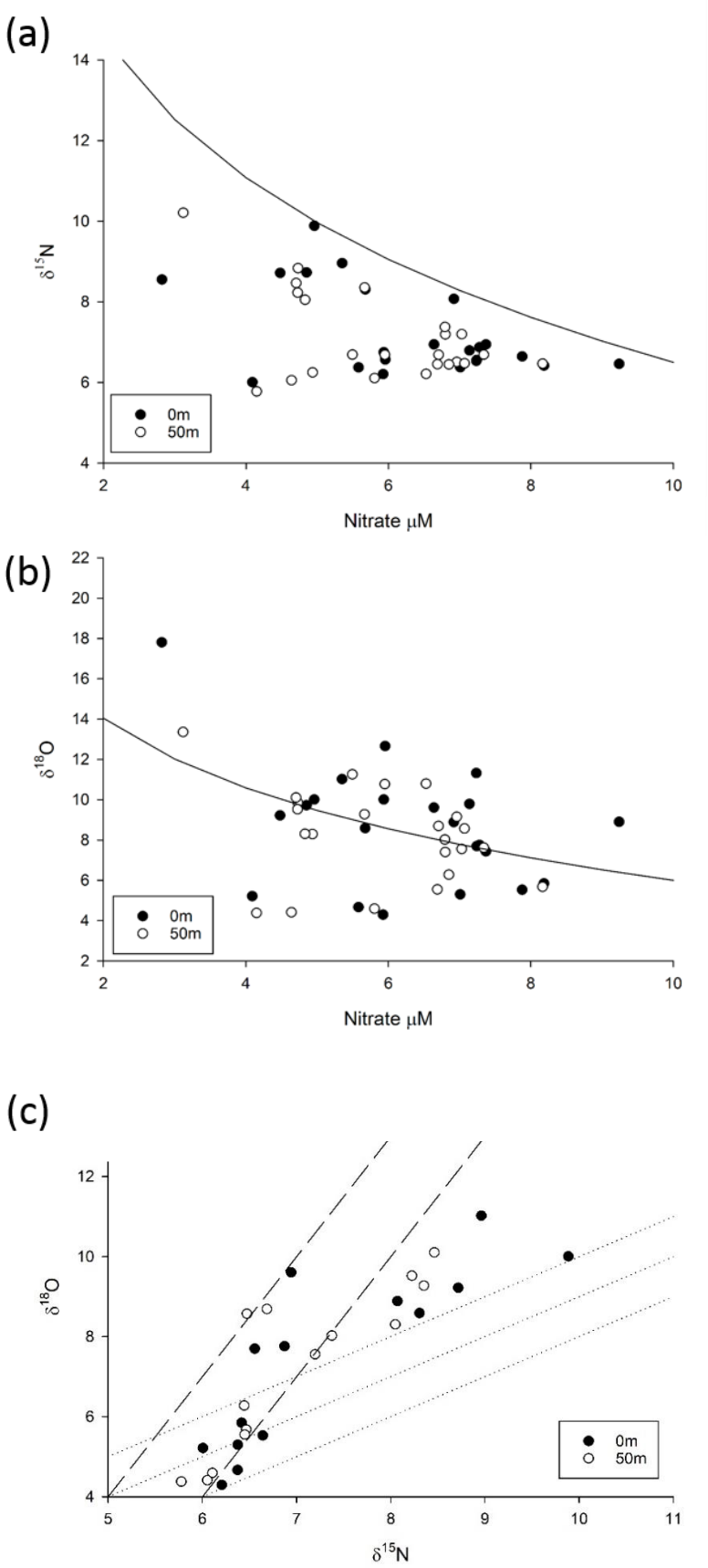

Figure 3.11. a) $\delta^{15}N_{NO3}$ vs. nitrate with Rayleigh fractionation line, b) $\delta^{18}O_{NO3}$ vs. nitrate with Rayleigh fractionation line and c) $\delta^{15}N_{NO3}$ vs. $\delta^{18}O_{NO3}$ with 1:1 dotted lines and 3:1 dashed lines for L4 between December 2014 and May 2016.

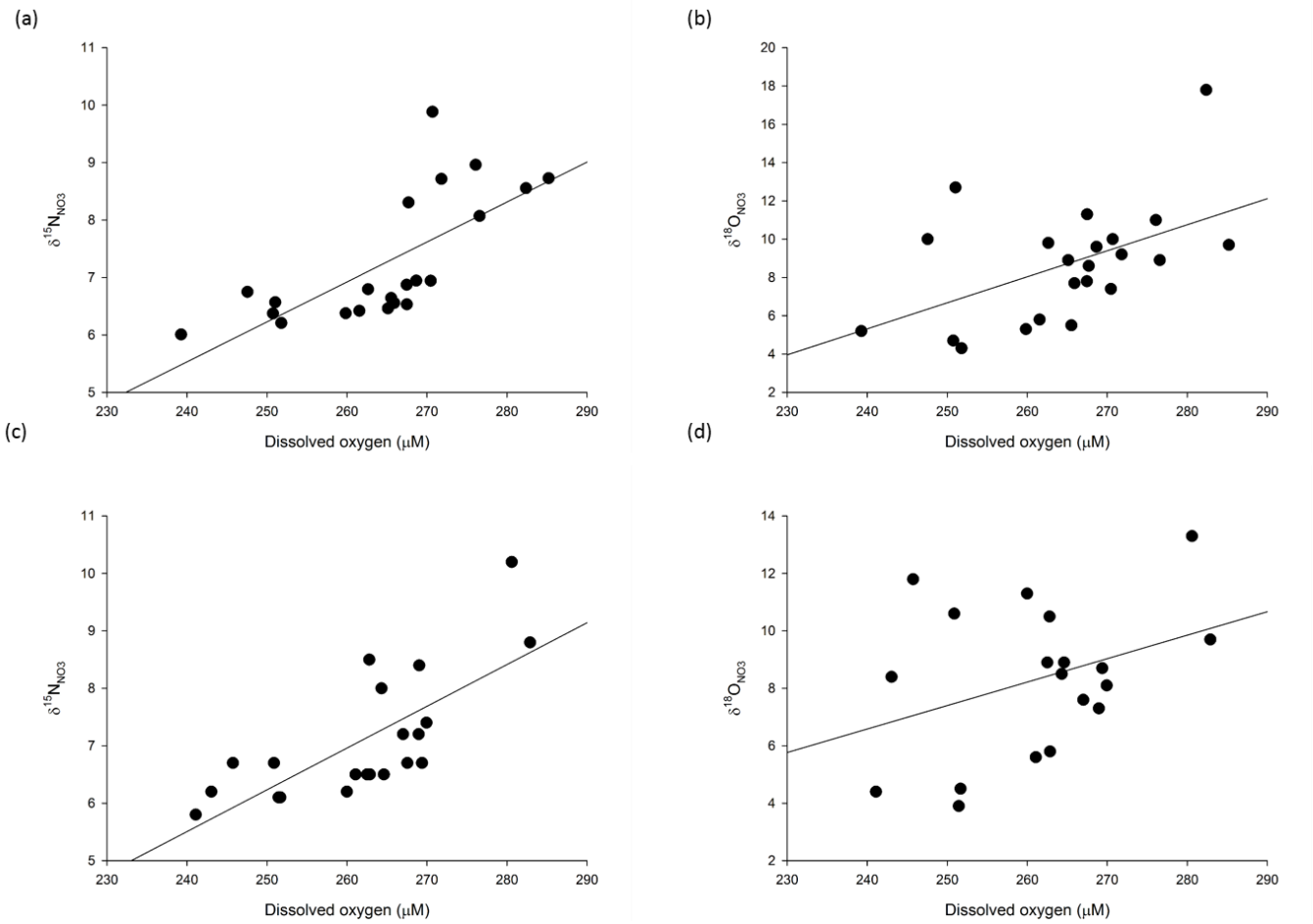

Figure 3.12. The $\delta^{15}N_{NO3}$ (a) and $\delta^{18}O_{NO3}$ (b) and dissolved oxygen for surface waters, and the $\delta^{15}N_{NO3}$ (c) and $\delta^{18}O_{NO3}$ (d) and dissolved oxygen at 50 m.

3.4 Discussion

The L4 site provided a well-studied region to investigate the potential of stable isotopes of nitrate to determine the sources of nitrate to the site and the physical, chemical and biological processes occurring throughout the year. $\delta^{15}N_{NO3}$ and $\delta^{18}O_{NO3}$ were sampled throughout the year, capturing the autumn to winter and winter to spring transition over the years 2014 to 2015 and 2015 to 2016. $\delta^{15}N_{NO3}$ and $\delta^{18}O_{NO3}$ could not be measured during the spring to summer and summer to autumn periods when nitrate concentrations were consistently below 1 µM. As a result, the main biological process captured was the spring bloom period.

3.4.1 Phytoplankton assimilation and *in-situ* remineralisation

During the spring period for each year there were exponential increases in both $\delta^{15}N_{NO3}$ and $\delta^{18}O_{NO3}$ at close to a 1:1 ratio in both the surface and at 50 m. Maximum values were over 10 ‰ for $\delta^{15}N_{NO3}$ and over 12 ‰ for $\delta^{18}O_{NO3}$. This increase in both $\delta^{15}N_{NO3}$ and $\delta^{18}O_{NO3}$ is most likely associated with the uptake of nitrate by phytoplankton, as it is one of the two processes (along with denitrification) to increase both the $\delta^{15}N_{NO3}$ and $\delta^{18}O_{NO3}$ at a 1:1 ratio (Sigman et al. 2009a). It is unlikely that denitrification was responsible for the enrichment in both $\delta^{15}N_{NO3}$ and $\delta^{18}O_{NO3}$ because the waters were well oxygenated (Figure 3.9c, 3.10c) and the change in both $\delta^{15}N_{NO3}$ and $\delta^{18}O_{NO3}$ was much lower than would be expected from the isotope effect by denitrification (ε =25-30%)(Sigman et al. 2009a). The main onset of the spring bloom occured during April as the water column begins to stratify but before the thermocline becomes permanently established (Pingree and Maddock 1977). During the time period where isotopes were measured there were similar dates for the onset of stratification as observed in previous years with the median date being 23rd April (Smyth et al. 2009). There was strong nitrate depletion in both the surface waters and at 50 m during April, with nitrate being consistently below the limit of detection between May and August. The length of the spring bloom is primarily controlled by the concentration of nitrate, and its subsequent exhaustion (Pingree and Griffiths 1978).

Rayleigh fractionation is likely the best way to describe the uptake signal at L4 during the spring bloom period as it describes isotope fractionation in a closed system where the reactant and product pools of nitrogen are not replenished or lost from the system. Using equation 1.3 (Chapter 1, Section 1.6) for 2015 to 2016, assuming a winter time $\delta^{15}N_{NO3}$ value of 6.4 ‰ as the initial value and a surface water winter maximum concentration of 8.3 µM, I can calculate the isotopic fractionation factor for the surface waters as nitrate is used up towards the end of April. The ε value was approximately 5.4 ‰ in the surface waters at L4. The ε value for the year 2014 to 2015 was 4.9 ‰ and was similar to 2015 to 2016 taking a winter time $\delta^{15}N_{NO3}$ value of 6.8 ‰ as the initial value and a surface water winter maximum concentration of 7.3 µM. These fractionation factors are in agreement with the accepted ε values for phytoplankton uptake (ε=5 ‰). There was a strong relationship between the $\delta^{15}N_{NO3}$ and the dissolved oxygen and nitrate concentration, which is a good indicator that nitrate assimilation was the dominant process taking place. The spring bloom uptake signal was observed in both the surface and bottom waters at L4 along with a corresponding decrease in both surface and bottom water nitrate concentrations. This indicated that the production signal is mixed throughout the water column as stratification was weak.

Stratification at L4 is not primarily driven by temperature with tidal and wind-mixing events being important (Huisman et al. 1999; Lewis and Allen 2009). The critical turbulence threshold is also likely to be as important as the critical depth in determining phytoplankton growth at L4 due to the water column being weakly stratified even in summer (Huisman et al. 1999; Lewis and Allen 2009). This weak stratification extends to depths of approximately 20 m during the summer months of June, July and August, before this stratification breaks down in September. This weak stratification means that unlike in more open shelf or open ocean regions, the nitrate concentration is depleted at both the surface and at depth, this results in the regeneration signal in the stable isotopes during the summer and autumn periods being mixed with any uptake signal from phytoplankton. Also as the nitrate concentrations are particularly low this means that any nitrate regenerated *in situ* is likely assimilated immediately meaning that no detectable signal can be measured using $\delta^{15}N_{NO3}$ and $\delta^{18}O_{NO3}$. It is likely that *in situ* remineralisation is taking place as

evidenced by the decline in oxygen saturation during the summer and autumn periods, particularly in the bottom waters.

During the 2014-2015 period there was also evidence of a much greater increase in $\delta^{18}O_{NO3}$ compared to $\delta^{15}N_{NO3}$. This is unlikely to be caused by assimilation alone. This particularly enriched $\delta^{18}O_{NO3}$ may be due to the source of the nitrate e.g. riverine or rainwater, however the increase at close to a 3:1 ratio implies that there was simultaneous nitrate assimilation and nitrification taking place in the water column, this has previously been observed in Monterey Bay, California (Wankel et al. 2007). Their model highlighted that multiple nitrogen cycling processes were occurring in the surface waters which highlighted the importance of ammonium consumption in which ammonium served as a substrate for nitrification (Wankel et al. 2006; Wankel et al. 2007). Their observations indicated that between 15 and 27 % of surface production was supported by nitrification in surface waters. Branching between nitrification and phytoplankton ammonium uptake despite potentially exerting a strong control on nitrate isotopic composition is relatively under studied (Wankel et al. 2007). Similar results were reported in the East China Sea, with water in the Subei shoal coastal region having a similar 3:1 increase, which suggested that the change in isotopes could arise not only from the mixing of water masses but also from the influence of nitrification in the presence of nitrate assimilation (Yuan et al. 2008; Liu et al. 2017).

3.4.2 Sources of nitrate

There was a typical seasonal cycle in nutrient conditions as expected at a temperate coastal site like L4. During the winter period the nutrient stock was reset to the yearly maximum. The supply of nitrate (and phosphate) set the upper limit of the spring bloom, which occured in April. Periods of low salinity, particularly during the winter are likely associated with periods of heavy outflow from the River Tamar (Siddorn et al. 2003). The relative influence of the Tamar river run-off is dependent on tidal range and the strength of the run off (Pingree and Griffiths 1978; Lewis and Allen 2009). The surface waters were more strongly influenced by the fresh water fluxes from the Tamar. Changes in maximum yearly nutrients and sporadic increases in nutrients at L4 are in part driven by the fluvial input from the Tamar (Rees et al. 2009a; Rees et al. 2009b). The system at L4 appeared to be predominantly nitrate

limited in regard to phytoplankton net growth, as phosphate was usually detectable throughout the summer months when nitrate concentrations approached zero. Only the sporadic fluvial inputs from the Tamar alleviated the nitrogen limitation during the summer (Rees et al. 2009b; Widdicombe et al. 2010). The breakdown of stratification and increased mixing events start to replenish nitrate to the surface waters during September.

Variations between the yearly maximum nutrient concentrations throughout the time series, and the changes in $\delta^{15}N_{NO3}$ and $\delta^{18}O_{NO3}$ over the winter period as a result of the different sources of nitrate to L4. There are several sources of nitrate to L4 outlined here:

1) Nitrate supplied from the open shelf via tidal intrusion into the English Channel.
2) Nitrate supplied via freshwater influence from the River Tamar.
3) Rainfall events (although increased rainfall will likely be associated with increased outflow from the River Tamar).
4) Nitrate remineralised *in situ* or from the sediments

Nitrate from different sources will have different end members, and the nitrate at L4 will be a combination of these. The sources of nitrate can be quantified using $\delta^{15}N_{NO3}$ and $\delta^{18}O_{NO3,}$ in conjunction with salinity and rainfall data. The increase in nitrate over the winter period during 2015 to 2016 was associated with an approximate decline of 0.3 in salinity at 50 m from 35.3 to 35, indicating that the supply of nitrate at L4 had a freshwater component from the Tamar. From November to March when stable isotopes could be measured the decrease in salinity was 0.2, from 35.2 to 35. This corresponded to an increase in nitrate from approximately 4 µM to 8.5 µM. Concomitantly, the $\delta^{15}N_{NO3}$ increased from 6 ‰ in November to 6.9 ‰ before the spring bloom, indicating a high $\delta^{15}N_{NO3}$ value associated with freshwater input from the Tamar. If I take Site E1 as an oceanic end-member where maximum nitrate concentrations only increased from 4 µM to 6 µM in spring, compared to L4 where maximum concentrations reach 8.5 µM in spring, then at least 2.5 µM of the nitrate supplied is of riverine origin. The riverine supply of nitrate at least 30 % of the total nitrate supplied at L4, giving a riverine $\delta^{15}N_{NO3}$ of 9 ‰. The 1.5 ‰ increase in $\delta^{18}O_{NO3}$ over the same time period would result in a riverine end member of 9.5 ‰.

During the previous year 2014 to 2015, there was no relationship between the increased nitrate and salinity, implying a lower contribution of a riverine nitrate. Rainfall between November 2014 and March 2015 was lower than 2015 – 2016; only 422 mm of rainfall fell compared to 503 mm. Lower rainfall would suggest less riverine input to L4.

Another potential source of nitrate to L4 is direct rainwater inputs. However, increased rainfall would also increase riverine input making it difficult to separate the two. Neglecting any mixing effects I can calculate the volume of rainwater required for a specific change in salinity and therefore the rainfall required to alter the isotopic concentration of the $\delta^{18}O_{NO3}$ in the water column using the following equation:

$$ppt = ((ppt0)*((h-d)/h)) + ((ppt\_rain)*(d/h)) \qquad \text{Eqn. 3.1}$$

Where ppt is the current depth-averaged salinity, and ppt0 is the initial salinity in a water-column with depth h (m) after a rainfall event (d; (m)). In this case, ppt_rain is the salinity (or $\delta^{18}O_{NO3}$/Nitrate concentration) of rainwater. Taking the total known rainfall over the winter period for 2015-2016 of approximately 0.5 m, and assuming a nitrate concentration of rainwater to be 20 mmol m^3, and a $\delta^{18}O_{NO3}$ of rainwater of 70 ‰ (Mayer et al. 2002; Hastings et al. 2003) then the rainfall between November and March has the potential to raise the $\delta^{18}O_{NO3}$ of the water column by the 1.5 ‰ observed in this study, and add 0.14 mmol m^3 of nitrate. It is likely that direct rainfall input and indirect input via rivers provide the means to raise the $\delta^{18}O_{NO3}$ over the winter period to the levels observed before the spring bloom.

Finally, nitrate may be remineralised *in situ* or from the sediments. As previously mentioned due to low levels of nitrate during the summer period and the weak stratification meaning that the water column is more mixed it makes it difficult to calculate a proportion of remineralised nitrate at L4. Any nitrate supplied from the sediments is unlikely to alter the isotopic ratio as sedimentary denitrification has an isotopic effect of 0 ‰ (Casciotti 2016).

3.4.3 Implications

Coastal and shelf environments are extremely important supporting large fisheries and providing numerous ecosystem services. Understanding the supply of

nitrate (and other macro nutrients) to the coastal environments is important. The management and health of these systems relies on an in depth understanding of the nutrient supply that fuels them. Current changes caused by anthropogenic impacts have the potential to change the functioning of these environments beyond the scope of natural variation. As L4 is a long term time-series changes can be quantified, understood, and potentially used to alter global policy on how coastal environments are utilised and protected. Several of these anthropogenic impacts could cause large changes to the nitrogen cycle in coastal regions.

Between 2013 and 2017 there was an overall decline in mean bottom water oxygen saturation (approximately 1 % each year) at the L4 site coinciding, with a decline in the N:P ratio (from 13.8 to 11.2) over the same time period (Table 3.1). The loss of nitrate relative to phosphate from L4 indicates a potential increase in denitrification and/or decrease in nitrification. These changes could potentially be linked to anthropogenic impacts on the coastal zone through inputs of nitrogen.

Since the industrial revolution the atmospheric carbon dioxide levels have increased due to human activity by almost 40 % (Sitch et al. 2015). This increase has been mitigated by the ability of the oceans to absorb carbon dioxide. However, the process has led to a decrease in surface-ocean pH by approximately 0.1 units. Current climate models predict that for the open ocean there may be a further decrease of 0.35 units by 2100. Coastal zone acidification rates are an order of magnitude greater than that observed in the open ocean (Waldbusser and Salisbury 2014). There is increasing evidence that in particular benthic biogeochemical cycling is affected by changes in pH. Laboratory investigations mimicking a decrease of 0.3 units reduced the sediment community oxygen consumption by 60 % and benthic nitrification rates by 94 % in a pre-spring bloom period. Benthic nitrification is and extremely important component of the nitrogen cycle making up a large proportion of ocean nitrification (Wyatt et al. 2010; Kitidis et al. 2011). Any reduction in this cycling may have global impacts on the balance of nitrification and denitrification and the supply of nutrients to the water column. Decreased pH is also expected to impact pelagic nitrification rates with a possible reduction in ammonium oxidation rates of 0.195 d^{-1} to 0.171 d^{-1} by the 2100 (Yool et al. 2007; Kitidis et al. 2011; Rees et al. 2016). Studies specific to the North West European Shelf predicted a 20 % reduction in North Sea water column nitrification rates at atmospheric carbon dioxide

concentrations of 1000 ppm (Blackford and Gilbert 2007). These changes have the potential to cause changes in the phytoplankton community, and impact future fisheries yields in shelf waters (Van Leeuwen et al. 2016).

Coastal environments have also been subject to greater nutrient loading with nitrogen inputs doubling in the past 50 years (Smith et al. 2003; Jickells et al. 2017). Increased nitrogen fluxes into coastal areas have led to widespread hypoxia. Denitrifying bacteria thrive in low oxygen environments and remove nitrate from the water. Hypoxic regions are also know to exacerbate ocean acidification because the consumption of oxygen driving hypoxia is coupled with the production of DIC including carbon dioxide gas (Gypens et al. 2011).

3.4.4 Conclusions

Overall the results from L4 indicate the potential for the stable isotopes of nitrate to be used investigate the uptake signal from phytoplankton and provide quantitative information on the potential sources of nitrate. Using station E1 as an oceanic end member, the nitrate available for primary production during the spring bloom period at L4 from a riverine source was calculated. At least 2.5 µM of the nitrate at L4 was from a riverine origin, with isotopic end members calculated at 9 ‰ for $\delta^{15}N_{NO3}$ and 9.5 ‰ for $\delta^{18}O_{NO3}$. This confirms the hypothesis that a proportion of the nitrate available for the spring bloom at L4 is from a riverine source. However, the limitations of using the method in a relatively mixed environment are highlighted as due to no clear separation in the surface and bottom water signals it is difficult to quantitatively separate the production signal from a regeneration signal, although there is evidence for assimilation and nitrification occurring at the same time. Also, as nitrate is depleted to below 1 µM, and often below detectable levels across the entire water column from late spring to autumn it makes the current denitrifier method used at Liverpool only useful during the autumn to spring bloom period when nitrate concentrations are higher. If the method was developed to use manual injections with larger volumes of sample then the time-series could be expanded into periods of lower nitrate concentration giving a more complete seasonal cycle in nitrate.

Chapter 4. Sources and cycling of nitrate in the Celtic Sea

4.1 Introduction

Shelf seas are important in the global nutrient and carbon cycles, with shelf seas in general being a net sink for carbon. The strong primary production in shelf seas leads to an annual drawdown of carbon dioxide from the atmosphere (Thomas et al. 2004). Shelf seas cover less than 8 % of the global ocean surface area, but are responsible for between 15-30 % of global ocean primary production (Wollast 1998; Simpson and Sharples 2012; Bauer et al. 2013). The Celtic Sea is a broad temperate shelf sea located to the south-west of the United Kingdom and south of Ireland. The strong seasonal cycle driven by the development of a seasonal thermocline and increased light drives a short intense spring bloom event. The surface mixed later (SML) and bottom mixed layer (BML) are separated by the seasonal thermocline which is strongest in the summer. Autotrophic processes dominate the SML with nutrient concentrations being low for much of the year when the water column is stratified. In contrast, the BML is dominated by respiratory processes and bacterial remineralisation of organic matter meaning nutrients are higher. During the winter, production in temperate shelf seas is limited by low solar insolation, while after the onset of seasonal stratification fixed nitrogen availability is the limiting factor for growth (Simpson and Sharples 2012).

The Celtic Sea is an important region for shelf-deep water exchange with exchange estimated at 3 $m^2 s^{-1}$, comparable to the Hebrides Shelf, and slightly lower than the North Sea where exchange has been estimated at 4 $m^2 s^{-1}$ (Holt et al. 2009; Huthnance 2010). There are strong internal tides at the shelf edge that can carry on-offshore exchange up to 1.3 $m^2 s^{-1}$. These internal tides mix and diffuse the cooler water below the surface mixed layer causing enhanced production at the shelf edge during the summer months (Joint et al. 2001). Ekman flow down the shelf slope provides a route for sediment transport off shelf (McCave et al. 2001).

The aim of this study was to investigate the nutrient supply, cycling and remineralisation across the Celtic Sea over a seasonal cycle using the stable isotopes $\delta^{15}N_{NO3}$ and $\delta^{18}O_{NO3}$. I present $\delta^{15}N_{NO3}$, $\delta^{18}O_{NO3}$ and $\delta^{15}N_{PN}$ from four process cruises (DY018, DY021, DY029 and DY033) across the Celtic Sea during 2014 and

2015 (Figure 4.1). I used $\delta^{15}N_{NO3}$, $\delta^{18}O_{NO3}$ data alongside temperature, salinity, oxygen and inorganic nutrient data to understand both the surface and bottom layer nutrient processes and to quantify the extent of nutrient remineralisation across the Celtic Sea over an annual cycle. The $\delta^{18}O_{NO3}$ stable isotope proxy for nitrogen regeneration processes was compared to estimates from apparent oxygen utilisation (AOU) allowing estimation of nutrient remineralisation from oxygen depletion. Comparisons were made to similar shelf sea dual isotope studies (Granger et al. 2013; Liu et al. 2017). The estimates of on shelf remineralisation can help better understand the nitrogen cycle for the Celtic Sea and consequently how much nitrate and carbon is supplied from the open ocean or regenerated *in situ* on shelf to maintain production.

The specific hypothesis investigated was that a large proportion of the nitrate across the Celtic Sea was derived from *in situ* regeneration of nitrate with a limited supply from the open ocean.

4.2 Methods

Four pelagic focused cruises collected samples for stable isotope analysis included in this chapter (Table 4.1). Each of these four cruises provided a snapshot of a different time-period relevant to the shelf sea nutrient cycle. DY018 captured the autumn bloom and the beginning of the breakdown of stratification in November and December 2014. DY021 captured the well mixed winter waters preceding the onset of stratification during March 2015. DY029 captured the onset of stratification and the spring bloom during April 2015 and DY033 captured the summer period of strong stratification in July 2015. The sampling strategy included: (a) repeat visits to 3 main stations, Site A, CCS and CS2, (b) on shelf transects, O and J and (c) cross shelf edge transects (Figure 4.1).

Table 4.1 Process cruises undertaken during the SSB sampling campaign

Cruise	Dates
DY018	09/11/14 to 02/12/14
DY021	01/03/15 to 26/03/15
DY029	01/04/15 to 30/04/15
DY033	11/07/15 to 03/08/15

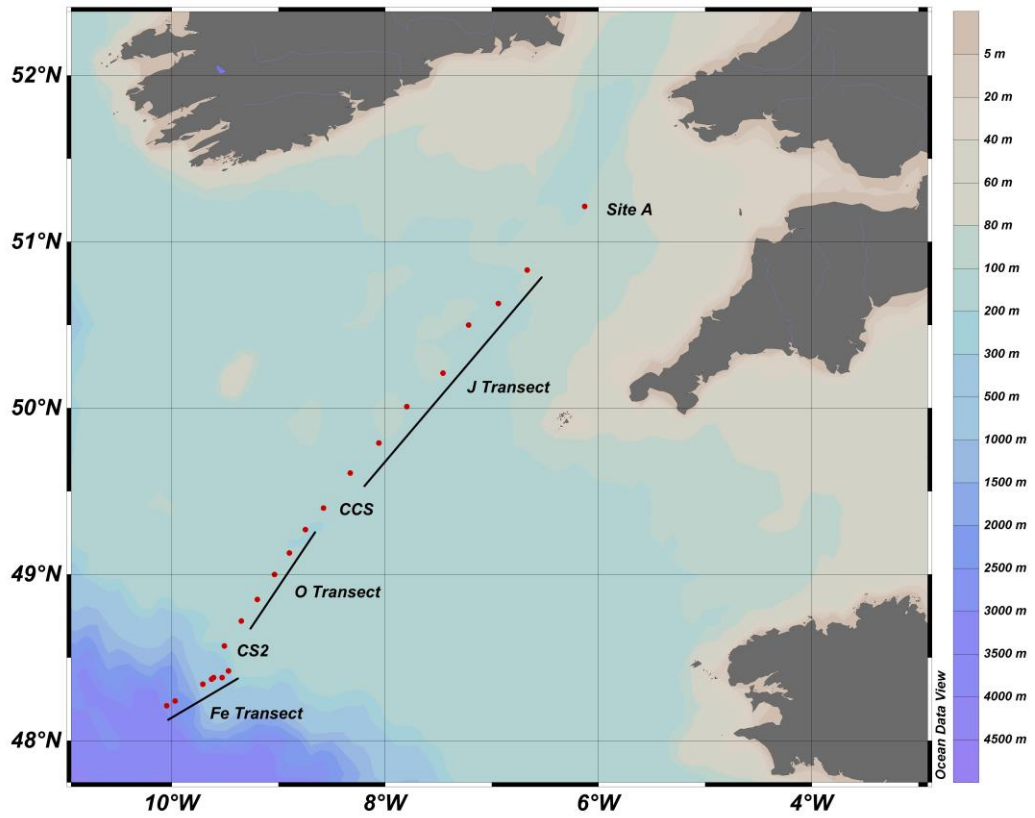

Figure 4.1 Celtic Sea process stations (CS2, CCS, and Benthic A), and transects (O, J and Fe) visited during each of the SSB process cruises during 2014 and 2015. Map generated with Ocean Data View (Schlitzer 2002).

Seawater samples were collected using a seabird CTD equipped with a 24-bottle rosette of 20L Niskin bottles. Seawater samples for $\delta^{15}N_{NO3}$ and $\delta^{18}O_{NO3}$ were filtered through Whatman glass fibre filters (GF/F, 0.7 µm pore size, pre-combusted at 450 ˚C for 4 hrs before acid washing, deionized water rinsing, and drying at 50 ˚C) into 60 ml HDPE (high density polyethylene) bottles and were stored frozen at -20 ˚C until analysis. Samples for the analysis of particulate nitrogen isotopes were collected by filtering between 1 L and 3 L of seawater onto a Whatman glass fibre

filter (GF/F 0.7 µm, prepared as above), stored frozen at -80 ˚C until analysis. Samples for $\delta^{18}O$ H_2O analysis were collected on DY029 and filtered through Whatman glass fibre filters (GF/F, 0.7 µm pore size, pre-combusted at 450 ˚C for 4 hrs before acid washing, deionized water rinsing, and drying at 50 ˚C) into 500 ml HDPE bottles with no headspace and stored in the fridge at <4 °C until analysis at the British Geological Survey.

Inorganic nutrients (nitrate+nitrite, nitrite, ammonium, phosphate and silicate) were collected via CTD sampling. Samples were collected from all sampled depths and refrigerated at 4 °C until analysis. Samples were analysed using standard colormetric autoanalyzer techniques (Brewer and Riley 1965; Mantoura and Woodward 1983; Kirkwood 1989; Zhang and Chi 2002). Dissolved oxygen concentrations were measured using Winkler whole bottle technique with an estimated accuracy of ±0.3 µmol kg^{-1}. These discrete measurements were used to calibrate the Seabird-43 dissolved oxygen sensor attached to the CTD frame (Langdon 2010). Fluorometric analysis of chl *a* was conducted by filtering 100 ml of seawater through 25 mm glass fibre filters and extracted in 90 % acetone at 4 °C. Chl a concentration was then measured using a Turner fluorometer using the Welschmeyer method (Welschmeyer 1994).

Apparent oxygen utilisation (AOU) was calculated as:

$$AOU\ (\mu M) = \text{saturated } O_2\ (\mu M) - \text{observed } O_2\ (\mu M) \qquad \text{Eqn. 4.1}$$

Saturated O_2 calculated as a function of temperature and salinity using equations by (Garcia and Gordon 1992). AOU is the difference between the measured dissolved oxygen concentration and its equilibrium saturation concentration in water with the same properties. Therefore, the AOU of a water sample is the sum of the biological activity since it was last at an equilibrium concentration with the atmosphere. Positive AOU values indicate water that has been out of contact with the atmosphere and where oxygen has been consumed via remineralisation, whereas a near zero or negative AOU value indicates concentrations close to saturation due to close contact with the atmosphere or biological production or low rates of respiration (Garcia and Levitus 2006). AOU was used to estimate nitrate released by respiration by assuming Redfield stoichiometry (Redfield 1963) of 138:106:16:1 (O:C:N:P):

1 mol O_2 consumed = 106/138 mol CO_2 +16/138 mol NO_3 + 1/138 mol H_3PO_4

= 0.77 CO_2 + 0.12 HNO_3 + 0.0072 H_3PO_4 Eqn. 4.2

AOU values were then used to calculate the percentage (%) and concentration (µM) of *in situ* remineralised nitrate using both the Redfield ratio and measured N:P ratio (Redfield 1963; Anderson 1995).

$\delta^{15}N_{NO3}$ and $\delta^{18}O_{NO3}$ were analysed using the 'Denitrifier Method' as described in Chapter 2 (Sigman et al. 2001; Casciotti et al. 2002; McIlvin and Casciotti 2011) at the LIFER laboratory in Liverpool using a customised Thermo – Finnigan Gas Bench II (with backflush) interfaced with a Thermo Fisher Delta V Advantage IRMS. Isotope ratios are reported as parts per thousand deviations from a known international standard. The isotope ratios are reported using delta notation (δ) with units per mil (‰):

$$\delta(X) = \left[\frac{R_{sample} - R_{standard}}{R_{standard}}\right].10^3[‰] \quad \text{Eqn. 4.3}$$

Where R=$^{15}N/^{14}N$, the ratio of the atom occurrence of the rare to common isotope. The reference values for $^{15}N/^{14}N$ and $^{18}O/^{16}O$ are N_2 in air and Vienna Standard Mean Ocean Water (VSMOW), respectively.

The proportion of remineralised nitrate (X) was quantified using the following equation:

$$\delta^{18}O_{measured} = \delta^{18}O_{nitrified}\,(X) + \delta^{18}O_{imported}\,(1\text{-}X) \quad \text{Eqn 4.4}$$

$$X = 1 - \left(\frac{\delta^{18}O_{measured} - \delta^{18}O_{nitrified}}{\delta^{18}O_{imported} - \delta^{18}O_{nitrified}}\right) \quad \text{Eqn 4.5}$$

$\delta^{18}O_{measured}$ was defined as the measured value of $\delta^{18}O_{NO3}$, $\delta^{18}O_{nitrified}$ was the $\delta^{18}O$ value of newly nitrified nitrate and $\delta^{18}O_{imported}$ was the value of $\delta^{18}O_{NO3}$ imported onto the shelf from the open ocean through cross-shelf exchange. The percentage of remineralised nitrate was calculated by multiplying the proportion of remineralised nitrate (X) by 100 and the concentration of newly nitrified nitrate was estimated by multiplying the proportion of remineralised nitrate (X) by the nitrate concentration.

The mixed layer depth at each station was calculated using the density difference of 0.03 kg m^3 from the near surface (CTD sample closest to the surface) (de Boyer Montégut et al. 2004).

4.3 Results

4.3.1 Temperature, salinity and density

The mean temperature in the surface mixed layer varied seasonally between the cruises and there were some small variations across each transect. During DY018 (hereafter called autumn), the mean temperature in the surface mixed layer off shelf was 12.3 ± 1.3 °C, while mean temperature on shelf was 13.1 ± 0.7 °C. The mean temperature in the bottom mixed layer off shelf was 11.8 ± 0.6 °C, similar to the on shelf mean temperature of 11.9 ± 0.8 °C. There was a small gradient in temperature across the shelf. The surface mixed layer of stations north of CCS were cooler (<13 °C), while stations closer to the shelf edge were warmer (>14 °C). The bottom mixed layer was also warmer near the shelf edge, with bottom water temperature near CS2 being higher than 13 °C, compared to on shelf waters (<12 °C; Figure 4.2a). During DY029 (hereafter called early or late spring), there were both vertical and horizontal gradients in temperature during both early and late transects. Mean surface mixed layer temperature during early spring was 11.5 ± 0.6 °C off shelf compared to 10.5 ± 0.6 °C on shelf (Figure 4.2b). The mean surface layer temperature off shelf in late spring was similar at 11.5 ± 0.1 °C and slightly warmer on shelf at 10.7 ± 0.6 °C, again coldest at the inner shelf stations (Figure 4.2c). The mean bottom water temperature in early spring was 11.2 ± 0.2 °C off shelf and 9.8 ± 0.5 °C on shelf, with cooler water further on shelf (Figure 4.2b). In late spring the bottom water mean temperature was the same off shelf at 11.2 ± 0.2 °C and on shelf at 9.8 ± 0.8 °C (Figure 4.2c). The shelf edge and off shelf were both slightly warmer than on shelf with temperature reaching above 11 °C in the surface waters compared to on shelf temperature below 11 °C (Figure 4.2a, Figure 4.2b). During DY033 (hereafter called summer), there were strong temperature gradients between the surface mixed layer and bottom mixed layer across the shelf and open ocean. The mean temperature in the surface mixed layer off shelf was 17.1 ± 0.4 °C, compared to slightly cooler on shelf temperature of 16.4 ± 0.6 °C, with the inner shelf stations cooler than those at

the shelf edge (Figure 4.2d). The mean temperature in the bottom mixed layer below the thermocline was 11.3 ± 0.2 °C off shelf, compared to 10.5 ± 0.6 °C on shelf.

There were well defined salinity gradients across the shelf with fresher water at the inner shelf stations gradually becoming more saline towards the shelf edge. The smallest gradients were observed during the autumn. The least saline water was at the innermost station 'Site A' with a salinity of 35.23 ± 0.01 across the whole water column, whilst the most saline waters were at the shelf edge and open ocean with salinity reaching 35.60 at most of the off shelf stations in the top 500 m depth (Figure 4.2e). Off shelf salinity was similar during both the spring and summer remaining close to 35.60 at most off shelf stations. The inner shelf stations had the lowest observed salinity during the spring and summer than in the autumn, with the innermost stations Site A reaching 35.04 during early spring (Figure 4.2f) and 34.94 in late spring (Figure 4.2g), with little variation observed across the water column. During the summer the surface mixed layer was fresher than the bottom mixed layer across the shelf and the surface waters at Site A were 34.72 ± 0.01, while the bottom mixed layer was 35.14 ± 0.1, both gradually increased towards the shelf edge (Figure 4.2h).

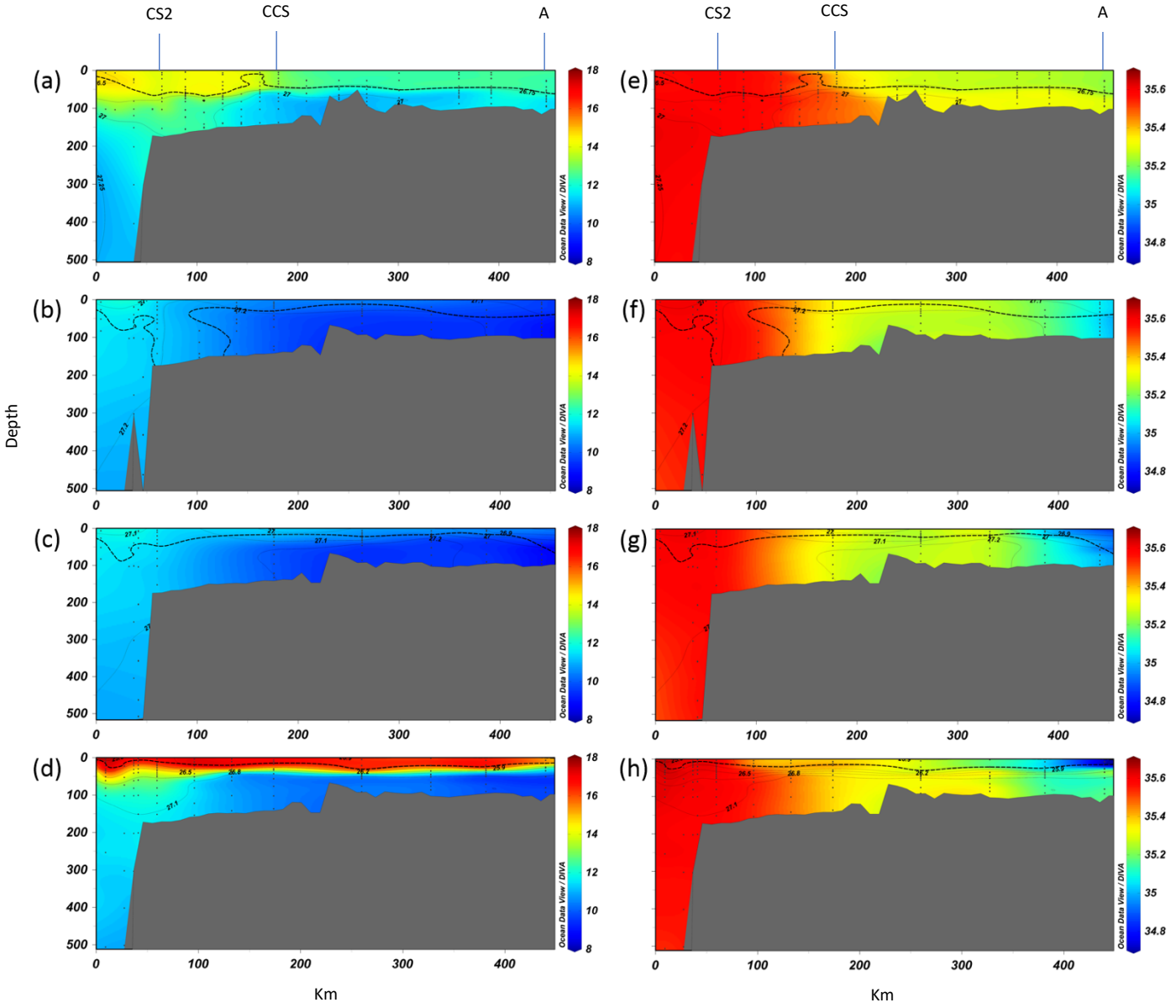

Figure 4.2. Temperature (°C) for cruises DY018 (a), DY029 early (b), DY029 late (c) and DY033 (d) across the Celtic Sea. Salinity for cruises DY018 (e), DY029 early (f), DY029 late (g) and DY033 (h) across the Celtic Sea. Data was plotted in ODV using DIVA gridding using GEBCO1 bathymetry, distance is plotted in km from the southernmost station over the shelf edge. Isobars show sigma theta (Density kg m^{-3} -1000), dots show sampling depths and the dotted line shows the mixed layer depth.

Density (presented as sigma theta = density (kg m^{-3}) – 1000) varied both across the shelf with depth and between each of the seasons. As expected the densest water was found off shelf at depths below 1500 m where density peaked at 27.5 kg m^{-3}. The least dense water was found at the surface during the summer where density was as low as 25.7 kg m^{-3}. During the spring cruise the least dense water observed was 26.9 kg m^{-3}. The surface density during the autumn was between the spring and summer, with a minimum density of 26.5 kg m^{-3} (Figure 4.3). During each of the seasons the densest surface waters were above 27.1 kg m^{-3} and occurred in spring and summer (Figure 4.3).

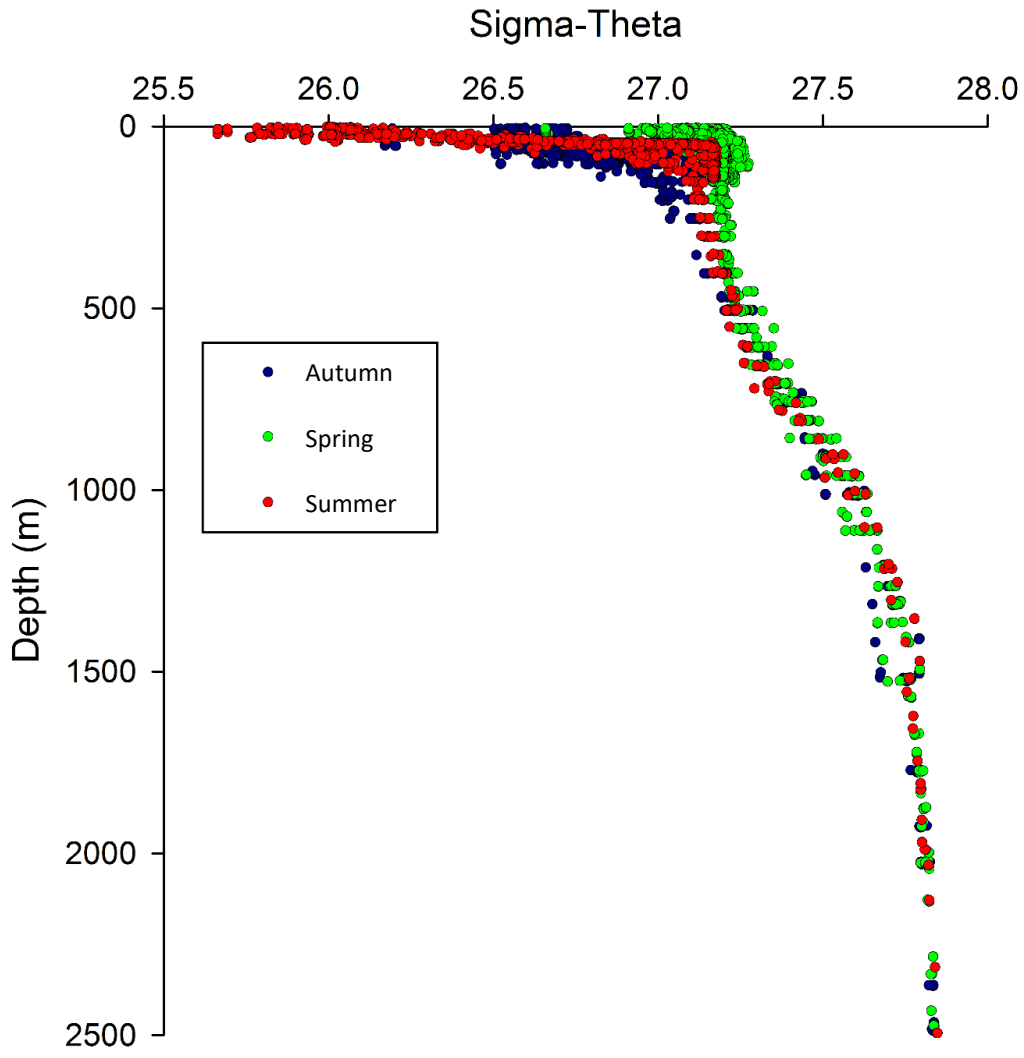

Figure 4.3. Depth (m) variation in sigma theta (Density kg m^{-3}-1000) for cruises DY018, DY029, and DY033 across the Celtic Sea.

During autumn a vertical gradient was observed between the surface waters and bottom waters, with a gradient between the furthest on shelf stations and those closer to the shelf edge. The density in the surface layer over the entire shelf and open ocean stations was between 26.5 kg m^{-3} and 26.75 kg m^{-3}, only decreasing to 26.5 kg m^{-3} at the outermost open ocean station off shelf. There was a weak density gradient between the surface and bottom layer with the bottom mixed layer being between 26.75 kg m^{-3} and 27.25 kg m^{-3} across the entire shelf and open ocean stations, only increasing at depths below 250 m off shelf (Figure 4.4a). During the spring period, a density gradient developed across the shelf, however it was weaker than that observed in autumn and summer. During the early spring the density ranged from no gradient at depth across the shelf and open ocean, with the shelf edge region having no density gradient across the water column. During late spring, the density gradient continued to develop, with density at the innermost shelf stations being the lowest at 26.9 kg m^{-3}, and the bottom mixed layer being between 27.1 kg m^{-3} and 27.3 kg m^{-3} (Figures 4.4b and 4.4c). During the summer the density depth gradient was at its strongest with surface waters below 25.9 kg m^{-3} and bottom waters above 27.1 kg m^{-3} across the shelf. The density layers at the shelf edge were thicker during the summer, with the gradient from 25.9 kg m^{-3} at the bottom of the mixed layer to 27.1 kg m^{-3} spread over 100 m (Figure 4.4d).

The mixed layer depth at each station was calculated using the density difference of 0.03 kg m^3 from the near surface (de Boyer Montégut et al. 2004). The deepest mixed layer depth was observed during autumn and was frequently deeper than 50 m across the shelf and open ocean. During the spring period, the water column transitioned from being full mixed to there being a mixed layer depth shallower than 20 m. During the summer the mixed layer depth was at its most stable across the shelf when the density gradients were maximum at depths between 20 m and 30 m depth. During the autumn the mixed layer was deeper than summer time, generally being deeper than 30 m on shelf (Figure 4.4).

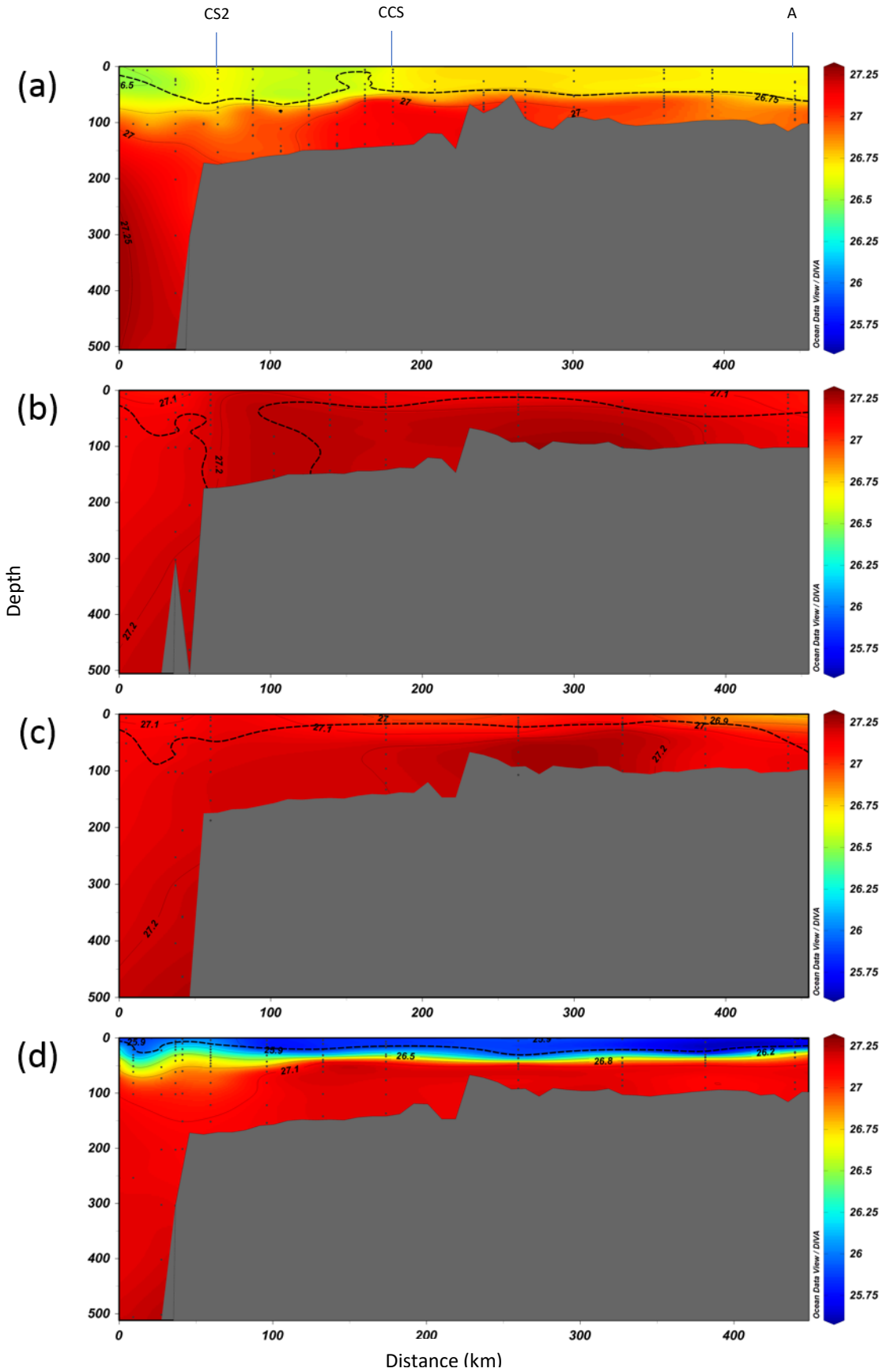

Figure 4.4. (a) to (d) Sigma theta (Density kg m^{-3} - 1000) for cruises DY018 Autumn (a), DY029 early Spring (b), DY029 late Spring (c) and DY033 Summer (d) across the Celtic Sea. Data was plotted in ODV using DIVA gridding using GEBCO1 bathymetry, distance is plotted in km from the shelf edge. Isobars show sigma theta (Density kg m^{-3} -1000), dots show sampling depths and the dotted line shows the mixed layer depth.

4.3.2 Inorganic nutrients, oxygen and fluorescence

Horizontal and vertical gradients were noted in both nitrate and phosphate concentrations during each cruise. In autumn, the nitrate concentration in the surface mixed layer was lower than the bottom mixed layer across the shelf and open ocean stations. The mean surface mixed layer nitrate was 2.3 ± 0.6 µM across the whole transect, being higher on shelf (2.6 ± 0.5 µM) than off shelf (1.8 ± 0.2 µM; Figure 4.5a). Mean bottom mixed layer nitrate concentrations were similar on shelf (8 ± 2.1 µM) and off shelf (8.7 ± 2.4 µM) but were more variable than the surface mixed layer (Figure 4.5a). During early spring when stratification was developing, there were large nitrate gradients across the shelf, as the mixed layer depth was more developed on the inner shelf than at the shelf edge and the spring bloom developed across the shelf. Off shelf nitrate concentrations (7.9 ± 0.7 µM) were higher than on shelf nitrate (5.7 ± 2.4 µM) in the surface mixed layer, however there was considerable variation in the on shelf nitrate (Figure 4.5b). The nitrate concentration in the upper 500 m was again higher off shelf (9.4 ± 1.2 µM) compared to the nitrate concentration on shelf in bottom mixed layer (6.0 ± 1.3 µM; Figure 4.5b). During late spring when stratification was more developed and the nitrate concentration in the surface mixed layer was lower on the shelf, stations from CCS towards the inner shelf were low (0.4 ± 0.3 µM), whereas concentrations at the shelf edge site CS2 were higher at 7.3 ± 0.3 µM. However, the shelf edge sites were the first to be visited during the second half of DY029 (Figure 4.5c and 4.5d). Nitrate in the bottom mixed layer (5.2 ± 2.4 µM) was more variable than during early spring between CCS to the inner shelf. Nitrate concentrations at the shelf edge station CS2 were again higher (8.4 ± 0.2 µM) in the bottom mixed layer (Figure 4.5c). During the summer, the mean nitrate concentration was below the limit of detection (0.02 µM) in the surface mixed layer on shelf. The nitrate concentrations at the off shelf stations were also generally below the limit of detection, with only stations Fe03 and Fe04 having measurable nitrate up to 0.2 µM (Figure 4.5d). During the summer variability in the nitrate concentration in the bottom mixed layer was 4.6 ± 3.9 µM, much of this variation was caused by the concentration rapidly increasing from the base of the mixed layer to a mean value of 8.6 ± 0.6 µM at bottom depths across the shelf (Figure 4.5d).

During the autumn, phosphate was lower in the surface mixed layer than in the bottom mixed layer. Mean phosphate concentration on shelf 0.3 ± 0.05 µM compared to 0.2 ± 0.01 µM off shelf (Figure 4.5e). Mean bottom layer phosphate was similar on and off shelf being 0.6 ± 0.1 µM across the shelf and up to 500m off shelf. The highest phosphate concentrations were found at the inner most shelf stations with phosphate concentrations close to 0.8 µM in the bottom mixed layer at Site A (Figure 5.4e). During the early spring off shelf phosphate concentrations in the surface mixed layer were 0.5 ± 0.05 µM compared to on shelf surface mixed layer concentrations of 0.4 ± 0.1 µM (Figure 4.5f). Bottom mixed layer phosphate concentrations were similar (0.6 ±0.1 µM) for off shelf stations and on shelf stations (Figure 4.5f). During late spring the surface mixed layer phosphate on shelf was low (0.1 ± 0.06 µM) from CCS inwards, while the shelf edge station CS2 remained higher at 0.5 ± 0.02 µM (Figure 4.5g). The bottom mixed layer phosphate concentrations were 0.4 ± 0.1 µM on shelf from CCS inwards and 0.5 ± 0.01 µM for CS2 (Figure 4.5g). During the summer phosphate concentrations in the surface mixed layer on shelf were low (0.04 ± 0.03 µM), off shelf concentrations were 0.06 ± 0.01 µM (Figure 4.5h). Mean bottom mixed layer phosphate was 0.4±0.3 µM on shelf, increasing rapidly from near zero at the base of the surface mixed layer to a mean bottom water concentration of 0.6 ± 0.1 µM (Figure 4.5h). Phosphate concentration increased at the innermost shelf station A, with bottom water concentrations of 0.8 µM during the summer, similar to autumn concentrations (Figure 4.5h).

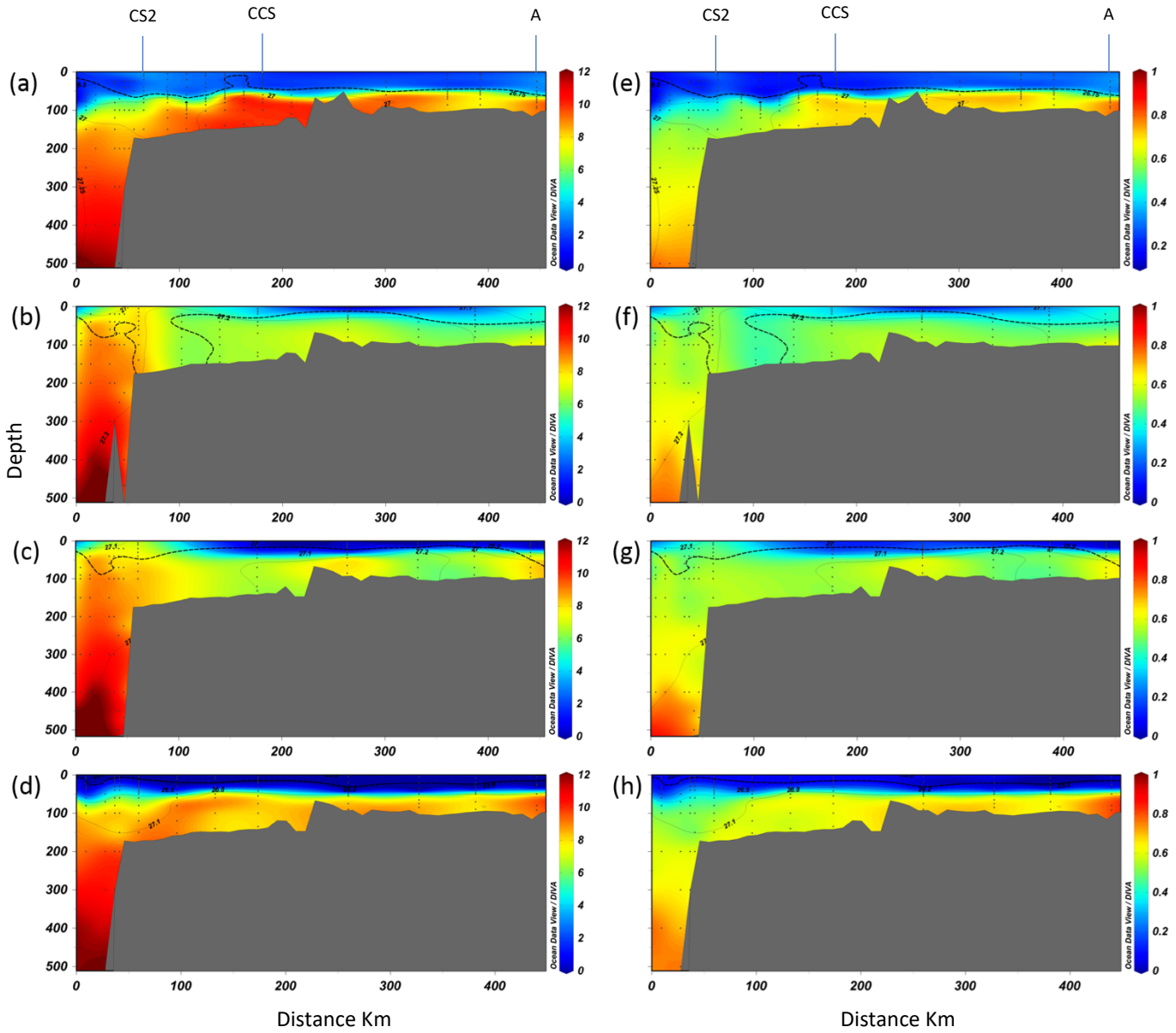

Figure 4.5. (a) to (d) concentrations of nitrate (µM) for cruises DY018 (a), DY029 early (b), DY029 late (c) and DY033 (d) across the Celtic Sea. Phosphate for cruises DY018 (e), DY029 early (f), DY029 late (g) and DY033 (h) across the Celtic Sea. Data was plotted in ODV using DIVA gridding using GEBCO1 bathymetry, distance is plotted in km from the southernmost station over the shelf edge. Isobars show sigma theta (Density kg m^{-3} - 1000), dots show sampling depths and the dotted line shows the mixed layer depth.

Nitrite concentrations during the autumn were highest in the surface mixed layer with mean concentration on shelf of 0.24 ± 0.05 µM, reaching up to 0.36 µM across the mid shelf and inner shelf regions. Off shelf nitrite concentrations were 0.22 ± 0.02 µM in the surface mixed layer (Figure 4.6a). Bottom mixed layer nitrite was low both on and off shelf, with off shelf values frequently below the limit of detection, and a mean value of 0.02 ± 0.04 µM. On shelf bottom mixed layer nitrite concentrations were 0.07 ± 0.06 µM (Figure 4.6a). During both early and late spring nitrite concentrations were highly variable across the shelf. This spatial variation is a construct of the time travelling across the shelf collecting samples, capturing different periods of the spring bloom at different times. During early spring, the highest nitrite concentrations were measured at the shelf edge reaching up to 0.36 µM at station O4 and reaching 0.21 µM at the shelf edge station CS2 (Figure 4.6b). During late spring the highest nitrate concentrations were measured across the inner shelf reaching 0.38 µM across J transect and 0.32 µM at site A (Figure 4.6c). During the summer period nitrite concentrations were low across much of the shelf with highest concentrations measured off shelf and at the shelf edge at the base of the surface mixed layer, reaching concentrations between 0.26 and 0.29 µM at a depth of 60 m across the Fe transect. On shelf nitrite was generally below 0.02 µM across the shelf, apart from a peak in the bottom 20 m of the inner shelf site A where concentrations reached 0.22 µM (Figure 4.6d).

Ammonium concentrations during the autumn were low across the surface and bottom mixed layer, reaching a maximum of 0.15 µM at station O3 across the outer shelf, but generally remaining below 0.1 µM across the shelf and open ocean stations (Figure 4.6e). Ammonium concentrations were also low during the early spring, peaking in the off shelf Fe transect at 0.35 µM but generally remaining below 0.1 µM on shelf (Figure 4.6f). During late spring ammonium concentrations were elevated compared to autumn and early spring across much of the shelf, highest concentrations were at the inner most site A where concentrations reached 0.83 µM at 30 m depth (Figure 4.6g). During the summer ammonium concentrations increased near the shelf edge below the base of the surface mixed layer, reaching concentrations of 1.1 µM between 40 and 50 m water depth. Elevated concentrations were also measured at site A reaching 0.33 µM at depths of 80 m (Figure 4.6h).

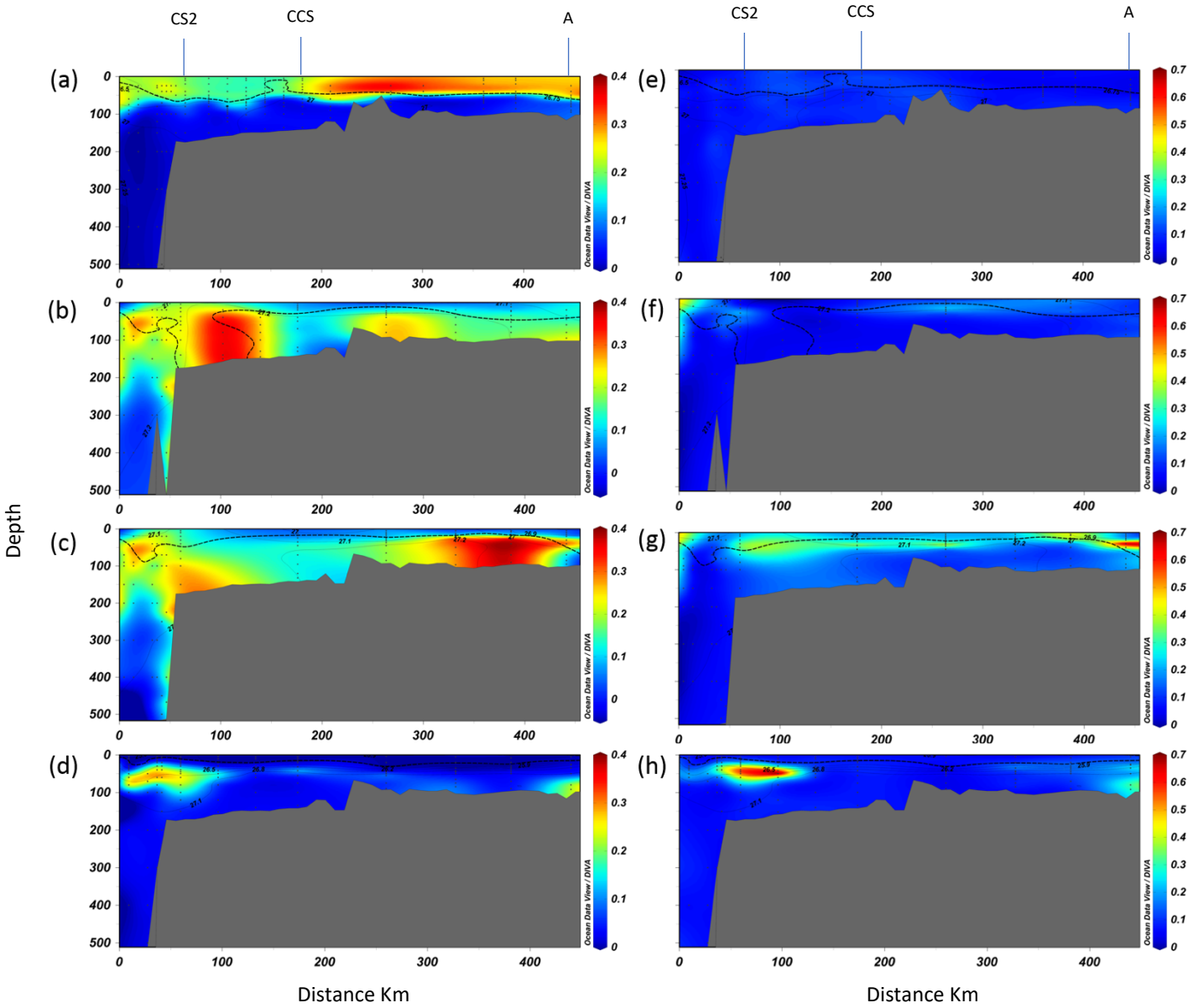

Figure 4.6. (a) to (d) concentrations of nitrite (µM) for cruises DY018 (a), DY029 early (b), DY029 late (c) and DY033 (d) across the Celtic Sea. Ammonium for cruises DY018 (e), DY029 early (f), DY029 late (g) and DY033 (h) across the Celtic Sea. Data was plotted in ODV using DIVA gridding using GEBCO1 bathymetry, distance is plotted in km from the southernmost station over the shelf edge. Isobars show sigma theta (Density kg m^{-3} -1000), dots show sampling depths and the dotted line shows the mixed layer depth.

The nitrate to phosphate ratio (N:P) during autumn was low in the surface mixed layer with an overall mean value of 10 ± 2 across both the shelf and open ocean stations. The ratio peaked between CCS and the Shelf edge where the ratio was between 11.2 and 14.2 (Figure 4.7a). Bottom mixed layer N:P ratios decreased from the open ocean towards the inner shelf from above 15 at the shelf edge to below 11 at the innermost three stations on shelf (Figure 4.7a). During the spring period the low N:P develops across the shelf, and by late spring much of the surface water apart from the shelf edge and innermost shelf station A have N:P below 7.5. Off shelf station N:P was higher generally being between 15 and 18 in the top 500 m water depth (Figure 4.7b). During the summer the N:P in the surface layer was low, particularly on shelf due to nitrate often being below the limit of detection. Bottom mixed layer N:P increased from the open ocean stations towards the coast across the shelf from ≥16 off shelf to ≤10 at the inner shelf stations. N:P increased from the base of the surface mixed layer across density gradients (Figure 4.7d).

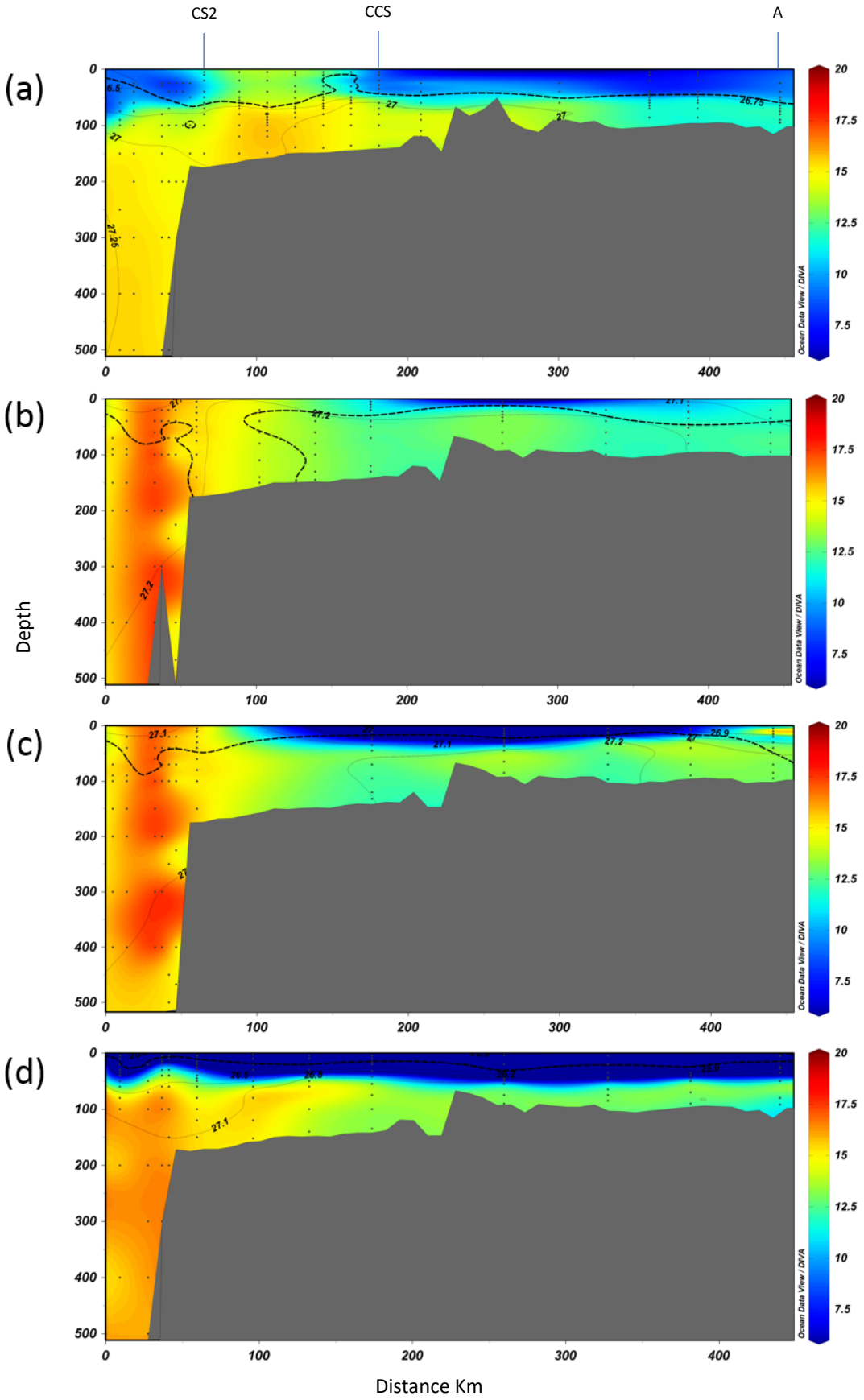

Figure 4.7. (a) to (d) nitrate to phosphate ratio for cruises DY018 (a), DY029 early (b), DY029 late (c) and DY033 (d) across the Celtic Sea. Data was plotted in ODV using DIVA gridding using GEBCO1 bathymetry, distance is plotted in km from the southernmost station over the shelf edge. Isobars show sigma theta (Density kg m^{-3} -1000), dots show sampling depths and the dotted line shows the mixed layer depth.

Dissolved oxygen concentrations during the autumn ranged from 208 µM to 256 µM across the shelf and open ocean stations (Figure 4a). Concentrations were higher in the surface mixed layer than the bottom mixed layer. Mean surface layer off shelf concentrations were 252 ± 1 µM and mean on shelf concentrations were 258 ± 3 µM. Surface mixed layer concentrations were highest between the mid and inner shelf regions were concentrations reached 265 µM (Figure 4.8a). Bottom mixed layer concentrations were 241 ± 6 µM off shelf compared to 232 ± 12 µM on shelf, with the lowest dissolved oxygen concentrations at the innermost shelf station site A at 208 µM (Figure 4.8a). During the early and late spring period there were high oxygen concentrations across the mid and inner shelf surface mixed layer where they reached 364 µM at station J6 in the central shelf during early spring (Figure 4.8b). During early spring bottom mixed layer oxygen concentrations were 264 ± 11 µM off shelf and 296 ± 10 µM on shelf, higher than in the previous autumn (Figure 4.8b). During late spring concentrations in the bottom mixed layer were similar at 264 ± 11 µM off shelf and 292 ± 12 µM on shelf (Figure 4.8c). During the summer dissolved oxygen concentrations in the surface mixed layer both on and off shelf were lower than in spring at 258 ± 5 µM and 259 ± 5 µM, respectively (Figure 4.8d). There was evidence of a subsurface chlorophyll maximum with oxygen concentrations between density layers of 26.2 kg m^{-3} and 27.1 kg m^{-3} at the base of the mixed layer having higher concentrations than the rest of the water column reaching over 300 µM across stations J2, J4 and J6 on the inner shelf (Figure 4.8d).

During the autumn period fluorescence, used as a proxy for chlorophyll concentration, was low across the water column being below 1 µg L^{-1} across the entire transect (Figure 4.8e). During the early and late spring periods fluorescence increased in the surface mixed layer with similar patterns to oxygen concentration, reaching concentrations above 6 µg L^{-1} across the on shelf stations (Figure 4.8f, g). There was again evidence for a subsurface chlorophyll maximum during the summer period with elevated fluorescence between the density layers 26.2 kg m^{-3} and 27.1 kg m^{-3}at the base of the mixed layer. Concentrations reached over 3 µg L^{-1} at both J4 and J6 on the inner shelf (Figure 4.8h).

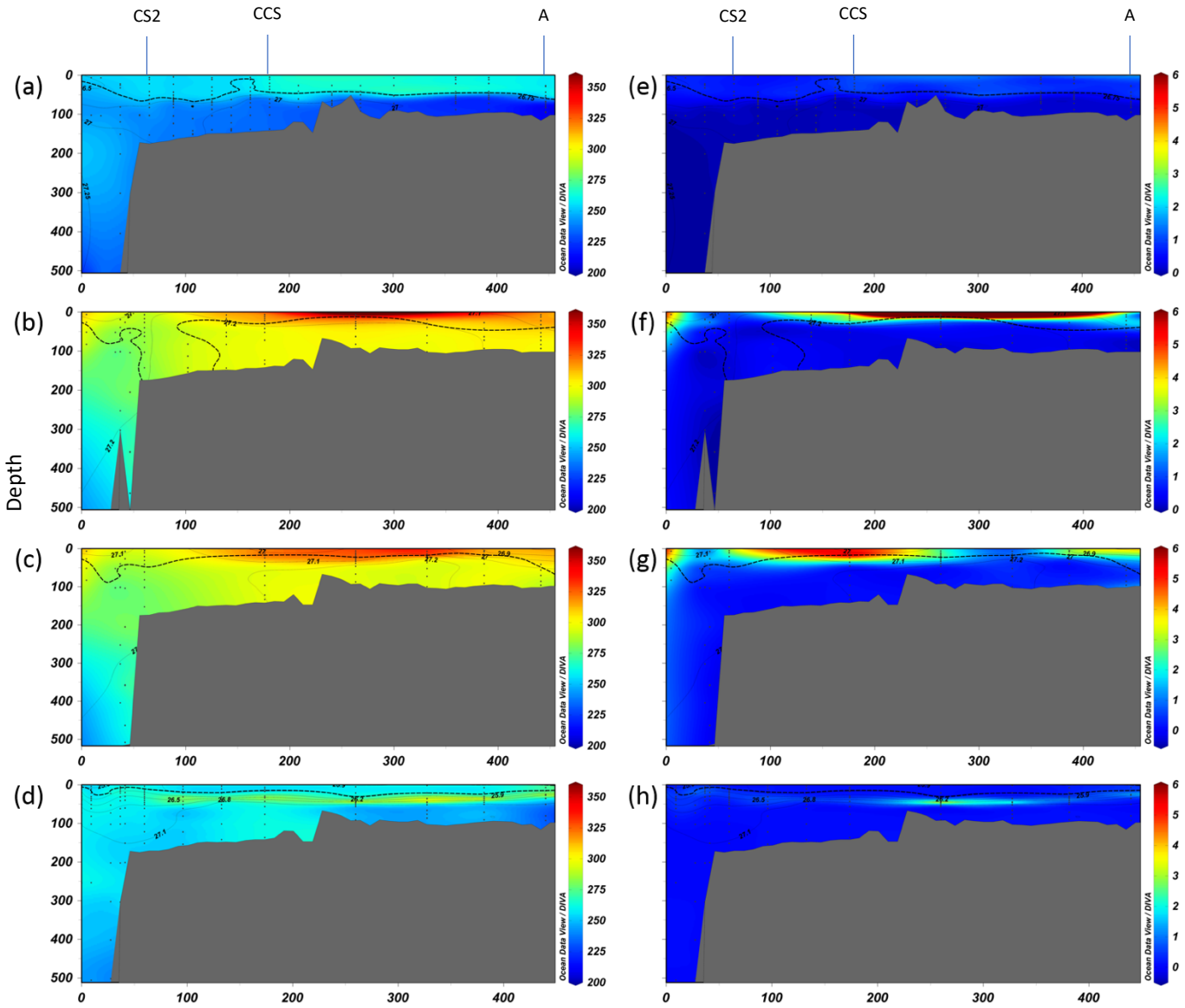

Figure 4.8. (a) to (d) dissolved oxygen concentration (µM) for cruises DY018 (a), DY029 early (b), DY029 late (c) and DY033 (d) across the Celtic Sea. CTD fluorescence (µg L^{-1}) for cruises DY018 (e), DY029 early (f), DY029 late (g) and DY033 (h) across the Celtic Sea. Data was plotted in ODV using DIVA gridding using GEBCO1 bathymetry, distance is plotted in km from the southernmost station over the shelf edge. Isobars show sigma theta (Density kg m^{-3} -1000), dots show sampling depths and the dotted line shows the mixed layer depth

The relationship between nitrate and dissolved oxygen is important for assessing new and regenerated production, this relationship changed throughout the year. During the autumn period the oxygen concentrations were lowest (< 265 μM) across the shelf, even in the surface layer. The lowest concentrations in the bottom mixed layer were associated with the highest nitrate concentrations on shelf (Figure 4.9). During the spring period, the water was well oxygenated across the shelf, with the highest oxygen concentrations (>300 μM) associated with the lowest nitrate concentrations in the surface mixed layer during the spring bloom. The lowest oxygen concentrations were in the bottom mixed layer in waters off the shelf and coincided with the highest nitrate concentrations. The summer period was the transition between the spring period and autumn period, oxygen concentrations decreased across the shelf, and nitrate concentration was close to zero in the surface mixed layer but beginning to increase at depth (Figure 4.9).

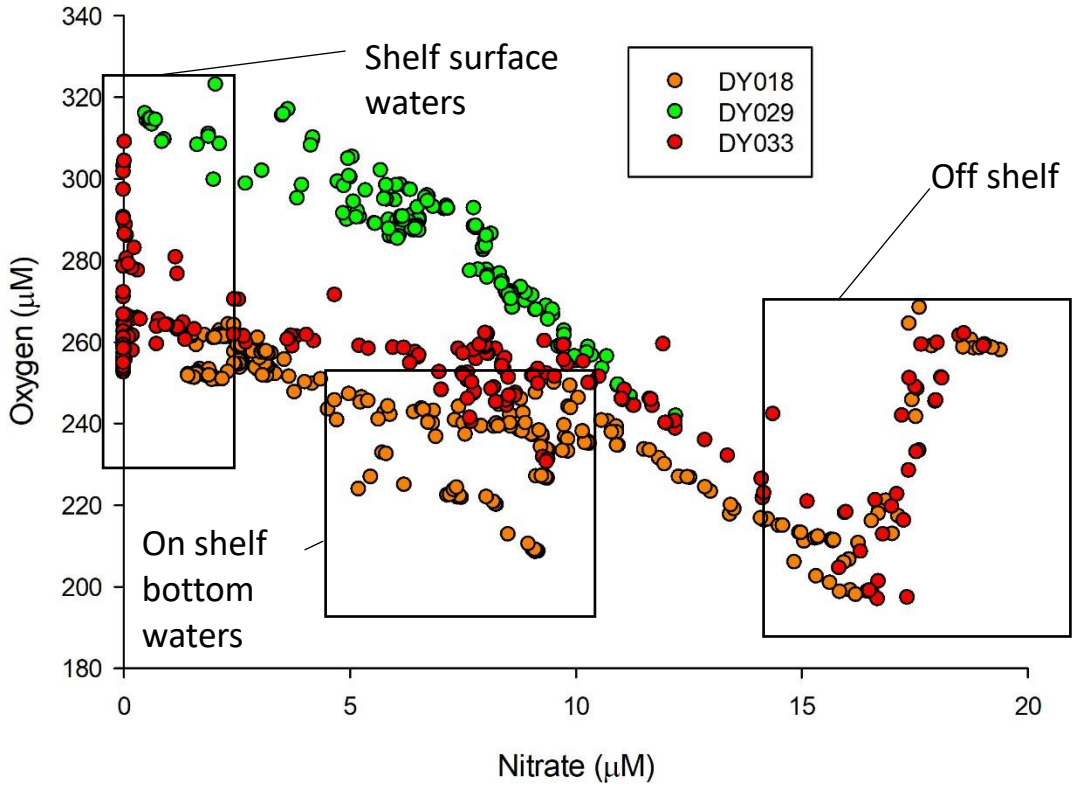

Figure 4.9. Nitrate (μM) vs. dissolved oxygen (μM) for each of the cruises DY018, DY029 and DY033 across the Celtic Sea.

Apparent oxygen utilisation (AOU), the difference between the equilibrium oxygen saturation concentration and the measured dissolved oxygen concentration

(Garcia and Gordon 1992) was calculated giving the apparent oxygen utilisation (AOU). During autumn with the deepening mixed layer depth, the AOU in the surface mixed layer on and off shelf was negative, being -9 ± 1 µM and -9 ± 2 µM, respectively. Bottom mixed layer AOU became more positive from off shelf to the middle and inner shelf regions. Mean off shelf bottom mixed layer AOU was +17 ± 6 µM while on shelf mean AOU was +23 ± 13 µM. Shelf stations on the inner shelf were most negative with the AOU at Site A being +44 ± 10 µM (Figure 4.10a). During the spring periods the surface AOU was negative reaching -59 µM across the central shelf regions (Figure 4.10b, c). During late spring bottom mixed layer AOU was also negative off shelf to almost 400 m water depth with mean concentration of -8 ± 10 µM. On shelf AOU in the bottom mixed layer was also negative across the entire shelf with AOU of -23 ± 13 µM (Figure 4.10c). During the summer period the surface mixed layer AOU concentrations were still negative on and off shelf. AOU increased rapidly from the base of the surface mixed layer, with bottom water AOU on the inner shelf being positive compared to either negative or close to zero values across the outer shelf and open ocean stations. Bottom water AOU at site A reached +37 µM at bottom depths, compared to +2.3 µM at CCS and +5.1 µM at CS2 (Figure 4.10d).

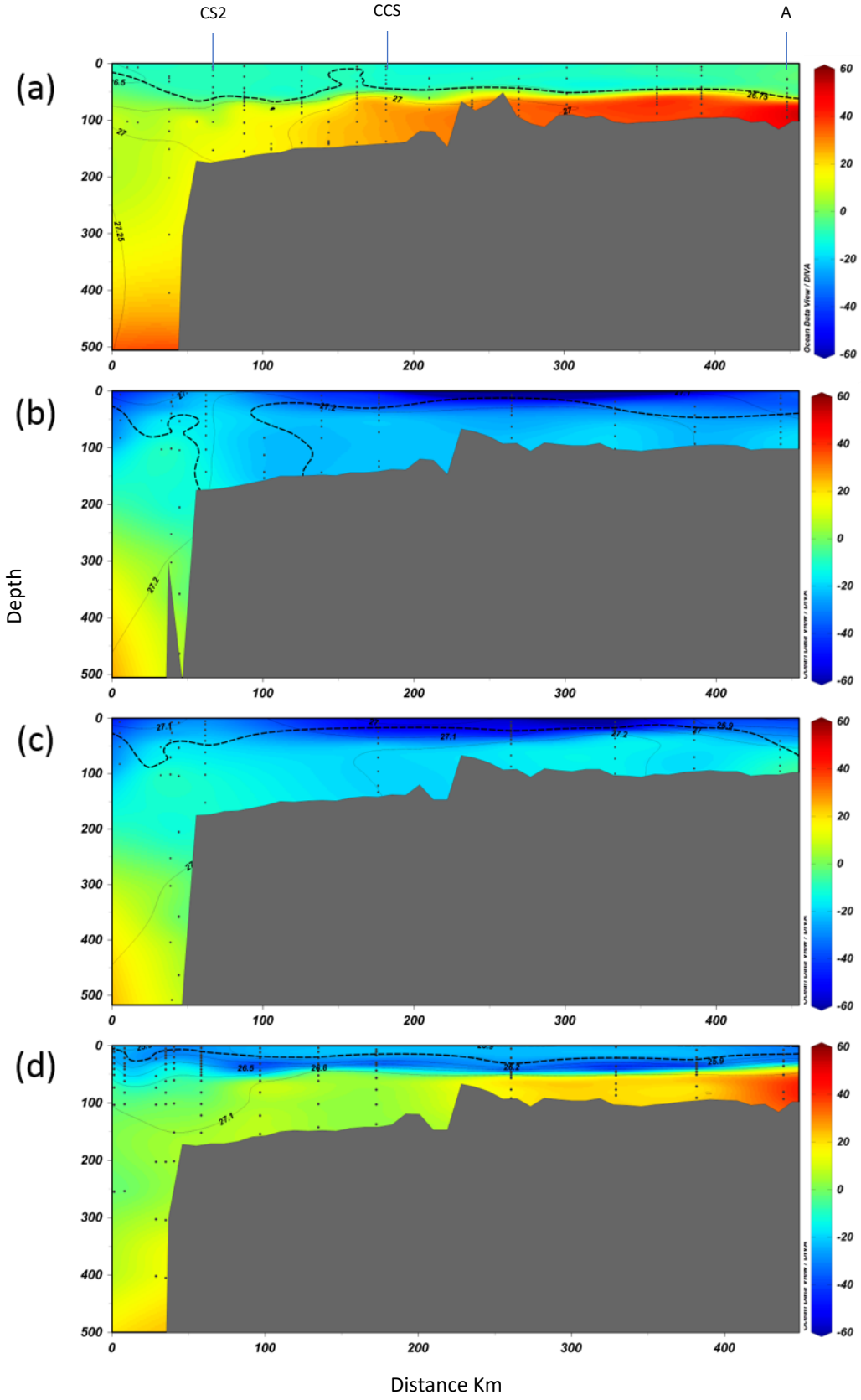

Figure 4.10 (a) to (d) Apparent Oxygen Utilisation (AOU) (µM) for cruises DY018 (a), DY029 early (b), DY029 late (c) and DY033 (d) across the Celtic Sea. Data was plotted in ODV using DIVA gridding using GEBCO1 bathymetry, distance is plotted in km from the southernmost station over the shelf edge. Isobars show sigma theta (Density kg m^{-3} -1000), dots show sampling depths and the dotted line shows the mixed layer depth.

Full depth profiles of both AOU and oxygen concentration reveal that the most negative AOU and highest oxygen concentrations were during the spring periods of DY029 in the surface waters, with oxygen decreasing off shelf to depths of 1000 m before increasing towards to the bottom (Figure 4.11a, b). Off shelf AOU concentrations were similar below 500 m off shelf for each cruise corresponding to a density of approximately 27.5 kg m^{-3} (Figure 4.11c, d). The positive AOU concentrations were associated with the bottom waters on shelf generally between 26.5 kg m^{-3} and 27 kg m^{-3}, while the negative summer concentrations were associated with the least dense on shelf waters when the stratification is strongest (Figure 4.11d).

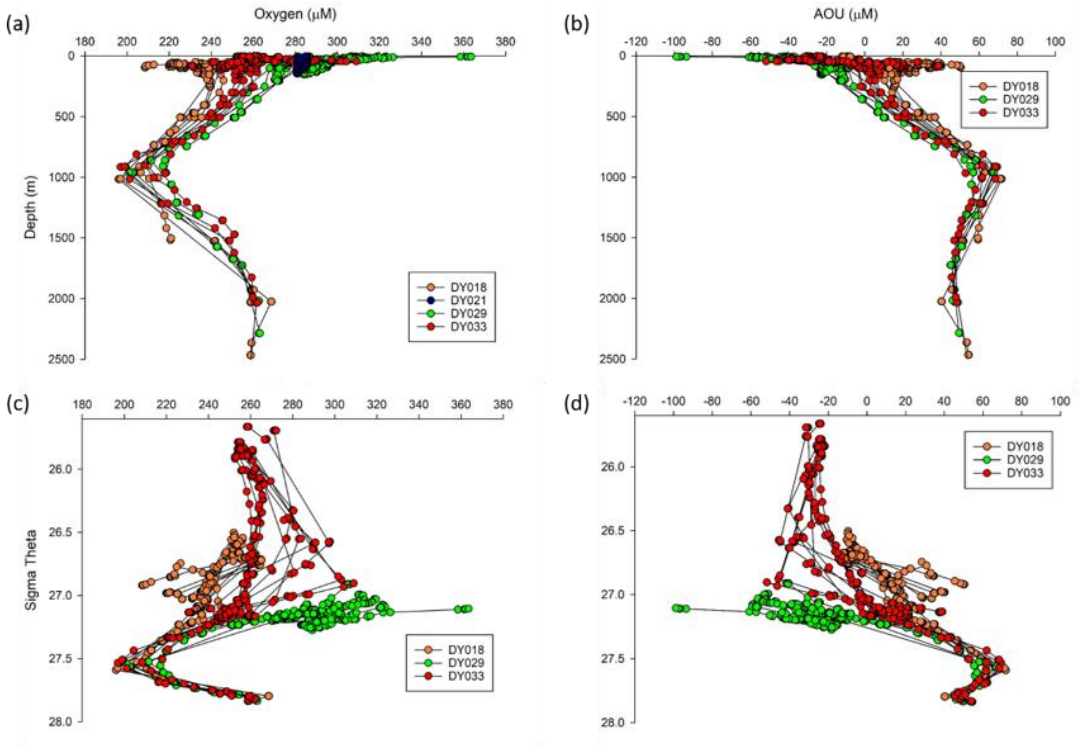

Figure. 4.11 Full depth profiles of (a) dissolved oxygen concentration (µM) and (b) AOU (µM) for cruises DY018, DY021, DY029 and DY033 across the Celtic Sea. Full depth isopycnal profiles for (c) dissolved oxygen concentration (µM) and (d) AOU (µM) for cruises DY018, DY021, DY029 and DY033 across the Celtic Sea.

4.3.3 Stable Isotopes

During the autumn, there were small variations in $\delta^{15}N_{NO3}$ across the shelf. Off shelf mean $\delta^{15}N_{NO3}$ was 4.6 ± 0.2 ‰, however all samples were collected at depths below 100 m. Mean on shelf $\delta^{15}N_{NO3}$ was 5.0 ± 0.3 ‰. $\delta^{15}N_{NO3}$ increased from a minimum of 4.6 ‰ at the shelf edge station, CS2, to a maximum of 5.6 ‰ at the most inner shelf station site A across the entire water column (Figure 4.12a; instrument precision was 0.2 ‰). $\delta^{15}N_{NO3}$ above and below the mixed layer depth were not significantly different on shelf ($p > 0.05$), with cross shelf gradients being larger than vertical gradients. $\delta^{18}O_{NO3}$ during the autumn ranged from 2.7 ‰ to 5.3 ‰ across the shelf, with the lowest values in the bottom mixed layer at the inner shelf stations. Mean off shelf $\delta^{18}O_{NO3}$ between the base of the mixed layer and 500 m water depth was 3.8 ± 0.4 ‰ (Figure 4.12e).

During the spring period, the surface water values for $\delta^{15}N_{NO3}$ and $\delta^{18}O_{NO3}$ increased across the shelf at a ratio close to 1:1 (Figure 4.12b; due to phytoplankton utilisation of nitrate). However, both $\delta^{15}N_{NO3}$ and $\delta^{18}O_{NO3}$ were above 6 ‰ in both the surface and bottom waters across much of the shelf at the beginning of the spring research cruise, with the most enriched values at the surface (Figure 4.12b). The increase in $\delta^{15}N_{NO3}$ and $\delta^{18}O_{NO3}$ was patchy across the shelf as the spring bloom gradually developed temporally and spatially. The maximum measured $\delta^{15}N_{NO3}$ and $\delta^{18}O_{NO3}$ were 11.6 ‰ and 11.9 ‰, respectively before nitrate concentrations decreased below the limit of detection (1 µM) for the denitrifier method (Figure 4.12b, c, f, g). Throughout the spring period, the bottom layer on shelf also became progressively enriched for both $\delta^{15}N_{NO3}$ and $\delta^{18}O_{NO3}$. During late spring, the bottom mixed layer $\delta^{15}N_{NO3}$ and $\delta^{18}O_{NO3}$ reached 7 ‰ on the outer shelf and shelf edge stations (Figure 4.12c).

During the summer $\delta^{15}N_{NO3}$ values were lower than the spring period across the shelf, with concentrations close to 4.5 ‰ at the shelf edge progressively increasing on shelf to a maximum of 6.7 ‰ at the inner most shelf stations J2 and site A (Figure 4.12d). $\delta^{18}O_{NO3}$ was lower at bottom depth on shelf stations, reaching a minimum of 3.2 ‰ at the innermost station site A (Figure 4.12h). Shelf edge stations were enriched in the surface, penetrating into the bottom mixed layer where $\delta^{18}O_{NO3}$ reached 6.6 ‰ at the shelf edge station CS2 (Figure 4.12h).

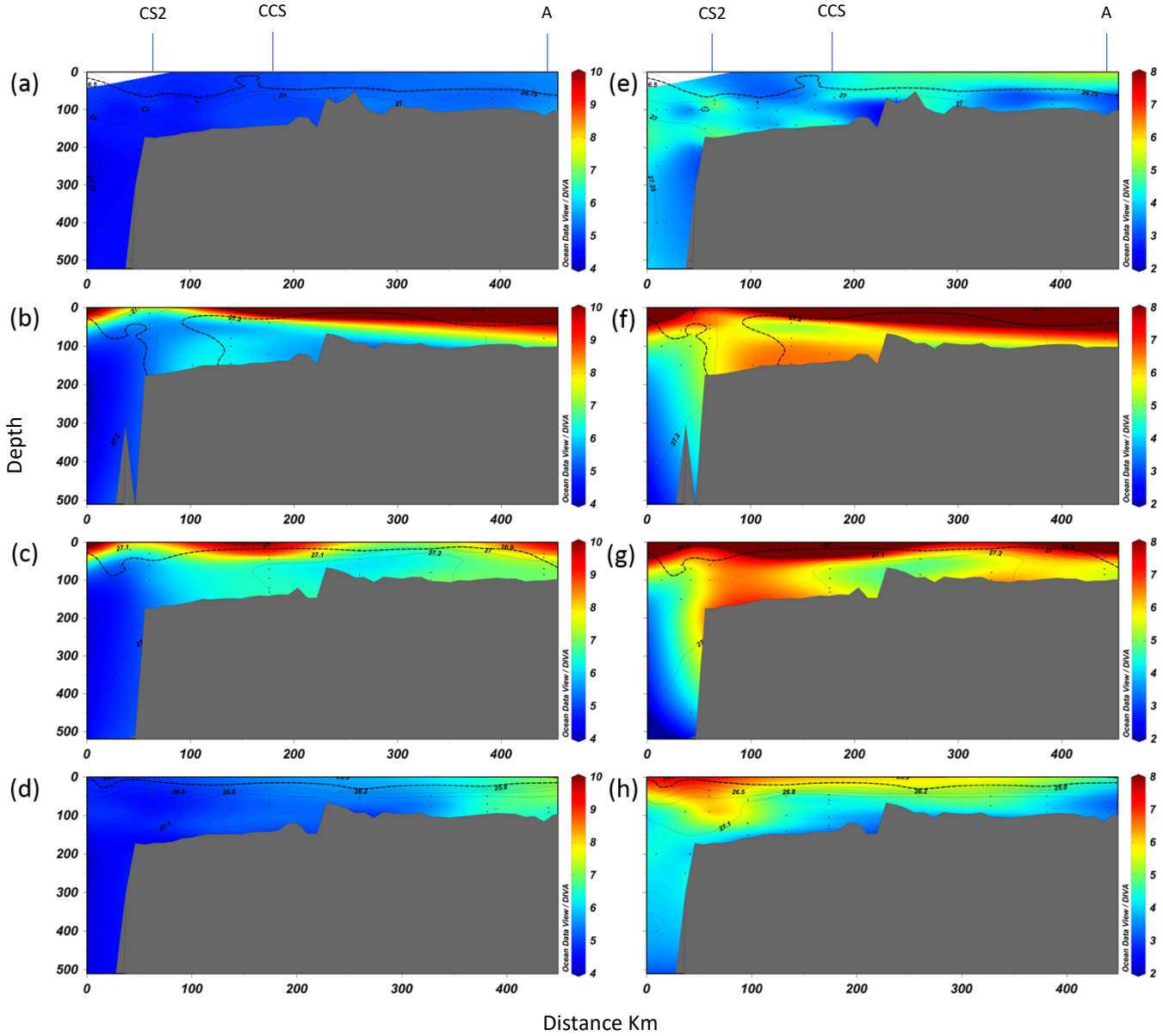

Figure 4.12. (a) to (d) $\delta^{15}N_{NO3}$ (‰) for cruises DY018 (a), DY029 early (b), DY029 late (c) and DY033 (d) across the Celtic Sea. $\delta^{18}O_{NO3}$ (‰) for cruises DY018 (e), DY029 early (f), DY029 late (g) and DY033 (h) across the Celtic Sea. Data was plotted in ODV using DIVA gridding using GEBCO1 bathymetry, distance is plotted in km from the southernmost station over the shelf edge. Isobars show sigma theta (Density kg m^{-3} - 1000), dots show sampling depths and the dotted line shows the mixed layer depth.

At stations where water depth was greater than 500 m, the off shelf $\delta^{15}N_{NO3}$ and $\delta^{18}O_{NO3}$ values were similar below 100 m (above a density of 27.3 kg m^{-3}) for all cruises (Figure 4.13a, b). The density in autumn shelf waters was the lowest with corresponding $\delta^{15}N_{NO3}$ similar to off shelf values of 4.8 ‰ (Figure 4.13c). Wintertime $\delta^{15}N_{NO3}$ and $\delta^{18}O_{NO3}$ were similar to early spring values across the shelf across similar density layers, although samples were only taken from the three process stations, CCS, Site A and CS2 (Figure 4.13c, d).

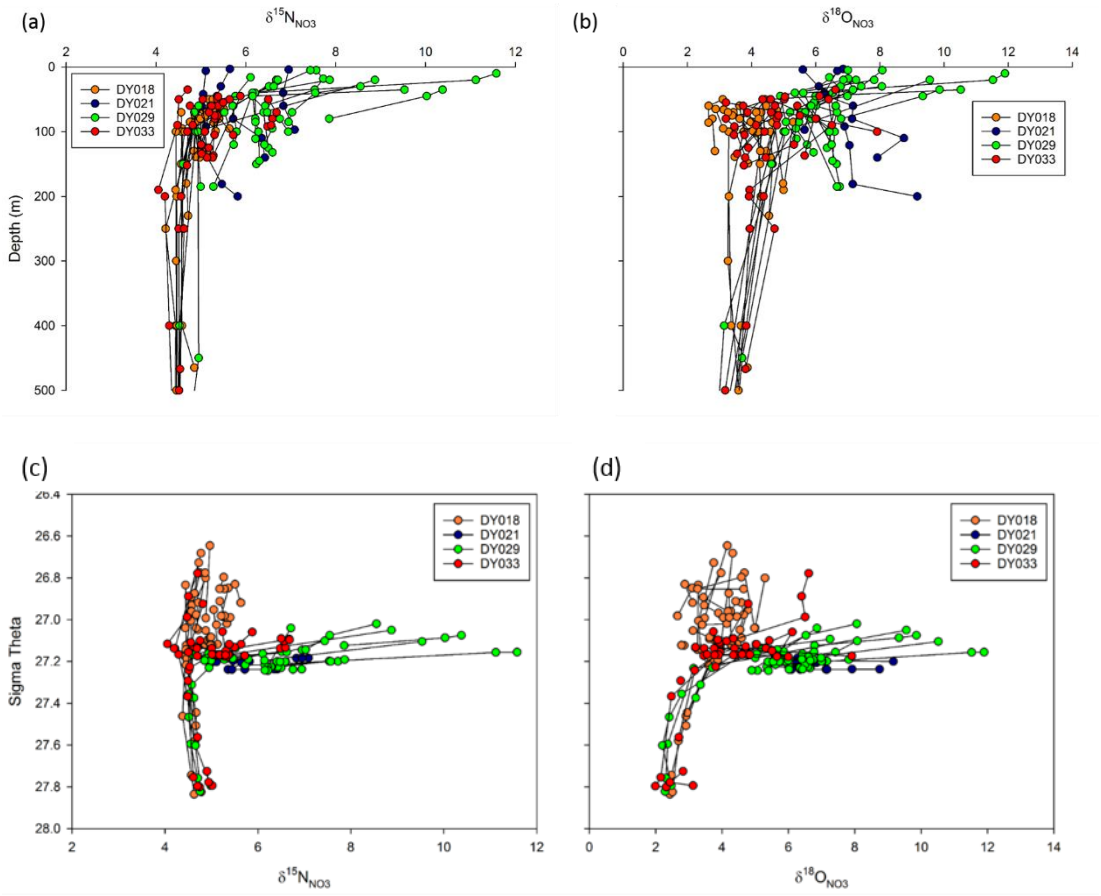

Figure 4.13. Full depth profiles of (a) $\delta^{15}N_{NO3}$ and (b) $\delta^{18}O_{NO3}$ for cruises DY018, DY021, DY029 and DY033 across the Celtic Sea. Full depth isopycnal profiles of (c) $\delta^{15}N_{NO3}$ and (d) $\delta^{18}O_{NO3}$ for cruises DY018, DY021, DY029 and DY033 across the Celtic Sea.

The relationship between $\delta^{15}N_{NO3}$ and $\delta^{18}O_{NO3}$ and nitrate varied between seasons. During spring, $\delta^{15}N_{NO3}$ and $\delta^{18}O_{NO3}$ increased as the nitrate concentration decreased, generally within the surface mixed layer. This increase was close to a 1:1 ($^{15}N=^{18}O$; Figure 4.14c), as expected from phytoplankton uptake within the surface mixed layer. Off shelf values for each of the cruises indicated that above 14 µM of

nitrate the $\delta^{15}N_{NO3}$ and $\delta^{18}O_{NO3}$ reached the expected values for deep off shelf water in the North Atlantic (Sigman et al. 2003) (Figure 4.14a,b). During the summer and autumn periods, the $\delta^{15}N_{NO3}$ and $\delta^{18}O_{NO3}$ were below the 1:1 ratio, with $\delta^{18}O_{NO3}$ lower than expected compared to $\delta^{15}N_{NO3}$ if uptake were the only process impacting the nitrate isotopes indicating that another process such as remineralisation was taking place. This deviation resulted in a positive Δ (15-18) value (Figure 4.14c).

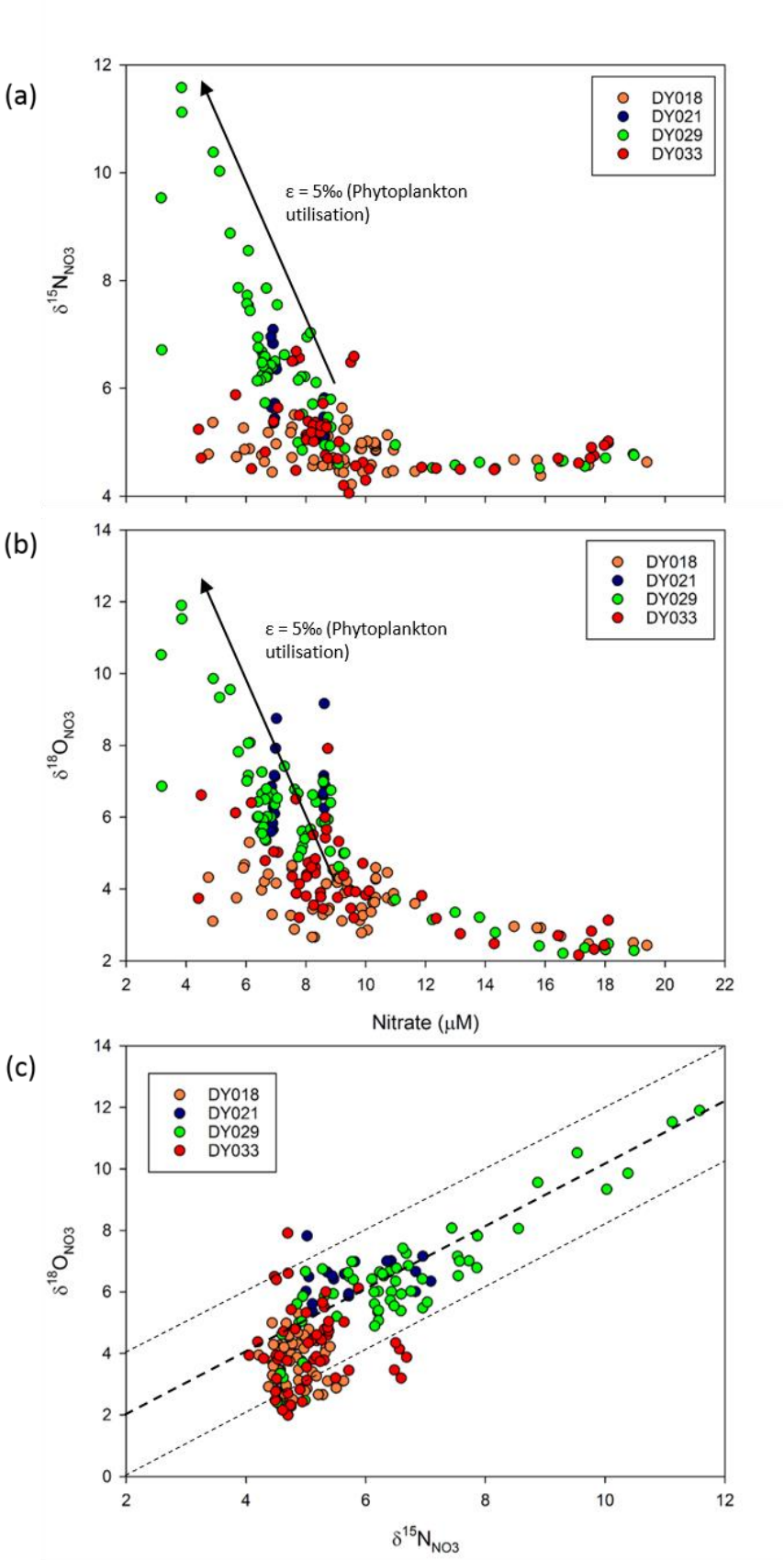

Figure 4.14.(a) $\delta^{15}N_{NO3}$ and (b) $\delta^{18}O_{NO3}$ plotted against nitrate for cruises DY018, DY021, DY029 and DY033 across the Celtic Sea. (c) $\delta^{15}N_{NO3}$ v $\delta^{18}O_{NO3}$ for cruises DY018, DY021, DY029 and DY033 across the Celtic Sea, with dashed lines showing the 1:1 increase with different end members.

The percentage and concentration of remineralised nitrate was calculated for bottom water below the mixed layer across the shelf for the summer period. Remineralised nitrate using the AOU was calculated using equation 4.2 & 4.3, and mean N:P ratio used for calculating remineralised nitrate using AOU was 14:1, lower than Redfield. Remineralised nitrate using the $\delta^{18}O_{NO3}$ was calculated using equations 4.4 and 4.5. A value of 3.8 ‰ was selected for the $\delta^{18}O_{imported}$ value, which was the mean off shelf $\delta^{18}O_{NO3}$ value between the base of the thermocline and 500 m water depth for each of the cruises. This value is critically evaluated in the discussion. The proportion of remineralised nitrate for both methods increases from the shelf edge towards the inner shelf. Between the shelf edge and CCS the percentage of remineralised nitrate is low using the AOU method (Tables 4.2 and 4.3) ranging from 4 to 10 % using Redfield and 2 to 10 % using measured N:P ratio. However, using the $\delta^{18}O_{NO3}$ to quantify the regenerated nitrate pool, I estimate that there was no local nitrate regeneration at any station apart from CCS (10%). This was due to the $\delta^{18}O_{NO3}$ value in this region being the same as the imported $\delta^{18}O_{NO3}$ value. Between CCS and Site A the percentage of remineralised nitrate was higher using both methods (Table 4.2). The AOU method estimated that at the inner shelf stations CCS, J6, J4, J2 and Site A, the percentage of remineralised nitrate was 4 %, 25 %, 29 %, 32 % and 47 %, respectively using Redfield, and 2.5 %, 18 %, 22 %, 24 % and 35 % using measured N:P ratio. The $\delta^{18}O_{NO3}$ method produced a similar pattern in increasing percentage of remineralised nitrate from 10 % at CCS, through to 20 % at J4 and J2 and 30 % at Site A (Table 4.2). The AOU method estimated that a maximum of 4.5 µM of the nitrate was remineralised at Site A using Redfield, and 3.5 µM using measured N:P ratio. This compared to 2.8 µM estimated by the isotope method. At each of the stations between CCS and the shelf edge less than 1 µM of nitrate was estimated to be remineralised *in situ* using the AOU method, whilst using the isotope method only 0.8 µM was remineralised at CCS (Table 4.2).

In autumn, the percentage and concentration of remineralised nitrate was calculated using a similar approach reported above using the $\delta^{18}O_{imported}$ value of 3.8 ‰ (Table 4.3). The remineralised nitrate for both methods increased from the shelf edge towards the inner shelf, and maximum concentrations of remineralised nitrate were higher than the summer period for both the AOU and stable isotope methods. Between CCS and the shelf edge, the AOU method using Redfield estimates that

between 22 % and 31 % of the nitrate was remineralised *in situ*, increasing from the shelf edge towards CCS. Using measured N:P ratios the AOU method estimates that between 16 % and 23 % was remineralised *in situ*. The stable isotope method, however estimates lower remineralisation at the stations between CCS and the shelf edge ranging between 0 and 23 % (Table 4.2, 4.3). Between CCS and Site A the percentage of remineralised nitrate was higher using both methods (Table 4.3). Estimates of remineralisation using the AOU method using Redfield were between 40 % and 65 % across the inner shelf stations, with the maximum percentage at Site A. Similarly using the measured N:P ratio the range across the inner shelf stations fell between 30 % and 49 %, with the maximum percentage at site A. The remineralised nitrate estimated from the isotope method was between 32 % and 59 % (although at Station J5 it was estimated that zero remineralisation was taking place). The highest remineralisation signal using the isotope method was at station J3. The AOU method using Redfield estimated the concentration of remineralised nitrate was between 1.9 µM and 3.2 µm across the outer shelf, and between 3.3 µM and 6 µM across the inner shelf. The AOU method using measured N:P ratio estimated that between 2.5 and 4.5µM of remineralised nitrate was present across the inner shelf, and between 1.5 and 2.1 µM was present across the outer shelf. This was compared well with the isotope method estimating between zero and 2.3 µM across the outer shelf and between 2.4 µM and 5 µM across the inner shelf (Table 4.3).

Table 4.2. On shelf mean values (± S.D) for bottom water samples for AOU (using Redfield), and AOU (using mean measured N:P ratio), and $\delta^{18}O_{NO3}$ from the inner shelf (A) to the shelf edge (CS2) during summer 2015. Subsequently *in situ* remineralised nitrate (%) and (µM) were calculated from each method using a $\delta^{18}O_{imported}$ value of 3.8‰.

Station	**Water column (WC) depth**	**WC Density Gradient**	**AOU (µM)**	**AOU Remin. N Redfield (%)**	**AOU Remin. N Redfield (µM)**	**AOU Remin. N N:P ratio (%)**	**AOU Remin. N N:P ratio (µM)**	**$\delta^{18}O_{NO3}$ (‰)**	**$\delta^{18}O_{NO3}$ Remin. N (%)**	**$\delta^{18}O_{NO3}$ Remin. N (µM)**
A	93	1.44	+37.5	47	4.5	35	3.4	3.2	30	2.8
J2	91	1.44	+20.8	32	2.5	24	1.9	3.2	30	2.3
J4	107	1.33	+20.9	29	2.5	22	1.9	3.4	20	1.7
J6	102	1.28	+18.2	25	2.2	18	1.6	-	-	-
CCS	137	1.32	+2.3	3.7	0.3	2.5	0.2	3.6	10	0.8
O2	142	1.34	+3.2	5	0.4	3.8	0.3	3.8	0	0
O4	154	1.35	+7.6	10	0.9	7.8	0.7	3.8	0	0
CS2	192	1.08	+5.1	6.4	0.6	5.3	0.5	3.9	0	0

Table 4.3. On shelf values for bottom water samples for AOU (using Redfield), AOU (using measured mean N:P ratio) and $\delta^{18}O_{NO3}$ from the inner shelf (A) to the shelf edge (CS2) during autumn 2014. Subsequently *in situ* remineralised nitrate (%) and (µM) were calculated from each method using a $\delta^{18}O_{imported}$ value of 3.8‰.

Station	**Water column (WC) depth**	**WC Density Gradient**	**AOU (µM)**	**AOU Remin. N Redfield (%)**	**AOU Remin. N Redfield (µM)**	**AOU Remin. N N:P ratio (%)**	**AOU Remin. N N:P ratio (µM)**	**$\delta^{18}O_{NO3}$ (‰)**	**$\delta^{18}O_{NO3}$ Remin. N (%)**	**$\delta^{18}O_{NO3}$ Remin. N (µM)**
A	93	0.22	+50.2	65	6.0	49	4.5	3.1	40	3.7
J2	91	0.17	+34.6	56	4.2	41	3.1	3.3	32	2.4
J3	86	0.27	+39.9	58	4.8	44	3.6	2.7	59	4.9
J5	99	0.26	+34.8	45	4.2	33	3.1	4	0	0
J6	100	0.27	+33.5	-	4.0		3.0	-	-	-
J8	130	0.37	+27.8	40	3.3	30	2.5	2.9	50	5.0
CCS	137	0.44	+26.8	31	3.2	23	2.4	4.3	0	0
O1	136	0.56	+23.6	27	2.8	20	2.1	3.8	9	0
O2	142	0.49	+23.3	27	2.8	20	2.1	-	-	-
O3	139	0.44	+19.3	23	2.3	17	1.7	3.5	23	2.3
O4	154	0.40	+17.1	23	2.1	16	1.5	3.9	5	0
O5	150	0.36	+16.0	21	1.9	16	1.4	4.3	0	0
CS2	192	0.37	+17.0	22	2.0	17	1.5	5	0	0

4.4 Discussion

The timing of the research cruise schedule provided a means to study the seasonality in physical, chemical and biological processes across the Celtic shelf sea. A strong seasonal cycle was evident between autumn 2014 and summer 2015 as expected. There were both cross shelf gradients and gradients between the surface mixed layer and bottom mixed layer for each of the cruises, which allowed different processes to be captured in the $\delta^{15}N_{NO3}$ and $\delta^{18}O_{NO3}$ relationship.

4.4.1 Seasonality in temperature, salinity and inorganic nutrients

The cruise in autumn 2014 captured the post autumn bloom period, when the mixed layer was deepening, before winter mixing occurred. Air temperature and subsequently surface water temperature was starting to decrease causing the mixed layer to deepen, as stratification started to weaken. The water temperature was lower across the inner shelf region compared to the shelf edge where more dynamic mixing occurs (Pingree and Mardell 1981). Throughout the cruise, waters both on and off shelf were still stratified and the mixed layer was generally being below 50 m in depth. During the spring period, the development of the spring bloom was captured as it developed across the shelf during the cruise, as the winter vertically mixed water column became stratified. Throughout the April cruise a weak thermocline developed and by May temperatures in the bottom mixed layer were below 11 °C while temperatures in the surface mixed layer were above 11 °C, with a surface mixed layer of approximately 50 m. Thermal stratification was strongest during the summer period, with maximum surface temperature of 16 °C. In each season the waters near the shelf edge remained warmer than further on shelf, likely due to the warmer waters from further south moving along in the slope current at the shelf edge (Huthnance 2010).

The salinity gradient across the Celtic sea can be utilised as a tracer for the influence of open-ocean and riverine waters. Salinity decreased further on shelf during each of the seasons. During autumn the salinity gradient between the shelf edge and inner shelf stations was the weakest observed. This indicated that riverine input to the shelf waters was the lowest of each of the seasons measured. During

spring 2015 the fresh water influence was stronger than in the autumn, extending further into the Celtic Sea, vertical shear enabled low salinity waters in the surface mixed layer extending further onto the shelf. During the summer period, there was greater influence from riverine sources was observed and suggested a greater transport of riverine nutrients to support production in the Celtic Sea, the lower salinity water in the surface again extending further across the shelf. There was potentially a greater on shelf flux of water during the summer and autumn periods in the bottom waters with the high salinity associated with off shelf water extending further onto the shelf (Figure 4.2 e, h). Estimates of the riverine nitrate supply to Site A and CCS available for the spring bloom using salinity gradients were estimated to be 30 % and 10 %, respectively (Ruiz-Castillo et al. 2018)

Throughout the seasonal nutrient cycle I expected nitrogen uptake to occur in the surface waters during spring, followed by remineralisation of organic matter in the bottom mixed layer during summer and autumn across the inner shelf that is more isolated from the off shelf supply of nitrate. During autumn the concentrations of nitrate and phosphate were low in the surface mixed layer, however there was some re-supply of nutrients from the bottom layer as the mixed layer depth increased. The increase in mixed layer depth enabled nutrients from the more nutrient rich bottom layer to be mixed up into the surface waters due to convective and wind driven mixing (Wihsgott et al. 2016). Nitrite concentration in the surface mixed layer was highest during the autumn period accumulating across the inner shelf stations to concentrations close to 0.4 µM, and the nitrate to phosphate ratio were low indicating that the waters were under saturated in nitrate relative to phosphate. This was consistent with previous studies that indicated nitrogen being the limiting nutrient in the Celtic Sea (Davis et al. 2014). During the spring following the onset of stratification nitrate concentrations rapidly decreased to close to zero due to uptake by phytoplankton. Throughout the summer stratified period the nitrate concentrations in the bottom layer increased while surface concentrations remained near zero until autumn. The N:P ratio remained below the Redfield 16:1 across the inner and middle shelf throughout the sampling period indicating that nitrogen was limiting across the shelf. This was followed by the breakdown of stratification and fully mixed water column during the winter, with the shelf resupplied with nitrate from waters off shelf and riverine sources and from nitrate remineralised *in situ*.

4.4.2 Uptake and remineralisation of nitrate

During this study the observations of $\delta^{15}N_{NO3}$ and $\delta^{18}O_{NO3}$ captured a snapshot of the processes occurring across the shelf during each of the seasons, and provided information on the sources of nitrate to the shelf. During the spring period the $\delta^{15}N_{NO3}$ and $\delta^{18}O_{NO3}$ were already enriched on shelf compared to off shelf values with the first station sampled at CCS having a $\delta^{15}N_{NO3}$ and $\delta^{18}O_{NO3}$ of 7.6 % and 7.0 % in the surface waters. This indicated that there was a pre-bloom episode of phytoplankton uptake causing enrichment before the onset of the main spring bloom event. Along with surface water enrichment the $\delta^{15}N_{NO3}$ and $\delta^{18}O_{NO3}$ of bottom waters were also both above 6 ‰ across the shelf during early spring, over 1‰ higher than off shelf $\delta^{15}N_{NO3}$ and over 2 ‰ higher than off shelf $\delta^{18}O_{NO3.}$ There are two possible explanations for this particularly enriched $\delta^{18}O_{NO3}$: (1) Atmospheric input of nitrate from rainwater with an enriched $\delta^{18}O_{NO3}$ signature, (2) influence of riverine water with elevated $\delta^{18}O_{NO3}$ signature.

(1) Between November 2014 and March 2015, there was 18 cm of rainfall at CCS, coinciding with a decrease in salinity of 0.1 g kg^{-1} over 100 m depth (Ruiz-Castillo et al. 2018). This indicated that between 42 and 48 % of the observed salinity changes in this 100 m depth layer may be attributed to rainfall during the winter time period (Ruiz-Castillo et al. 2018). Across the outer shelf approximately 26 % of the salinity change was a result of precipitation during the same period (Ruiz-Castillo et al. 2018). Heavy rainfall events across the shelf during the winter have the potential to deposit nitrate into the water column, and for the strong winter mixing to distribute the rainwater across the water column. $\delta^{18}O_{NO3}$ of nitrate in rainwater is much higher than that of the corresponding $\delta^{15}N_{NO3}$, as evidenced by enriched $\delta^{18}O_{NO3}$ in rainwater samples collected in Bermuda (one of the only datasets of $\delta^{18}O_{NO3}$ in rainwater available) $\delta^{18}O_{NO3}$ ranged from 60 to 87 ‰ and $\delta^{15}N_{NO3}$ ranged from -2.1 to -5.8 ‰ (Hastings et al. 2003). Therefore, heavy rain events have the potential to elevate $\delta^{18}O_{NO3}$ relative to $\delta^{15}N_{NO3}$ across the shelf. Neglecting any mixing effects I can calculate the volume of rainwater required for a specific change in salinity and therefore the rainfall required to alter the isotopic concentration of $\delta^{18}O_{NO3}$ in the water column using the equation:

$$ppt = ((ppt0^*)((h-d)/h)) + ((ppt\_rain)^*(d/h)) \qquad \text{Eqn 4.6}$$

Where ppt is the current depth-averaged salinity, and ppt0 is the initial salinity in a water-column with depth h (m) after a rainfall event (d; (m)). In this case, ppt_rain is the salinity (or $\delta^{18}O_{NO3}$) of rainwater. If I take a water depth of 100 m (similar to CCS), a $\delta^{18}O_{NO3}$ of rainwater of 60 to 87 ‰, and rainfall of 0.18m with nitrate concentration of 40 mmol m^{-3} over the winter period; then the rainfall can elevate $\delta^{18}O_{NO3}$ across the 100 m by between 0.5 and 0.9 ‰, almost half of the change observed.

(2) The other likely input of $\delta^{18}O_{NO3}$ is from a riverine source with enriched values compared to the open ocean supply of nitrate. The salinity gradient across the Celtic Sea shows that there was a mixing of the oceanic and riverine water across the shelf, with the surface salinity decreasing at Site A from 35.4 to 35.0 between the spring and summer period, then increasing again in the latter half of the year indicating that low salinity water was spreading across the Celtic Sea. At CCS, bottom water salinity increased over the summer period reaching a maximum during the winter period before the spring bloom, indicating transport of high salinity water onto the shelf in the bottom layer. Estimates of the riverine nitrate supply to Site A and CCS available for the spring bloom using salinity gradients were estimated to be 30 % and 10 %, respectively using long term mooring and river discharge data (Ruiz-Castillo et al. 2018). Therefore, $\delta^{18}O_{NO3}$ across the shelf is a mixture of riverine and oceanic water. Bottom water $\delta^{18}O_{NO3}$ at Site A during the spring period was approximately 6.8 ‰ compared to 6 to 6.5 ‰ for the on shelf stations at CCS and the outer shelf. Using mixing effects only and assuming that the sites were linearly connected, this would indicate the riverine source of $\delta^{18}O_{NO3}$ was close to 13.8 ‰, however this underestimates $\delta^{18}O_{NO3}$ at CCS by approximately 1 ‰. When using the change in $\delta^{15}N_{NO3}$ in bottom water during the spring period of 7 ‰ at Site A and 6.6 ‰ across the outer shelf the riverine $\delta^{15}N_{NO3}$ would be estimated at 10.5 ‰, although this again underestimates the $\delta^{15}N_{NO3}$ at CCS by approximately 0.6 ‰. High $\delta^{15}N_{NO3}$ values are often seen in estuaries and rivers with values from German rivers (Rhine, Elbe, Weser, Ems and Eider) that discharge into the North Sea being between 8.2 ‰ and 11.3 ‰ although $\delta^{18}O_{NO3}$ values were much lower between 0.4 ‰ and 2.2 ‰, indicating nitrate derived from sewage or soil nitrification (Johannsen et al. 2008). High $\delta^{18}O_{NO3}$ values have been associated with riverine nitrate with values up to 19

% in the Eastern United States associated with watersheds with significant agricultural and urban land use (Mayer et al. 2002). Considering that the riverine source of nitrate to the Celtic Sea is the Bristol Channel catchment with several large cities on the banks (Jonas and Millward 2010), then the values calculated for $\delta^{15}N_{NO3}$ and $\delta^{18}O_{NO3}$ fall within expected values.

The real scenario is likely to be a combination of both riverine influence and rainfall over winter, elevating both $\delta^{15}N_{NO3}$ and $\delta^{18}O_{NO3}$. Rainwater is the probable cause that elevates $\delta^{18}O_{NO3}$ relative to $\delta^{15}N_{NO3}$, particularly nearer the shelf edge where there was less influence from riverine water. The other process which enriched both $\delta^{15}N_{NO3}$ and $\delta^{18}O_{NO3}$ across the shelf was primary production taking place before the main on-set of stratification and spring bloom, potentially driven by a large rainfall event leading a salinity change and stratifying the water column for a short period (Jardine et al. 2017; Figure 4.15). This rainfall event coincided with an expected salinity decrease, which increased surface buoyancy and kick-started a stratification event before the main temperature controlled stratification occurred during the spring.

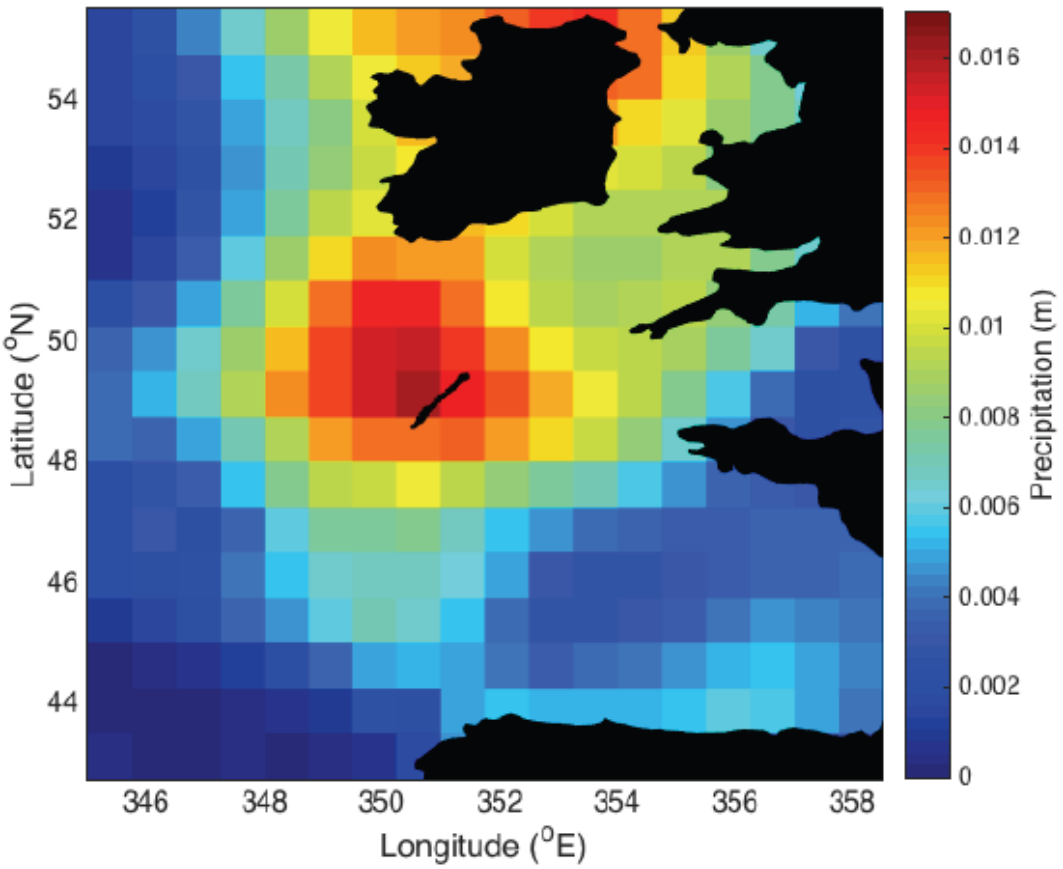

Figure 4.15. Precipitation across the Celtic Sea during the 25th and 26th of March 2015 (taken from Jardine et al., AGU Poster 2017)

Any uptake of nitrate by phytoplankton during the winter spring transition time would be expected to enrich both $\delta^{15}N_{NO3}$ and $\delta^{18}O_{NO3}$ at a 1:1 ratio. This production signal could then be mixed through the water column if stratification broke down, meaning that both $\delta^{15}N_{NO3}$ and $\delta^{18}O_{NO3}$ were higher than expected before the onset of the main spring bloom. This would have implications on both the scenarios discussed previously, with riverine water potentially having lower isotope ratios than calculated.

Liu et al., 2017 investigated nitrate isotopes during the spring bloom in the East China Sea. They found that $\delta^{15}N_{NO3}$ and $\delta^{18}O_{NO3}$ varied between water masses, with the Yellow Sea Coastal Current Water having much higher $\delta^{15}N_{NO3}$ and $\delta^{18}O_{NO3}$ (13.2 ‰ and 18.8 ‰, respectively) than the Yellow Sea Mixed Water (6.3 to 8.2 ‰, respectively and Yellow Sea Warm Current Water (6.2 to 9.7 ‰, respectively). Of particular relevance to this study, $\delta^{18}O_{NO3}$ was particularly high and higher than the

$\delta^{15}N_{NO3}$, comparable to the high values in spring in the Celtic Sea. The high $\delta^{18}O_{NO3}$ was attributed to multiple sources of nitrate, with 71 % of the nitrate from atmospheric deposition(Liu et al. 2017).

During the main spring bloom period, $\delta^{15}N_{NO3}$ and $\delta^{18}O_{NO3}$ both increase at close to a 1:1 ratio to a maximum of 11.6 ‰ and 11.9 ‰, respectively before nitrate concentrations decreased below 1 µM. As phytoplankton consume nitrate (and ammonium, nitrite and other N compounds) they leave the remaining nitrate pool progressively enriched in ^{15}N and ^{18}O due to preferential take up of ^{14}N relative to ^{15}N (Altabet and Francois 2001). The quantitative relationship between $\delta^{15}N_{NO3}$ and nitrate consumption can be described using first order Rayleigh fractionation (Mariotti et al. 1981) (as described in Chapter 1, equation 1.3).

During summer the relationship between $\delta^{15}N_{NO3}$ and $\delta^{18}O_{NO3}$ in the bottom waters can help investigate the regeneration signal on shelf. Quantitatively, the degree of nitrate recycling can be determined by using $\delta^{18}O_{NO3}$ and $\delta^{18}O_{H2O}$ (the $\delta^{18}O$ of background water). The light $\delta^{18}O_{NO3}$ values due to remineralisation are defined as 1.1 ‰ plus $\delta^{18}O_{H2O}$ (Sigman et al. 2009b). The specific $\delta^{18}O_{nit}$ value (the value of newly nitrified nitrate) of 1.1 % above ambient seawater was used as this was estimated from $\delta^{18}O_{NO3}$ in the eastern Mediterranean, where subsurface nitrate originates exclusively from *in situ* remineralisation (Sigman et al. 2009b). $\delta^{18}O_{H2O}$ was collected at 24 locations across the Celtic Sea during the spring cruises (DY029). $\delta^{18}O_{H2O}$ across the shelf was 0.6 ±0.1 ‰, giving a newly nitrified nitrate signal of between 1.6 ‰ and 1.8 ‰. A value of 1.7 ‰ was chosen for newly nitrified nitrate across the Celtic Sea.

An $\delta^{18}O_{imported}$ value of 3.8 ‰ was used, this was the mean $\delta^{18}O_{NO3}$ between the base of the mixed layer and 500 m off shelf, encompassing the density layers entrained onto the shelf during winter. Sensitivity analysis shows that the relationship between $\delta^{18}O_{imported}$ and the percentage of remineralised nitrate is non-linear, with the values close to the measured value having a larger proportionate effect on the value. i.e. a change of 0.1 ‰ from 3.8 ‰ to 3.9 ‰ increases the percentage remineralised nitrate by 4 %, however an increase of 1 ‰ from 3.8 ‰ to 4.8 ‰ only increases the remineralised nitrate by 28 ‰. This demonstrates that

choosing the correct value is important as the effects are non-linear following a second order polynomial relationship.

The two methods applied in this study to estimate the percentage and concentration of nitrate demonstrated a similar pattern of regeneration across the Celtic sea. During the summer the regenerated nitrate signal across the outer shelf stations from CCS to the shelf edge was below 10 % for both methods. At the inner shelf stations the regenerated signal was higher for both methods, with the regenerated signal increasing towards the innermost station, Site A. Despite the overall agreement of the two methods in the general pattern of remineralisation across the shelf they vary by up to 17 % at Site A when Redfield was used. AOU using Redfield estimated that 47 % of the nitrate at Site A was remineralised *in situ*, compared to only 30 % using the stable isotope method. At all other stations the disparity was within 10 % for Redfield and often below 5 % when using the measured N:P ratio, with the stable isotope method usually indicating that less nitrate was remineralised relative to that estimated using AOU. An exception to this was at CCS, where the stable isotope method estimated that 10 % of the nitrate was remineralised compared to 3.7 % for the AOU method using Redfield. The remineralisation signal in the autumn was similar to summer using both methods, with more nitrate being remineralised across the inner shelf stations. The maximum percentage of remineralised nitrate using the AOU method was at Site A, with 65 % of the nitrate estimated to be remineralised *in situ* using Redfield and 49 % remineralised *in situ* using the N:P ratio, compared to 40 % estimated by the isotope method. The maximum regenerated nitrate estimated by the isotope method was at station J3, with 59 % of the nitrate estimated to be remineralised *in situ*, compared to 58 % estimated by the Redfield AOU method. Across the outer shelf the AOU method estimated higher regeneration, (over 20 %) at each of the stations from CCS to the shelf edge, compared to much lower estimates using the stable isotope method that were under 10 % for all stations apart from O3.

The higher percentage of remineralised nitrate across the inner shelf region compares well with Granger et al., (2013) who investigated the proportion of remineralised nitrate across the Bering Sea. They estimated that between 20 % and 100 % of the nitrate across the inner shelf was remineralised *in situ* as the inner shelf was isolated from the off shelf supply of nitrate over the winter period. The inner

shelf regions of the Celtic Sea fall within this estimate for both summer and autumn period remineralisation, and the inner shelf.

The results of this study imply that there was more local nitrate regeneration occurring during both the summer and autumn across the inner shelf compared to the outer shelf. This indicates that the inner shelf stations are potentially more isolated from an off shelf supply of nitrate during the summer and autumn than those stations located from CCS towards the shelf edge, and that those stations at the shelf edge are potentially supplied by off shelf nitrate during the summer and autumn periods. This hypothesis is supported by the intrusion of higher salinity bottom waters at the shelf edge, as indicated, for example, with the on shelf movement of the 35.7 and 35.6 isohalines at a speed of around 0.8 km d^{-1} (Figure 4.16a and b). Using the change in salinity, (Ruiz-Castillo et al. 2018) estimated that approximately 0.4 mmol m^{-3} of nitrate at CCS was attributed to on shelf transport during the summer.

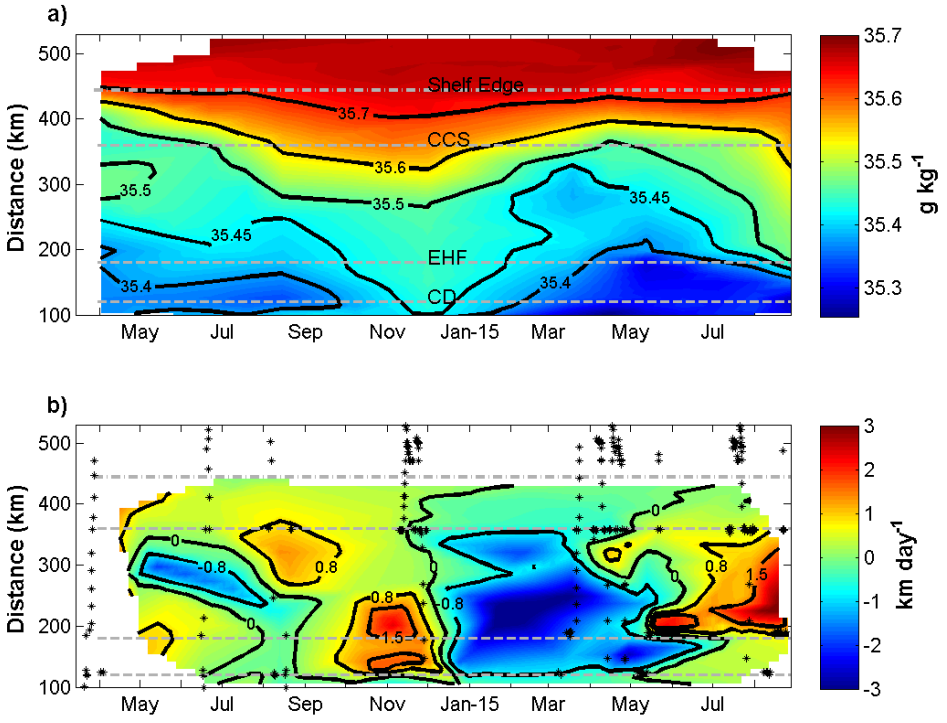

Figure 4.16. (a) Bottom water absolute salinity (80 m) along the transect and (b) velocities calculated from the salinity displacement. Taken from Ruiz-Castillo et al., 2018.

Estimates of remineralisation have impacts on carbon uptake and export from the Celtic Sea. If the nitrate fuelling production during the summer and autumn periods is driven by regenerated nitrate then any carbon within the system is also regenerated

and not lost to the sediments, leading to minimal carbon drawdown from the atmosphere and reducing the ability of the shelf to take up carbon. This signal is seen across the inner shelf in both the AOU estimates of regeneration and the stable isotope estimates of regeneration. The outer shelf however, is flushed with 'new' off –shelf nitrate during the summer and autumn periods, and this suggests that the production across the outer shelf during the summer and autumn is fuelled by 'new' nitrate with minimal nitrate regenerated *in situ*.

There were differences in remineralised nitrate estimated using the two methods. The percentage of regenerated nitrate using the stable isotope method was generally lower to AOU, with the difference between methods being most pronounced at the outer shelf region. There are several potential reasons for this disparity. Firstly, the AOU method is the difference between the dissolved oxygen concentration and its equilibrium saturation. If off shelf nitrate rich water is supplied to the shelf during the summer and autumn this may be effectively transporting a low AOU value, but will be supplying 'new' nitrate to the bottom layer and is therefore not representative of local oxygen consumption. The stable isotope method however is a true measure of regeneration as the only process that can lower the $\delta^{18}O_{NO3}$ in nitrate is nitrification. This leads to low rates of remineralisation taking place in the bottom waters across the outer shelf during the summer and autumn periods. AOU calculated using the measured N:P ratios rather than Redfield were closer to the estimates using stable isotopes, this is due to much of the shelf generally being below Redfield ratio for the majority of the year.

Across the inner shelf, where both methods indicate higher remineralisation, the values using the isotope method represent an under estimate of remineralisation. This underestimate is because of the off shelf end member chosen for the $\delta^{18}O_{imported}$ (3.8 ‰), which would only be a true end member if the entire shelf was completely flushed with off shelf nitrate. In reality a percentage of the nitrate available across the shelf (up to 30 % at the innermost station Site A) is from riverine sources with a unique end-member that is likely higher than the off shelf value chosen. Choosing a more riverine end-member value based off the 30 % influence at Site A, then potentially over 70 % of the nitrate was remineralised *in situ* during the autumn period. Similarly, using the estimated 10 % riverine influence at CCS then over 15 % of the nitrate was remineralised *in situ* during the autumn.

Overall, the results illustrate that a significant proportion of the nitrate across the inner shelf was remineralised during the summer and autumn periods. In contrast, the proportion of nitrate remineralised was lower across the outer shelf to CCS, and instead, an off shelf supply of nitrate was relatively more important during summer and autumn than previously thought. These results therefore challenge the classical view we have of the shelf where wintertime flushing supplies the majority of nitrate for the spring bloom and suggest that a combination of riverine, on shelf transport of nitrate from the shelf edge during the summer and *in situ* remineralisation maintain the nitrate pool on shelf during the summer and autumn periods.

Chapter 5. Nitrogen cycling across the Hebrides Shelf

5.1 Introduction

The Hebrides Shelf, which lies to the west of Scotland and north of Ireland makes up the north western region of the NW European Shelf, covering approximately 9 % of the total NW European Shelf area. There have been numerous long-term observational and modelling studies that show that there is significant exchange of water between Hebrides shelf and the open ocean, with ocean-shelf water exchange estimated at 3 $m^2 s^{-1}$. This is the same as the exchange estimate for the Celtic Sea (3 $m^2 s^{-1}$), and slightly less than the North Sea (4 $m^2 s^{-1}$; (Holt et al. 2009; Huthnance 2010)). The down-welling circulation along the Hebrides shelf is important for the export of carbon to the open ocean (Huthnance et al. 2009), being driven by the warm saline water flowing northwards along the shelf edge. This warm current lies above the 500 m bathymetric contour and below the seasonal thermocline that develops in spring and persists through to the autumn (Booth and Ellett 1983; Huthnance 1986). The large exchange between the Hebrides shelf and Atlantic make this region a good place to investigate the potential for the cross-shelf exchange of nitrate and the imprint this would have on $\delta^{15}N_{NO3}$ and $\delta^{18}O_{NO3}$.

Shelf seas are responsible for 15 to 30 % of global ocean primary production, whilst occupying only ~8 % of ocean surface area and thus play a disproportionately large role in global productivity and the global carbon cycle (Wollast 1998). In temperate shelf seas, there is a strong seasonal cycle, controlled by the development of a seasonal thermocline which along with improved light conditions, drives a short spring bloom event. The seasonal thermocline separates the surface mixed layer (SML) from the bottom mixed layer (BML). The SML is characterised by having low nutrient concentrations throughout most of the year due to uptake of nutrients by phytoplankton. In contrast, nutrients in the BML are higher throughout the year due to respiratory processes and bacterial remineralisation of organic matter.

Nitrate (NO_3^-) is one of the essential inorganic macronutrients for marine phytoplankton. Nitrate limits production within most shelf sea environments (Gruber 2004), and therefore the supply of nitrate to shelf seas has implications for the efficiency of the biological carbon pump (or shelf sea carbon pump) (Thomas et al.

2004). As phytoplankton take up nitrate during the spring bloom, summer and autumn periods, they produce organic matter, which as it sinks is either remineralised, lost to sediments or transported off shelf or is consumed by higher trophic levels (although this in turn produces organic matter on shelf). The relative magnitude of each of these processes is important to quantify in order to fully understand the nutrient cycles in shelf seas.

Stable isotopes, specifically the stable nitrogen and oxygen isotopes of nitrate ($\delta^{15}N_{NO3}$ and $\delta^{18}O_{NO3}$, respectively) are useful tools to unravel the complex nutrient cycling and transport within the shelf sea system. The signatures of $\delta^{15}N_{NO3}$ and $\delta^{18}O_{NO3}$ are fractionated during nitrogen cycling processes. The primary N cycling process in temperate shelf sea surface waters that fractionates the aforementioned isotopes is the consumption of nitrate by phytoplankton. The $\delta^{15}N$ and $\delta^{18}O$ of surface water nitrate increases at a 1:1 ratio ($^{15}\varepsilon=^{18}\varepsilon$) as nitrate is progressively depleted by phytoplankton utilisation of the lighter isotope (Altabet and Francois 2001). If there is no resupply of nitrate to the surface waters then $\delta^{15}N_{NO3}$ and $\delta^{18}O_{NO3}$ become increasingly enriched in ^{15}N and ^{18}O respectively following Rayleigh fractionation patterns. Differences in the isotopic effect between $\delta^{15}N_{NO3}$ and $\delta^{18}O_{NO3}$ arise during production of nitrate. Nitrification 'resets' the $\delta^{18}O_{NO3}$ signature as oxygen atoms are derived from water. This process gives a $\delta^{18}O_{NO3}$ signature approximately 1.1 ‰ above that of the background $\delta^{18}O$ of seawater, as there is a small fractionation effect associated with nitrification. Therefore, the $\delta^{18}O_{NO3}$ signature is disconnected from the $\delta^{15}N_{NO3}$ (which relies on the $\delta^{15}N$ of the fixed nitrogen pool) as it loses any previous enrichment signal from denitrification, utilisation or partial unitisation by phytoplankton (Casciotti et al. 2002; Sigman et al. 2005; Sigman et al. 2009b). These processes which cause differences in the isotopic effect on nitrogen and oxygen atoms has led to the development of the parameter Δ (15-18), which is defined as the difference between $\delta^{15}N_{NO3}$ and $\delta^{18}O_{NO3}$ (Rafter et al. 2013). This parameter can give information on the sources of remineralised NO_3^- ; as a deviation away from a 1:1 relationship causes a shift in the Δ (15-18). Low Δ (15-18) values can indicate the addition of low ^{15}N due to remineralisation of organic matter that has recently been fixed, while a high Δ (15-18) can indicate remineralisation in low nitrate areas where $\delta^{15}N$ values of organic matter are close to 5 ‰ due to complete uptake (Knapp et al. 2008; Rafter et al. 2013).

This study investigated the post autumn bloom nutrient cycling and remineralisation across the Hebrides shelf system using the stable isotopes $\delta^{15}N_{NO3}$ and $\delta^{18}O_{NO3}$. I present four cross-shelf transects of $\delta^{15}N_{NO3}$ and $\delta^{18}O_{NO3}$ measurements – A, C, E and F across the Hebrides Shelf (Figure 5.1). I used $\delta^{15}N_{NO3}$ and $\delta^{18}O_{NO3}$ data alongside temperature, salinity, oxygen and inorganic nutrient data to understand both the surface and bottom layer nutrient processes and to quantify the extent of nutrient remineralisation across the Hebrides Shelf in October and November 2014. The parameter Δ (15-18) was used to investigate changes in the $\delta^{15}N_{NO3}$ and $\delta^{18}O_{NO3}$ relationship across the Hebrides Shelf, shelf edge and open ocean. The $\delta^{18}O_{NO3}$ stable isotope proxy for nitrogen regeneration processes was compared to estimates from apparent oxygen utilisation (AOU) allowing estimation of nutrient remineralisation from oxygen depletion. The $\delta^{18}O_{NO3}$ and AOU methods were used to calculate the percentage of remineralised nitrate on the shelf. The $\delta^{18}O_{NO3}$ estimates were then compared to other shelf sea studies that utilised $\delta^{15}N_{NO3}$ and $\delta^{18}O_{NO3}$ including in the Bering Sea (Granger et al. 2013) and in the East China Sea (Liu et al. 2017). The estimates of on shelf remineralisation can help better understand the nitrogen cycling for the Hebrides Shelf and consequently how much nitrate and carbon is supplied from the open ocean or regenerated *in situ* on shelf. This in turn will further improve models of carbon flux and budgets of the north-west European continental shelf.

5.2 Methods

DY017 was a Shelf Sea Biogeochemistry process cruise to the Outer Hebrides. The research cruise took place on board the RRS Discovery from 20th October 2014 to 11th November 2014, capturing the end of the stratification period and beginning of the breakdown in stratification and onset of winter mixing. The Outer Hebrides is immediately to the west of the UK and North of Ireland and is known to be a key region for the exchange of water, nutrients and carbon between the continental shelf and North Atlantic Ocean (Holt et al. 2009; Huthnance 2010; Painter et al. 2016). Six of the seven planned transects were completed with the seventh transect (B) abandoned due to poor weather (Figure 5.1). Transects ranged from between 100 km to 150 km with transect D being the shortest and C being the longest. Isotope data was analysed from four of the six completed transects. Water

depth ranged from 60 m at the innermost stations on transect G to over 2500 m at the oceanic stations on each transect.

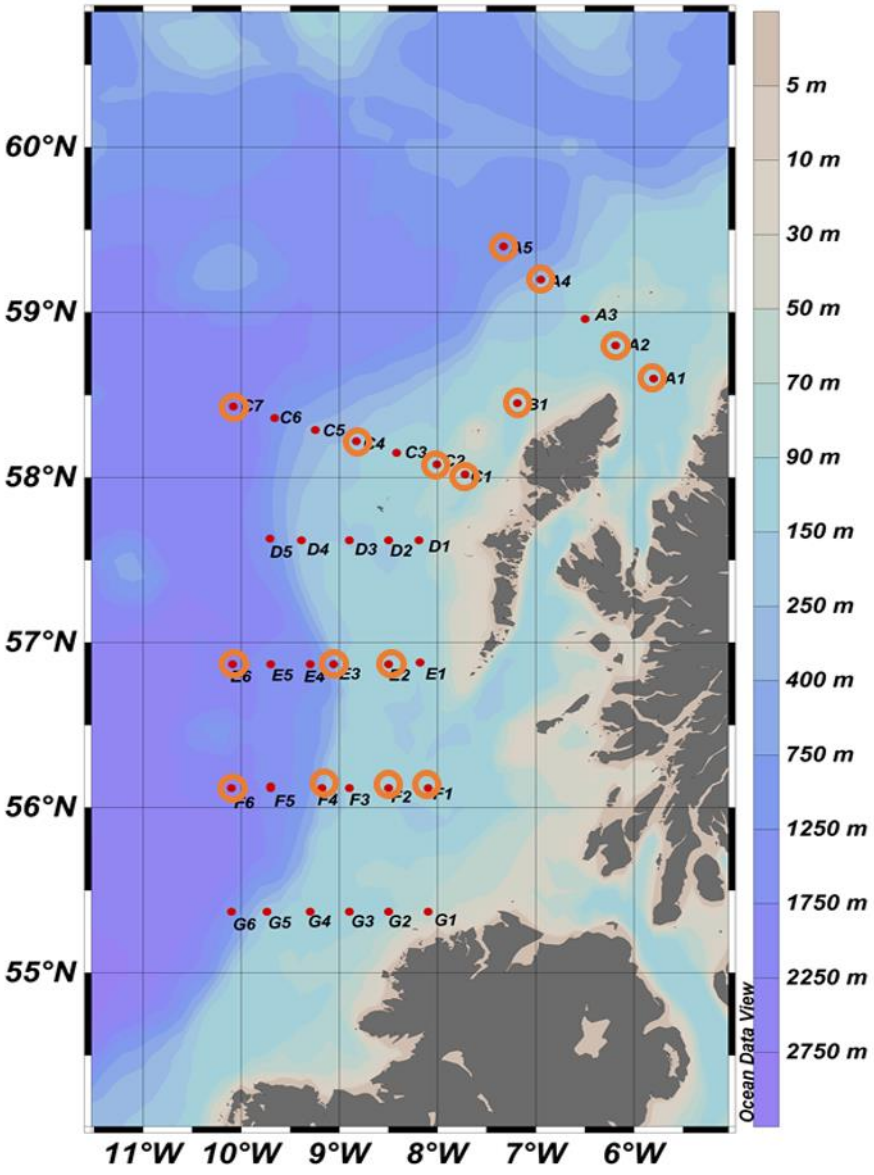

Figure 5.1. Map of the Hebrides/Malin Shelf area showing sampling stations during DY017 October-November 2014. The orange circles show stations where water samples for $\delta^{15}N_{NO3}$ and $\delta^{18}O_{NO3}$ were collected.

Seawater samples were collected using a rosette equipped with a seabird CTD, fluorescence and oxygen sensor package and 24-20 L Niskin bottles. Seawater samples for $\delta^{15}N$ and $\delta^{18}O$-nitrate analysis were filtered through Whatman glass fibre filters (GF/F, 0.7 µm pore size, pre-combusted at 450 ˚C for 4hrs before acid washing, deionized water rinsing, and drying at 50 ˚C) into 60 ml high density polyethylene

(HDPE) bottles and were stored frozen at -20 ˚C until analysis. Sampling was performed by Nealy Carr (University of Liverpool).

Inorganic nutrients (nitrate+nitrite, phosphate and silicate) were collected via CTD sampling. Samples were collected from all sampled depths and refrigerated at 4°C until analysis. Samples were analysed on a Skalar Sanplus autoanalyser (Brewer and Riley 1965; Grasshoff 1976; Mantoura and Woodward 1983; Kirkwood 1989; Zhang and Chi 2002). Dissolved oxygen concentrations were measured using Winkler whole bottle technique with an estimated accuracy of ± 0.3 µmol kg^{-1}. These discrete measurements were used to calibrate the Seabird-43 dissolved oxygen sensor attached to the CTD frame (Langdon 2010).

Apparent oxygen utilisation (AOU) was calculated as:

$$\text{AOU } (\mu M) = \text{saturated } O_2\ (\mu M) - \text{observed } O_2\ (\mu M). \qquad \text{Eqn 5.1}$$

Saturated O_2 calculated as a function of temperature and salinity using equations by (Garcia and Gordon 1992). AOU is the difference between the measured dissolved oxygen concentration and its equilibrium saturation concentration in water with the same properties. Therefore, the AOU of a water sample is the sum of the biological activity since it was last at an equilibrium concentration with the atmosphere. Positive AOU values indicate water that has been out of contact with the atmosphere and potential *in-situ* remineralisation, whereas a near zero or negative AOU value indicates concentrations close to saturation due to close contact with the atmosphere or biological production or low respiration (Garcia and Levitus 2006). AOU was used to calculate nitrate released by respiration by assuming Redfield stoichiometry (Redfield 1963)of 138:106:16:1 (O:C:N:P):

$$1 \text{ mol } O_2 \text{ consumed} = 106/138 \text{ mol } CO_2 + 16/138 \text{ mol } HNO_3 + 1/138 \text{ mol } H_3PO_4$$

$$= 0.77\ CO_2 + 0.12\ HNO_3 + 0.0072\ H_3PO_4 \qquad \text{Eqn 5.2}$$

AOU values were then used to calculate the percentage (%) and concentration (µM) using equation 5.3 using both Redfield stoichiometry and measured N:P ratio for stations with a positive AOU value.

$\delta^{15}N_{NO3}$ and $\delta^{18}O_{NO3}$ were analysed using the 'Denitrifier Method' as described in Chapter 2 (Sigman et al. 2001; Casciotti et al. 2002; McIlvin and Casciotti 2011) at the LIFER laboratory in Liverpool using a customised Thermo – Finnigan Gas Bench

II (with backflush) interfaced with a Thermo Fisher Delta V Advantage IRMS. Isotope ratios are reported as parts per thousand deviations from a known international standard. The isotope ratios are reported using delta notation (δ) with units per mil (‰):

$$\delta(X) = \left[\frac{R_{sample} - R_{standard}}{R_{standard}}\right].10^3[‰] \qquad \text{Eqn 5.3}$$

Where R=$^{15}N/^{14}N$, the ratio of the atom occurrence of the rare to common isotope. The reference values for $^{15}N/^{14}N$ and $^{18}O/^{16}O$ are N_2 in air and Vienna Standard Mean Ocean Water (VSMOW), respectively. The proportion of remineralised nitrate (X) can be quantified using the following equation:

$$\delta^{18}O_{measured} = \delta^{18}O_{nitrified}\,(X) + \delta^{18}O_{imported}\,(1\text{-}X) \qquad \text{Eqn 5.4}$$

$$X = 1 - \left(\frac{\delta^{18}O_{measured} - \delta^{18}O_{nitrified}}{\delta^{18}O_{imported} - \delta^{18}O_{nitrified}}\right) \qquad \text{Eqn 5.5}$$

$\delta^{18}O_{measured}$ was defined the measured value of $\delta^{18}O_{NO3}$, $\delta^{18}O_{nitrified}$ was the $\delta^{18}O$ value of newly nitrified nitrate (1.7 ‰) and $\delta^{18}O_{imported}$ was the value of $\delta^{18}O_{NO3}$ imported onto the shelf from the open ocean through cross-shelf exchange (Eq. 5.4). The percentage of remineralised nitrate can be calculated by multiplying the proportion of remineralised nitrate (X) by 100 and the concentration of newly nitrified nitrate can then be calculated by multiplying the proportion of remineralised nitrate (X) by the nitrate concentration (Eq. 5.5).

5.3. Results

5.3.1 Temperature, salinity and density

The mean temperature in the surface mixed layer was 12.3 ± 0.4 °C across all transects (Figure 5.2). There were small horizontal gradients in temperature across the mixed layer of each transect, with the shelf being on average only 0.3 °C warmer than the open ocean. The mixed layer on shelf was 12.2 ± 0.3 °C, compared to 11.9 ± 0.4 °C off shelf (Figure 5.2). Temperature in the surface mixed layer was similar between north to south transects, with the southern transect mean temperature being comparable to the northern stations. The mean surface mixed layer temperature across transect F was 12.3 ± 0.2 °C compared to 12.1 ± 0.4 °C for transect C and 12.2 ± 0.3 °C for transect A. Temperature remained above 12 °C across most of

transect A where the water column was weakly stratified (Figure 5.2a). There was a decrease in temperature with depth closer to the shelf edge, with southernmost stations being the warmest, shelf edge stations from transect E and F had a bottom water temperature of approximately 11 °C, compared to 10 °C at the more northern transects C and D (Figure 5.2).

The mean salinity in the surface mixed layer was 35.23 ± 0.17 across all transects (Figure 5.2). There was a horizontal salinity gradient from freshest at the inner shelf becoming more saline at the shelf edge and open-ocean. Compared to the rest of the transects, the water was 0.35 fresher at the innermost stations on the most northern transects, A1 and A2, with mean water column salinity of 34.78 ± 0.03 and 34.93 ± 0.13 respectively (Figure 5.2f). The SML was fresher (34.77 ± 0.01) at station A2 compared to the BML (35.03 ± 0.03; Figure 5.2f). Salinity increased towards the shelf edge with off shelf mixed layer salinity of 35.4 ± 0.01 across the entire data set. There was a pronounced salinity gradient across the shelf along Transect C with a minimum salinity of 35.11 ± 0.01 at station C2 (Figure 5.2g). The salinity gradient was less pronounced along Transects D through to F with the freshest on shelf mixed layer water being approximately 35.20. There were no horizontal or vertical gradients in salinity in the surface 500 m at off shelf stations, apart from a fresher spike at A5, the outermost sampling station 35.33 (Figure 5.2f).

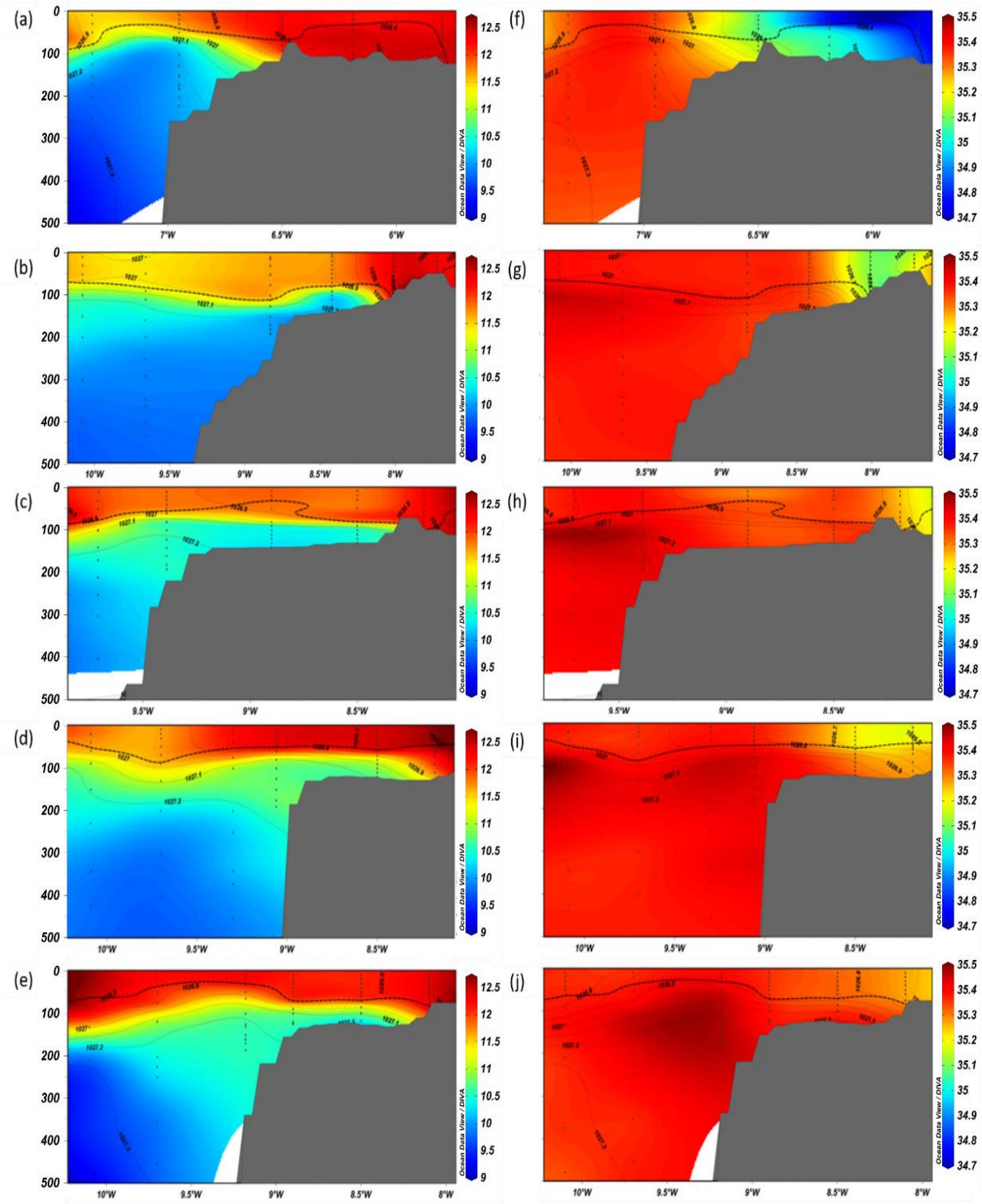

Figure 5.2. (a) to (e) Temperature (°C) for transects A, C, D, E and F across the Hebrides Shelf during October and November 2014. (f) to (j) Salinity for transects A, C, D, E and F across the Hebrides during October and November 2014. Data was plotted in ODV using DIVA gridding using GEBCO1 bathymetry. Isobars show density (kg m^{-3}), dots show sampling depths and the dotted line shows the mixed layer depth.

Density is reported as sigma theta (Density kg m^{-3} - 1000). As expected density increased with depth, the densest waters were found off shelf at 27.8 kg m^{-3} at 2000 m (Figure 5.3). Throughout this chapter the cross shelf transects have been presented between the surface and 500 m depth, as the density surfaces connecting the shelf and open ocean were captured and there was no significant increase in density below 500 m depth before reaching close to 1km (Figure 5.3). Density between the surface and 500 m ranged from 26.3 kg m^{-3} to 27.4 kg m^{-3}, with variations between transects, across the shelf and open ocean. Surface waters along Transect A had the lowest density waters at 26.3 kg m^{-3}, whilst density in surface waters along the other transects was between 26.6 kg m^{-3} and 27.4 kg m^{-3} (Figure 5.3).

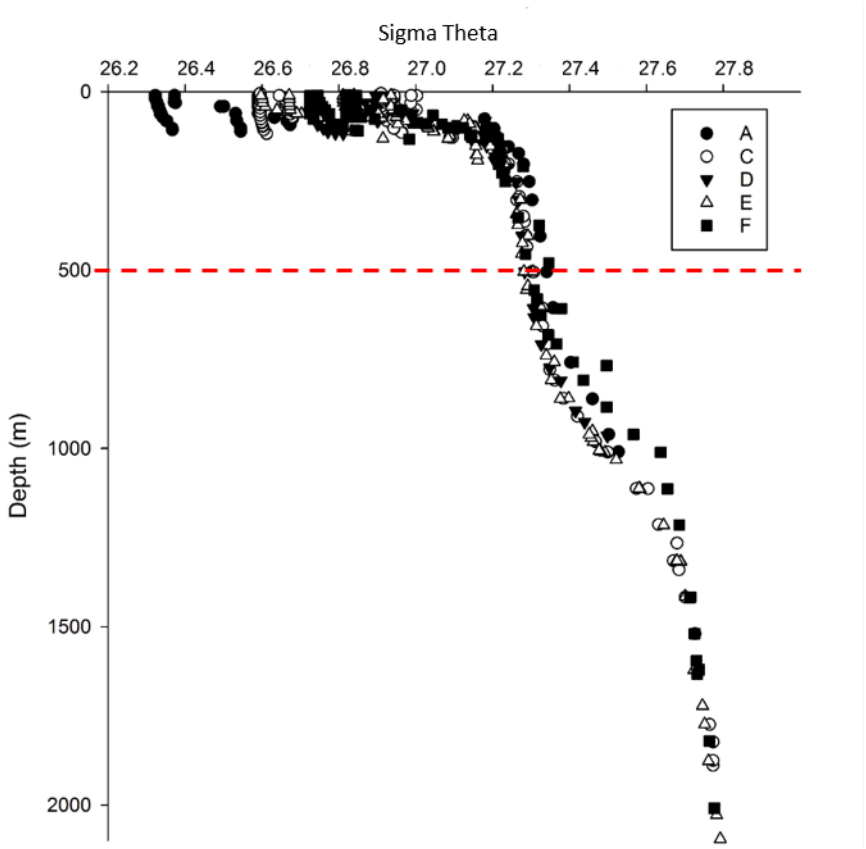

Figure 5.3. Depth (m) variation in sigma theta (density kg m^{-3} -1000) for each of the transects A – F across the Hebrides Shelf during October and November 2014.

Each of the transects had similar off shelf densities of between 27.2 kg m^{-3} and 27.4 kg m^{-3} between 200 m (approximate depth of the shelf edge) and 500 m depth, and surface density of between 26.8 kg m^{-3} and 26.9 kg m^{-3} (Figure 5.4). There were vertical and horizontal gradients in density observed across the shelf.

Transect A had the largest cross-shelf gradient in density at the innermost stations Surface density was 26.4 kg m^{-3} and the shelf edge stations had a density of 27 kg m^{-3} (Figure 5.4a).The horizontal density gradient for transects C to F was less pronounced than transect A, with density increasing from approximately 26.6 kg m^{-3} to 26.9 kg m^{-3} in the surface waters and 26.7 kg m^{-3} to 27.2 kg m^{-3} in the bottom water depths towards the shelf edge (Figure 5.4b, 5.4c, 5.4d 5.4e).

The mixed layer depth at each station was calculated using the density difference of 0.03kg m^3 from the near surface (CTD sample closest to the surface; (de Boyer Montégut et al. 2004). The mixed layer depth varied across the shelf and open ocean (Figure 5.4f, 5.4g, 5.4h, 5.4i, 5.4j). The water column was fully mixed at the innermost stations on Transects A, C, D and F. The mixed layer depth for stations closer to the shelf edge and the open ocean was between 50 m and 100 m across the transects (Figure 5.4f, 5.4g, 5.4h, 5.4i, 5.4j). The overall increase in density relative to *in situ* surface density across the entire water column was lowest at the inner most shelf stations, indicating weaker stratification. The lowest increase was observed along transect A with the density difference being less than 0.2 kg m^{-3} across the three on shelf stations, indicating much weaker stratification than the open ocean (Figure 5.4f). There was a small increase in density difference at the outermost shelf stations of transects C and D to approximately 0.3 kg m^{-3} between the surface and sediments, and another increase at the outermost shelf stations of transect E and F to approximately 0.4 kg m^{-3} between the surface and benthos; indicating that the strength of on shelf stratification increased towards the south (Figure 5.4g, 5.4h, 5.4i, 5.4j).

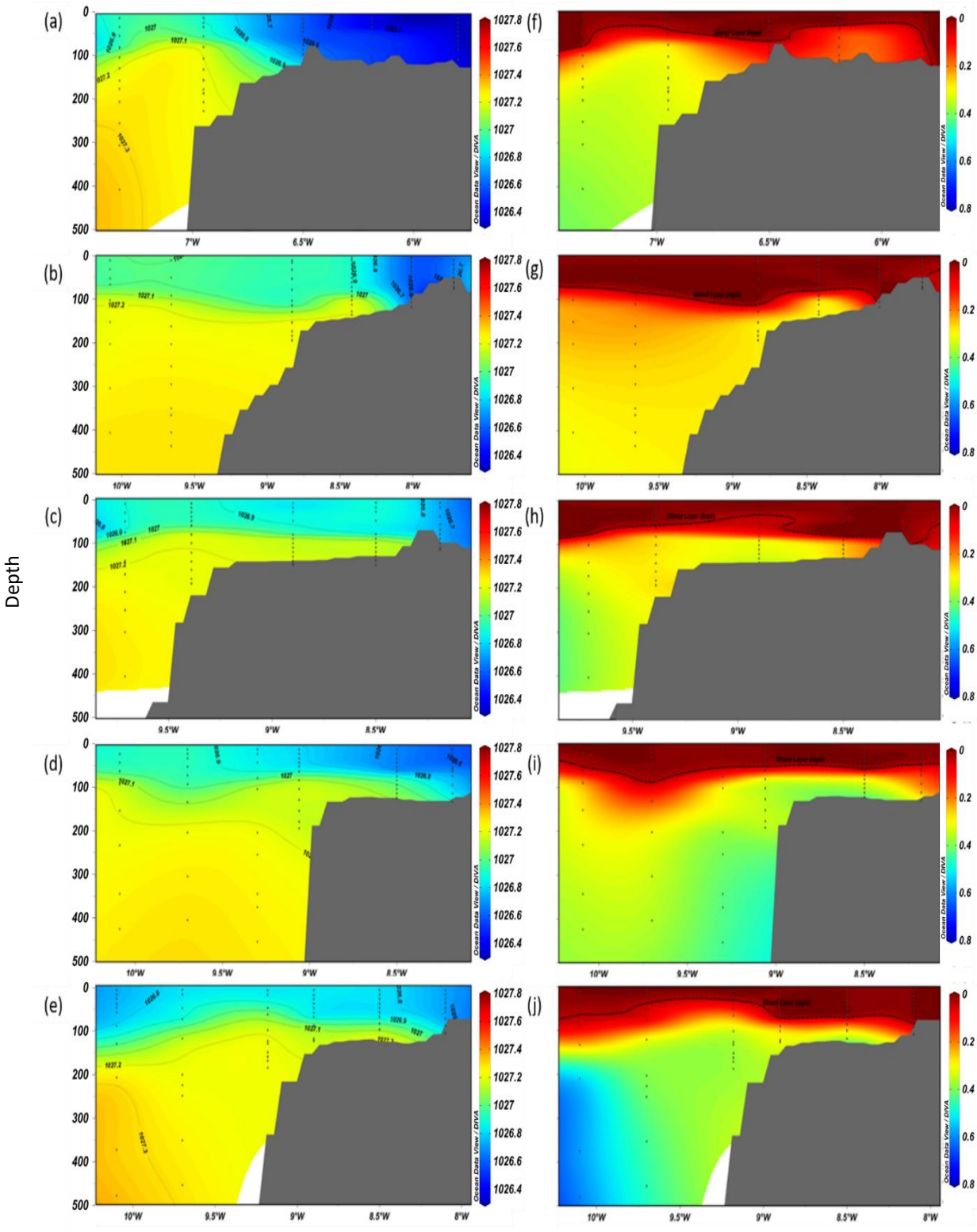

Figure 5.4. (a) to (e) Density (kg m^{-3}) for transects A, C, D, E and F across the Hebrides Shelf during October and November 2014 to 500m water depth. (f) to (j) Density difference (kg m^{-3}) from the surface for transects A, C, D, E and F across the Hebrides Shelf during October and November 2014 to 500m water depth. Data was plotted in ODV using DIVA gridding and GEBCO1 bathymetry. Isobars show density (kg m^{-3}), dots show sampling depths and the dotted line shows the mixed layer depth**.**

5.3.2 Inorganic nutrients, oxygen and fluorescence

There were both vertical and horizontal gradients in nitrate and phosphate across all transects. In general, nitrate concentrations in the mixed layer on the shelf (4.7 ± 0.7 µM) were slightly lower than off shelf nitrate (5.0 ± 1.0 µM; Figure 5.5). Bottom layer (defined as the below the mixed layer to the sediments) mean nitrate concentrations were 10.1 ± 3.6 µM on the shelf, and were more variable horizontally across the shelf than nitrate in the surface mixed layer. At the innermost stations, where stratification was weakest or the water column was mixed, nitrate concentrations were almost uniform with depth at stations A1, A2, B1, C1 and C2 with mean water column concentrations of 3.8 ± 0.2 µM, 4.5 ± 0.1 µM, 4.2 ± 0.1 µM, 4.6 ± 0.1 µM and 4.5 ± 0.1 µM (Figure 5.5a, 5.5b). The highest concentrations were found on transect C where the water column was still stratified, reaching a maximum of over 14 µM in the bottom layer at stations C3 and C4 (Figure 5.5b). These differences were primarily caused by the change in stratification. At the inner shelf stations, nitrate was mixed over the entire water column, while at stations closer to the shelf edge the nitrate had accumulated in the bottom mixed layer of the stratified water column. Overall the nitrate inventory was similar across similar water depths at different stations.

The vertical patterns in phosphate were similar to nitrate. The mean surface mixed layer phosphate concentration across all transects was 0.36 ± 0.04 µM. There was no change in overall mean surface mixed layer phosphate concentrations between the on shelf and off shelf stations both having a concentration of 0.36 ± 0.04 µM (Figure 5.5). The innermost stations, where stratification was the weakest, or the water column was completely mixed, had an almost uniform phosphate concentration throughout the entire water column at stations A1, A2, B1, C1 and C2 with mean water column concentrations of 0.39 ± 0.01 µM, 0.37 ± 0.14 µM, 0.34 ± 0.01 µM, 0.36 ± 0.01 µM and 0.36 ± 0.01 µM respectively (Figure 5.5f, 5.5g). The highest concentrations were found on transect C, reaching a maximum of over 0.9 µM in the bottom layer at station C4 (Figure 5.5g). These differences were primarily caused by the change in stratification, as at the inner shelf stations the phosphate was mixed over the entire water column, whilst at those stations closer to the shelf edge the phosphate had accumulated in the bottom mixed layer.

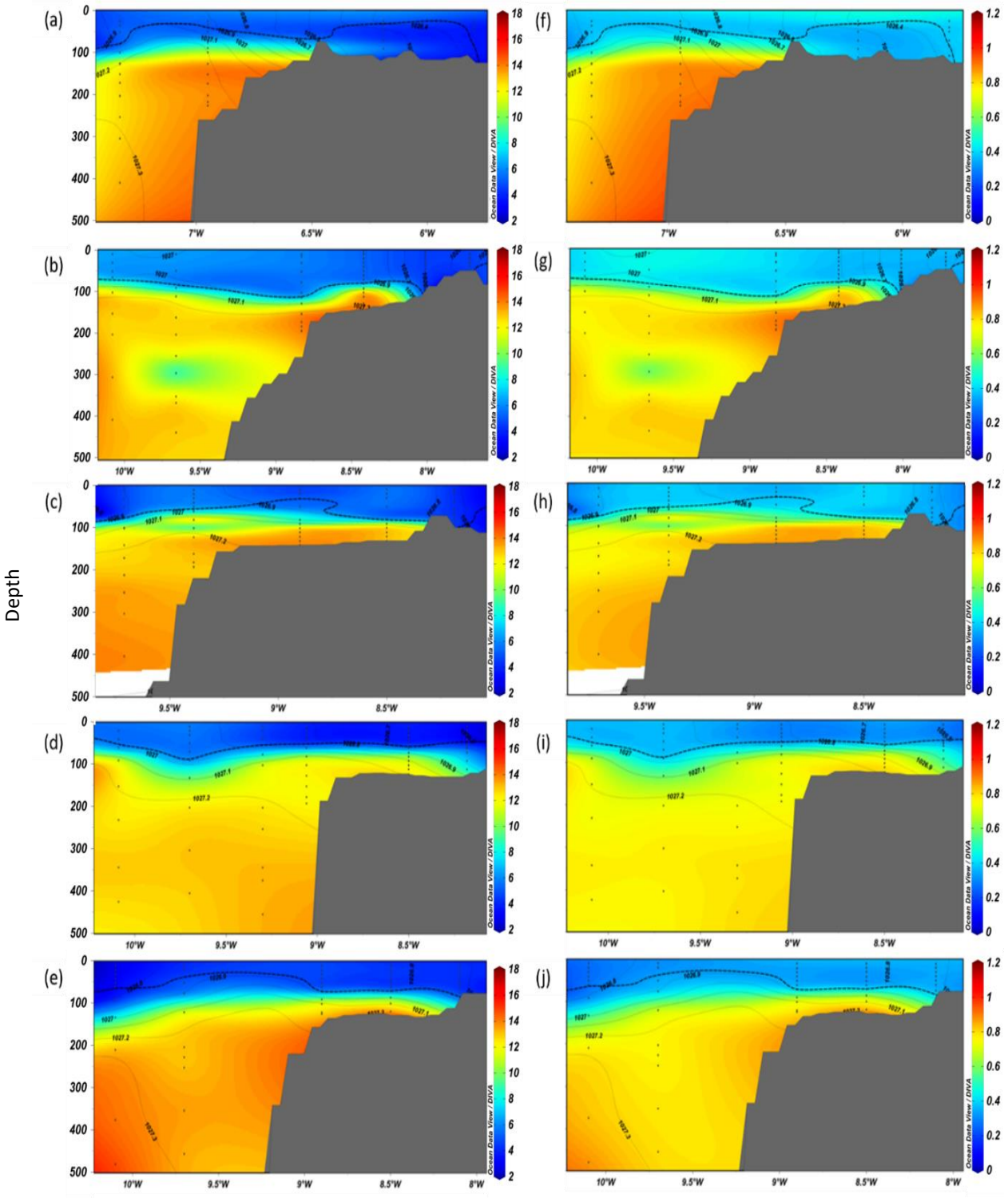

Figure 5.5. (a) to (e) concentrations of nitrate (µM) for transects A, C, D, E and F across the Hebrides Shelf during October and November 2014. (f) to (j) concentrations of phosphate (µM) for transects A, C, D, E and F across the Hebrides Shelf during October and November 2014. Data was plotted in ODV using DIVA gridding and GEBCO1 bathymetry. Isobars show density (kg m^{-3}), dots show sampling depths and the dotted line shows the mixed layer depth.

As expected, the highest nitrate concentrations were found in the denser waters off shelf with concentrations exceeding 12 µM at depths greater than 150 m (generally >27.2 kg m^{-3}) and increasing with density and depth (Figures 5.5 and 5.6a). Deep water off shelf nitrate concentrations approached 20 µM at 1000 m depth where density was approximately 27.5 kg m^{-3}, typical for North Atlantic deep waters (Figures 5.5 and 5.6a). Similarly, to nitrate concentrations, the highest phosphate concentrations were found in deeper more dense waters off shelf with concentrations exceeding 0.7 µM at depths greater than 150 m (generally >27.2 kg m^{-3}). Deep water off shelf phosphate concentrations were approximately 1.2 µM by 1000 m depth (approximately 27.5 kg m^{-3}), typical of North Atlantic deep water (Figures 5.5 and 5.6b).

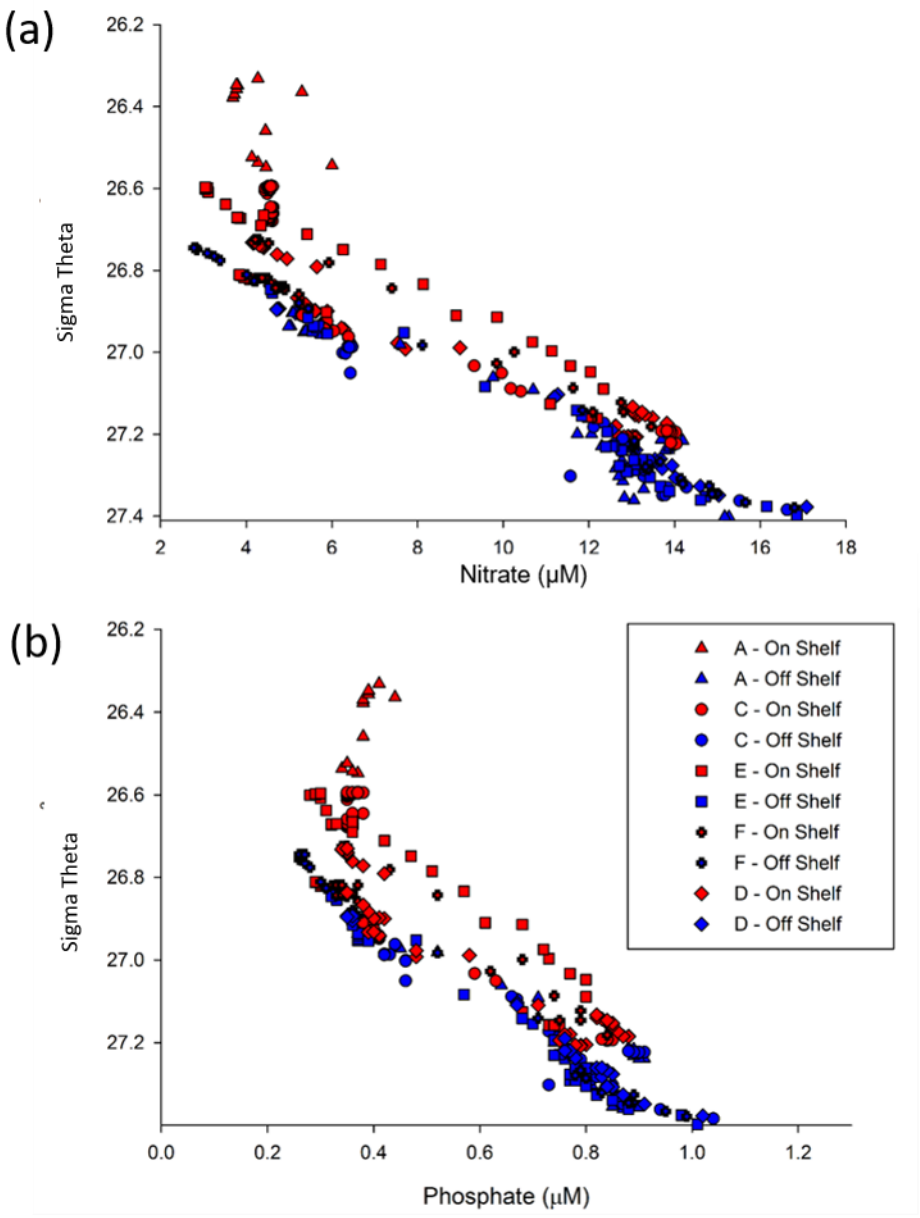

Figure 5.6. (a) Nitrate plotted against density (to 500m water depth) for each transect (on shelf and off shelf), (b) Phosphate plotted against density (to 500m water depth) for each transect (on shelf and off shelf).

The nitrate to phosphate ratio (N:P) deviated horizontally across the shelf and vertically. There was no difference in the surface mixed layer N:P ratio between on shelf (13.1 ± 1.2) and off shelf (13.9 ± 1.3; Figure 5.7). There was a gradient in the bottom layer with the mean N:P of 15.1 ± 1.4 on shelf, while off shelf N:P ratios below the mixed layer ranged between 16.8 and 17 between the base of the mixed layer and 500 m depth, increasing to over 19 by 1000 m and remaining homogenous to the sea floor. In general, the N:P ratio increased towards the open ocean, in both

the surface mixed layer and at depth. The lowest N:P for each transect was found at the innermost shelf regions were all transects apart from the southernmost (F) and had an N:P ratio below 12 (Figure 5.7e). The lowest N:P was found at station A1 where the water column was fully mixed with a mean water column N:P of 9.9 ± 0.3, and generally showed an increased towards the shelf edge (Figure 5.7a).

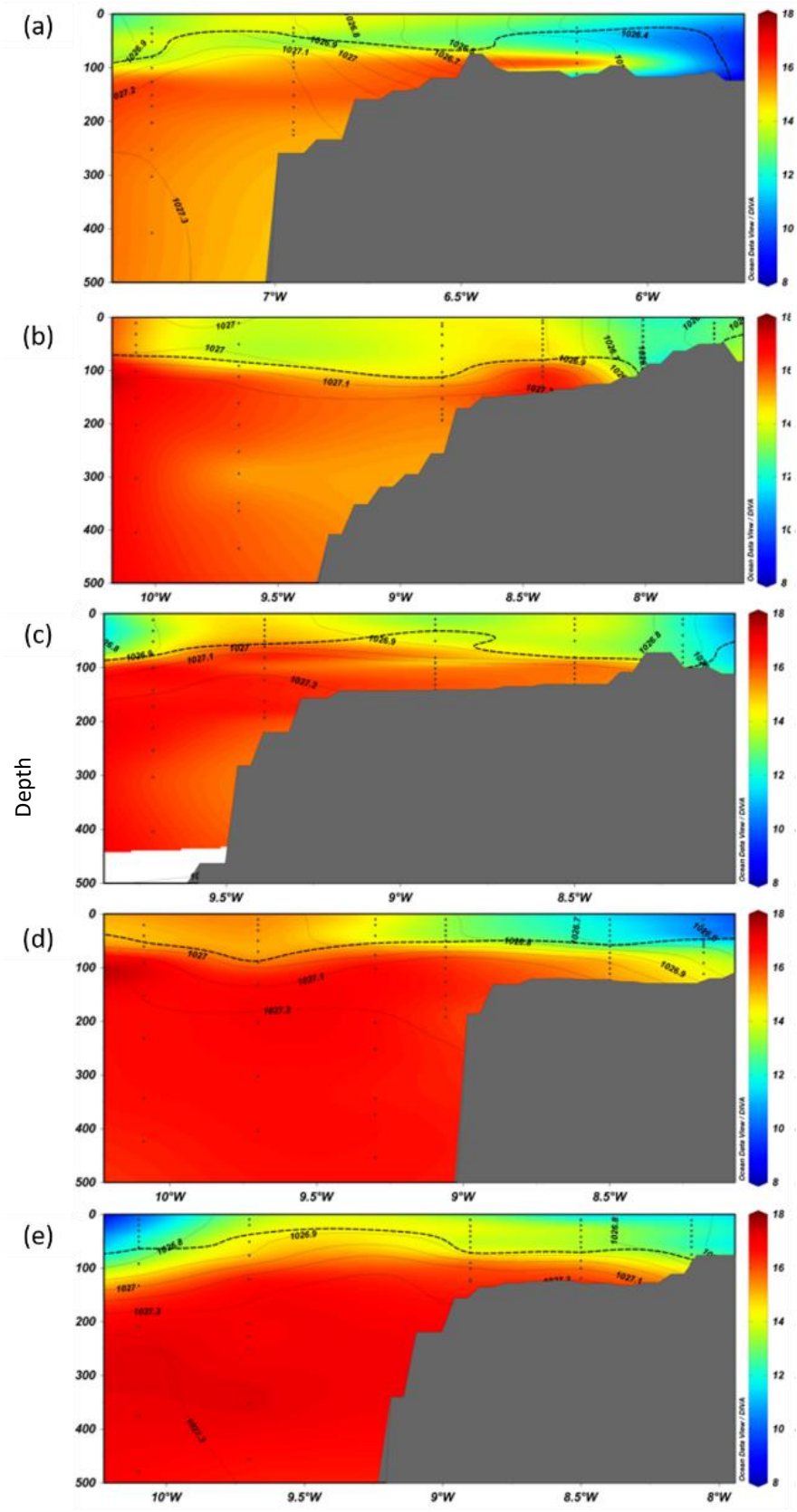

Figure 5.7. (a) to (e) Nitrate: Phosphate ratio for transects A, C, D, E and F across the Hebrides Shelf during October and November 2014. Data was plotted in ODV using DIVA gridding and GEBCO1 bathymetry. Isobars show density (kg m^{-3}), dots show sampling depths and the dotted line shows the mixed layer depth.

Oxygen concentrations ranged from 230 µM to 296 µM across all transects. Surface water oxygen concentrations at the majority of stations were >280 µM, apart from the well mixed stations furthest on shelf. The mean surface mixed layer oxygen concentrations were 278 ± 4 µM across the entire data set. There was a small but significant increase in surface mixed layer oxygen concentration between the on shelf (278 ± 3 µM) and off shelf (284 ± 3 µM) stations (T-value = -12.09, DF = 49, P= <0.05; Figure 5.8). As expected, there were strong gradients in dissolved oxygen concentration with depth across the on shelf regions, with the lowest concentrations approaching 230 µM near the seabed along each transect. This represents a reduction of over 40 µM with respect to surface concentrations. The area of lowest oxygen concentrations along each transect was variable, being broadest along transect D (Figure 5.8c). The stations furthest on shelf had more uniform dissolved oxygen concentrations with depth. This was particularly clear at stations B1 and C1 (Figure 5.8b), where there was less than a 0.5 µM difference between surface and bottom depth oxygen concentrations. Off shelf oxygen concentrations ranged between 250 and 280 µM between the base of the surface mixed layer and 500 m depth. Higher oxygen concentrations were generally observed in the open ocean away from the lower values associated with the shelf and shelf edge (Figure 5.8a, 5.8b, 5.8c, 5.8d, 5.8e).

CTD fluorescence was used as an indirect measure of pigment concentration as only surface chlorophyll was collected during the cruise at a limited number of stations. CTD fluorescence concentrations ranged from below the limit of detection (0.01 µg L^{-1}) to 0.38 µg L^{-1} and were higher in the off shelf open ocean surface waters (0.29 ± 0.05 µg L^{-1}) compared to on shelf surface waters (0.22 ± 0.04 µg L^{-1}). The fluorescence signal was apparent in bottom depths at the furthest on shelf stations, A1, A2, B1, C1, C2 and D1, possibly due to the deeper surface mixed layer and recent breakdown of stratification at these stations (Figure 5.8f, 5.8g, 5.8h). Fluorescence below the surface mixed layer on shelf was low, with a mean value of 0.07 ± 0.06 µg L^{-1} often falling below the limit of detection. Off shelf fluorescence between the base of the mixed layer and 500 m depth was also low with a mean value of 0.04 ± 0.06 µg L^{-1} often falling below the limit of detection (Figure 5.8). There was some evidence of an on shelf subsurface chlorophyll maximum in

transects A, C, D and F (Figure 5.8f, 5.8g, 5.8h, 5.j), where the maximum chlorophyll concentrations were deeper in the water column. This was particularly clear in transect D, where chlorophyll concentrations approached 0.3 µg L^{-1} at depths between 50 m and 100 m (Figure 5.8h).

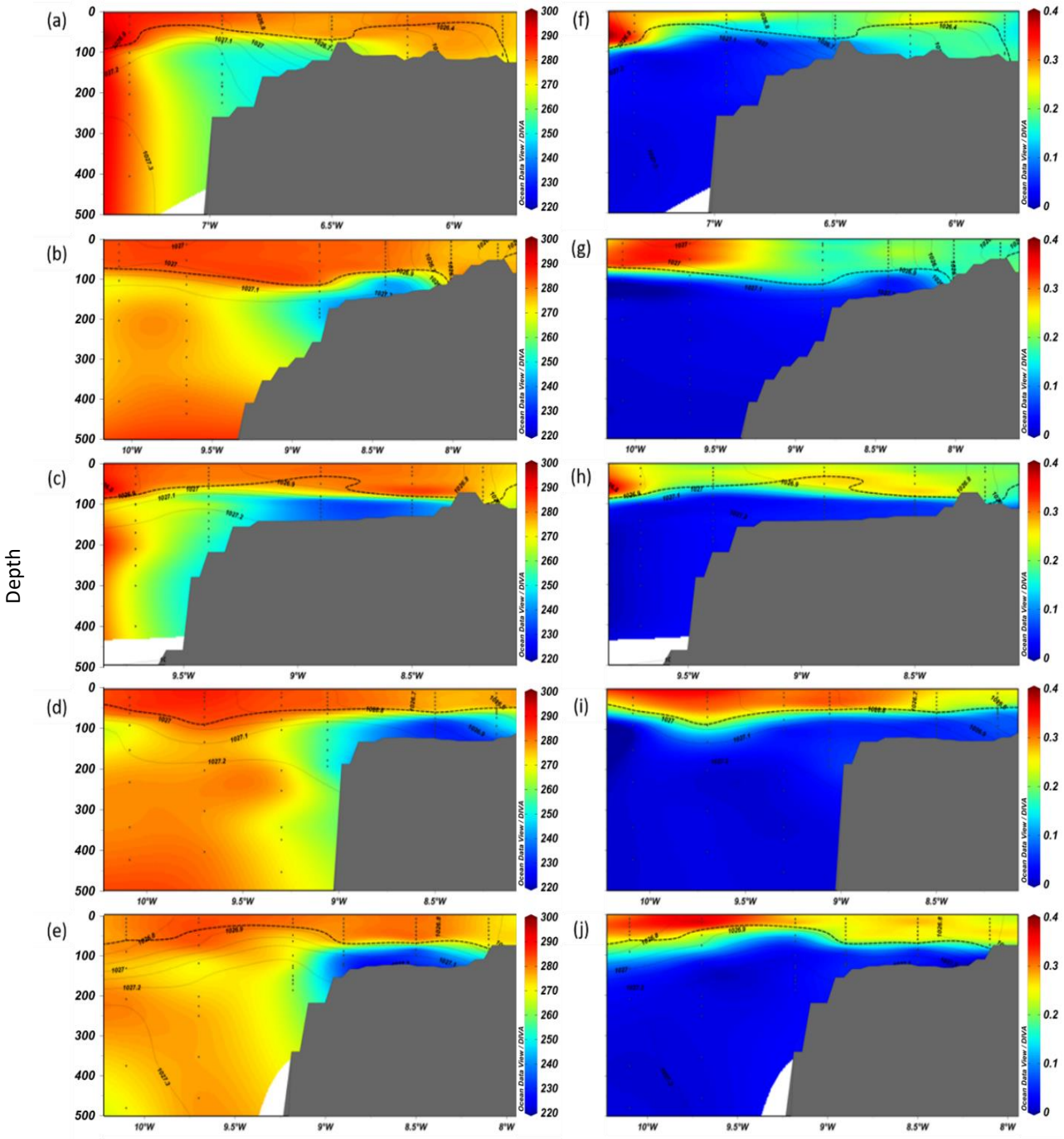

Figure 5.8. (a) to (e) Dissolved oxygen concentration (µM) for transects A, C, D, E and F across the Hebrides Shelf during October and November 2014. (f) to (j) CTD fluorescence (µg L^{-1}) for transects A, C, D, E and F across the Hebrides Shelf during October and November 2014. Data was plotted in ODV using DIVA gridding and GEBCO1 bathymetry. Isobars show density (kg m^{-3}), dots show sampling depths and the dotted line shows the mixed layer depth.

Oxygen concentrations were lowest (<230 µM) on shelf between 26.8 kg m^{-3} and 27.2 kg m^{-3} in the bottom waters (Figure 5.9). The lowest oxygen concentrations were observed on transects D, E and F where oxygen concentrations were all below 240 µM in the bottom layer (Figure 5.9). Oxygen concentrations off shelf were consistently higher than those found on shelf, with the lowest oxygen concentration being ~ 250 µM (Figure 5.9).

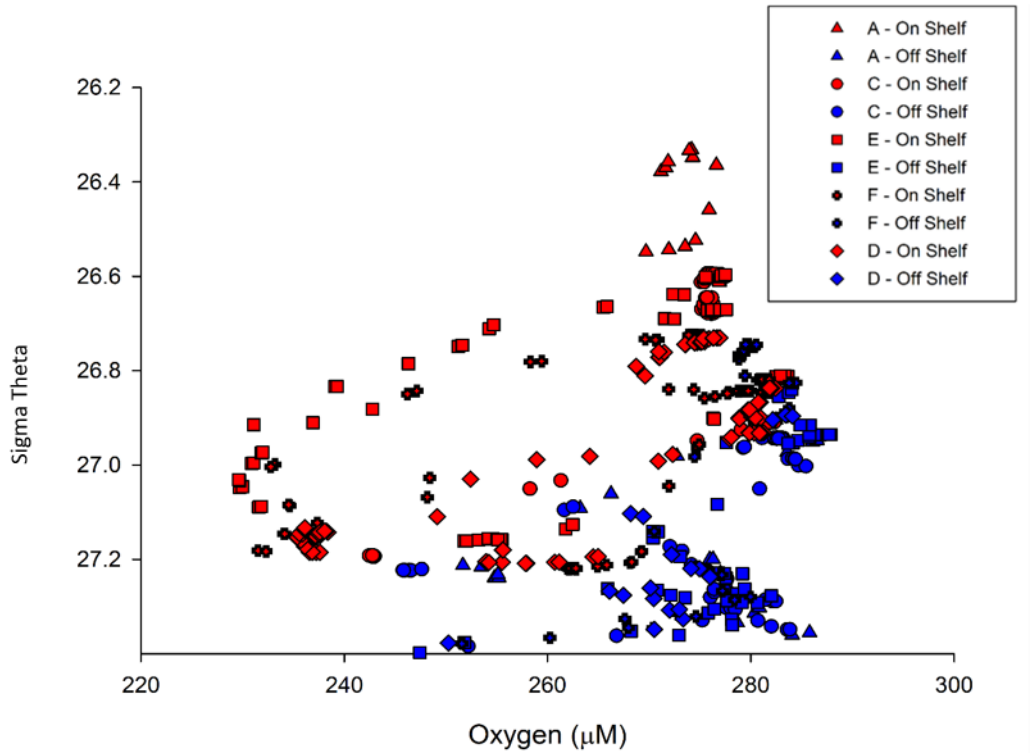

Figure 5.9. Dissolved oxygen concentration with density between the surface and 500m water depth for each of the transects showing (on shelf and off shelf)

The difference between the measured dissolved oxygen concentration and the equilibrium oxygen saturation concentration (Garcia and Gordon 1992) was calculated giving the apparent oxygen utilisation (AOU). The AOU represents the biological activity that the water sample has experienced since it was last at equilibrium with the atmosphere. Negative AOU values are associated with water that has recently been in contact with the atmosphere or where primary production has taken place, while positive AOU values are associated with water that is under saturated in dissolved oxygen due to consumption of oxygen via respiration or remineralisation of organic matter. The surface mixed layer across all transects had a

negative AOU value reaching up to -20μM. The AOU at the innermost on shelf stations (A1, A2, B1, C1, C2 and D1) was negative throughout the entire water column (Figure 5.10a, 5.10b, 5.10c). These low AOU values were consistent across the mixed layer in all transects both on shelf and in the open ocean. Transect A had the lowest overall AOU values across the shelf, with only station A4 having a positive AOU between 26 μM and 29 μM in the bottom layer (Figure 5.10a). The most positive AOU values were found on shelf in the bottom layer. AOU was highest (47 μM) at station F2 (Figure 5.10e). The distinctive feature across transects C, D, E and F was the persistent area of positive AOU between the mid-shelf region and the shelf edge in the bottom mixed layer (Figure 5.10b, 5.10c, 5.10d, 5.10e) The AOU across these stretches ranged from 26 μM in transect A, to 47 μM in transect F. The widest stretch of strongly positive AOU was across transect D, covering a distance of over 80 km (Figure 5.10c).

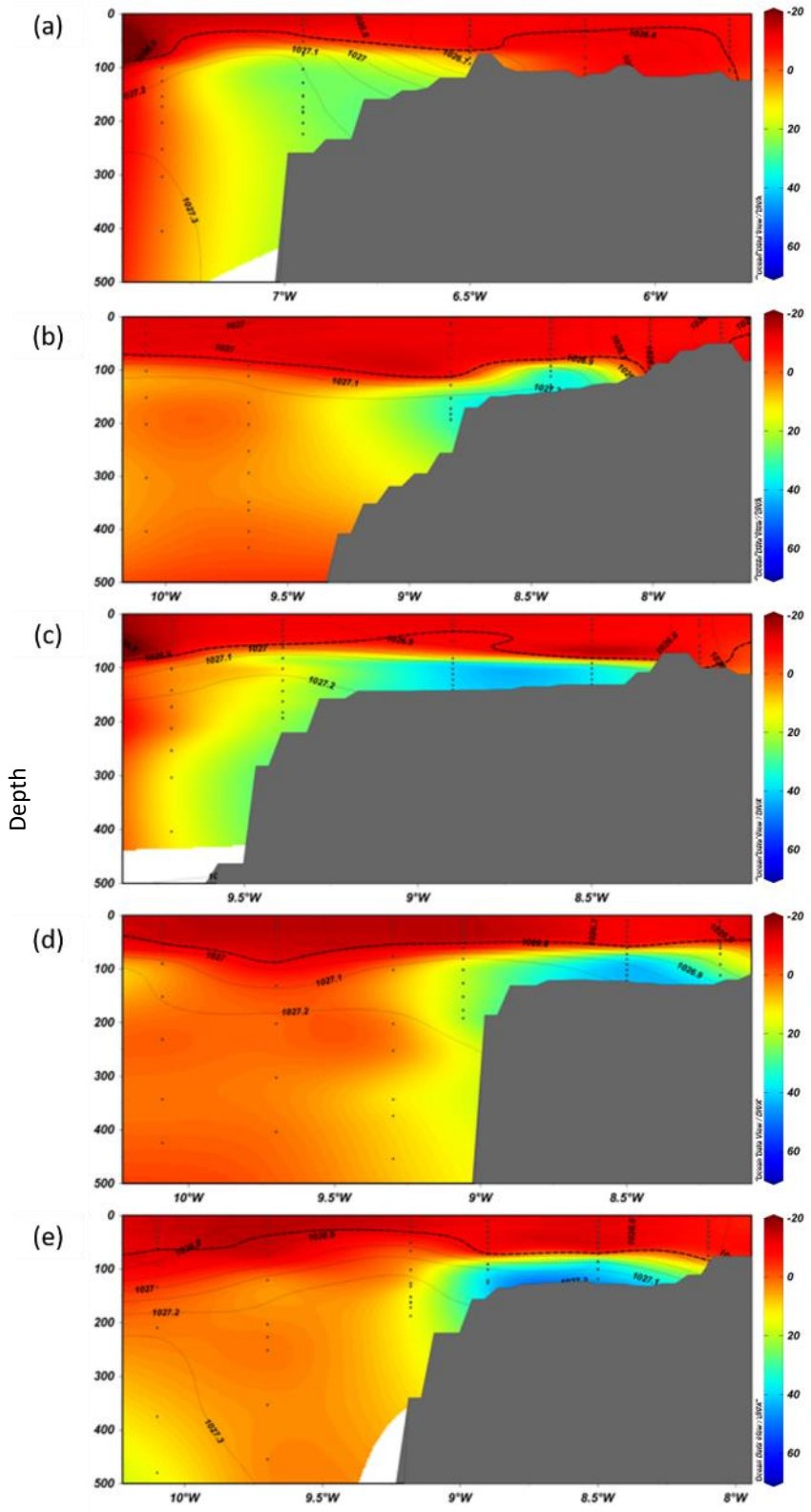

Figure 5.10. (a) to (e) Apparent oxygen utilisation (AOU) (µM) for transects A, C, D, E and F across the Hebrides Shelf during October and November 2014. Data was plotted in ODV using DIVA gridding and GEBCO1 bathymetry. Isobars show density (kg m^{-3}), dots show sampling depths and the dotted line shows the mixed layer depth.

There were clear cross shelf relationships between nitrate and oxygen concentration. The lowest oxygen concentrations were associated with the bottom layer at stratified on shelf stations, where nitrate concentrations were relatively high. In contrast, oxygen concentrations were lower than both the surface mixed layer and the off shelf waters between the base of the surface mixed layer and 500 m depth. The lowest dissolved oxygen concentrations (~ 230 µM) were found at stations D1, D2 and E2 (Figure 5.8c, 5.8d, 5.11). Well oxygenated water was found off shelf in both the surface and at depth, with nitrate ranging between 2.8 µM at the surface and 13µM at depth. At on shelf stations that were fully mixed or close to fully mixed water column there was well oxygenated water (≥265 µM), but lower nitrate concentrations (approximately 4 µM). These concentrations were similar to the surface mixed layer concentrations on shelf (Figure 5.11).

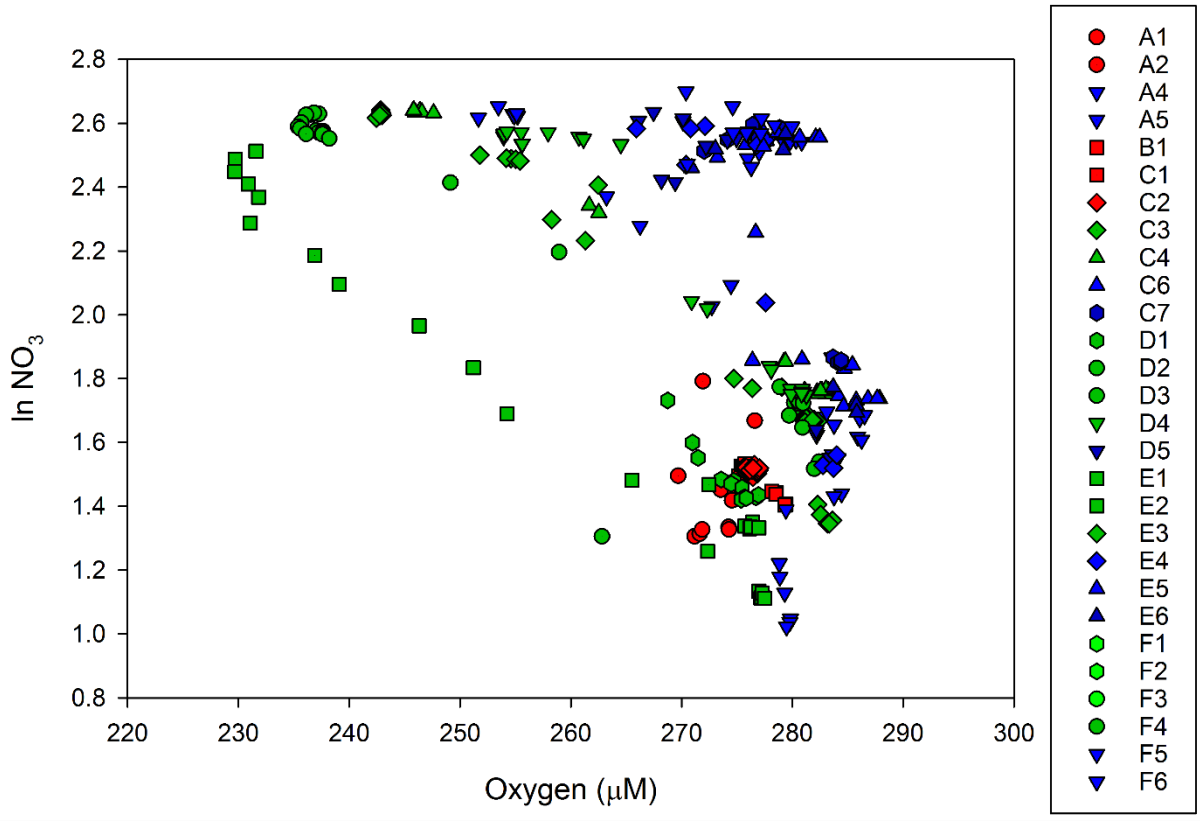

Figure 5.11. Dissolved oxygen concentration (µM) with ln NO_3 (µM) for each station, red indicates on shelf mixed stations, green indicates on shelf stratified stations and blue indicates off shelf stations (up to 500m depth).

5.3.3 Stable Isotopes

Mean $\delta^{15}N_{NO3}$ and $\delta^{18}O_{NO3}$ values were highest in the surface mixed layer, with on shelf values of 5.8 ± 0.5 ‰ and 4.4 ± 1.3 ‰, respectively excluding stations A1 and A2 where there was a strong influence from the Scottish Coastal Current with different nitrate isotope end members (Figure 5.12). $\delta^{15}N_{NO3}$ and $\delta^{18}O_{NO3}$ values were lower in the bottom layer than the surface mixed layer both on and off the shelf. Mean bottom layer on shelf $\delta^{15}N_{NO3}$ and $\delta^{18}O_{NO3}$ were 4.9 ± 0.3 ‰ and 3.0 ± 0.4 ‰, respectively (excluding stations A1 and A2).

Low values of $\delta^{18}O_{NO3}$ (<3.5 ‰) were found at stratified stations on shelf and coincided with the lowest dissolved oxygen concentrations near the sediments (Figure 5.12e, 5.12f, 5.12g, 5.12h), with the lowest $\delta^{18}O_{NO3}$ values (1.7 ‰) being found at bottom depths at station C2. $\delta^{18}O_{NO3}$ across all on shelf transects, except transect A, were < 3.5‰ in the bottom layer. The Δ (15-18) ranged from -0.3 to >3 ‰ on shelf. In general, the Δ (15-18) was higher at the stations furthest on shelf, with bottom values reaching over 3‰. The highest Δ (15-18) coincided with shelf stations with the lowest $\delta^{18}O_{NO3}$, stations C1 and C2 reaching 2.9 ‰ and 3.0 ‰, respectively.

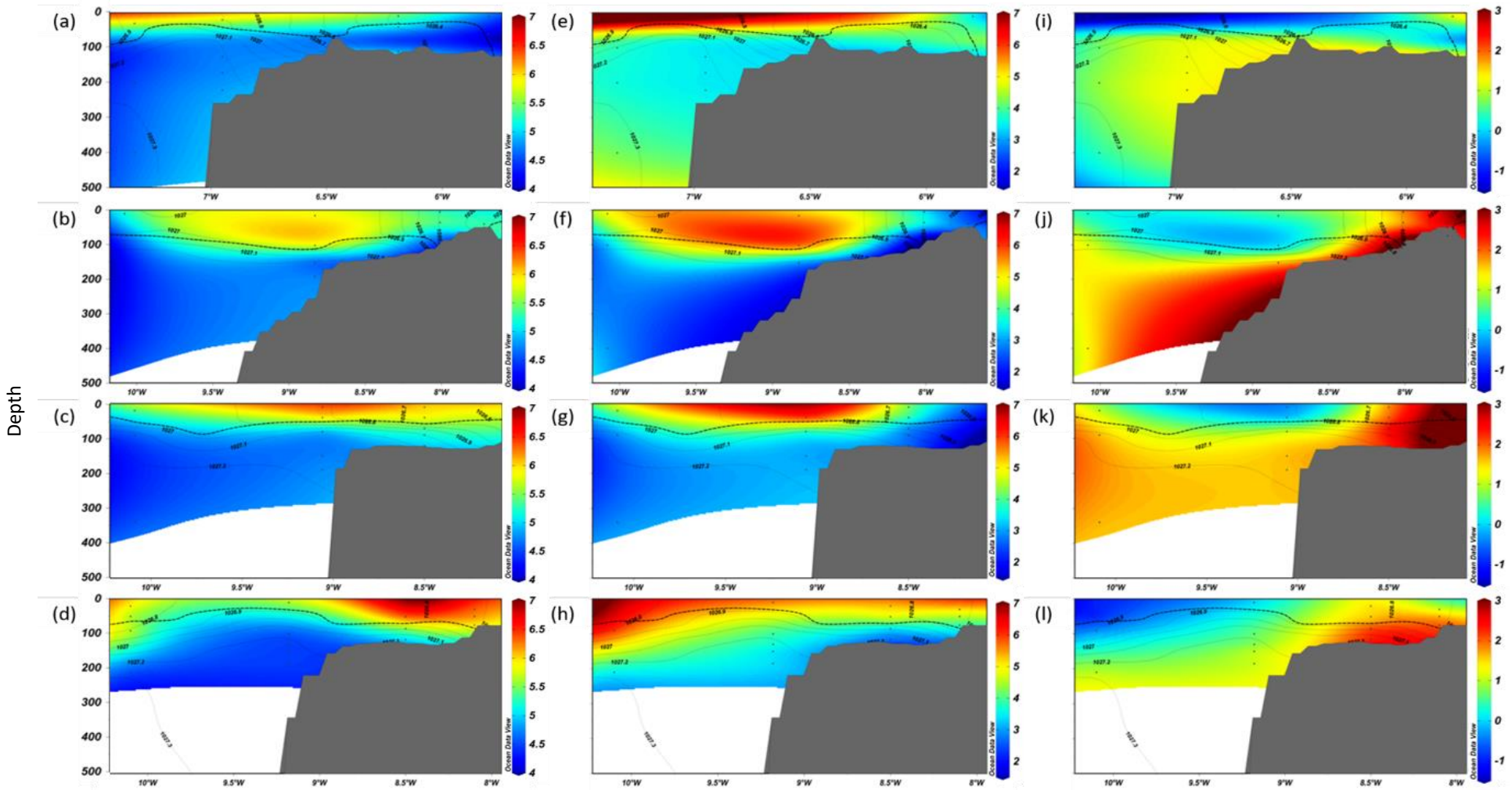

Figure 5.12. $\delta^{15}N_{NO3}$, $\delta^{18}O_{NO3}$ and Δ (15-18) for transects A, C, E and F across the Hebrides Shelf during October and November 2014. Data was plotted in ODV using DIVA gridding and GEBCO1 bathymetry. Isobars show density (kg m^{-3}), dots show sampling depths and the dotted line shows the mixed layer depth.

$\delta^{15}N_{NO3}$ and $\delta^{18}O_{NO3}$ varied with density across the shelf. In general, $\delta^{15}N_{NO3}$ decreased with increasing density. The lower density water on shelf had higher $\delta^{15}N_{NO3}$ and $\delta^{18}O_{NO3}$ values decreased with density and depth. Off shelf, values increased for $\delta^{15}N_{NO3}$. The $\delta^{15}N_{NO3}$ and $\delta^{18}O_{NO3}$ above 27.4 kg m^{-3} was 4.8 ‰ and 2.3 ‰, respectively, which is close to North Atlantic deep water (Sigman et al. 2009b) (Figure 5.13). Several of the stations furthest on shelf (A1, A2, B1, C1 and C2) with the lowest densities of between 26.3 kg m^{-3} and 26.7 kg m^{-3} did not fit the general trend in $\delta^{15}N_{NO3}$ across the rest of the stations. This a result of the increased mixing and influence of fresh water at these stations. $\delta^{18}O_{NO3}$ values were more variable than the $\delta^{15}N_{NO3}$ with respect to density (Figure 5.13). The stations furthest on shelf (A1, A2, B1, C1 and C2) in the least dense waters were split into two main groups. Stations A1 and A2 had high $\delta^{18}O_{NO3}$ between 4.9 ‰ and 6.3 ‰ while stations B1, C1 and C2 had much lower $\delta^{18}O_{NO3}$ between 1.7 ‰ and 3.7 ‰. In general, $\delta^{18}O_{NO3}$ at the remaining stations decreased with increasing density (and depth), reaching a mean value of 2.4 ‰ at densities above 27.4 kg m^{-3}. Stations between densities of 26.6 kg m^{-3} and 27.4 kg m^{-3} were more variable than $\delta^{15}N_{NO3}$, with a range between 2 ‰ and 7 ‰.

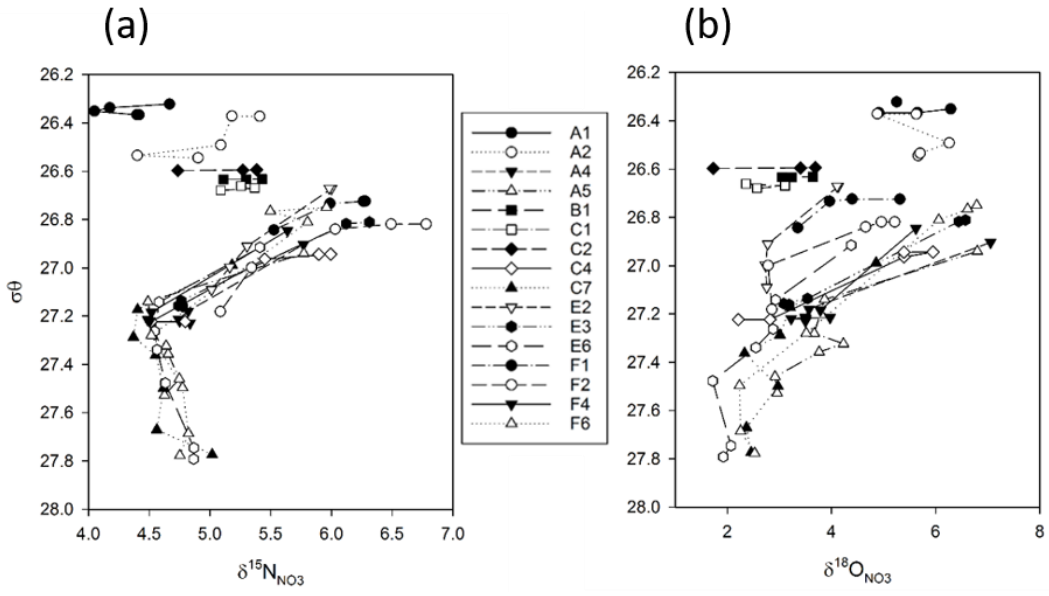

Figure 5.13. Full depth isopycnal profiles of (a) $\delta^{15}N_{NO3}$ and (b) $\delta^{18}O_{NO3}$ for transects A, C, E and F across the Hebrides Shelf during October and November 2014

The cross-shelf relationship between $\delta^{15}N_{NO3}$ and $\delta^{18}O_{NO3}$ and nitrate was complex and several patterns were identified (Figure 5.14). Firstly, as per Rayleigh

dynamics, as the nitrate concentration decreased, the $\delta^{15}N_{NO3}$ and $\delta^{18}O_{NO3}$ increased (Figure 5.14a). The low concentrations of nitrate found in the surface mixed layer were associated with the most enriched $\delta^{15}N_{NO3}$ and $\delta^{18}O_{NO3}$ values of ≥7 ‰ in some areas. This is a signal for biological utilisation of nitrate and it is particularly clear in the open ocean stations and stratified on shelf stations. At the on shelf mixed stations A1 and A2, $\delta^{15}N_{NO3}$ was lower (< 5.5 ‰) throughout the water column and the nitrate concentrations were lower here (Figure 5.14a). There were deviations in the Rayleigh fractionation signal in $\delta^{18}O_{NO3}$ at stations B1, C1 and C2, which had much lower $\delta^{18}O_{NO3}$ of between 1.7 ‰ and 3.7 ‰ associated with nitrate of 4 μM, falling below the expected Rayleigh fractionation observed off shelf (Figure 5.14b). Low $\delta^{18}O_{NO3}$ values were also associated with higher nitrate on shelf at bottom water stratified stations (Figure 5.14b). There were large variations in $\delta^{15}N_{NO3}$ to $\delta^{18}O_{NO3}$ ratio, with the on shelf mixed stations A1 and A2 in particular having enriched $\delta^{18}O_{NO3}$ compared to $\delta^{15}N_{NO3}$. Similar patterns were observed in the shelf edge and off shelf stations on transect A (Figure 5.14c). The on shelf mixed stations B1, C1 and C2 were generally below the 1:1 line where $\delta^{18}O_{NO3}$ was relatively light compared to $\delta^{15}N_{NO3}$ (Figure 5.14c). The relationship between $\delta^{15}N_{NO3}$ and $\delta^{18}O_{NO3}$ at on shelf mixed stations were variable, with some stations falling below the 1:1 line, whilst off shelf stations (apart from transect A) were close to the expected North Atlantic values (Figure 5.14c).

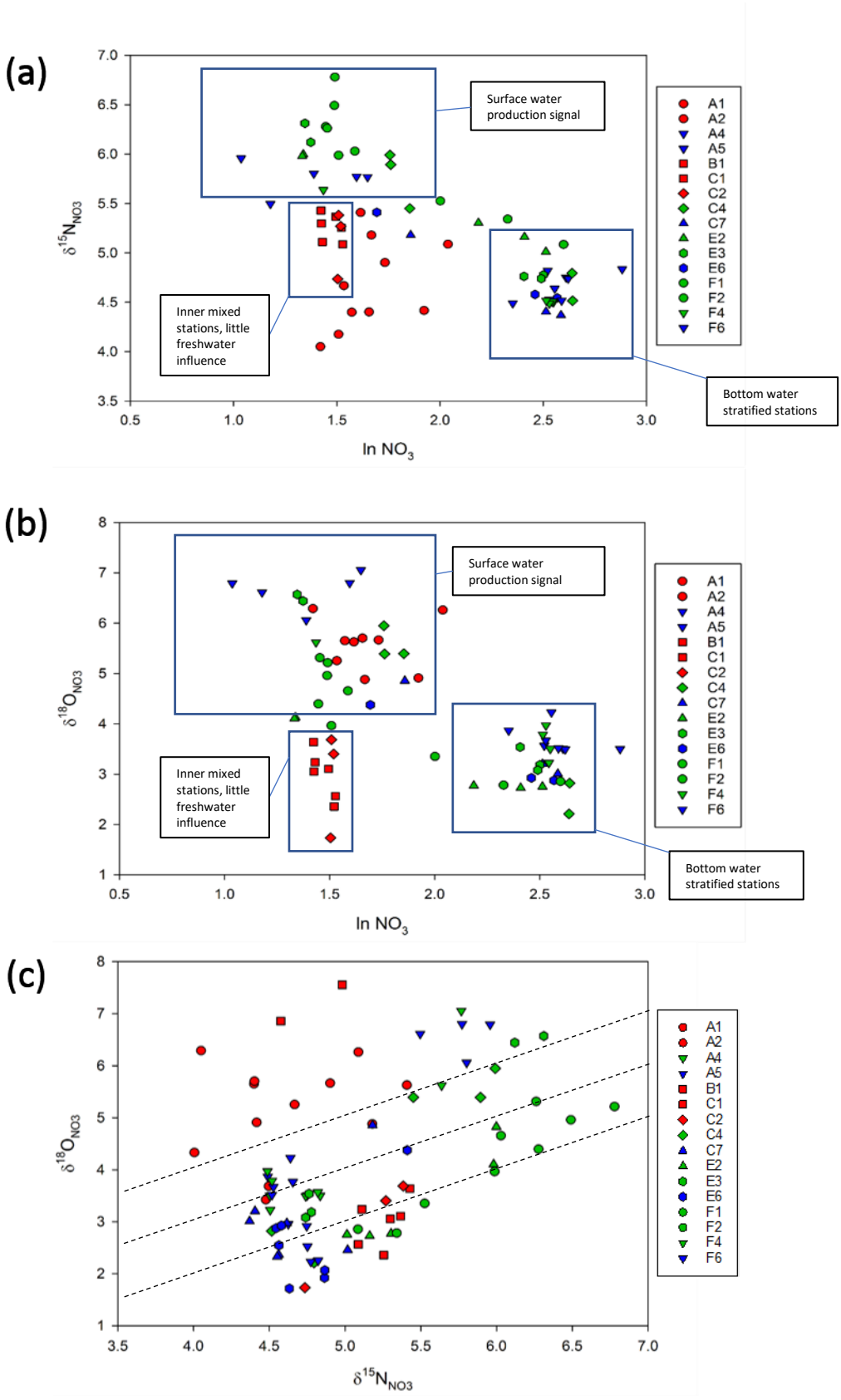

Figure 5.14. (a) $\delta^{15}N_{NO3}$ and (b) $\delta^{18}O_{NO3}$ plotted against ln NO_3^- in Rayleigh space and (c) $\delta^{15}N_{NO3}$ v. $\delta^{18}O_{NO3}$ (with 1:1 lines) for transects A, C, E and F across the Hebrides Shelf during October and November 2014.

5.3.4 Stable isotopes, AOU and remineralisation

As oxygen concentrations decreased from >270 µM to 230 µM, there was an increase in Δ (15-18) from 0.5 ‰ to over 2.5 ‰ (Figure 5.15). However, the inshore stations displayed an increase in Δ (15-18) without a corresponding decrease in oxygen concentration. These were stations B1, C1 and C2, where the water column was fully mixed and the water column was well oxygenated (Table 5.1).

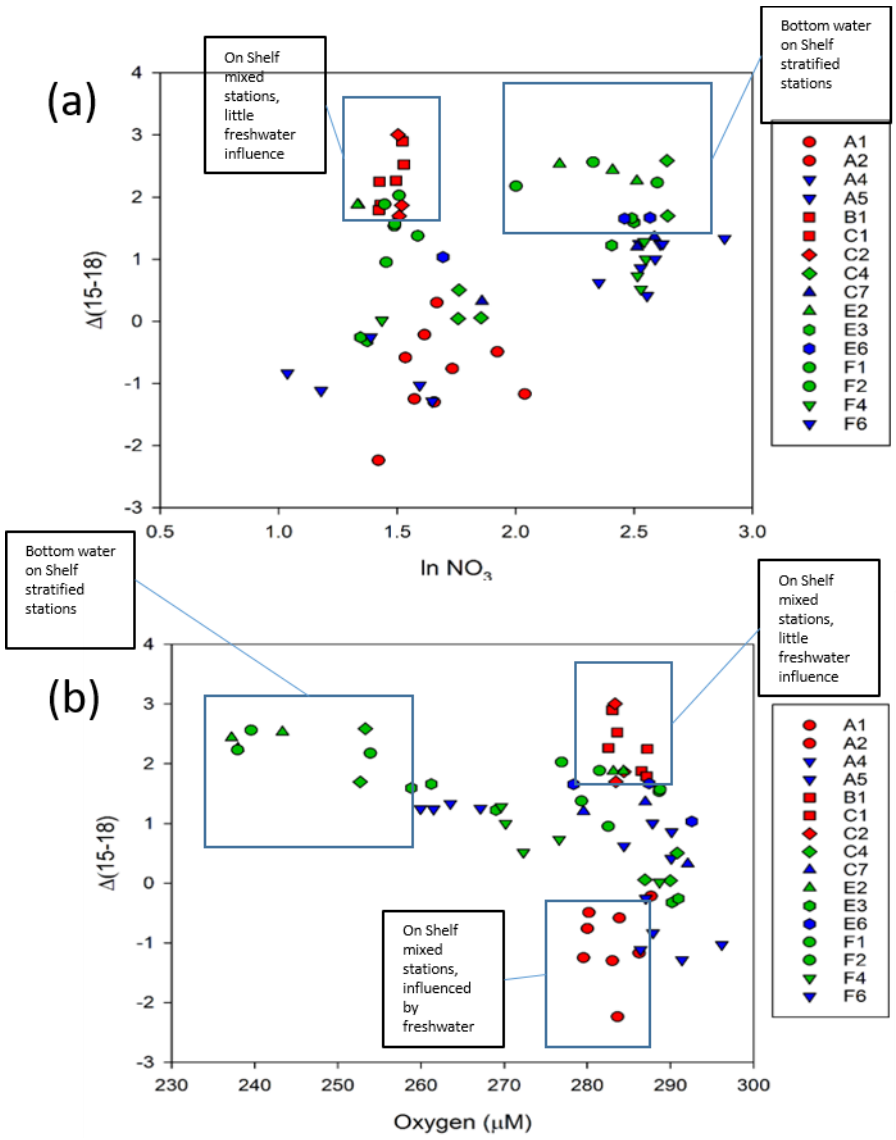

Figure 5.15. (a) Δ (15-18) plotted against ln NO_3^- (b) Δ (15-18) plotted against dissolved oxygen concentration (µM) for transects A, C, E and F across the Hebrides Shelf during October and November 2014

At stations furthest on shelf (A1, B1, C1, C2), where stratification was weak or the water column was mixed, the AOU was negative due to waters recently being in contact with the atmosphere (Table 5.1). The AOU was higher below the base of the surface mixed layer at the more strongly stratified on shelf stations. Based on the AOU value using Redfield, up to 47 ± 1 % of the nitrate was remineralised *in situ* at station E2 representing a nitrate concentration of up to 5.2 ± 0.3 µM. However, using AOU based on the measured N:P ratio only 43 ± 1 % was remineralised *in situ*. For other on shelf stratified stations AOU ranged between 18 % at stations A4 and E3 and 44 % at station F2 using Redfield, and 16 % and 40 % using the measured N:P ratio (Table 5.1)

The proportion of remineralised nitrate determined using stable isotopes was quantified using equation 5.5, and a $\delta^{18}O_{imported}$ value of 3.5 ‰. The $\delta^{18}O_{NO3}$ value was lower than the imported value at these stratified on shelf stations correlating with the strongest density gradients in the water column and suggested that up to 78 % of the nitrate (up to 10.2 µM) was remineralised *in situ* in the bottom mixed layer station C4, and 39 % remineralised in the BML at station E2 and F2. The innermost stations (besides station A1 that had a higher $\delta^{18}O_{NO3}$ value that was influenced by the Scottish Coastal Current) that were weakly stratified or mixed had a larger range in the $\delta^{18}O_{NO3}$ across the water column due to this mixing. However, there was potentially up to 94 % (up to 4.2 µM) of the nitrate at C2 remineralised *in situ*. The other on shelf mixed stations B1 and C1 potentially had up to 28 % and 50 % on the nitrate remineralised *in situ* (Table 5.1).

Table 5.1. On shelf mean values (± S.D) for samples below the mixed layer for AOU (using Redfield), AOU (using measured N:P ratio), and $\delta^{18}O_{NO3}$. Subsequently in-situ remineralised nitrate (%) and (µM) were calculated from each method using a $\delta^{18}O_{imported}$ value of 3.5‰. Stations at on shelf stratified stations are coloured in green, while mixed/weakly stratified stations are shown in red.

Station	Water column (WC) depth	WC Density Gradient	AOU (µM)	AOU Remin. N Redfield (%)	AOU Remin. N Redfield (µM)	AOU Remin. N N:P ratio (%)	AOU Remin. N N:P ratio (µM)	$\delta^{18}O_{NO3}$ (‰)	$\delta^{18}O_{NO3}$ Remin. N (%)	$\delta^{18}O_{NO3}$ Remin. N (µM)
A1	107	0.04	-4	0	0	0	0	3.7	0	0
A4	224	0.33	20 ± 10	18 ± 8	2.4 ± 1.2	17 ± 8	2.2 ± 1.1	3.5 ± 0	0	0
B1	75	0.01	-11	0	0	0	0	3.3 ± 0.3	0 - 28	0 - 1.2
C1	76	0.03	-8	0	0	0	0	2.6	50	2.3
C2	118	0.02	-9 ± 1	0	0	0	0	2.9 ± 1.1	0 - 94	0 - 4.2
C4	194	0.28	31 ± 9	26 ± 6	3.7 ± 1.0	24 ± 6	3.4 ± 1.0	2.5 ± 0.4	33 - 78	4.3 - 10.2
E2	123	0.42	43 ± 5	47 ± 1	5.1 ± 0.6	43 ± 1	4.7 ± 0.6	2.8 ± 0	39	4.3
E3	191	0.35	17 ± 11	18 ± 9	2.1 ± 1.0	16 ± 9	1.9 ± 1.2	3.3 ± 0.2	0 - 22	0 - 2.4
F1	107	0.12	16 ± 8	28 ± 12	1.9 ± 1.0	27 ± 12	1.8 ± 0.8	3.3	11	0 - 0.7
F2	118	0.36	43 ± 3	44 ± 3	5.2 ± 0.3	40 ± 3	4.7 ± 0.3	2.8 ± 0	39	4.6
F4	187	0.38	10 ± 7	-	-	-	-	3.6 ± 0.3	0 - 11	-

5.4. Discussion

The timing of the research cruise in autumn provided a unique opportunity to investigate the post autumn bloom nutrient cycling and remineralisation across the Hebrides shelf system at the breakdown of summer stratification across the shelf and throughout the cruise. In this study there were varying degrees of water column stability across the Hebrides shelf during the time of sampling in October and November 2014. The physics, nutrient and water column dynamics were distinctly different between each of the transects sampled through A to F. There were both cross shelf gradients across each transect and differences between transects, allowing different processes to be captured in the $\delta^{15}N_{NO3}$ and $\delta^{18}O_{NO3}$ relationship.

5.4.1 Surface water characteristics

The off shelf waters for transect A were still stratified and had higher concentrations of chlorophyll than below the mixed layer indicating recent production. The surface mixed layer $\delta^{15}N_{NO3}$ was enriched, with highest values at the most oceanic station, A5, corresponding with the highest chlorophyll and dissolved oxygen concentrations. This enriched $\delta^{15}N_{NO3}$ (and $\delta^{18}O_{NO3}$) signal was associated with uptake of nitrate by phytoplankton, and can be described using first order Rayleigh fractionation. The signal for $\delta^{18}O_{NO3}$ in the waters below the mixed layer was also enriched when compared to the off shelf regions of the other transects, this implied that the off shelf waters of transect A potentially had a different source of nitrate than the other off shelf transects, as a result of the greater influence of the Scottish Coastal Current (Booth and Ellett 1983). $\delta^{15}N_{NO3}$ for transects C, E and F was also enriched in the surface mixed layer at stratified stations, indicating recent uptake of nitrate by phytoplankton, again corresponding with higher concentrations of dissolved oxygen and chlorophyll than found below the mixed layer.

5.4.2 In-situ remineralisation on shelf

The cycling of nutrients within shelf sea bottom waters is dominated by respiratory processes in the water column and sediments that convert particulate matter back into dissolved constituents (equation 5.1). This is in contrast to the

surface waters where the dominant process of phytoplankton utilisation draws nutrients down to low concentrations in spring and summer and winter time mixing replenishes the surface waters with nutrients (although respiration and recycling do take place in surface waters) (Simpson and Sharples 2012). The microbial process that regenerates nutrients such as nitrate and phosphate can be simplified to:

$$\text{Organic matter} + O_2 \rightarrow \text{Liberated simple nutrients} + CO_2 + H_2O \qquad \text{Eqn 5.6}$$

Using ^{137}Cs from the Sellafield nuclear plant the Hebrides shelf is estimated to have residence times that are close to a year (Prandle 1984), and the Scottish Coastal Current takes approximately 9 months to transit from the Irish Sea to the mid-Hebrides Shelf region (McKay et al. 1986; McCubbin et al. 2002). These long residence times on shelf coupled with stratification allow the lower oxygen regions associated with respiration to develop on shelf.

Apparent oxygen utilisation provides a means to quantify *in situ* nutrient regeneration. Despite the potential for AOU to provide estimates for nutrient regeneration there are problems associated with these measurements, particularly in shallow and dynamic shelf seas such as the Hebrides shelf. There are a number of factors which can influence oxygen concentration within the water column. Temperature, oxygen exchange with the atmosphere and biological production all influence dissolved oxygen concentration in the water column and therefore AOU, making it difficult to unravel simultaneous processes and calculate accurate remineralisation in a dynamic environment such as a shelf sea (Topcu and Brockmann 2015). The timescale for oxygen equilibration with the atmosphere was important as the positive AOU values across the water column at the inner shelf mixed stations indicated that the waters had been in contact with the atmosphere recently. The timescale for O_2 equilibration can be calculated using:

$$T = \frac{h}{K_g} \qquad \text{Eqn 5.7}$$

Where T = air-sea exchange timescale, h = the mixed layer depth (m) and K_g = the gas transfer coefficient (1.4×10^{-4} m s^{-1}) (Kihm and Körtzinger 2010). Using this I can calculate that at the inner shelf stations where depths were 75 m then it would take 6.25 days for the oxygen to come into equilibrium with the atmosphere. Therefore, while oxygen equilibration is relatively rapid, thus eroding the AOU

signal, the stable isotope signal is longer lived because it relies on water column mixing and/or mixing with nitrate of a different isotope signal.

Unlike AOU, $\delta^{15}N_{NO3}$ and $\delta^{18}O_{NO3}$ are therefore important tools to quantify nutrient regeneration across the shelf system as they are not influenced by the multiple factors that cause changes in oxygen concentration on shelf, in particular equilibration with the atmosphere. Using dual stable isotopes it is possible to separate the multiple factors influencing the nutrient cycle on shelf (Casciotti 2016).

Quantitatively, the degree of nitrate recycling can be determined by using $\delta^{18}O_{NO3}$ and $\delta^{18}O_{H2O}$ as described in Chapter 4. Light $\delta^{18}O_{NO3}$ values due to remineralisation are defined as 1.1 ‰ plus $\delta^{18}O_{H2O}$ (Sigman et al. 2009b). The specific $\delta^{18}O_{nit}$ value of 1.1 % above ambient seawater was used as this was estimated from $\delta^{18}O_{NO3}$ in the eastern Mediterranean where subsurface nitrate originates exclusively from *in situ* remineralisation (Sigman et al. 2009b). $\delta^{18}O_{H2O}$ was not measured during the Hebrides shelf cruise, however there were samples taken during the Shelf Sea Biogeochemistry programme in the Celtic Sea during April 2015. $\delta^{18}O_{H2O}$ across the shelf was 0.6 ± 0.1 ‰, giving a newly nitrified nitrate signal of between 1.6 ‰ and 1.8 ‰. A value of 1.7 ‰ is chosen for newly nitrified nitrate on the Hebrides shelf.

The $\delta^{18}O_{imported}$ value was difficult to quantify due to only having samples from the autumn period, therefore a value of 3.5 ‰ was taken based upon off shelf measured $\delta^{18}O_{NO3}$ between the base of the mixed layer and a density of 27.3 kg m^{-3}, which roughly translates to between 100 m and 500 m water depth and encompasses the density of water likely to be entrained onto the shelf in winter, setting a baseline for the $\delta^{18}O_{NO3}$. A critical analysis of the $\delta^{18}O_{imported}$ value was included in Chapter 4.

Transect A was the most northern and the first to be sampled. Stratification across the shelf stations of transect A was starting to breakdown, with the density gradient between the surface and bottom waters being the weakest of all the on shelf regions, less than 0.2 kg m^{-3} between the surface and sediments at stations A1, A2 and A3. There was a stronger salinity gradient along Transect A compared to the other transects across the shelf, implying that it was influenced by outflow of fresher water from the Minch, which separates the Hebrides from mainland Scotland. The Minch is part of the Scottish Coastal Current which flows northwards, and influences

not only the salinity but the nutrient profile at the innermost stations particularly on transect A. This is evident in the nitrate to phosphate ratio across transect A, with lower N:P values (below 10 at station A1) than any of the other transects.

The weak stratification was confirmed with AOU values close to zero or negative across much of the inner shelf region of transect A in both the surface and bottom layers, with only station A4 having a strongly positive AOU in the bottom waters where the waters were more strongly stratified. The negative AOU values indicate that the waters on shelf of transect A were saturated in dissolved oxygen having recently been mixed into contact with the atmosphere. Any remineralisation signal present in the bottom water at the inner stations of transect A would have been mixed between the surface and the bottom layers as stratification weakened highlighting that AOU cannot be used to calculate a percentage of remineralised nitrate or other nutrients at these inner stations. At the shelf edge station A4, where the waters were more strongly stratified the AOU was still positive, and using Redfield indicated that 18 ± 8 % of the nitrate was remineralised *in situ*, equating to 2.4 ± 1.2 µM. Using the measured N:P ratio the values were lower indicating that 17 ± 8 % of the nitrate was remineralised *in situ*, equating to 2.2 ± 1.1 µM.

There were two factors making it difficult to use $\delta^{18}O_{NO3}$ to calculate the *in-situ* remineralisation of nitrate across transect A; 1) the influence of Scottish Coastal Current freshwater from the Minch and 2) the recent breakdown of stratification. This weakening stratification meant that unlike the more stratified stations the surface water signal related to production and the bottom water signal (often linked to remineralisation) for both $\delta^{15}N_{NO3}$ and $\delta^{18}O_{NO3}$ was starting to be mixed throughout the water column, potentially removing any signal of remineralisation. $\delta^{18}O_{NO3}$ at station A1 where stable isotope samples were collected was 3.7 ‰, above the 3.5 ‰ used as an imported value of $\delta^{18}O_{NO3}$ from off shelf, indicating that if this imported value were correct then any remineralisation signal had been removed due to mixing. The other factor making it difficult to calculate remineralisation at the inner shelf stations across transect A using stable isotopes was the clear influx of fresher water from the Scottish Coastal Current. This fresher water will bring with it nitrate of unknown $\delta^{15}N_{NO3}$ and $\delta^{18}O_{NO3}$, resulting in the imported $\delta^{18}O_{NO3}$ was likely different from the off shelf known values due to mixing of both off shelf waters and fresher waters from the Scottish Coastal Current. $\delta^{18}O_{NO3}$ in the bottom waters at the

stratified station A4 was 3.5 ‰, the same as the imported $\delta^{18}O_{NO3}$, and indicated that there was little to no remineralisation taking place, however the imported value may be influenced by the fresher water from the Scottish Coastal Current, meaning there is the potential for remineralisation to be taking place *in situ* as the AOU predicts.

Transect C was similar to transect A as the innermost stations were mixed or were weakly stratified. However, stratification was stronger than transect A across the mid and outer shelf, and although the innermost stations were slightly fresher there was much less of a salinity gradient than transect A, being only approximately 0.10 fresher, likely influenced by recirculation in the South Minch surface waters (Hill et al. 1997). Weak stratification was confirmed by AOU values close to zero or negative at the innermost stations C1 and C2, suggesting that any regeneration signal had been overwritten. The stations between the mid shelf and shelf edge were stratified and AOU was strongly positive in the bottom mixed layer. Calculating the percentage of remineralised nitrate using Redfield AOU gave 26 ± 6 %, equating to 3.7 ± 1.0 µM of the total nitrate regenerated *in situ*. Using the measured N:P ratio the percentage of remineralised nitrate was 24 ± 6 %, equating to 3.4 ± 1 µM of the total nitrate remineralised *in situ*.

The inner stations of transect C were much less influenced by the Scottish Coastal Current, suggesting that the imported $\delta^{18}O_{NO3}$ was likely similar to the value chosen for calculations. Despite this, the mixed water column potentially overwrote the $\delta^{18}O_{NO3}$ signal in the bottom layer. $\delta^{18}O_{NO3}$ at stations B1, C1 and C2 were highly variable within the water column indicating that the waters were stratified until recently, and still provide an insight into the remineralisation that was dominating the bottom mixed layer. $\delta^{18}O_{NO3}$ at station C1 was below the imported $\delta^{18}O_{NO3}$ across the entire water column and was at low of 2.6 ‰ at a bottom depth of 74 m, indicated that approximately 50 % (2.3 µM) of the nitrate was regenerated *in situ*. Station C2 was also mixed with $\delta^{18}O_{NO3}$ values ranging from 1.8 ‰ to 3.7 ‰ across the water column, indicating that up to 94 % (4.2 µM) of the nitrate may have been remineralised *in situ*. Station C4 that was still more strongly stratified, the bottom mixed layer $\delta^{18}O_{NO3}$ was 2.5 ± 0.4 ‰ indicating that between 33 and 78 % of the nitrate was remineralised *in situ* equating to 4.3 - 10.2 µM. This lower end of this estimate is close to the AOU estimate of 26 ± 6 % *in situ* remineralised nitrate.

The southernmost transects E and F were stratified across the entire shelf, with stronger density gradients across the water column with a 0.4 kg m^{-3} difference between the surface and seafloor at all stations except the innermost E1 and F1 (this compares with less than 0.2 kg m^{-3} across transect A stations). The high salinity observed (35.20) implied that there was little influence of fresher water from the Scottish Coastal Current in contrast to transect A and the innermost stations of transect C. The most positive AOU values were in the bottom mixed layer at the stratified inner shelf stations E2 and F2 which were the innermost stations with clear stratification. Using Redfield AOU, 47 ± 1 % and 44 ± 3 % of the nitrate was calculated to be remineralised *in situ* equating to 5.1 ± 0.6 µM and 5.2 ± 0.3 µM, at stations E2, and F2 respectively. These stations are likely representative of the inner shelf stations from transects A and C whilst they were still stratified. At station F1 where stratification was weaker the AOU indicated less of a regeneration signal with only 28 ± 12 % remineralised *in situ* using Redfield, and 27 ± 12 % using the measured N:P ratio.

The $\delta^{18}O_{NO3}$ signal in the bottom layer also indicated that *in situ* remineralisation was taking place. Estimates of *in situ* remineralisation at the strongly stratified stations E2 and F2 were 39 %, equating to 4.3 µM and 4.6 µM respectively. At station F1 where the mixed layer was deeper and density gradients were weaker the $\delta^{18}O_{NO3}$ estimated that 11 % of nitrate was remineralised *in situ*, however the remineralisation signal could be weak due to the deepening mixed layer and weaker stratification. Station E3 was also stratified but much closer to the shelf edge, and could be more influenced by the open ocean nutrient supply when compared to the inner shelf stations E2 and F2. $\delta^{18}O_{NO3}$ was much closer to the imported $\delta^{18}O_{NO3}$ value from the open ocean, and indicated that between 0 and 22 % of the nitrate in the bottom layer was remineralised *in situ*. This compared well with the measured N:P ratio AOU estimate of remineralisation at E3 which was 17 ± 9 %.

There have been several other studies that have utilised the use of stable isotopes in shelf seas systems. Granger *et al*. (2013) analysed pre-spring bloom samples in the Bering Sea over two seasons and concluded that between 20 % and 100 % of the nitrate across the inner shelf was remineralised *in situ* due to isolation from the off shelf supply of nitrate over the winter period. Although the current study analyses samples from the autumn a similar pattern was observed with the inner shelf

regions being more isolated from the deep ocean supply. Inner shelf stations had greater *in situ* regeneration and a gradient was observed from the middle to outer shelf in the percentage of remineralised nitrate.

More recently (Liu et al. 2017) investigated the nitrogen biogeochemistry during the spring bloom in the East China Sea. They observed that $\delta^{15}N_{NO3}$ and $\delta^{18}O_{NO3}$ varied between water masses, with the Yellow Sea Coastal Current Water having much higher $\delta^{15}N_{NO3}$ and $\delta^{18}O_{NO3}$ (13.2 ‰ and 18.8 ‰, respectively) than the two other water masses (Yellow Sea Mixed Water and Yellow Sea Warm Current Water (6.3 to 8.2 ‰ and 6.2 to 9.7 ‰, respectively). Liu et al noted that $\delta^{18}O_{NO3}$ was higher than $\delta^{15}N_{NO3}$, which reflected the multiple sources of nitrate including atmospheric deposition which accounted for 71 % of the external nitrate input. These higher $\delta^{15}N_{NO3}$ and $\delta^{18}O_{NO3}$ from terrestrial sources could imply that the end member $\delta^{18}O_{NO3}$ chosen for this study may potentially underestimate the remineralisation taking place.

The high percentages of nitrate regenerated locally on the Hebrides Shelf during autumn 2014 indicated that primary productivity was supported by remineralised nitrate over large areas of the shelf region. This demonstrated that the Hebrides Shelf retained and utilised nutrients to fuel the highly productive system when potentially isolated from the deep ocean supply of nutrients. $\delta^{18}O_{NO3}$ is essentially a tracer of the capacity of the shelf to resupply fixed nitrogen for production. Estimates of autumn remineralisation have impacts on the carbon uptake and export from the system. If nitrate is remineralised *in situ* then the carbon within the system is also regenerated and not buried in the shelf sediments. Any carbon regenerated is not lost from the shelf unless it is transported off shelf at the shelf edge. This can potentially lead to outgassing of carbon dioxide in regions with high *in situ* remineralisation rates. The north-west European shelf accounts for a significant proportion of global carbon export, estimated to remove up to 40 % of the carbon sequestered from each growing season before the onset of the next (Holt et al. 2009). If *in situ* remineralisation rates are higher than expected this would have an impact on global carbon export estimates and the current understanding of the shelf sea carbon cycle. Air sea CO_2 fluxes were investigated during the Hebrides cruise ranged from -14.6 to 12.4 mmol C m^{-2} d^{-1} (Painter et al. 2016). Positive fluxes at the inner shelf shallow mixed stations indicated there was outgassing of carbon dioxide

to the atmosphere, while the outer shelf stations and off shelf stations were sinks of carbon dioxide. The whole shelf was estimated to be a weak carbon sink in autumn 2014 (-0.0021 ± 0.0044 Tg C d^{-1}), with the large standard deviation associated with inner shelf outgassing stations (Painter et al. 2016). Overall the conclusions drawn from Painter et al., 2016 agree well with the conclusions drawn from the estimates of regeneration across the shelf as found in this study. The inner shelf stations are more reliant on regenerated nitrate however this was difficult to quantify as the waters were recently mixed. The potential for carbon export at the outer shelf stations meant that despite some regeneration taking place they were carbon dioxide sinks during the autumn.

5.4.3 Conclusions

This study was the first to collect samples for the analysis of $\delta^{15}N_{NO3}$ and $\delta^{18}O_{NO3}$ on the Hebrides Shelf, providing a means to independently quantify the amount of nitrate remineralised locally. This study estimated that a significant proportion of the nitrate across the Hebrides Shelf was remineralised *in situ* during the autumn period before the shelf was re-supplied with nitrate from off shelf supply over winter. Estimates for the inner shelf were ≤94 % of the nitrate present may be due to local remineralisation, whilst at the middle and outer shelf 78 % may be due to local remineralisation, although likely to be closer to 40 %. The southern transects E and F were likely representative of the wider shelf before stratification had started to breakdown, showing the potential for the stable isotopes $\delta^{15}N_{NO3}$ and $\delta^{18}O_{NO3}$ to be used to investigate nitrogen cycling in a seasonally stratified shelf sea (Figure 5.16). Therefore, this study provided a unique opportunity to critically evaluate the use of stable isotopes across a dynamic environment as stratification broke down. Across the inner shelf where the waters were recently mixed, the surface uptake signal and bottom water nitrification signal were mixed and so it was more difficult to quantify the potential remineralisation using stable isotopes due to the dilution of the two values and impossible to quantify it using AOU as the oxygen had already equilibrated with the atmosphere (Figure 5.15). The mid shelf stratified regions provided the best estimates of remineralisation using both methods as the surface uptake signal and bottom water nitrification signal were distinct, owing to mixing of isotopic end members and minimal changes in oxygen concentration due to mixing

(Figure 5.16). The shelf edge region was most connected to the off shelf supply of nitrate, which supplied ‘new’ nitrate, with less *in situ* remineralisation taking place. This signal was observed in the isotope values as the off shelf nitrate supply mixed with the on shelf remineralisation signal, representing the overall proportion of new versus regenerated production.

a)

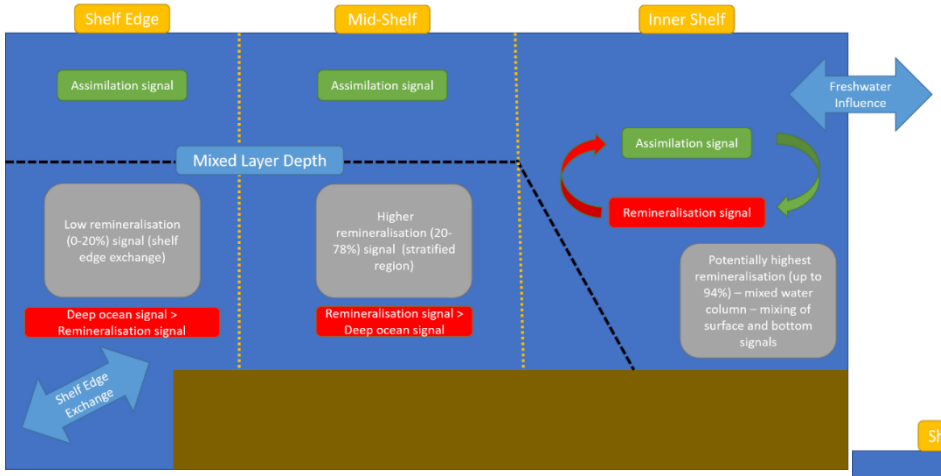

b)

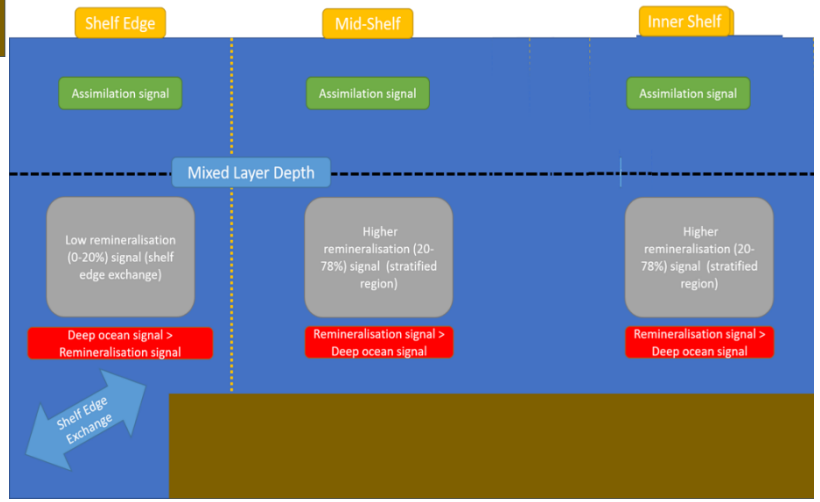

Figure 5.16. Schematic showing the stable isotope signals occurring across the Hebrides Shelf during autumn 2014 across the shelf edge, mid shelf and inner shelf regions at a) northern shelf stations where stratification was breaking down, and b) southern shelf stations where the shelf waters were still stratified.

Chapter 6. Review of isotope datasets & conclusions

6.1. Review of isotope datasets

$\delta^{15}N_{NO3}$ and $\delta^{18}O_{NO3}$ have been collected from several published datasets in Shelf Sea and estuarine regions (Dähnke et al. 2010; Granger et al. 2013; Brown et al. 2015; Liu et al. 2017). Data were collected from a diverse range of polar and temperate shelf seas the Bering Sea (Granger et al. 2013), the Chukchi Shelf Sea and Canadian Basin (Brown et al. 2015), the German Bight in the North Sea (Dähnke et al. 2010), and the East China Sea (classed as a warm temperate region) (Liu et al. 2017) for comparing with the data presented in this thesis.

The study of the proportion of remineralised nitrate in the Bering Sea (Granger et al. 2013) provided a useful comparison to the data presented in this thesis, as it is from a similar sized shelf with the potential for the inner shelf to be isolated from the off shelf supply of nitrate. The separation of the surface uptake signal, and bottom water remineralisation signal can be identified in both datasets (Figure 6.1a, 6.1b). The off shelf deep water $\delta^{15}N_{NO3}$ in the Bering Sea was more enriched than off shelf waters in this study, particularly those taken from off shelf stations in the Celtic Sea (SSB) due to the inter basin differences between the Pacific (the source of nitrate to the Bering Sea) and the North Atlantic (the major source of nitrate to the Celtic Sea) (Sigman et al. 2009b). However, both data sets indicate the same processes occurring in the $\delta^{15}N_{NO3.}$ The $\delta^{18}O_{NO3}$ was similar between both Granger's and this study with and enriched and remineralised signal evident in both, and a similar off shelf deep water value.

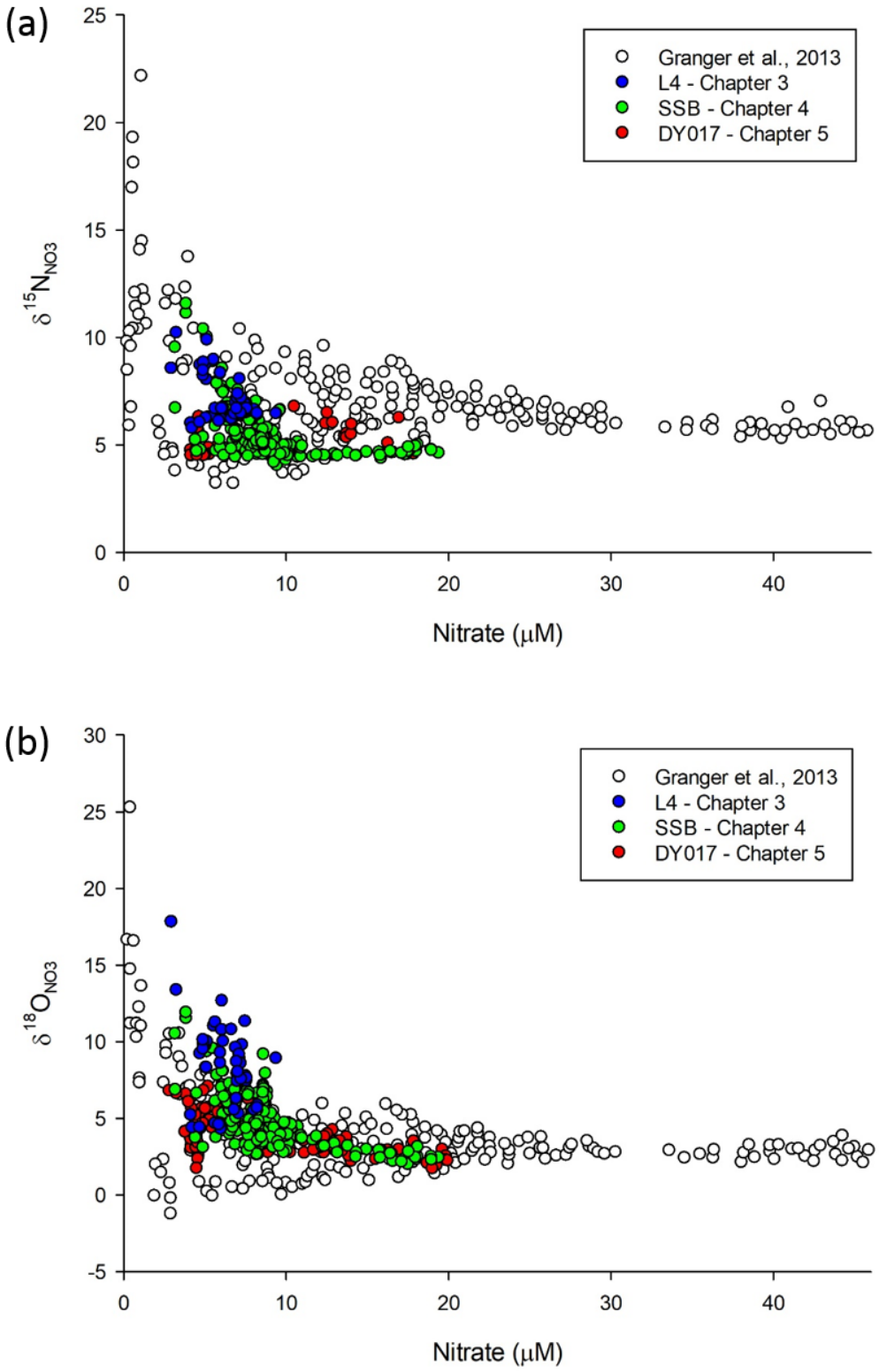

Figure 6.1 (a) Combined nitrate and $\delta^{15}N_{NO3}$ data for this thesis compared to data from the Bering Sea (Granger et al., 2013) (b) Combined nitrate and $\delta^{18}O_{NO3}$ data for this thesis compared to data from the Bering Sea (Granger et al., 2013).

The $\delta^{15}N_{NO3}$ to $\delta^{18}O_{NO3}$ measured in this thesis was compared to the studies in the Chukchi Shelf Sea and Canadian Basin (Brown et al. 2015), the German Bight in the North Sea (Dähnke et al. 2010), and the East China Sea (Liu et al. 2017). The studies highlight the different processes that affect the $\delta^{15}N_{NO3}$ to $\delta^{18}O_{NO3}$ ratio. The $\delta^{15}N_{NO3}$ to $\delta^{18}O_{NO3}$ ratio in the L4 data-set was similar to the samples from East China Sea, with a similar 3:1 gradient observed at L4 to the coastal current in the East China Sea. The samples from the German Bight demonstrated particularly high $\delta^{15}N_{NO3}$ relative to $\delta^{18}O_{NO3}$ associated with run off from the continent, whilst my samples were relatively enriched in $\delta^{18}O_{NO3}$ compared to $\delta^{15}N_{NO3}$. The study in the Chukchi Shelf Sea and Canadian Basin observed coupled partial nitrification-denitrification, driving the decrease in $\delta^{18}O_{NO3}$ and a sediment source of ^{15}N enriched ammonium driving up the $\delta^{15}N_{NO3}$.

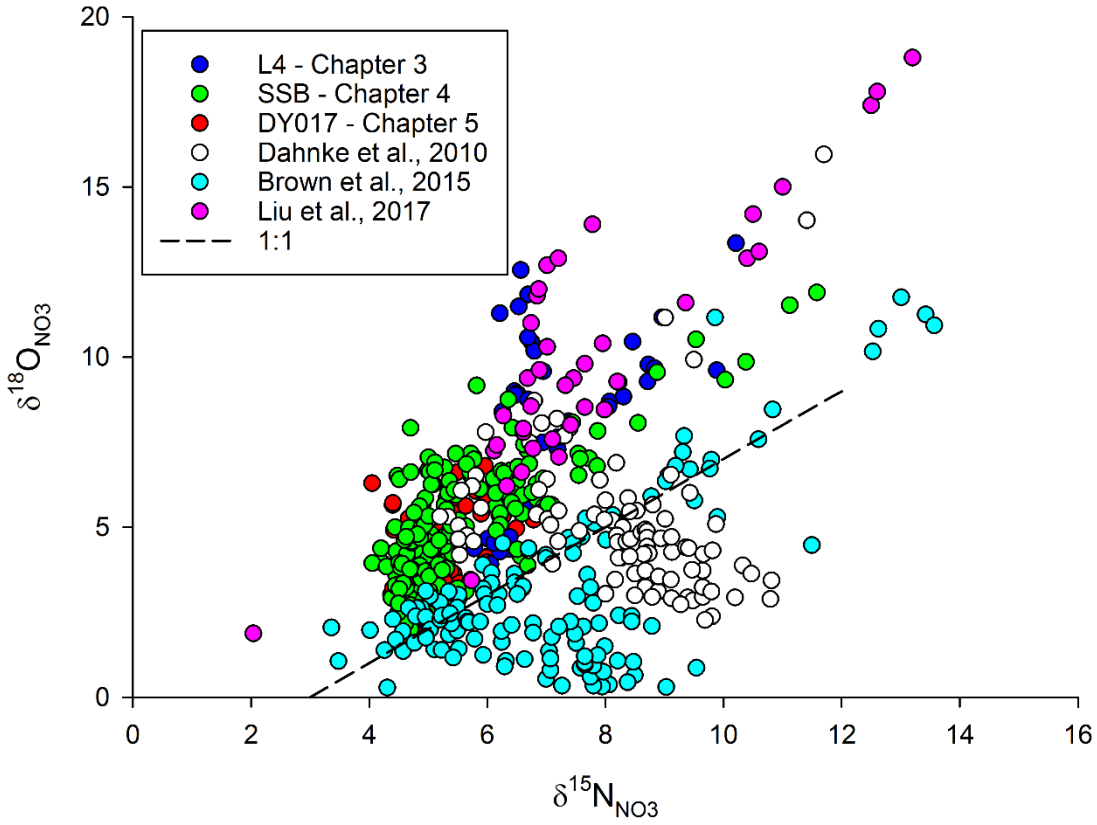

Figure 6.2. The relationship between $\delta^{15}N_{NO3}$ and $\delta^{18}O_{NO3}$ for this thesis compared to data from the Chukchi Shelf Sea and Canadian Basin (Brown et al., 2015), the German Bight in the North Sea (Dahnke et al., 2010), and the East China Sea (Liu et al., 2017).

This study was the first to analyse the stable isotopes of nitrate across a shelf sea for an entire seasonal cycle. The results of this study have provided the first comprehensive seasonal assessment of the regeneration of nitrogen in the North West European shelf seas using stable isotopes of nitrate. This study has provided valuable insight into the different biogeochemical processes occurring across the shelf, and the sources of nitrate that sustains productivity on the shelf during different periods of the annual shelf sea nutrient cycle.

6.2 Impacts of the research presented

This study used stable isotope measurements of $\delta^{15}N_{NO3}$ and $\delta^{18}O_{NO3}$ to critically analyse the nitrogen cycle within three shelf sea environments across the North West European shelf. Nitrate isotopes provide an integrative tracer of the biogeochemical processes occurring across the shelf sea ecosystem and gives the potential for the shelf sea carbon cycle to be evaluated.

The time-series from the L4 site (Chapter 3) provided an understanding of using stable isotopes in a particularly dynamic mixed near shore environment. They captured the spring bloom period, with a strong nitrate assimilation signal. The main sources of nitrate to the system were also detected in the stable isotope nitrogen and oxygen values corresponding to changes in salinity and nitrate concentration. The results confirm the hypothesis that a proportion of the nitrate supplied to L4 is of riverine origin, and that this can be identified using $\delta^{15}N_{NO3}$ and $\delta^{18}O_{NO3}$. The study also highlighted the difficulty of using stable isotopes in a relatively well mixed coastal environment where seasonal depletion of nitrate occurred in both the surface and bottom mixed layers.

The stable isotope measurements from the Celtic Sea (Chapter 4) provided new insight into the supply and cycling on nitrogen across the shelf and delivers important conclusions as part of the NERC Shelf Sea Biogeochemistry programme. The data analysed highlighted key biogeochemical processes occurring across the Celtic Sea over an annual cycle including the spring bloom, and *in situ* remineralisation. Along the full transect the inner shelf stations become increasingly isolated from the off shelf supply of nitrate throughout the summer and autumn periods with these inner shelf regions rely on *in situ* remineralisation to provide nitrate during the summer and to a greater extent the autumn. Riverine supply of

nitrate was greater at these inner shelf stations providing a significant proportion of the nitrate for primary production, with the contribution of rivers decreasing towards the shelf edge. The outer shelf bottom waters from CCS (lying approximately 120 km from the shelf edge) were supplied with nitrate from off shelf during the summer and autumn with little *in situ* remineralisation taking place. These findings suggest that regenerated nitrate was particularly important across the inner shelf during summer and autumn. Contrastingly, across the outer shelf a new supply of off shelf nitrate was potentially important during the summer and autumn periods with salinity intrusion onto the shelf in the bottom layer (see Figure 4.16). This study therefore challenges the classical view we have of the shelf where wintertime flushing supplies the majority of nitrate for the spring bloom and suggests that a combination of riverine, on shelf transport of nitrate from the shelf edge during the summer and *in situ* remineralisation maintain the nitrate pool on shelf. These conclusions have implications for understanding the processes that cause the Celtic Sea to be an overall sink for carbon dioxide (Huthnance et al. 2009) and demonstrate how important an understanding of the nitrogen cycling processes across the shelf are to improve predictive marine biogeochemical and ecosystems models and marine policy.

The data from the Hebrides Shelf (Chapter 5) provided an opportunity to study the post autumn bloom time period during the breakdown of stratification. Four cross shelf transects were utilised using the stable isotope method at varying degrees of stratification across the shelf. The study confirms the hypothesis that a large proportion of the nitrate across the Hebrides shelf was remineralised *in situ* during the autumn period before the shelf was resupplied with nitrate from the off shelf during the winter. Despite being recently mixed the northern inner shelf stations still retained an isotopic signature associated with remineralisation providing useful estimates of the proportion of remineralisation.

6.3 Critical evaluation of research

Despite this work providing new insights into the nitrogen cycle in the North West European shelf seas, and shelf seas in general the study highlighted limitations in $\delta^{15}N_{NO3}$ and $\delta^{18}O_{NO3}$ to provide accurate results in highly mixed environments. It also highlighted the future need for sampling for accurate end -

member isotopes, particularly $\delta^{18}O_{NO3}$ when calculating the percentage of remineralised nitrate in a region with multiple nitrate sources.

The high precision of denitrifier method used for isotopic analysis is vital for this work to separate the different biogeochemical processes and calculate accurate proportions of remineralised nitrate. Throughout this work there was a large amount of method development at the LIFER Lab at the University of Liverpool to ensure that the results obtained were accurate and that the error was low enough to feel confident in drawing conclusion from the work.

6.4 Future research priorities

The marine nitrogen and carbon cycles are likely to be influenced by anthropogenic induced changes. Shelf seas in particular are heavily affected by human activities and are likely to feel the greatest impacts of perturbations to the nitrogen cycle. The warming climate and subsequent decreases in ocean pH are likely to lead to an increase in oxygen deficient zones within the ocean. A decrease in pH is likely to inhibit the microbial community and cause a decrease in nitrification (Beman et al. 2011). An increase in oxygen deficient zones within the ocean is likely to increase denitrification potentially unbalancing the global nitrogen cycle (Devol and Hartnett 2001). Results from model decadal analysis of the North West European shelf highlight that between 325,000 and 365,000 km^2 of shelf bottom waters were vulnerable to oxygen deficiency including the Celtic Sea (Ciavatta et al. 2016).

The current inputs of fixed nitrogen due to human activity now matches that naturally fixed in the marine biosphere (Jickells et al. 2017). These large increases significantly impact coastal and shelf regions first. The North Sea, however has seen a decline in productivity since the 1980s (Capuzzo et al. 2018), with policy changes to reduce run off aiming to limit the effects of eutrophication and oxygen depletion (Lenhart et al. 2010). The reduction in phosphate inputs, however has been much greater than the reduction in nitrogen inputs, changing not only nutrient availability, but the stoichiometric ratio of nutrients available to phytoplankton (Burson et al. 2016). These results show the importance of understanding the nutrient cycles within shelf seas in regard to changes in policy, and the potential for policy changes to cause major changes in coastal region nutrient dynamics.

This work has highlighted how important understanding the role of shelf seas are in the nitrogen and carbon cycles. It is important that we continue to increase our understanding of the complex processes occurring in these highly dynamic environments in a changing world and use it to improve predictive climate models.

7. References

Altabet MA, Francois R (2001) Nitrogen isotope biogeochemistry of the Antarctic Polar Frontal Zone at 170 W. Deep Sea Research Part II: Topical Studies in Oceanography 48: 4247-4273

Altabet MA, Murray DW, Prell WL (1999) Climatically linked oscillations in Arabian Sea denitrification over the past 1 my: Implications for the marine N cycle. Paleoceanography 14: 732-743

Anderson LA (1995) On the hydrogen and oxygen content of marine phytoplankton. Deep sea research part I: Oceanographic research papers 42: 1675-1680

Antia N, Harrison P, Oliveira L (1991) The role of dissolved organic nitrogen in phytoplankton nutrition, cell biology and ecology. Phycologia 30: 1-89

Bates NR, Astor YM, Church MJ, Currie K, Dore JE, Gonzalez-Davila M, Lorenzoni L, Muller-Karger F, Olafsson J, Santana-Casiano JM (2014) A Time-Series View of Changing Surface Ocean Chemistry Due to Ocean Uptake of Anthropogenic CO_2 and Ocean Acidification. Oceanography 27: 126-141

Bauer JE, Cai W-J, Raymond PA, Bianchi TS, Hopkinson CS, Regnier PA (2013) The changing carbon cycle of the coastal ocean. Nature 504: 61

Beman JM, Chow C-E, King AL, Feng Y, Fuhrman JA, Andersson A, Bates NR, Popp BN, Hutchins DA (2011) Global declines in oceanic nitrification rates as a consequence of ocean acidification. Proceedings of the National Academy of Sciences 108: 208-213

Berman T (2001) The role of DON and the effect of N: P ratios on occurrence of cyanobacterial blooms: implications from the outgrowth of Aphanizomenon in Lake Kinneret. Limnology and Oceanography 46: 443-447

Beusen AH, Bouwman AF, Van Beek LP, Mogollón JM, Middelburg JJ (2016) Global riverine N and P transport to ocean increased during the 20th century despite increased retention along the aquatic continuum. Biogeosciences 13: 2441

Bigg GR, Rohling EJ (2000) An oxygen isotope data set for marine waters. Journal of Geophysical Research: Oceans 105: 8527-8535

Biscaye PE, Flagg CN, Falkowski PG (1994) The shelf edge exchange processes experiment, SEEP-II: an introduction to hypotheses, results and conclusions. Deep Sea Research Part II: Topical Studies in Oceanography 41: 231-252

Blackford J, Gilbert F (2007) pH variability and CO2 induced acidification in the North Sea. Journal of Marine Systems 64: 229-241

Booth DA, Ellett D (1983) The Scottish continental slope current. Continental Shelf Research 2: 127-146

Böttjer D, Dore JE, Karl DM, Letelier RM, Mahaffey C, Wilson ST, Zehr J, Church MJ (2017) Temporal variability of nitrogen fixation and particulate nitrogen export at Station ALOHA. Limnology and Oceanography 62: 200-216

Boyer EW, Howarth RW, Galloway JN, Dentener FJ, Green PA, Vörösmarty CJ (2006) Riverine nitrogen export from the continents to the coasts. Global Biogeochemical Cycles 20

Brewer P, Riley J (1965) The automatic determination of nitrate in sea water Deep Sea Research and Oceanographic Abstracts. Elsevier, pp 765-772

Bronk D, See J, Bradley P, Killberg L (2007) DON as a source of bioavailable nitrogen for phytoplankton. Biogeosciences 4: 283-296

Bronk DA (2002) Dynamics of DON. Biogeochemistry of marine dissolved organic matter 384: p153-247

Brown ZW, Casciotti KL, Pickart RS, Swift JH, Arrigo KR (2015) Aspects of the marine nitrogen cycle of the Chukchi Sea shelf and Canada Basin. Deep Sea Research Part II: Topical Studies in Oceanography 118: 73-87

Burson A, Stomp M, Akil L, Brussaard CP, Huisman J (2016) Unbalanced reduction of nutrient loads has created an offshore gradient from phosphorus to nitrogen limitation in the North Sea. Limnology and Oceanography 61: 869-888

Capone DG, Ferrier MD, Carpenter EJ (1994) Amino acid cycling in colonies of the planktonic marine cyanobacterium Trichodesmium thiebautii. Applied and Environmental Microbiology 60: 3989-3995

Capone DG, O'Neil JM, Zehr J, Carpenter EJ (1990) Basis for diel variation in nitrogenase activity in the marine planktonic cyanobacterium Trichodesmium thiebautii. Applied and environmental microbiology 56: 3532-3536

Capone DG, Zehr JP, Paerl HW, Bergman B, Carpenter EJ (1997) Trichodesmium, a globally significant marine cyanobacterium. Science 276: 1221-1229

Capuzzo E, Lynam CP, Barry J, Stephens D, Forster RM, Greenwood N, McQuatters-Gollop A, Silva T, Leeuwen SM, Engelhard GH (2018) A decline in primary production in the North Sea over 25 years, associated with reductions in zooplankton abundance and fish stock recruitment. Global change biology 24

Carpenter EJ, Harvey HR, Fry B, Capone DG (1997) Biogeochemical tracers of the marine cyanobacterium Trichodesmium. Deep Sea Research Part I: Oceanographic Research Papers 44: 27-38

Casciotti KL (2016) Nitrogen and oxygen isotopic studies of the marine nitrogen cycle. Annual review of marine science 8: 379-407

Casciotti KL, Sigman DM, Hastings MG, Böhlke J, Hilkert A (2002) Measurement of the oxygen isotopic composition of nitrate in seawater and freshwater using the denitrifier method. Analytical Chemistry 74: 4905-4912

Ciavatta S, Kay S, Saux-Picart S, Butenschön M, Allen J (2016) Decadal reanalysis of biogeochemical indicators and fluxes in the North West European shelf-sea ecosystem. Journal of Geophysical Research: Oceans 121: 1824-1845

Codispoti L, Brandes JA, Christensen J, Devol A, Naqvi S, Paerl HW, Yoshinari T (2001) The oceanic fixed nitrogen and nitrous oxide budgets: moving targets as we enter the anthropocene? Scientia Marina 65: 85-105

Cohen Y, Gordon LI (1978) Nitrous oxide in the oxygen minimum of the eastern tropical North Pacific: Evidence for its consumption during denitrification and possible mechanisms for its production. Deep Sea Research 25: 509-524

Dähnke K, Emeis K, Johannsen A, Nagel B (2010) Stable isotope composition and turnover of nitrate in the German Bight. Marine Ecology Progress Series 408: 7-18

Dalsgaard T, Thamdrup B, Canfield DE (2005) Anaerobic ammonium oxidation (anammox) in the marine environment. Research in Microbiology 156: 457-464

Davis CE, Mahaffey C, Wolff GA, Sharples J (2014) A storm in a shelf sea: Variation in phosphorus distribution and organic matter stoichiometry. Geophysical Research Letters 41: 8452-8459
de Boyer Montégut C, Madec G, Fischer AS, Lazar A, Iudicone D (2004) Mixed layer depth over the global ocean: An examination of profile data and a profile-based climatology. Journal of Geophysical Research: Oceans 109
Devol AH, Hartnett HE (2001) Role of the oxygen-deficient zone in transfer of organic carbon to the deep ocean. Limnology and Oceanography 46: 1684-1690
Diaz F, Raimbault P (2000) Nitrogen regeneration and dissolved organic nitrogen release during spring in a NW Mediterranean coastal zone (Gulf of Lions): implications for the estimation of new production. Marine Ecology Progress Series: 51-65
Dugdale R, Goering J (1967) Uptake of new and regenerated forms of nitrogen in primary productivity 1. Limnology and oceanography 12: 196-206
Finni T, Kononen K, Olsonen R, Wallström K (2001) The history of cyanobacterial blooms in the Baltic Sea. AMBIO: A Journal of the Human Environment 30: 172-178
Forster P, Ramaswamy V, Artaxo P, Berntsen T, Betts R, Fahey DW, Haywood J, Lean J, Lowe DC, Myhre G (2007) Changes in atmospheric constituents and in radiative forcing. Chapter 2 Climate Change 2007 The Physical Science Basis
Gallon J (2001) N2 fixation in phototrophs: adaptation to a specialized way of life. Plant and Soil 230: 39-48
Galloway JN, Dentener FJ, Capone DG, Boyer EW, Howarth RW, Seitzinger SP, Asner GP, Cleveland CC, Green P, Holland EA (2004) Nitrogen cycles: past, present, and future. Biogeochemistry 70: 153-226
Garcia HE, Gordon LI (1992) Oxygen solubility in seawater: Better fitting equations. Limnology and oceanography 37: 1307-1312
Garcia HE, Levitus S (2006) World Ocean Atlas 2005. Vol. 3, Dissolved oxygen, apparent oxygen utilization, and oxygen saturation
Gonfiantini R (1978) Standards for stable isotope measurements in natural compounds. Nature 271: 534
Granger J, Prokopenko M, Sigman D, Mordy C, Morse Z, Morales L, Sambrotto R, Plessen B (2011) Coupled nitrification-denitrification in sediment of the eastern Bering Sea shelf leads to 15N enrichment of fixed N in shelf waters. Journal of Geophysical Research: Oceans 116
Granger J, Prokopenko MG, Mordy CW, Sigman DM (2013) The proportion of remineralized nitrate on the ice-covered eastern Bering Sea shelf evidenced from the oxygen isotope ratio of nitrate. Global Biogeochemical Cycles 27: 962-971
Granger J, Sigman DM (2009) Removal of nitrite with sulfamic acid for nitrate N and O isotope analysis with the denitrifier method. Rapid Communications in Mass Spectrometry 23: 3753-3762
Granger J, Sigman DM, Needoba JA, Harrison PJ (2004) Coupled nitrogen and oxygen isotope fractionation of nitrate during assimilation by cultures of marine phytoplankton. Limnology and Oceanography 49: 1763-1773
Grasshoff K (1976) Filtration and storage. Methods of seawater analysis: 21-30
Gruber N (2004) The dynamics of the marine nitrogen cycle and its influence on atmospheric CO 2 variations The ocean carbon cycle and climate. Springer, pp 97-148

Gruber N, Sarmiento JL (1997) Global patterns of marine nitrogen fixation and denitrification. Global Biogeochemical Cycles 11: 235-266

Gypens N, Lacroix G, Lancelot C, Borges AV (2011) Seasonal and inter-annual variability of air–sea CO2 fluxes and seawater carbonate chemistry in the Southern North Sea. Progress in oceanography 88: 59-77

Hastings MG, Sigman DM, Lipschultz F (2003) Isotopic evidence for source changes of nitrate in rain at Bermuda. Journal of Geophysical Research: Atmospheres 108

Hill A, Horsburgh K, Garvine R, Gillibrand P, Slesser G, Turrell W, Adams R (1997) Observations of a density-driven recirculation of the Scottish coastal current in the Minch. Estuarine, Coastal and Shelf Science 45: 473-484

Holt J, Harle J, Proctor R, Michel S, Ashworth M, Batstone C, Allen I, Holmes R, Smyth T, Haines K (2009) Modelling the global coastal ocean. Philosophical Transactions of the Royal Society of London A: Mathematical, Physical and Engineering Sciences 367: 939-951

Huisman J, van Oostveen P, Weissing FJ (1999) Critical depth and critical turbulence: two different mechanisms for the development of phytoplankton blooms. Limnology and oceanography 44: 1781-1787

Huthnance J (1986) The Rockall slope current and shelf-edge processes. Proceedings of the Royal Society of Edinburgh, Section B: Biological Sciences 88: 83-101

Huthnance JM (1995) Circulation, exchange and water masses at the ocean margin: the role of physical processes at the shelf edge. Progress in Oceanography 35: 353-431

Huthnance JM (2010) The northeast Atlantic margins

Huthnance JM, Holt JT, Wakelin SL (2009) Deep ocean exchange with west-European shelf seas. Ocean Science 5: 621-634

Huttunen I, Lehtonen H, Huttunen M, Piirainen V, Korppoo M, Veijalainen N, Viitasalo M, Vehviläinen B (2015) Effects of climate change and agricultural adaptation on nutrient loading from Finnish catchments to the Baltic Sea. Science of the Total Environment 529: 168-181

Jackson GA, Williams PM (1985) Importance of dissolved organic nitrogen and phosphorus to biological nutrient cycling. Deep Sea Research Part A Oceanographic Research Papers 32: 223-235

Jahnke R, Nelson J, Richards M, Robertson C, Rao A, Jahnke D (2008) Benthic primary productivity on the Georgia midcontinental shelf: Benthic flux measurements and high-resolution, continuous in situ PAR records. Journal of Geophysical Research: Oceans 113

Jickells T, An Z, Andersen KK, Baker A, Bergametti G, Brooks N, Cao J, Boyd P, Duce R, Hunter K (2005) Global iron connections between desert dust, ocean biogeochemistry, and climate. science 308: 67-71

Jickells T, Buitenhuis E, Altieri K, Baker A, Capone D, Duce R, Dentener F, Fennel K, Kanakidou M, LaRoche J (2017) A reevaluation of the magnitude and impacts of anthropogenic atmospheric nitrogen inputs on the ocean. Global Biogeochemical Cycles 31: 289-305

Johannsen A, Dähnke K, Emeis K (2008) Isotopic composition of nitrate in five German rivers discharging into the North Sea. Organic Geochemistry 39: 1678-1689

Joint I, Wollast R, Chou L, Batten S, Elskens M, Edwards E, Hirst A, Burkill P, Groom S, Gibb S (2001) Pelagic production at the Celtic Sea shelf break. Deep Sea Research Part II: Topical Studies in Oceanography 48: 3049-3081

Jonas P, Millward G (2010) Metals and nutrients in the Severn Estuary and Bristol Channel: contemporary inputs and distributions. Marine Pollution Bulletin 61: 52-67

Kao SJ, Terence Yang JY, Liu KK, Dai M, Chou WC, Lin HL, Ren H (2012) Isotope constraints on particulate nitrogen source and dynamics in the upper water column of the oligotrophic South China Sea. Global Biogeochemical Cycles 26

Karl D, Michaels A, Bergman B, Capone D, Carpenter E, Letelier R, Lipschultz F, Paerl H, Sigman D, Stal L (2002) Dinitrogen fixation in the world's oceans. Biogeochemistry 57: 47-98

Karsh KL, Granger J, Kritee K, Sigman DM (2012) Eukaryotic assimilatory nitrate reductase fractionates N and O isotopes with a ratio near unity. Environmental science & technology 46: 5727-5735

Kihm C, Körtzinger A (2010) Air-sea gas transfer velocity for oxygen derived from float data. Journal of Geophysical Research: Oceans 115

Kirkwood D (1989) Simultaneous determination of selected nutrients in sea water. International Council for the Exploration of the Sea (ICES)

Kitidis V, Laverock B, McNeill LC, Beesley A, Cummings D, Tait K, Osborn MA, Widdicombe S (2011) Impact of ocean acidification on benthic and water column ammonia oxidation. Geophysical Research Letters 38

Knapp AN, DiFiore PJ, Deutsch C, Sigman DM, Lipschultz F (2008) Nitrate isotopic composition between Bermuda and Puerto Rico: Implications for N2 fixation in the Atlantic Ocean. Global Biogeochemical Cycles 22

Kuenen JG (2008) Anammox bacteria: from discovery to application. Nature Reviews Microbiology 6: 320

Kustka AB, Sañudo-Wilhelmy SA, Carpenter EJ, Capone D, Burns J, Sunda WG (2003) Iron requirements for dinitrogen-and ammonium-supported growth in cultures of Trichodesmium (IMS 101): Comparison with nitrogen fixation rates and iron: Carbon ratios of field populations. Limnology and Oceanography 48: 1869-1884

Langdon C (2010) Determination of Dissolved Oxygen in Seawater by Winkler Titration Using The Amperometric Technique

Lenhart H-J, Mills DK, Baretta-Bekker H, Van Leeuwen SM, Van Der Molen J, Baretta JW, Blaas M, Desmit X, Kühn W, Lacroix G (2010) Predicting the consequences of nutrient reduction on the eutrophication status of the North Sea. Journal of Marine Systems 81: 148-170

Lewis K, Allen J (2009) Validation of a hydrodynamic-ecosystem model simulation with time-series data collected in the western English Channel. Journal of Marine Systems 77: 296-311

Li M, Lee YJ, Testa JM, Li Y, Ni W, Kemp WM, Di Toro DM (2016) What drives interannual variability of hypoxia in Chesapeake Bay: Climate forcing versus nutrient loading? Geophysical Research Letters 43: 2127-2134

Liu K-K, Tang TY, Gong G-C, Chen L-Y, Shiah F-K (2000) Cross-shelf and along-shelf nutrient fluxes derived from flow fields and chemical hydrography observed in the southern East China Sea off northern Taiwan. Continental Shelf Research 20: 493-523

Liu SM, Altabet MA, Zhao L, Larkum J, Song GD, Zhang GL, Jin H, Han LJ (2017) Tracing Nitrogen Biogeochemistry During the Beginning of a Spring Phytoplankton Bloom in the Yellow Sea Using Coupled Nitrate Nitrogen and

Oxygen Isotope Ratios. Journal of Geophysical Research: Biogeosciences 122: 2490-2508
Luo Y-W, Lima ID, Karl DM, Deutsch CA, Doney SC (2014) Data-based assessment of environmental controls on global marine nitrogen fixation. Biogeosciences 11: 691-708
Mahaffey C, Reynolds S, Davis CE, Lohan MC (2014) Alkaline phosphatase activity in the subtropical ocean: insights from nutrient, dust and trace metal addition experiments. Frontiers in Marine Science 1: 73
Mahaffey C, Williams RG, Wolff GA, Mahowald N, Anderson W, Woodward M (2003) Biogeochemical signatures of nitrogen fixation in the eastern North Atlantic. Geophysical Research Letters 30
Mantoura R, Woodward E (1983) Optimization of the indophenol blue method for the automated determination of ammonia in estuarine waters. Estuarine, Coastal and Shelf Science 17: 219-224
Mariotti A, Germon J, Hubert P, Kaiser P, Letolle R, Tardieux A, Tardieux P (1981) Experimental determination of nitrogen kinetic isotope fractionation: some principles; illustration for the denitrification and nitrification processes. Plant and soil 62: 413-430
Mayer B, Boyer EW, Goodale C, Jaworski NA, Van Breemen N, Howarth RW, Seitzinger S, Billen G, Lajtha K, Nadelhoffer K (2002) Sources of nitrate in rivers draining sixteen watersheds in the northeastern US: Isotopic constraints. Biogeochemistry 57: 171-197
McCave I, Hall IR, Antia A, Chou L, Dehairs F, Lampitt R, Thomsen L, Van Weering T, Wollast R (2001) Distribution, composition and flux of particulate material over the European margin at 47–50 N. Deep Sea Research Part II: Topical Studies in Oceanography 48: 3107-3139
McCubbin D, Leonard KS, Brown J, Kershaw PJ, Bonfield RA, Peak T (2002) Further studies of the distribution of technetium-99 and caesium-137 in UK and European coastal waters. Continental Shelf Research 22: 1417-1445
McIlvin MR, Casciotti KL (2011) Technical updates to the bacterial method for nitrate isotopic analyses. Analytical Chemistry 83: 1850-1856
McKay W, Baxter M, Ellett D, Meldrum D (1986) Radiocaesium and circulation patterns west of Scotland. Journal of Environmental Radioactivity 4: 205-232
Mulholland MR, Heil CA, Bronk DA, O'Neil JM, Bernhardt P (2002) Does nitrogen regeneration from the N2 fixing cyanobacteria Trichodesmium spp. fuel Karenia brevis blooms in the Gulf of Mexico. Harmful algae: 47-49
Muller-Karger FE, Varela R, Thunell R, Luerssen R, Hu C, Walsh JJ (2005) The importance of continental margins in the global carbon cycle. Geophysical research letters 32
Painter SC, Hartman SE, Kivimäe C, Salt LA, Clargo NM, Bozec Y, Daniels CJ, Jones SC, Hemsley VS, Munns LR (2016) Carbon exchange between a shelf sea and the ocean: The Hebrides Shelf, west of Scotland. Journal of Geophysical Research: Oceans 121: 4522-4544
Pauly D, Christensen V, Guénette S, Pitcher TJ, Sumaila UR, Walters CJ, Watson R, Zeller D (2002) Towards sustainability in world fisheries. Nature 418: 689
Pingree R, Griffiths D (1978) Tidal fronts on the shelf seas around the British Isles. Journal of Geophysical Research: Oceans 83: 4615-4622
Pingree R, Maddock L (1977) Tidal residuals in the English Channel. Journal of the Marine Biological Association of the United Kingdom 57: 339-354

Pingree R, Mardell G (1981) Slope turbulence, internal waves and phytoplankton growth at the Celtic Sea shelf-break. Phil Trans R Soc Lond A 302: 663-682
Porter M, Inall M, Green J, Simpson J, Dale A, Miller P (2016) Drifter observations in the summer time Bay of Biscay slope current. Journal of Marine Systems 157: 65-74
Prandle D (1984) A modelling study of the mixing of 137Cs in the seas of the European continental shelf. Phil Trans R Soc Lond A 310: 407-436
Qi H, Coplen TB, Geilmann H, Brand WA, Böhlke JK (2003) Two new organic reference materials for δ13C and δ15N measurements and a new value for the δ13C of NBS 22 oil. Rapid Communications in Mass Spectrometry 17: 2483-2487
Rabalais N, Diaz RJ, Levin L, Turner R, Gilbert D, Zhang J (2010) Dynamics and distribution of natural and human-caused hypoxia. Biogeosciences 7: 585
Rabalais NN, Turner RE (2006) Oxygen depletion in the Gulf of Mexico adjacent to the Mississippi River Past and Present Water Column Anoxia. Springer, pp 225-245
Rafter PA, DiFiore PJ, Sigman DM (2013) Coupled nitrate nitrogen and oxygen isotopes and organic matter remineralization in the Southern and Pacific Oceans. Journal of Geophysical Research: Oceans 118: 4781-4794
Redfield AC (1963) The influence of organisms on the composition of seawater. The sea 2: 26-77
Rees AP, Gilbert JA, Kelly-Gerreyn BA (2009a) Nitrogen fixation in the western English Channel (NE Atlantic ocean). Marine Ecology Progress Series 374: 7-12
Rees AP, Hope SB, Widdicombe CE, Dixon JL, Woodward EMS, Fitzsimons MF (2009b) Alkaline phosphatase activity in the western English Channel: elevations induced by high summertime rainfall. Estuarine, Coastal and Shelf Science 81: 569-574
Rees AP, Tait K, Widdicombe CE, Quartly GD, McEvoy AJ, Al-Moosawi L (2016) Metabolically active, non-nitrogen fixing, Trichodesmium in UK coastal waters during winter. Journal of plankton research 38: 673-678
Riemann B, Carstensen J, Dahl K, Fossing H, Hansen JW, Jakobsen HH, Josefson AB, Krause-Jensen D, Markager S, Stæhr PA (2016) Recovery of Danish coastal ecosystems after reductions in nutrient loading: a holistic ecosystem approach. Estuaries and Coasts 39: 82-97
Ruiz-Castillo E, Sharples J, Hopkins JE, Woodward E (2018) Seasonality in the cross-shelf physical structure and the implications for nutrients supplies to a temperate shelf sea. Progress in Oceanography In Review
Saba GK, Steinberg DK, Bronk DA (2011) The relative importance of sloppy feeding, excretion, and fecal pellet leaching in the release of dissolved carbon and nitrogen by Acartia tonsa copepods. Journal of Experimental Marine Biology and Ecology 404: 47-56
Schlitzer R (2002) Interactive analysis and visualization of geoscience data with Ocean Data View. Computers & geosciences 28: 1211-1218
Seitzinger S, Harrison JA, Böhlke J, Bouwman A, Lowrance R, Peterson B, Tobias C, Drecht GV (2006) Denitrification across landscapes and waterscapes: a synthesis. Ecological Applications 16: 2064-2090
Seitzinger SP, Giblin AE (1996) Estimating denitrification in North Atlantic continental shelf sediments Nitrogen cycling in the North Atlantic Ocean and its watersheds. Springer, pp 235-260

Shapiro G, Huthnance J, Ivanov V (2003) Dense water cascading off the continental shelf. Journal of Geophysical Research: Oceans 108
Sharples J, Middelburg JJ, Fennel K, Jickells TD (2017) What proportion of riverine nutrients reaches the open ocean? Global Biogeochemical Cycles 31: 39-58
Sharples J, Moore CM, Hickman AE, Holligan PM, Tweddle JF, Palmer MR, Simpson JH (2009) Internal tidal mixing as a control on continental margin ecosystems. Geophysical Research Letters 36
Siddorn J, Allen J, Uncles R (2003) Heat, salt and tracer transport in the Plymouth Sound coastal region: a 3-D modelling study. Journal of the Marine Biological Association of the United Kingdom 83: 673-682
Sigman D, Altabet M, McCorkle D, Francois R, Fischer G (2000) The δ15N of nitrate in the Southern Ocean: nitrogen cycling and circulation in the ocean interior. Journal of Geophysical Research: Oceans 105: 19599-19614
Sigman D, Altabet M, Michener R, McCorkle D, Fry B, Holmes R (1997) Natural abundance-level measurement of the nitrogen isotopic composition of oceanic nitrate: an adaptation of the ammonia diffusion method. Marine Chemistry 57: 227-242
Sigman D, Karsh K, Casciotti K (2009a) Ocean process tracers: nitrogen isotopes in the ocean
Sigman D, Robinson R, Knapp A, Van Geen A, McCorkle D, Brandes J, Thunell R (2003) Distinguishing between water column and sedimentary denitrification in the Santa Barbara Basin using the stable isotopes of nitrate. Geochemistry, Geophysics, Geosystems 4
Sigman DM, Casciotti KL, Andreani M, Barford C, Galanter M, Böhlke J (2001) A bacterial method for the nitrogen isotopic analysis of nitrate in seawater and freshwater. Analytical chemistry 73: 4145-4153
Sigman DM, DiFiore PJ, Hain MP, Deutsch C, Wang Y, Karl DM, Knapp AN, Lehmann MF, Pantoja S (2009b) The dual isotopes of deep nitrate as a constraint on the cycle and budget of oceanic fixed nitrogen. Deep Sea Research Part I: Oceanographic Research Papers 56: 1419-1439
Sigman DM, Granger J, DiFiore PJ, Lehmann MM, Ho R, Cane G, van Geen A (2005) Coupled nitrogen and oxygen isotope measurements of nitrate along the eastern North Pacific margin. Global Biogeochemical Cycles 19
Simpson JH, Sharples J (2012) Introduction to the physical and biological oceanography of shelf seas. Cambridge University Press
Sipler RE, Gong D, Baer SE, Sanderson MP, Roberts QN, Mulholland MR, Bronk DA (2017) Preliminary estimates of the contribution of Arctic nitrogen fixation to the global nitrogen budget. Limnology and Oceanography Letters 2: 159-166
Sitch S, Friedlingstein P, Gruber N, Jones S, Murray-Tortarolo G, Ahlström A, Doney SC, Graven H, Heinze C, Huntingford C (2015) Recent trends and drivers of regional sources and sinks of carbon dioxide. Biogeosciences 12: 653-679
Smith SV, Swaney DP, Talaue-Mcmanus L, Bartley JD, Sandhei PT, McLAUGHLIN CJ, Dupra VC, Crossland CJ, Buddemeier RW, Maxwell BA (2003) Humans, hydrology, and the distribution of inorganic nutrient loading to the ocean. AIBS Bulletin 53: 235-245
Smyth TJ, Fishwick JR, Al-Moosawi L, Cummings DG, Harris C, Kitidis V, Rees A, Martinez-Vicente V, Woodward EM (2009) A broad spatio-temporal view of the Western English Channel observatory. Journal of Plankton Research 32: 585-601

Sohm JA, Webb EA, Capone DG (2011) Emerging patterns of marine nitrogen fixation. Nature Reviews Microbiology 9: 499
Solomon S (2007) Climate change 2007-the physical science basis: Working group I contribution to the fourth assessment report of the IPCC. Cambridge university press
Southward AJ, Langmead O, Hardman-Mountford NJ, Aiken J, Boalch GT, Dando PR, Genner MJ, Joint I, Kendall MA, Halliday NC (2005) Long-term oceanographic and ecological research in the Western English Channel. Advances in marine biology 47: 1-105
Sparholt H, Bertelsen M, Lassen H (2007) A meta-analysis of the status of ICES fish stocks during the past half century. iCes Journal of Marine science 64: 707-713
Sterner RW (1990) The ratio of nitrogen to phosphorus resupplied by herbivores: zooplankton and the algal competitive arena. The American Naturalist 136: 209-229
Thomas H, Bozec Y, Elkalay K, De Baar HJ (2004) Enhanced open ocean storage of CO2 from shelf sea pumping. Science 304: 1005-1008
Topcu H, Brockmann U (2015) Seasonal oxygen depletion in the North Sea, a review. Marine pollution bulletin 99: 5-27
Trowbridge J, Lentz S (1998) Dynamics of the bottom boundary layer on the northern California shelf. Journal of Physical Oceanography 28: 2075-2093
Tsunogai S, Watanabe S, Sato T (1999) Is there a "continental shelf pump" for the absorption of atmospheric CO2? Tellus B 51: 701-712
Tupas L, Koike I (1990) Amino acid and ammonium utilization by heterotrophic marine bacteria grown in enriched seawater. Limnology and Oceanography 35: 1145-1155
Van Leeuwen S, Le Quesne W, Parker E (2016) Potential future fisheries yields in shelf waters: a model study of the effects of climate change and ocean acidification. Biogeosciences 13: 441
Waldbusser GG, Salisbury JE (2014) Ocean acidification in the coastal zone from an organism's perspective: multiple system parameters, frequency domains, and habitats. Annual review of marine science 6: 221-247
Wankel SD, Kendall C, Francis CA, Paytan A (2006) Nitrogen sources and cycling in the San Francisco Bay Estuary: A nitrate dual isotopic composition approach. Limnology and Oceanography 51: 1654-1664
Wankel SD, Kendall C, Pennington JT, Chavez FP, Paytan A (2007) Nitrification in the euphotic zone as evidenced by nitrate dual isotopic composition: Observations from Monterey Bay, California. Global Biogeochemical Cycles 21
Wasmund N, Nausch G, Matthäus W (1998) Phytoplankton spring blooms in the southern Baltic Sea—spatio-temporal development and long-term trends. Journal of plankton research 20: 1099-1117
Welschmeyer NA (1994) Fluorometric analysis of chlorophyll a in the presence of chlorophyll b and pheopigments. Limnology and Oceanography 39: 1985-1992
Widdicombe C, Eloire D, Harbour D, Harris R, Somerfield P (2010) Long-term phytoplankton community dynamics in the Western English Channel. Journal of Plankton Research 32: 643-655
Wihsgott J, Hopkins J, Sharples J, Jones E, Balfour C (2016) Long-term mooring observations of full depth water column structure spanning 17 months, collected in a temperate shelf sea (Celtic Sea). British Oceanographic Data Centre, Natural Environment Research Council, accessed 3

Wollast R (1993) Interactions of carbon and nitrogen cycles in the coastal zone Interactions of C, N, P and S biogeochemical cycles and global change. Springer, pp 195-210
Wollast R (1998) Evaluation and comparison of the global carbon cycle in the coastal zone and in the open ocean. The sea 10: 213-252
Wu J, Sunda W, Boyle EA, Karl DM (2000) Phosphate depletion in the western North Atlantic Ocean. Science 289: 759-762
Wyatt NJ, Kitidis V, Woodward EMS, Rees AP, Widdicombe S, Lohan M (2010) Effects of high CO2 on the fixed nitrogen inventory of the Western English Channel. Journal of plankton research 32: 631-641
Xue D, Botte J, De Baets B, Accoe F, Nestler A, Taylor P, Van Cleemput O, Berglund M, Boeckx P (2009) Present limitations and future prospects of stable isotope methods for nitrate source identification in surface-and groundwater. Water research 43: 1159-1170
Yan W, Mayorga E, Li X, Seitzinger SP, Bouwman A (2010) Increasing anthropogenic nitrogen inputs and riverine DIN exports from the Changjiang River basin under changing human pressures. Global Biogeochemical Cycles 24
Yool A, Martin AP, Fernández C, Clark DR (2007) The significance of nitrification for oceanic new production. Nature 447: 999
Yuan D, Zhu J, Li C, Hu D (2008) Cross-shelf circulation in the Yellow and East China Seas indicated by MODIS satellite observations. Journal of Marine Systems 70: 134-149
Zhang J-Z, Chi J (2002) Automated analysis of nanomolar concentrations of phosphate in natural waters with liquid waveguide. Environmental science & technology 36: 1048-1053

Appendices

1. Samples collected at L4 time-series 2014 to 2016

Date	Depth (m)	$\delta^{15}N_{NO3}$	$\delta^{18}O_{NO3}$
02/12/2014	0	6.6	8.0
08/12/2014	0	6.7	10.0
15/12/2014	0	6.6	12.7
27/01/2015	0	6.5	8.9
02/02/2015	0	6.8	9.8
09/02/2015	0	6.5	11.3
16/02/2015	0	6.9	7.4
10/03/2015	0	8.7	9.7
07/04/2015	0	8.6	17.8
16/11/2015	0	6.0	5.2
07/12/2015	0	6.4	4.7
05/01/2016	0	6.2	4.3
02/02/2016	0	6.4	5.8
16/02/2016	0	6.4	5.3
23/02/2016	0	6.6	5.5
29/02/2016	0	6.6	7.7
07/03/2016	0	6.9	7.8
14/03/2016	0	6.9	9.6
21/03/2016	0	8.1	8.9
04/04/2016	0	8.7	9.2
11/04/2016	0	8.3	8.6
18/04/2016	0	9.9	10.0
24/04/2016	0	9.0	11.0
02/12/2014	50	6.2	8.3
08/12/2014	50	6.7	11.3
15/12/2014	50	6.7	10.8
27/01/2015	50	6.2	10.8
02/02/2015	50	6.5	9.1
09/02/2015	50	6.7	7.6
16/02/2015	50	7.2	7.4
10/03/2015	50	8.8	9.8
07/04/2015	50	10.2	13.4
16/11/2015	50	5.8	4.4
07/12/2015	50	6.1	4.6
05/01/2016	50	6.1	4.4
02/02/2016	50	6.5	5.7
16/02/2016	50	6.4	6.3
23/02/2016	50	6.5	5.6
29/02/2016	50	6.5	8.6
07/03/2016	50	7.2	7.6
14/03/2016	50	6.7	8.7
21/03/2016	50	7.4	8.0

04/04/2016	50	8.0	8.3
11/04/2016	50	8.4	9.3
24/04/2016	50	8.2	9.5
03/05/2016	50	8.5	10.1

2. Samples collected across the Celtic Sea during DY018, DY021, DY029 and DY033

Cruise	Lat	Long	Site	Depth	$\delta^{15}N_{NO3}$	$\delta^{18}O_{NO3}$
DY018	49.40	-8.58	CCS	130	5.1	4.5
DY018	49.40	-8.58	CCS	67	5.0	4.8
DY018	49.40	-8.58	CCS	130	4.8	4.3
DY018	49.40	-8.58	CCS	70	4.9	4.3
DY018	49.27	-8.75	O1	100	4.9	3.8
DY018	49.27	-8.75	O1	60	5.0	3.6
DY018	49.13	-8.90	O2	140	5.0	4.6
DY018	49.13	-8.90	O2	80	5.0	3.6
DY018	49.13	-8.90	O2	66	4.9	3.1
DY018	49.00	-9.04	O3	139	4.9	3.5
DY018	49.00	-9.04	O3	102	5.0	4.2
DY018	48.85	-9.20	O4	149	4.6	3.9
DY018	48.85	-9.20	O4	95	4.6	3.5
DY018	48.85	-9.20	O4	85	4.8	4.0
DY018	48.72	-9.35	O5	150	4.6	4.3
DY018	48.72	-9.35	O5	100	4.6	4.2
DY018	48.72	-9.35	O5	70	4.6	3.4
DY018	48.21	-10.05	Fe01	2450	4.6	2.4
DY018	48.21	-10.05	Fe01	1500	4.6	2.5
DY018	48.21	-10.05	Fe01	850	4.4	2.9
DY018	48.21	-10.05	Fe01	400	4.4	3.7
DY018	48.21	-10.05	Fe01	250	4.2	3.9
DY018	48.21	-10.05	Fe01	100	4.8	4.3
DY018	48.24	-9.97	Fe02	2000	4.8	2.5
DY018	48.24	-9.97	Fe02	1000	4.6	2.7
DY018	48.24	-9.97	Fe02	400	4.5	3.7
DY018	48.24	-9.97	Fe02	200	4.5	4.3
DY018	48.24	-9.97	Fe02	100	4.6	4.2
DY018	48.37	-9.63	Fe04	990	4.7	2.9
DY018	48.37	-9.63	Fe04	850	4.7	3.0
DY018	48.37	-9.63	Fe04	500	4.5	3.6
DY018	48.37	-9.63	Fe04	300	4.4	3.3
DY018	48.37	-9.63	Fe04	100	4.4	3.3
DY018	48.38	-9.53	Fe06	465	4.9	3.9

DY018	48.38	-9.53	Fe06	400	4.6	3.4
DY018	48.38	-9.53	Fe06	200	4.6	3.3
DY018	48.38	-9.53	Fe06	100	4.7	3.7
DY018	48.42	-9.47	Fe07	230	4.7	4.5
DY018	48.42	-9.47	Fe07	150	4.7	4.7
DY018	48.42	-9.47	Fe07	100	4.7	4.6
DY018	48.57	-9.51	CS2	190	4.4	5.0
DY018	48.57	-9.51	CS2	85	4.9	5.3
DY018	48.57	-9.51	CS2	180	4.7	5.0
DY018	48.57	-9.51	CS2	75	4.9	4.7
DY018	49.61	-8.33	J8	130	5.0	2.9
DY018	49.61	-8.33	J8	80	5.0	2.8
DY018	49.79	-8.06	J7	75	5.1	3.4
DY018	49.79	-8.06	J7	70	5.3	4.1
DY018	49.79	-8.06	J7	50	5.2	4.4
DY018	50.21	-7.46	J5	99	5.3	4.0
DY018	50.21	-7.46	J5	80	5.4	4.2
DY018	50.21	-7.46	J5	60	5.2	4.5
DY018	50.63	-6.94	J3	86	5.3	2.7
DY018	50.63	-6.94	J3	60	5.2	2.7
DY018	50.63	-6.94	J3	50	5.4	3.1
DY018	50.83	-6.67	J2	86	5.3	4.7
DY018	50.83	-6.67	J2	70	5.2	3.3
DY018	50.83	-6.67	J2	50	5.3	4.6
DY018	51.21	-6.13	A	95	5.6	3.1
DY018	51.21	-6.13	A	65	5.5	2.9
DY021	51.21	-6.13	A	97	7.1	5.6
DY021	51.21	-6.13	A	60	6.8	5.8
DY021	51.21	-6.13	A	40	6.8	6.3
DY021	51.21	-6.13	A	4	7.0	5.6
DY021	49.40	-8.58	CCS	140	6.4	7.9
DY021	49.40	-8.58	CCS	110	6.4	8.7
DY021	49.40	-8.58	CCS	80	5.7	7.1
DY021	49.40	-8.58	CCS	60	5.7	7.2
DY021	48.57	-9.51	CS2	200	5.8	9.2
DY021	48.57	-9.51	CS2	181	5.5	7.2
DY029	49.40	-8.58	CCS	125	6.5	6.3
DY029	49.40	-8.58	CCS	70	6.4	6.7
DY029	49.40	-8.58	CCS	60	6.4	6.0
DY029	49.40	-8.58	CCS	35	7.5	7.2
DY029	49.40	-8.58	CCS	18	7.7	7.0
DY029	49.40	-8.58	CCS	5	7.6	7.0
DY029	48.57	-9.51	CS2	80	5.3	5.9
DY029	48.57	-9.51	CS2	55	5.5	5.9

DY029	48.57	-9.51	CS2	45	5.8	7.0
DY029	48.57	-9.51	CS2	16	6.1	6.4
DY029	48.85	-9.20	O4	150	6.2	6.6
DY029	49.13	-8.90	O2	145	6.3	6.5
DY029	49.13	-8.90	O2	100	6.3	6.6
DY029	49.13	-8.90	O2	80	6.2	6.0
DY029	49.13	-8.90	O2	40	6.2	5.3
DY029	49.13	-8.90	O2	20	7.9	7.8
DY029	49.40	-8.58	CCS	120	5.7	6.5
DY029	49.40	-8.58	CCS	40	6.1	5.6
DY029	49.40	-8.58	CCS	20	11.1	11.5
DY029	49.40	-8.58	CCS	10	11.6	11.9
DY029	51.21	-6.13	A	80	7.9	6.8
DY029	51.21	-6.13	A	45	10.0	9.3
DY029	51.21	-6.13	A	35	10.4	9.9
DY029	48.57	-9.51	CS2	185	5.3	6.7
DY029	48.57	-9.51	CS2	100	5.8	6.4
DY029	48.57	-9.51	CS2	60	5.7	6.6
DY029	48.57	-9.51	CS2	30	6.5	6.8
DY029	48.24	-9.97	Fe02	1972	4.8	2.3
DY029	48.24	-9.97	Fe02	1550	4.7	2.3
DY029	48.24	-9.97	Fe02	950	4.6	2.4
DY029	48.24	-9.97	Fe02	400	4.5	3.1
DY029	48.24	-9.97	Fe02	100	4.9	5.0
DY029	48.24	-9.97	Fe02	20	8.9	9.6
DY029	48.34	-9.71	Fe03	1477	5.0	2.5
DY029	48.34	-9.71	Fe03	950	4.7	2.2
DY029	48.34	-9.71	Fe03	750	4.5	2.4
DY029	48.34	-9.71	Fe03	650	4.5	2.8
DY029	48.34	-9.71	Fe03	150	4.6	4.6
DY029	48.34	-9.71	Fe03	60	4.9	5.9
DY029	48.38	-9.61	Fe05	741	4.6	3.2
DY029	48.38	-9.61	Fe05	650	4.6	3.3
DY029	48.38	-9.61	Fe05	450	5.0	3.7
DY029	48.38	-9.61	Fe05	100	4.9	5.0
DY029	48.38	-9.61	Fe05	70	5.5	5.2
DY029	48.38	-9.61	Fe05	20	6.7	7.3
DY029	48.57	-9.51	CS2	185	5.0	6.7
DY029	48.57	-9.51	CS2	70	4.9	5.6
DY029	48.57	-9.51	CS2	30	6.6	7.4
DY029	48.57	-9.51	CS2	5	7.4	8.1
DY029	49.40	-8.58	CCS	132	6.6	5.9
DY029	49.40	-8.58	CCS	120	6.4	5.7
DY029	49.40	-8.58	CCS	95	6.6	5.4

DY029	49.40	-8.58	CCS	70	6.5	5.5
DY029	49.40	-8.58	CCS	45	6.1	6.0
DY029	49.40	-8.58	CCS	35	9.5	10.5
DY029	51.21	-6.13	A	85	7.0	5.5
DY029	51.21	-6.13	A	70	7.0	5.7
DY029	51.21	-6.13	A	40	7.5	6.5
DY029	51.21	-6.13	A	30	8.6	8.1
DY029	50.50	-7.22	J4	100	6.9	6.4
DY029	50.50	-7.22	J4	80	6.8	6.0
DY029	50.01	-7.80	J6	111	6.2	5.4
DY029	50.01	-7.80	J6	85	6.2	5.1
DY029	50.01	-7.80	J6	45	6.2	4.9
DY029	50.01	-7.80	J6	20	6.7	6.9
DY033	49.40	-8.58	CCS	137	5.3	5.7
DY033	49.40	-8.58	CCS	80	5.3	6.0
DY033	49.40	-8.58	CCS	50	5.4	4.6
DY033	49.40	-8.58	CCS	45	5.9	6.1
DY033	49.40	-8.58	CCS	140	5.3	4.4
DY033	49.40	-8.58	CCS	80	5.3	4.8
DY033	49.40	-8.58	CCS	60	5.4	4.7
DY033	48.57	-9.51	CS2	190	4.1	3.9
DY033	48.57	-9.51	CS2	90	4.5	6.5
DY033	48.57	-9.51	CS2	50	4.5	6.4
DY033	48.57	-9.51	CS2	35	4.7	6.6
DY033	48.24	-9.97	Fe02	1960	4.7	2.3
DY033	48.24	-9.97	Fe02	1800	4.7	2.0
DY033	48.24	-9.97	Fe02	1550	4.6	2.2
DY033	48.24	-9.97	Fe02	780	4.5	2.5
DY033	48.24	-9.97	Fe02	400	4.3	3.8
DY033	48.24	-9.97	Fe02	200	4.2	4.4
DY033	48.34	-9.71	Fe03	1465	5.0	3.1
DY033	48.34	-9.71	Fe03	1350	4.9	2.4
DY033	48.34	-9.71	Fe03	1250	4.9	2.8
DY033	48.37	-9.63	Fe04	900	4.7	2.7
DY033	48.37	-9.63	Fe04	500	4.5	3.2
DY033	48.37	-9.63	Fe04	250	4.5	3.9
DY033	48.37	-9.63	Fe04	90	4.8	4.8
DY033	48.38	-9.53	Fe06	467	4.5	3.8
DY033	48.38	-9.53	Fe06	250	4.6	4.7
DY033	48.38	-9.53	Fe06	200	4.6	3.9
DY033	48.38	-9.61	Fe05	714	4.5	2.8
DY033	48.85	-9.20	O4	152	4.7	3.8
DY033	48.85	-9.20	O4	120	5.0	5.3
DY033	48.85	-9.20	O4	60	4.8	5.4

DY033	49.13	-8.90	O2	140	5.1	3.8
DY033	49.13	-8.90	O2	100	5.1	4.4
DY033	49.13	-8.90	O2	50	5.0	4.3
DY033	51.21	-6.13	A	92	6.5	3.5
DY033	51.21	-6.13	A	80	6.6	3.2
DY033	50.83	-6.67	J2	90	6.6	4.1
DY033	50.83	-6.67	J2	70	6.7	3.9
DY033	50.83	-6.67	J2	50	6.5	4.3
DY033	50.50	-7.22	J4	105	5.7	3.4
DY033	50.50	-7.22	J4	75	5.4	4.8
DY033	50.50	-7.22	J4	50	5.6	5.0
DY033	50.01	-7.80	J6	100	4.7	7.9
DY033	50.01	-7.80	J6	75	5.3	5.5
DY033	50.01	-7.80	J6	55	5.5	3.2
DY033	49.40	-8.58	CCS	134	5.0	3.6
DY033	49.40	-8.58	CCS	70	5.2	4.6
DY033	49.40	-8.58	CCS	46	5.4	5.0
DY033	49.40	-8.58	CCS	125	5.2	3.9
DY033	49.40	-8.58	CCS	105	5.3	3.8
DY033	49.40	-8.58	CCS	60	5.2	3.7
DY021	49.40	-8.58	CCS	45	5.4	6.4
DY021	49.40	-8.58	CCS	30	5.4	6.1
DY021	49.40	-8.58	CCS	3	5.6	6.9
DY021	48.57	-9.51	CS2	121	5.0	7.0
DY021	48.57	-9.51	CS2	92	5.1	6.9
DY021	48.57	-9.51	CS2	61	5.0	6.6
DY021	48.57	-9.51	CS2	42	5.0	6.3
DY021	48.57	-9.51	CS2	6	5.1	6.7

3. Samples collected during DY017 (Hebrides Shelf)

Cruise	Lat	Long	Site	Depth	$\delta^{15}N_{NO3}$	$\delta^{18}O_{NO3}$
DY017	58.60	-5.80	A1	107	4.4	4.9
DY017	58.60	-5.80	A1	102	4.4	5.6
DY017	58.60	-5.80	A1	81	4.0	6.3
DY017	58.60	-5.80	A1	60	4.2	
DY017	58.60	-5.80	A1	10	4.7	5.3
DY017	58.80	-6.19	A2	110	4.9	5.7
DY017	58.80	-6.19	A2	80	4.4	5.7
DY017	58.80	-6.19	A2	40	5.1	6.3
DY017	58.80	-6.19	A2	29	5.2	4.9
DY017	58.80	-6.19	A2	9	5.4	5.6
DY017	59.20	-6.95	A4	221	4.8	3.5
DY017	59.20	-6.95	A4	172	4.8	3.5
DY017	59.20	-6.95	A4	126	4.7	3.5

DY017	59.20	-6.95	A4	75	4.8	3.6
DY017	59.20	-6.95	A4	20	5.8	7.1
DY017	59.40	-7.33	A5	997	4.6	3.0
DY017	59.40	-7.33	A5	852	4.7	2.9
DY017	59.40	-7.33	A5	600	4.7	3.8
DY017	59.40	-7.33	A5	401	4.6	4.2
DY017	59.40	-7.33	A5	200	4.5	3.7
DY017	59.40	-7.33	A5	100	4.5	3.9
DY017	59.40	-7.33	A5	30	5.8	6.8
DY017	58.45	-7.19	B1	50	5.1	3.2
DY017	58.45	-7.19	B1	30	5.3	3.1
DY017	58.45	-7.19	B1	10	5.4	3.6
DY017	58.02	-7.72	C1	74	5.1	2.6
DY017	58.02	-7.72	C1	50	5.4	3.1
DY017	58.02	-7.72	C1	40	5.3	2.4
DY017	58.08	-8.01	C2	75	4.7	1.7
DY017	58.08	-8.01	C2	36	5.4	3.7
DY017	58.08	-8.01	C2	5	5.3	3.4
DY017	58.22	-8.83	C4	192	4.8	2.2
DY017	58.22	-8.83	C4	152	4.5	2.8
DY017	58.22	-8.83	C4	112	5.5	5.4
DY017	58.22	-8.83	C4	102	6.0	5.9
DY017	58.22	-8.83	C4	16	5.9	5.4
DY017	58.43	-10.08	C7	1863	5.0	2.5
DY017	58.43	-10.08	C7	1299	4.6	2.4
DY017	58.43	-10.08	C7	999	4.6	3.0
DY017	58.43	-10.08	C7	800	4.6	2.3
DY017	58.43	-10.08	C7	400	4.4	3.0
DY017	58.43	-10.08	C7	101	4.4	3.2
DY017	58.43	-10.08	C7	10	5.2	4.9
DY017	56.87	-8.50	E2	121	5.0	2.8
DY017	56.87	-8.50	E2	90	5.2	2.7
DY017	56.87	-8.50	E2	71	5.3	2.8
DY017	56.87	-8.50	E2	40	6.0	4.1
DY017	56.87	-8.50	E2	10	6.0	4.1
DY017	56.87	-9.06	E3	190	4.8	3.2
DY017	56.87	-9.06	E3	150	4.7	3.1
DY017	56.87	-9.06	E3	80	4.8	3.5
DY017	56.87	-9.06	E3	40	6.1	6.4
DY017	56.87	-9.06	E3	10	6.3	6.6
DY017	56.87	-10.09	E6	2066	4.9	1.9
DY017	56.87	-10.09	E6	1700	4.9	2.1
DY017	56.87	-10.09	E6	998	4.6	1.7
DY017	56.87	-10.09	E6	730	4.6	2.5
DY017	56.87	-10.09	E6	340	4.5	2.9

DY017	56.87	-10.09	E6	90	4.6	2.9
DY017	56.87	-10.09	E6	20	5.4	4.4
DY017	56.12	-8.10	F1	102	5.5	3.3
DY017	56.12	-8.10	F1	75	6.0	4.0
DY017	56.12	-8.10	F1	50	6.3	4.4
DY017	56.12	-8.10	F1	30	6.3	5.3
DY017	56.12	-8.50	F2	116	5.1	2.9
DY017	56.12	-8.50	F2	85	5.3	2.8
DY017	56.12	-8.50	F2	70	6.0	4.7
DY017	56.12	-8.50	F2	51	6.5	5.0
DY017	56.12	-8.50	F2	20	6.8	5.2
DY017	56.12	-9.18	F4	185	4.5	3.5
DY017	56.12	-9.18	F4	150	4.5	3.2
DY017	56.12	-9.18	F4	130	4.5	4.0
DY017	56.12	-9.18	F4	100	4.5	3.8
DY017	56.12	-9.18	F4	10	5.6	5.6
DY017	56.12	-10.10	F6	1980	4.8	2.5
DY017	56.12	-10.10	F6	1200	4.8	2.3
DY017	56.12	-10.10	F6	760	4.8	2.2
DY017	56.12	-10.10	F6	210	4.5	3.5
DY017	56.12	-10.10	F6	91	5.8	6.1
DY017	56.12	-10.10	F6	50	5.5	6.6
DY017	56.12	-10.10	F6	20	6.0	6.8

4. Samples collected for $\delta^{18}O_{H2O}$

CRUISE	EVENT	$\delta^{18}O_{H2O}$
DY029	CHRISTCHURCH	-0.1
DY029	STOUR	-6.1
DY029	UW1	0.5
DY029	UW2	0.6
DY029	UW3	0.6
DY029	UW4	0.6
DY029	UW5	0.7
DY029	UW6	0.6
DY029	UW7	0.6
DY029	UW8	0.7
DY029	UW9	0.7
DY029	EV051	0.4
DY029	EV051	0.6
DY029	EV051	0.7
DY029	EV054	0.6
DY029	EV090	0.7
DY029	EV099	0.7
DY029	EV105	0.7

DY033	EV008	0.7
DY033	EV104	0.7
DY033	EV135	0.3
DY033	EV135	0.7
DY033	EV135	0.7
DY033	EV160	0.7
DY033	EV161	0.6
DY033	EV192	0.6
DY033	EV194	0.6
DY033	EV196	0.6
DY033	EV199	0.6
DY029	EV102	0.7